Hawthorne, Christopher (2017) *Physiological and pharmacological modelling in neurological intensive care and anaesthesia.* MD thesis.

http://theses.gla.ac.uk/8721/

Physiological and Pharmacological Modelling in Neurological Intensive Care and Anaesthesia

Dr Christopher Hawthorne

BSc, MBBS, FRCA, FFICM

Submitted in fulfilment of the requirements for the

Degree of Doctor of Medicine

School of Medicine, Dentistry and Nursing

College of Medical, Veterinary and Life Sciences

University of Glasgow

May 2017

Abstract

Mathematical models of physiological processes can be used in critical care and anaesthesia to improve the understanding of disease processes and to guide treatment. This thesis provides a detailed description of two studies that are related through their shared aim of modelling different aspects of brain physiology.

The Relationship Between Transcranial Bioimpedance and Invasive Intracranial Pressure Measurement in Traumatic Brain Injury Patients (BioTBI) Study describes an attempt to model intracranial pressure (ICP) in patients admitted with severe traumatic brain injury (TBI). It is introduced with a detailed discussion of the monitoring and modelling of ICP in patients with TBI alongside the rationale for considering transcranial bioimpedance (TCB) as a non-invasive approach to estimating ICP. The BioTBI Study confirmed a significant relationship between TCB and invasively measured ICP in ten patients admitted to the neurological intensive care unit (NICU) with severe TBI. Even when using an adjusted linear modelling technique to account for patient covariates, the magnitude of the relationship was small (r-squared = 0.32) and on the basis of the study, TCB is not seen as a realistic technique to monitor ICP in TBI.

Target controlled infusion (TCI) of anaesthetic drugs exploit known pharmacokinetic pharmacodynamic (PKPD) models to achieve set concentrations in the plasma or an effect site. Following a discussion of PKPD model development for the anaesthetic drug propofol, the Validation Study of the Covariates Model (VaSCoM) describes a joint PKPD study of the Covariates Model. Pharmacokinetic validation of plasma concentrations predicted by the model in forty patients undergoing general anaesthesia confirmed a favourable overall bias (3%) and inaccuracy (25%) compared to established PKPD models. The first description of the pharmacodynamic behaviour of the Covariates Model is provided with an estimated rate constant for elimination from the effect site compartment (k_{e0}) of 0.21 to 0.27 min^{-1}.

Table of Contents

List of Tables

List of Figures

Acknowledgements

I am indebted to my supervisors Professor John Kinsella and Dr Ian Piper. John seemed to know what I was interested in before I did and his mentorship from my research fellow years, through my clinical lectureship and now into my consultant post has been invaluable. Ian has been an inspiration on how to make research enjoyable and has been a constant source of ideas and advice. Both of them have been instrumental in making sure that this thesis has reached completion. Ian has apparently retired now and John keeps threatening to, but if I can be as enthused as they currently are at a similar stage in my career, I will be delighted.

Two members of the research group at the Academic Unit of Anaesthesia deserve particular mention. Tara Quasim was my advisor throughout my MD. She can be pretty harsh but always fair (so she says) and I might never have started writing without her. I am very grateful she stuck with me. Martin Shaw is an incredible source of knowledge of mathematics, statistics and coding. He showed extraordinary patience when teaching a novice the ways of 'R' and 'the Greek'. Without his training and help there is no way the analyses in this thesis would have been successful.

The BioTBI Study was supported by funding from the National Institute of Academic Anaesthesia. Patients were recruited from the Neurological Intensive Care Unit at the Institute of Neurological Sciences and my special thanks go to the relatives who allowed me to collect the data for this study. Traumatic Brain Injury is a devastating diagnosis and I was constantly struck by how charitable our patients' relatives were at such a difficult time. My colleagues in the Departments of Neuroanaesthesia and Neurosurgery have always been supportive and encouraging. They are a fantastic bunch of people to work with and learn from. In particular, Linda Stewart has not only been a continuous source of backing for my research but also guidance in my clinical work. The critical care nursing staff is an exceptional group. They work with determination and compassion and it is an honour to be part of the team.

Details of Work and Collaboration

During completion of the BioTBI and VaSCoM Studies I was employed first as a Clinical Research Fellow, then as a Clinical Lecturer at the Academic Unit of Anaesthesia, Pain and Critical Care Medicine, University of Glasgow. For the writing-up phase of the studies, I have been employed as a Consultant in Anaesthesia and Neurocritical Care at the Institute of Neurological Sciences, Glasgow.

Throughout the period of study I have been enrolled in the Postgraduate Research Program of Doctor of Medicine at the University of Glasgow. I have participated in the compulsory courses and attended appropriate additional research training.

Both of the BioTBI and the VaSCoM Studies recruited patients in the acute hospital environment. The BioTBI Study was conducted in the Neurological Intensive Care Unit (Ward 61) at the Institute of Neurological Sciences, while the VaSCoM Study was conducted in the operating theatre suite at the Golden Jubilee National Hospital.

The research presented in this thesis is my own. I was responsible for patient recruitment, data collection and analysis for both the BioTBI and VaSCoM Studies. Details of the contribution of others are provided for each of the relevant chapters below.

Chapter 2

The introduction to monitoring and modelling of intracranial pressure in traumatic brain injury was adapted and expanded from a review article co-authored with Ian Piper. He provided invaluable historical background and guided me towards key literature in the field.

Chapter 3

The protocol for the BioTBI Study was developed with input from Ian Piper and Martin Shaw using their prior knowledge of transcranial bioimpedance from a previous animal study.

Chapter 4

The nursing staff on Ward 61 were exceptionally generous in keeping accurate notes of any nursing interventions that could influence the measurements made during the BioTBI Study. Martin Shaw provided advise on writing R code for data import and analysis. The circle fitting function required for Cole-Cole plots of bioimpedance data was adapted from his previous work.

Chapter 5

The related and future work section references work completed using data collected during the BioTBI Study in collaboration with other researchers. Details of the collaborating researchers are provided in the appropriate references. Of particular note, Ashleigh Ward used data from BioTBI to compare indices of cerebral autoregulation for her research project in completion of a BSc in Critical Care and Perioperative Medicine.

Chapter 7

The protocol for the VaSCoM Study was written and the research ethics approval process completed prior to my involvement by Stefan Schraag, Mani Chandra and Nick Sutcliffe.

Chapter 8

Shiona McKelvie was instrumental in co-ordinating the first approach to patients prior to recruitment to the VaSCoM Study. Each recruited patient required a team of three clinicians in theatre for anaesthesia, data collection and blood

sampling. The core team was myself, Stefan Schraag and Shiona McKelvie. Nick Sutcliffe assisted with several patients and the anaesthetists and anaesthetic nursing staff at the Golden Jubilee National Hospital kindly provided assistance when required. I was not personally present for the study of two out of the forty patients. Propofol concentrations in whole blood samples were analysed by Mel Priston at C3P Analysis. As for the BioTBI Study, Martin Shaw provided advise on writing R code for data import and analysis. This was particularly important when deciphering the input requirements of the *desolve* and *nlmeODE* Packages.

Chapter 9

As detailed above for the BioTBI Study, the related and future work section references work completed using data collected during the VaSCoM Study in collaboration with other researchers. Details of the collaborating researchers are provided in the appropriate references. Of particular note, Andrew Croall used data from VaSCoM to calculate a non-parametric k_{e0} for propofol during his research project in completion of a BSc in Critical Care and Perioperative Medicine.

Publications

Directly Related to the Work of the Thesis

Papers

Hawthorne C, Piper I Monitoring and Modelling of Intracranial Pressure in Patients with Traumatic Brain Injury. *Frontiers in Neurology* 2014; **5**.

Hawthorne C, Shaw M, Piper I, Moss L. Transcranial Bioimpedance Measurement as a Non-Invasive Estimate of Intracranial Pressure. 16th International Symposium on Intracranial Pressure and Neuromonitoring (Submitted to conference proceedings); 2016; Boston, Massachusetts.

Abstracts

Hawthorne C, Chandra M, McKelvie S, Sutcliffe N, Schraag S. Methods and interim results of a validation study of the Covariates Model for target-controlled infusion of propofol. British Journal of Anaesthesia. 2012;109(4):658P-9P.

Hawthorne C, Schraag S, Suttcliffe N, McKelvie S, Shaw M, Chandran M. Abstract PR437: Calculating the Keo for the Covariates Model for Target Controlled Infusion of Propofol. Anesthesia & Analgesia. 2016;123(3S_Suppl):552-3.

Hawthorne C, Schraag S, Suttcliffe N, McKelvie S, Shaw M, Chandran M. Abstract PR438: Validation Study of the Covariates Model for Target Controlled Infusion of Propofol. Anesthesia & Analgesia. 2016;123(3S_Suppl):554-5.

Using Data Collected During the Work of the Thesis

Papers

Georgatzis K, Lal P, **Hawthorne C**, Shaw M, Piper I, Tarbert C, et al. Artefact in Physiological Data Collected from Patients with Brain Injury: Quantifying the Problem and Providing a Solution Using a Factorial Switching Linear Dynamical Systems Approach. Acta Neurochir Suppl. 2016;122:301-5.

Shaw M, Piper I, **Hawthorne C**. Multi-resolution Convolution Methodology for ICP Waveform Morphology Analysis. Acta Neurochir Suppl. 2016;122:41-4.

Lal P, Williams CK, Georgatzis K, **Hawthorne C**, McMonagle P, Piper I, et al. Detecting artifactual events in vital signs monitoring data. 2016. In: Machine Learning for Healthcare Technologies. Institution of Engineering and Technology, Healthcare Technologies; [7-32].

Shaw M, Moss L, **Hawthorne C**, Kinsella J, Piper I, editors. Investigation of the relationship between the burden of raised ICP and the length of stay in a neuro-intensive care unit. 16th International Symposium on Intracranial Pressure and Neuromonitoring (Submitted to conference proceedings); 2016; Boston, Massachusetts.

Hawthorne C, Sutcliffe N. Total intravenous anaesthesia. Anaesthesia & Intensive Care Medicine. 2016;17(3):166-8.

Georgatzis K, Williams CKI, **Hawthorne C**. Input-Output Non-Linear Dynamical Systems applied to Physiological Condition Monitoring. In: Finale D-V, Jim F, David K, Byron W, Jenna W, editors. Proceedings of the 1st Machine Learning for Healthcare Conference; Proceedings of Machine Learning Research: PMLR; 2016. p. 1-16.

Abstracts

Hawthorne C, Shaw M, Moss L, Piper I, Elliott R, Lee C, et al. 761: Improvements to the optimal cerebral perfusion pressure calculation. Critical Care Medicine. 2016;44(12):266.

Ward A, **Hawthorne C**, Shaw M. Cerebral autoregulation model extension using high frequency ICU data. British Journal of Anaesthesia Research Forum (Submitted to conference proceedings); 2016; Glasgow, UK.

Croall A, **Hawthorne C**, Shaw M, editors. Modelling the effect site compartment in a target controlled infusion of Propofol. British Journal of Anaesthesia Research Forum (Submitted to conference proceedings); 2016; Glasgow, UK.

Abbreviations and Definitions

Abbreviation	Definition
A	Age
a-v PE Difference	Arterial-venous performance error difference
AAGBI	Association of Anaesthetists of Great Britain and Ireland
ABP	Arterial blood pressure
AEP	Auditory evoked potential
AIC	Akaike information criterion
BIA	Bioelectrical impedance analysis
BioTBI	Transcranial bioimpedance and invasive intracranial pressure measurement in traumatic brain injury patients
BIS	Bispectral index
BMI	Body mass index
BrainIT	Brain monitoring with information technology
BSR	Burst suppression ratio
CA	Cerebral autoregulation
CBF	Cerebral blood flow
CCIP	Computer-controlled infusion pump

$C_e(50)$	Concentration of drug in the effect site compartment at 50% of maximum effect
C_e	Concentration of drug in the effect site compartment
CHART-ADAPT	Connecting healthcare and research through a data analysis provisioning technology
Cl	Clearance
C_n	Concentration of drug in compartment n in a multi-compartment model
C_p	Concentration of drug in plasma
CRF	Clinical record form
csv	Comma separated value
CT	Computed tomography
$CUP_{propofol}$	Canonical univariate parameter for propofol
DAP	Diastolic arterial pressure
DoA	Depth of Anaesthesia
E	Effect
E_0	Baseline effect with no drug present
EDTA	Ethylenediaminetetraacetic acid
EDV	End diastolic velocity

EEG	Electroencephalogram
E_{max}	Maximum difference in drug effect from baseline
FDA	Food and Drug Administration
G	Gender
GABA	γ-Aminobutyric acid
HPLC	High performance liquid chromatography
EIT	Electrical impedance tomography
FFT	Fast Fourier transform
IoC	Index of consciousness
ICH	Intracranial hypertension
ICP	Intracranial pressure
iCPP	Invasive cerebral perfusion pressure
IIH	Idiopathic intracranial hypertension
IMPACT	International Mission on Prognosis and Clinical Trial Design in traumatic brain injury
K_{e0}	Rate constant for elimination from the effect site compartment
K_{1n}	Rate constant for movement of drug from compartment *1* to *n*

LBM	Lean body mass
MAP	Mean arterial blood pressure
MCA	Middle cerebral artery
MDPE	Median prediction error
MDAPE	Median absolute performance error
mFV	Mean flow velocity
MRI	Magnetic resonance imaging
nCPP	Non-invasive cerebral perfusion pressure
NHS	National Health Service
NICE	National Institute of Health and Care Excellence
NIRS	Near-infrared spectroscopy
NONMEM	Non-linear mixed effect model
ONSD	Optic nerve sheath diameter
PBPK	Physiologically based pharmacokinetic
PhA	Phase angle
PE	Percentage performance error
pEEG	Processed electroencephalography

PI	Pulsatility index
PK	Pharmacokinetic
PKPD	Pharmacokinetic pharmacodynamic
PSV	Peak systolic velocity
R_0	Resistance measured at zero frequency
RCT	Randomised Controlled Trial
REG	Rheoencephalography
R_{inf}	Resistance measured at infinite frequency
T	Temperature
TBI	Traumatic brain injury
TCB	Transcranial bioimpedance
TCD	Transcranial Doppler
TCI	Target controlled infusion
TIVA	Total intravenous anaesthesia
TMD	Tympanic membrane displacement
t_{peak}	Time to peak effect site concentration
VaSCoM	Validation Study of the Covariates Model
VEP	Visual evoked potential

V_n	Volume of compartment n in a multi-compartment model
WBZ_c	Whole body impedance measurement at maximum reactance
WBZ_{norm}	Normalised whole body impedance measurement
Z_c	Impedance measured at frequency where reactance is maximal

1   Introduction to Mathematical Modelling in Neurological Intensive Care and Anaesthesia

1.1   The Need for Modelling

In anaesthesia and critical care medicine, patients undergo continuous monitoring of their physiological systems. Developments in healthcare information systems mean that increasingly vast quantities of physiological data are being stored. There is mounting recognition that despite the significant time and resources that are consumed to collect these data, they are not being used to their full potential(1). In the ideal situation, data can be used to guide clinical management, predict outcomes and improve understanding of disease processes. To achieve this ideal, there is a need to utilise the advances in methods for the study of dynamic systems and in particular the techniques of mathematical modelling(2).

1.2   The Principles of Modelling

A model is a representation of reality and can only ever be an approximation of that reality(3). Mathematical models can be described in terms of their purpose or in terms of the approach to the modelling process (Figure 1.1).

The approach to mathematical modelling can be to either model the data or to model the system(4). In a data driven approach there is no need for existing knowledge of the physiological system of interest. Instead, these models can be considered as a "black box" where statistical modelling techniques are used to describe available experimental data. In contrast, for a physiologically derived model there is a requirement for existing knowledge of the system and the model is developed to represent this knowledge.

The purpose of mathematical modelling of physiological systems can be considered as predictive, explanatory or both. A predictive model aims to predict the future behaviour of the system under investigation. Meanwhile, an explanatory model aims to improve the understanding of the system of interest.
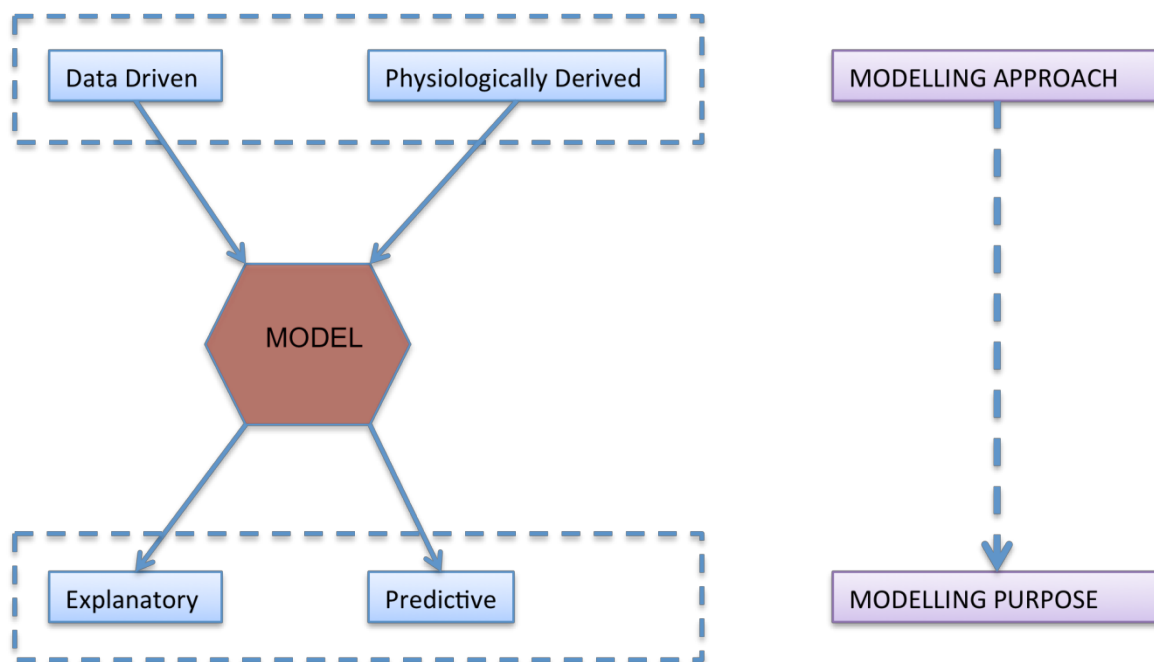
Figure 1.1: The relationship between modelling approach and modelling purpose.

The process of mathematical modelling involves the stages of model building, model identification, model simulation and model validation. The details of this process will vary significantly depending on the specific model being developed (Table 1.1).

Model Type	Model Features	Model Type	Model Features
Deterministic	Fixed model inputs provide fixed model outputs	Stochastic	Model outputs account for randomness observed in physiological systems
Static	Model describes system at single point in time	Dynamic	Model describes system as it changes in time
Discrete	Model samples physiological data at distinct time points	Continuous	Model of physiological system is allowed to change at any point in time

Table 1.1: Categorisation of physiological models.

1.3 Modelling of the Brain

The clinical settings of the two studies presented in this thesis were firstly the neurological intensive care unit (NICU) and secondly the operating theatre, specifically in patients undergoing general anaesthesia to facilitate surgery. In

both of these settings there is a need to model either the effects of disease processes or of specific therapies on the physiology of the brain.

The NICU provides the facilities and expertise to care for patients who suffer severe brain injuries with a variety of aetiologies ranging from trauma and vascular events to infection and malignancy. In these patients, specialised devices, such as the intracranial pressure monitor, can be used to monitor the disease process and thus inform treatment decisions. Modelling of the data provided by these devices has led to an improved understanding of the pathological processes following brain injury. There is an increasing demand to develop "non-invasive" monitoring and so avoid the potential complications of devices that require placement within the brain parenchyma.

The first study (BioTBI) is a pilot study to model the relationship between transcranial bioimpedance (TCB) and invasively measured intracranial pressure (ICP) in patients with traumatic brain injury (TBI). Without existing knowledge of the relationship between TCB and ICP the model derived is primarily data driven. It is an example of a stochastic, static, discrete model. The ultimate aim of this study was to begin development of a non-invasive technique to estimate ICP.

General anaesthesia can be regarded as a triad of hypnosis (or unconsciousness), analgesia (or pain relief) and muscle relaxation. The target sites of drugs used to achieve the hypnotic component of general anaesthesia are within the brain. There is therefore a call for models that can predict the dosing requirements to achieve adequate delivery of drugs to the brain and then to predict the clinical effects of these drugs.

The second study (VaSCoM) is a validation study of a three compartment pharmacokinetic (PK) model for the intravenous anaesthetic drug propofol. The "Covariates Model"(5) is an update to a model (The Marsh Model(6)) in wide clinical use that was previously adapted to account for the observed pharmacokinetic data. It is an example of a deterministic, dynamic, continuous model. The dual aims of this study were to firstly validate the pharmacokinetic component of the model and secondly to expand the model to account for

pharmacodynamic behaviour. This involved the use of processed electroencephalography (pEEG), a non-invasive brain monitoring technique, to quantify the effect of propofol on the brain.

A narrative review of the literature and discussion of existing models relevant to the two studies is provided in this thesis. The BioTBI and VaSCoM studies are not only related by their shared aim of modelling aspects of the brain, but also through the approach taken to the modelling process. All of the data collected were converted into standardised non-proprietary formats, while all of the analyses were performed using the open source statistical programming environment "R"(7). The consequence of this is that all data and models can be shared with interested research groups with diverse expertise in fields ranging from medicine to mathematics and clinical physics to computing science.

2 Monitoring and Modelling of Intracranial Pressure in Patients with Traumatic Brain Injury

2.1 Overview

Since Monro published his observations on the nature of the contents of the intracranial space in 1783 there has been investigation of the unique relationship between the contents of the skull and the intracranial pressure (ICP). This is particularly true following traumatic brain injury (TBI), where it is clear that elevated ICP due to the underlying pathological processes is associated with a poorer clinical outcome. Consequently, there is considerable interest in monitoring and manipulating ICP In patients with TBI.

The two techniques most commonly used in clinical practice to monitor ICP are via an intraventricular or intraparenchymal catheter with a microtransducer system. Both of these techniques are invasive and are thus associated with complications such as haemorrhage and infection. For this reason, significant research effort has been directed towards development of a non-invasive method to measure ICP. In this introduction there will be a detailed review of the existing non-invasive ICP monitoring technology. The final section will then be an overview of the theory underlying the BioTBI study.

The principle aims of ICP monitoring in TBI are to allow early detection of secondary haemorrhage and to guide therapies that limit intracranial hypertension and optimise cerebral perfusion. However, information from the ICP value and the ICP waveform can also be used to assess the intracranial volume-pressure relationship, estimate cerebrovascular pressure reactivity and attempt to forecast future episodes of intracranial hypertension.

The following introduction to monitoring and modelling of intracranial pressure in patients with traumatic brain injury is an updated and extended version of a previously published review article(8).

2.2 Introduction to Traumatic Brain Injury

The pathophysiology of TBI can divided into primary and secondary injury. The primary injury may include focal haematomas, contusions or diffuse injury that leads to a cycle of hypoxic ischaemic injury associated with inflammatory and neurotoxic processes (Figure 2.1). This secondary injury is exacerbated by secondary physiological insults such as hypoxia, hypo or hypercarbia, hypotension, hyperthermia and hypo or hyperglycaemia. A rise in ICP, or intracranial hypertension (ICH), is a secondary insult that can result from the primary injury, vascular engorgement, obstruction to cerebrospinal fluid (CSF) flow or cerebral oedema. It is known to be associated with poorer outcomes(9), which has led to considerable interest in its monitoring and manipulation in patients who have suffered TBI.
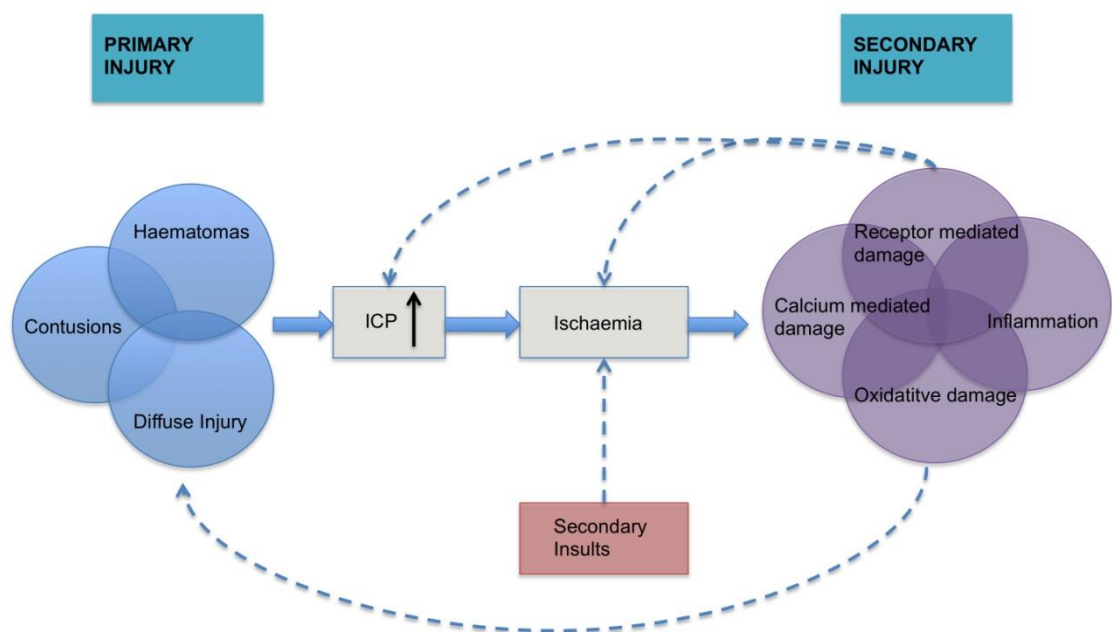
Figure 2.1: The inter-relationship between primary and secondary injury in TBI. Secondary physiological insults can potentiate ischaemia and lead to exacerbation of secondary injury. ICP = intracranial pressure. Adapted from Maas *et al*(10).

Normal ICP in healthy adults is usually regarded as 5 to 15 mmHg(11) and in TBI an ICP of >20 mmHg is widely accepted as ICH(12). The principle aims of ICP

monitoring in TBI are to allow early detection of secondary haemorrhage and to guide therapies that limit ICH. In addition, measurement of ICP and mean arterial pressure (MAP) allows calculation of cerebral perfusion pressure (CPP):

$$CPP = MAP - ICP \qquad (2.1)$$

Attempts can then be made to optimise cerebral perfusion pressure with the aim of preventing cerebral ischaemia.

There is ongoing debate over the central role of ICP monitoring in the clinical management of TBI. This is particularly relevant in the context of a recent randomised controlled trial (RCT) that did not show an outcome benefit in patients undergoing ICP monitoring with a treatment threshold of 20 mmHg when compared to patients that were not monitored(13). The purpose of this review is therefore to reconsider some of the basic science underlying ICP monitoring and the intracranial pressure-volume relationship in adults. With this pretext there will then be support for the arguments of other authors for the use of ICP as "more than a number" or a generic treatment threshold(14). Instead, the information within ICP trends and the ICP waveform can be used to provide individualised treatment thresholds and forecast future episodes of ICH.

2.3   Concepts and Historical Perspectives

2.3.1 Intracranial Contents

The Monro-Kellie hypothesis describes the relationship between the contents of the skull(15). In 1783, Monro published his observations that: the brain was enclosed in a non-expandable case of bone; the substance of the brain was nearly incompressible; the volume of the blood in the cranial cavity was therefore constant or nearly constant; and a continuous outflow of venous blood from the cranial cavity was required to make room for the continuous incoming arterial blood. Experiments performed by Kellie and Abercrombie supported these observations but they, like Monro, did not account for the role of CSF.

As the important role of CSF was recognised, the Monro-Kellie hypothesis was revised to its current form where with an intact skull, the sum of the volumes of

the brain, intracranial blood and CSF are constant. Therefore an increase in one necessitates a decrease in one or both of the remaining two. As the brain parenchyma is essentially non-compressible, compensation is achieved through extrusion of CSF or venous blood.

2.3.2 Intracranial Pressure Measurement

Lundberg systematically described the technique of continuous ICP monitoring using an intraventricular catheter in a series of 130 patients with suspected intracranial space occupying lesions(16). He then went on to confirm the feasibility of the technique in a series of 30 patients with TBI(17).

In his seminal paper, Lundberg identified three typical patterns of ICP fluctuation which have come to be known as "A", "B" and "C" waves. A waves are steep rises in ICP to a plateau of 50 mmHg or more and are sustained for 5 – 20 minutes before falling rapidly. They represent a critical reduction in intracranial compliance. B waves occur with a frequency of 0.5 to 2 waves per minute and are rhythmic oscillations to 20-30 mmHg above the baseline but without a sustained period of intracranial hypertension. C waves are not thought to be of pathophysiological importance, probably a reflection of Traube-Hering waves originating in the arterial pressure and are of much smaller amplitude to B waves.

While Lundberg and colleagues were developing the role of ICP monitoring in man, Langfitt's group were examining primates to carefully characterise the transmission of pressure across the intracranial compartments(18, 19). The phenomenon of pressure underestimation was fully defined in experimental studies of extradural brain compression where progressive loss of transmission of ICP across the tentorial hiatus occurred, with the pressure in the posterior fossa and lumbar subarachnoid space progressively under-reading the ventricular pressure and eventually returning to normal pressure.

2.3.3 The Intracranial Volume-Pressure Relationship

The intracranial volume-pressure curve demonstrates how small increases in volume of one of the intracranial components can be compensated by a

reduction in CSF or blood volume (Figure 2.2). However, these compensatory measures are quickly exhausted and any subsequent increase in volume leads to an exponential increase in ICP. Measurement of this volume-pressure relationship is most often incorrectly referred to as intracranial compliance. According to conventional terminology it should be referred to as elastance (change in pressure per unit change in volume, $\Delta P/\Delta V$)(20, 21). Due to the exponential nature of the volume-pressure relationship as depicted in Figure 2.2, being able to quantify elastance is attractive clinically as in theory it will increase during the volume compensation phase more rapidly than ICP and should therefore be predictive of impending volume decompensation.
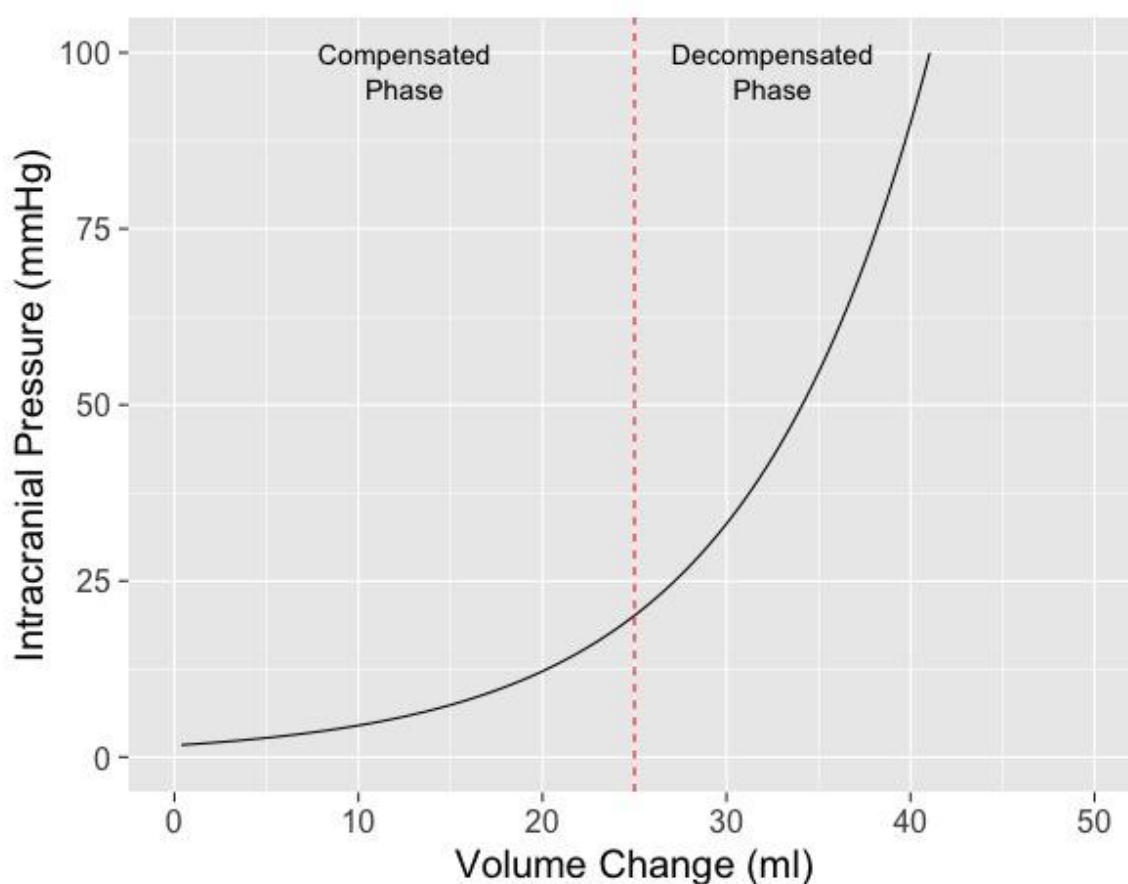
Figure 2.2: Cerebral volume-pressure curve showing the exponential relationship between ICP and an increase in volume of one of the intracranial components. The red line marks the point of decompensation.

The first full mathematical description of the craniospinal volume-pressure relationship was published by Marmarou in 1973(22). Since then, several research groups have contributed physiological simulation models of ICP dynamics of varying complexity. These models aim to improve understanding of

ICP pathophysiology and thus assist in the development of appropriate treatment strategies. A detailed comparative review on this subject has been provided by Wakeland and Goldstein(23). The early work of Marmarou and colleagues shall be discussed below as it provides an introduction to many important concepts surrounding ICP dynamics.

Through his interest in the pathological state of hydrocephalus, Marmarou developed a mathematical model of the CSF system that produced a general solution for the CSF pressure(22). The model parameters were verified in a series of experiments on adult cats(24). In these studies, the CSF pressure was measured both intracranially at the cisterna magna and in the lumbar subarachnoid space in response to bolus injections (Figure 2.3).
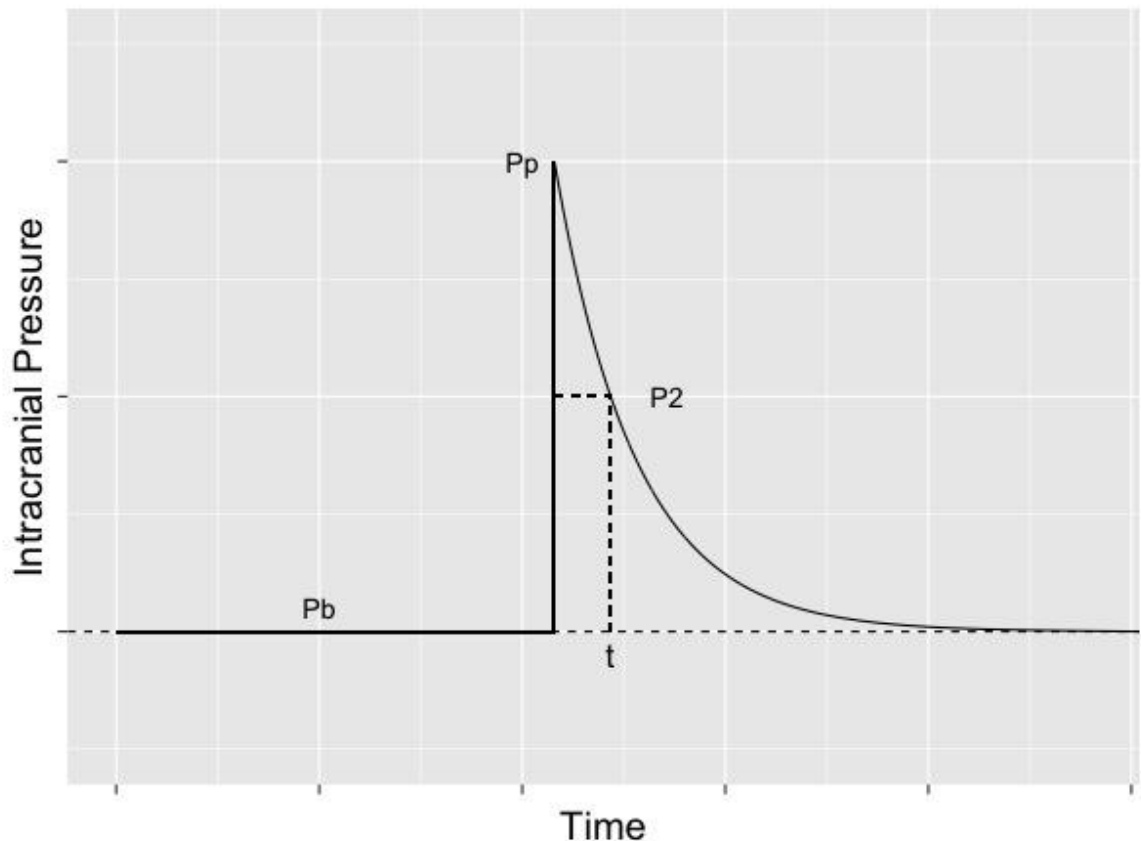
Figure 2.3: Demonstration of intracranial pressure changes following a bolus volume injection V$_0$ where: P$_b$ is the baseline ICP, P$_p$ is the peak pressure and P$_2$ refers to the pressure point on the return trajectory at time t.

Of particular note in this work, was the introduction of the pressure-volume index (PVI). Marmarou confirmed the non-linear relationship between changes in craniospinal volume and pressure. However, by plotting changes in volume

against the log to the base ten of pressure, a straight-line relationship could be defined (Figure 2.4). The slope of this line is termed the PVI and is the notional volume required to raise ICP tenfold. Unlike elastance or compliance, the PVI characterises the craniospinal volume-pressure relationship over the whole physiological range of ICP and can be calculated from:

$$PVI = \frac{V_0}{log_{10}\left(\frac{P_p}{P_b}\right)}$$

(2.2)

where V_0 is the bolus injection volume, P_p is the peak pressure and P_b is the baseline ICP.
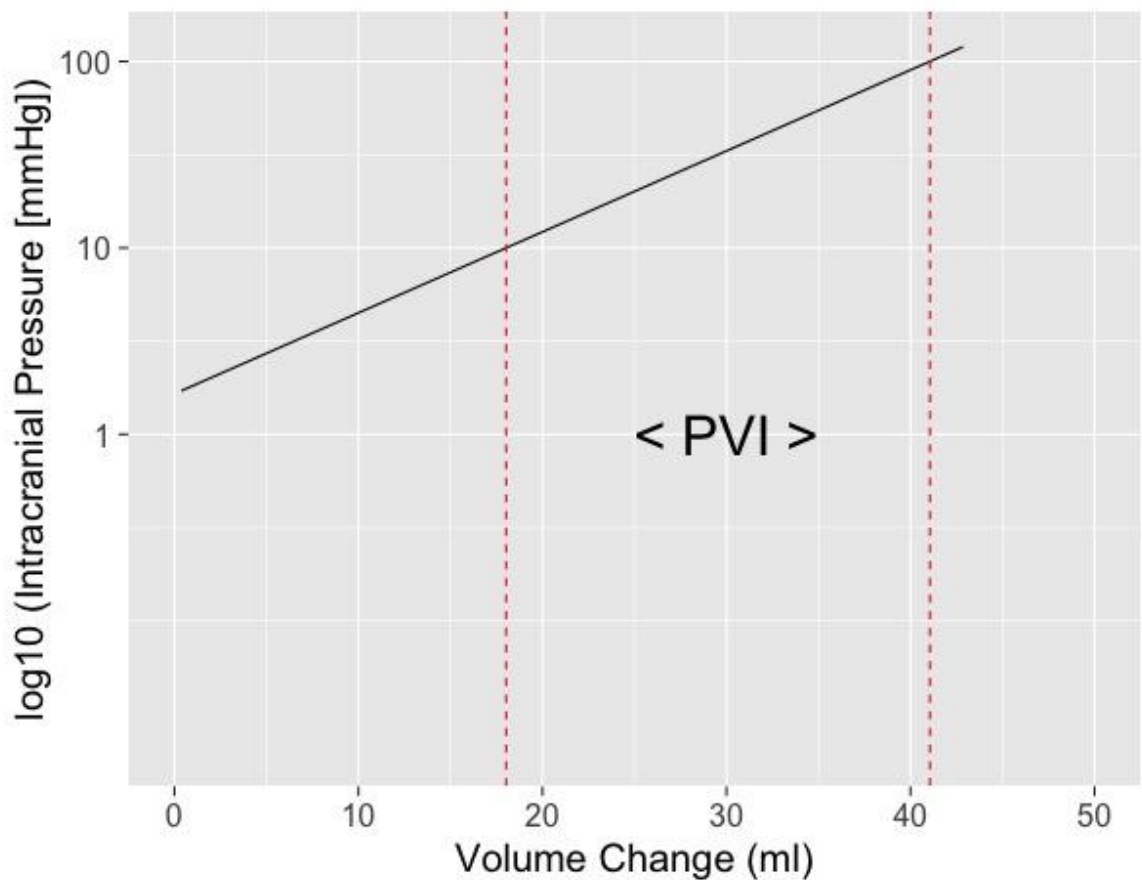
Figure 2.4: Log$_{10}$ ICP vs intracranial volume relationship defined by Marmarou(22). The pressure volume index (PVI) is the notional volume which when added to the craniospinal volume causes a ten-fold rise in ICP.

Marmarou's mathematical model developed an improved understanding not only of craniospinal elastance but also of the inter-relationships of the static and dynamic processess of formation, storage and absorption of CSF. Previously, Davson had demonstrated that by withdrawing CSF at the estimated rate of CSF production (approximately 0.3 ml/min), it was possible to determine the cerebral venous pressure(25). This value could then be substituted into the steady-state ICP equation:

$$ICP = P_{ssp} + \left(I_f \times R_o\right) \qquad (2.3)$$

where P_{ssp} is sagital sinus pressure, I_f is CSF formation rate and R_o is CSF outflow resistance. Marmarou extended Davson's work and his general solution for ICP allowed the derivation of an equation for CSF outflow resistance based on the bolus injection technique (Figure 2.3)(22, 24):

$$R_o = t \times \frac{P_b}{(PVI)log_{10}\left\{\dfrac{\left(P_2/P_p\right)\left(P_p - P_b\right)}{\left(P_2 - P_b\right)}\right\}} \qquad (2.4)$$

In TBI management, it is useful to know CSF outflow resistance when determining the aetiology of raised ICP. In general terms, causes of ICH can be categorised into "vascular" and "non-vascular" mechanisms. Vascular mechanisms include active cerebral vasodilation due to stimuli such as increased arterial carbon dioxide levels or decreased CPP with intact pressure autoregulation, passive distension of cerebral vessels in the absence of autoregulation or venous outflow obstruction. Non-vascular mechanisms include increased brain mass due to cerebral edema or an expanding extradural, subdural or intracerebral mass. A further non-vascular mechanism is an increase in CSF outflow resistance secondary to obstruction of the normal CSF pathway.

The importance of vascular factors and the state of cerebral blood flow (CBF) autoregulation as a determinant of craniospinal elastance was shown clearly by the work of Gray and Rosner(26, 27). The autoregulation of CBF will be discussed later, however, through a series of studies in adult cats, Gray and Rosner demonstrated that with CPP levels greater than 50 mm Hg, there was a linear

increase in PVI with increasing CPP. Similarly, with CPPs below 50 mmHg, further reduction in CPP was also associated with increased PVI, as well as reduced CBF. This work illustrated that the PVI is a complex function of CPP and that the direction of the CPP-PVI relationship is dependent on whether CPP is above or below the autoregulatory range for CBF. The importance of the state of autoregulation on PVI has been supported recently by Lavinio *et al*(28). In a series of brain injured patients admitted to the intensive care unit (ICU), PVI results were significantly different if a transcranial Doppler (TCD) derived assessment of middle cerebral artery (MCA) flow velocity (FV) revealed defective cerebral autoregulation.

Despite the potential for providing valuable information on the intracranial pressure-volume relationship, the PVI is not routinely measured in clinical management of severe TBI. Variability between measurements is high because of the difficulty in rapid manual injection at a constant rate. As a result, an average of repeated measures is usually required. In addition, there is an infection risk associated with injecting fluid into the subarachnoid space via an intraventricular catheter(29-31) and a risk of provoking secondary ICP rises following injection as a consequence of vasodilation(32). Thus, an interest in deriving estimates of the intracranial pressure-volume relationship indirectly through analysis of the ICP waveform has become a research focus.

2.3.4 The ICP Waveform

The ICP waveform has three consistent peaks that are related to the arterial pulse waveform (Figure 2.5), although their exact aetiology is the subject of some debate(33). Avezaat and van Eijndhoven systematically studied the ICP waveform pulse amplitude (ICP_{plse}) as a measure of craniospinal elastance(32, 34). In recognition of the limitations of the PVI related to the need for volume injection or withdrawal, they exploited the fact that with each cardiac cycle there is a pulsatile increase in cerebral blood volume. This is the equivalent of a small intracranial volume injection (dV), and the ICP_{plse} is the pressure change (dP) in response to that volume increment and should consequently be directly related to the craniospinal elastance (dP/dV) (Figure 2.6). Therefore, as craniospinal elastance increases (compliance decreases) the ICP_{plse} should increase. The observation that as ICP increases so does the amplitude of the

intracranial pressure pulsations is not a new one, having been first described in 1866 by Leyden(35).
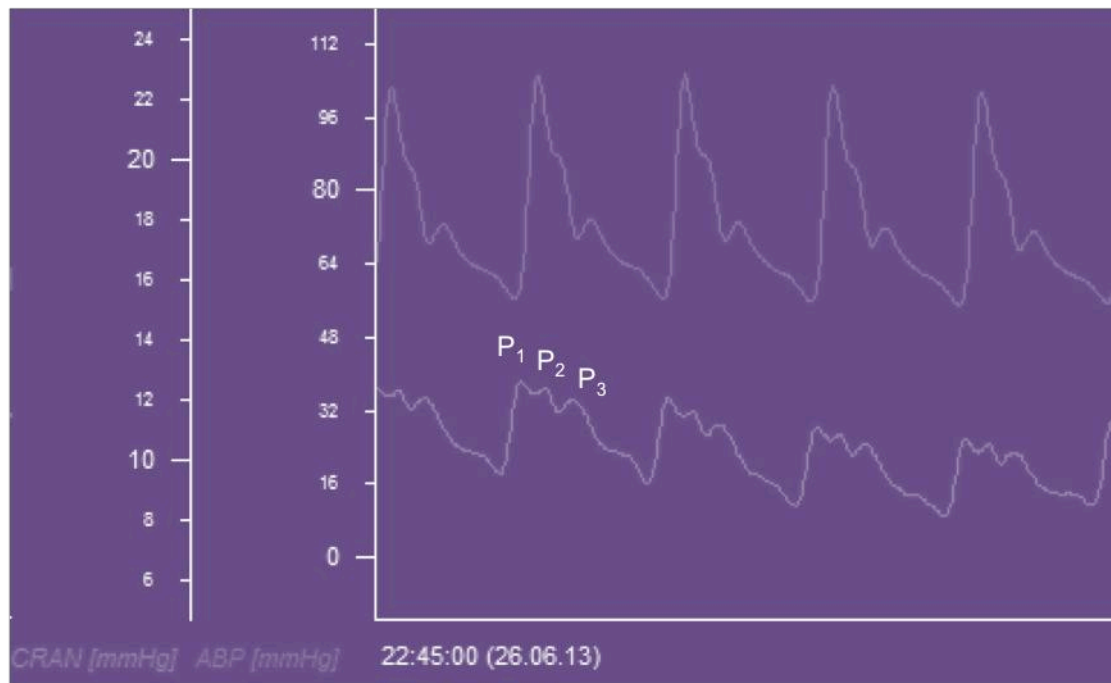
Figure 2.5: ICP waveform recorded from a Raumedic intraparenchymal catheter and displayed beneath an arterial waveform recorded from the radial artery in a patient with TBI. CRAN = intracranial pressure, ABP = arterial blood pressure, P_1 = percussion wave, P_2 = tidal wave, P_3 = dicrotic wave.

The mathematical description of the exponential craniospinal volume-pressure relationship was extended by Avezaat and Van Eijndhoven:

$$ICP = P_{eq}e^{E_1 dV} + P_0 \qquad (2.5)$$

where P_{eq} is intracranial equilibrium pressure, E_1 is the elastance coefficient and determines the elastance at a given pressure and P_0 is ICP at zero elastance. The term P_0 was introduced into the pressure-volume equation primarily for mathematical convenience. It allows the volume-pressure curve as a whole to shift up or down its axis, which allows for correction of pressure transducer reference position and postural changes. Mathematically, P_0 is the pressure at zero elastance and must therefore have physiological significance as a determinant of the normal intracranial equilibrium pressure (P_{eq}). Löfgren showed that alterations in central venous pressure (CVP) can shift the pressure-

volume curve up or down its axis(36), which would suggest CVP may be a factor determining P_0.
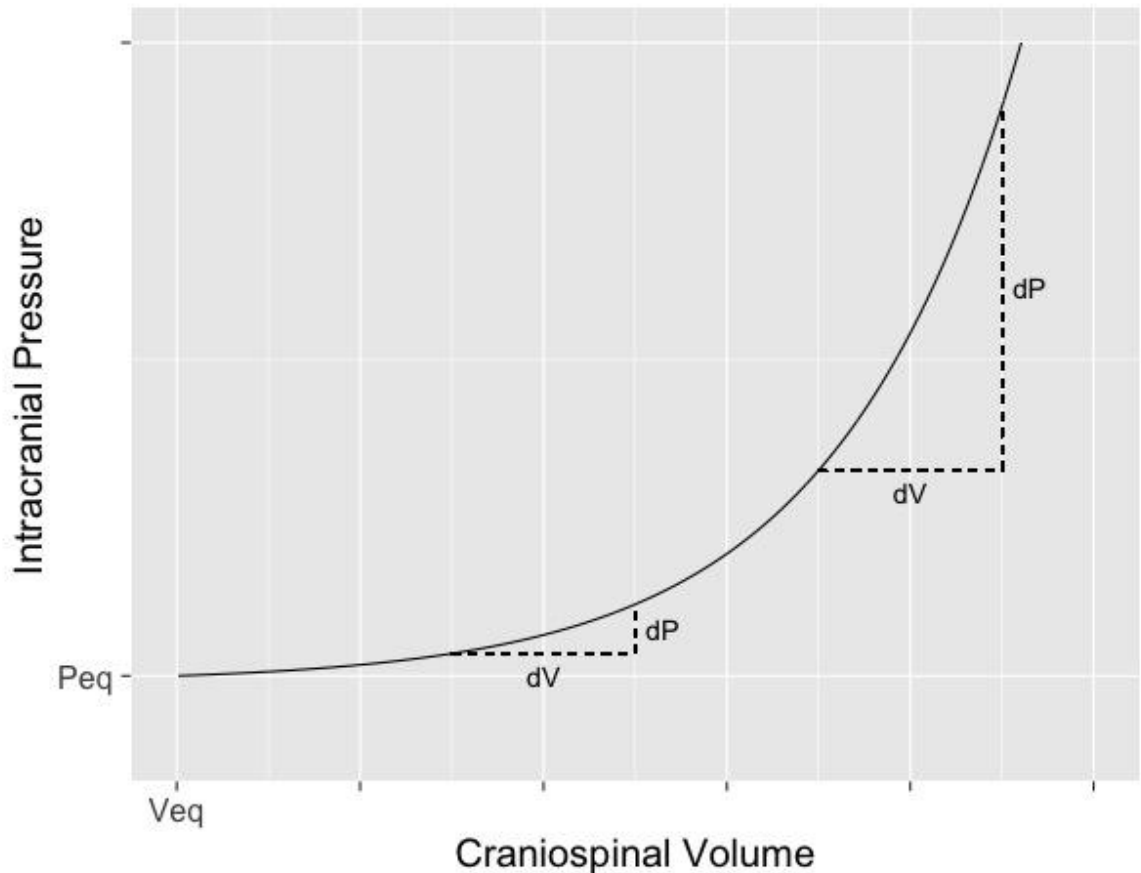
Figure 2.6: Craniospinal volume-pressure relationship demonstrating that for the same increase in craniospinal volume (dV) the ICP response (dP) increases when total craniospinal volume increases. Peq = intracranial equilibrium pressure, Veq = intracranial equilibrium volume. Adapted from Avezaat and Van Eijndhoven(32).

To allow validation of ICP_{plse} as a measure of elastance, Avezaat and Van Eijndhoven compared the relationship of ICP_{plse} versus ICP and elastance, as invasively measured by volume injection, versus ICP. This was performed in a series of 58 patients undergoing ICP monitoring for a variety of neurosurgical indications. A linear relationship between both ICP_{plse} and ICP and invasively measured elastance and ICP was confirmed, supporting the mono-exponential relationship between intracranial volume and ICP. However, the correlation between these relationships was weak.

Of particular note in the above study, was the observation that there was a disproportionate increase in ICP_{plse} during plateau waves, which was thought

secondary to an increase in dV due to defective cerebral vascular muscle tone. To explore this phenomenon further, they monitored ICP_{plse} while manipulating ICP in adult dogs by inflating an epidural balloon. They found the ICP_{plse} increased linearly with ICP up until a pressure of around 60 mmHg (Figure 2.7). At this pressure a breakpoint occurred and the ICP_{plse} increased more rapidly with increasing ICP. It was postulated that the breakpoint marked the loss of CBF autoregulation, which will be dealt with in more detail below.
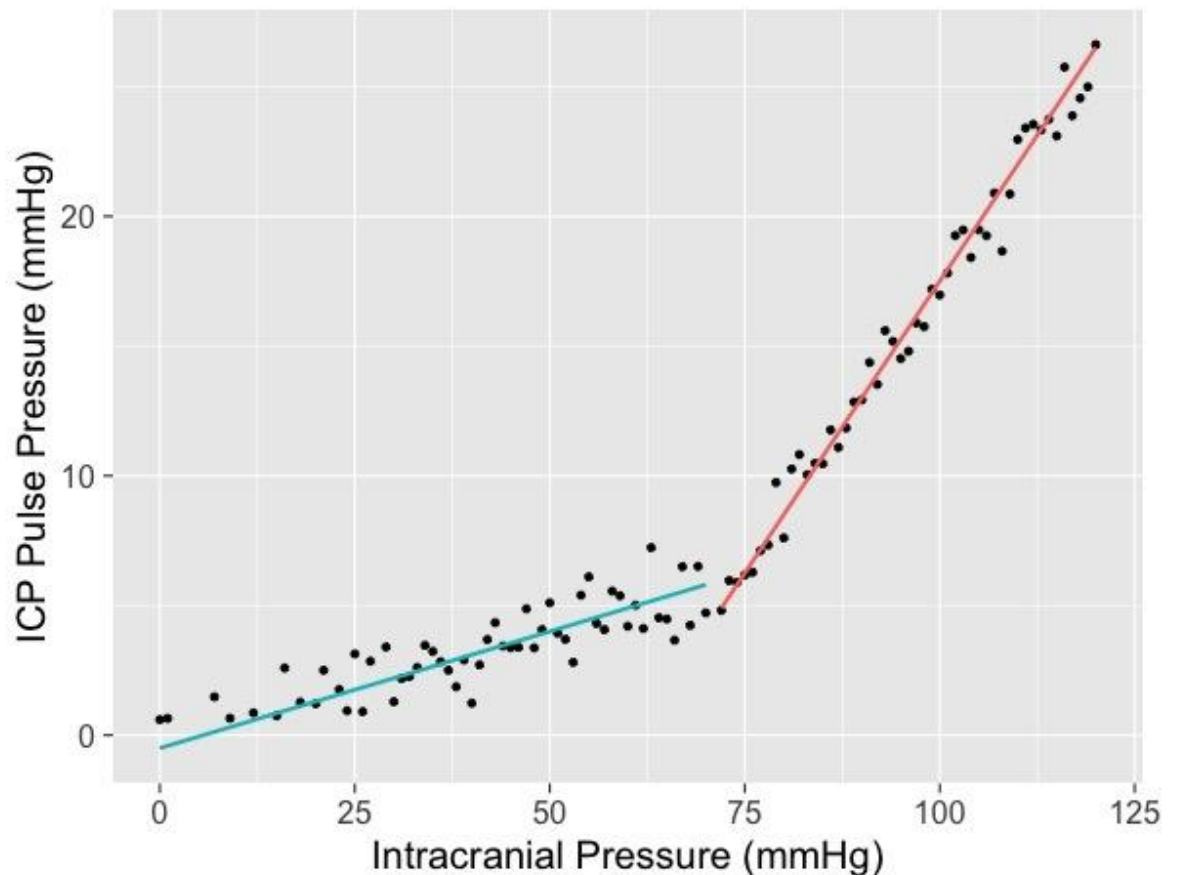
Figure 2.7: ICP_{plse} plotted against ICP, demonstrating a direct linear relationship. A breakpoint occurs at an ICP of approximately 60 mmHg where the slope of the relationship increases. Adapted from Avezaat and van Eijndhoven (32).

The major limitation of using ICP_{plse} as a measure of craniospinal elastance (dP/dV) is the need to assume that the volume of pulsatile blood (dV) is constant. This is unlikely to be the case in severe brain injury because of the associated cardiovascular complications. Therefore, the clinical utility of this technique is limited unless the pulsatile blood volume can be controlled for.

2.3.5 Cerebral Autoregulation

2.3.5.1   Principles of Cerebral Autoregulation

As suggested earlier, one of the principle clinical reasons to monitor ICP is to allow calculation of cerebral perfusion pressure. This is useful because, in theory, maintenance of a CPP within the limits of cerebral autoregulation will result in maintenance of adequate cerebral blood flow to meet the metabolic demands of the brain(37). Regulation of flow is achieved by active dilation and constriction of cerebral arterioles in response to changes of CPP and is illustrated in Figure 2.8. A number of physiological mechanisms are known to be involved in this process and Hamner and Tan have recently quantified the relative contributions of sympathetic, cholinergic and myogenic mechanisms(38). By measuring CBF while manipulating CPP, and utilising pharmacological blockade of the three mechanisms, they were able to demonstrate the effect that each had on cerebral autoregulation in healthy volunteers. Of note, they found that 38% of the pressure-flow relationship was unexplained by these mechanisms, implying that others must also be important.

The physiological range of autoregulation, is regarded as 50 to 150 mmHg in healthy adults(37). When CPP is below the lower limit of the autoregulatory range, vessels within the arterial-arteriolar bed tend to passively vasoconstrict. Conversely, when CPP is above the upper limit, passive vasodilation occurs. Using measures of CBF including intra-arterial xenon clearance(39) and transcranial Doppler flow velocity of the MCA(40), it has been demonstrated that disordered cerebral autoregulation occurs after severe TBI and is associated with worse outcome.
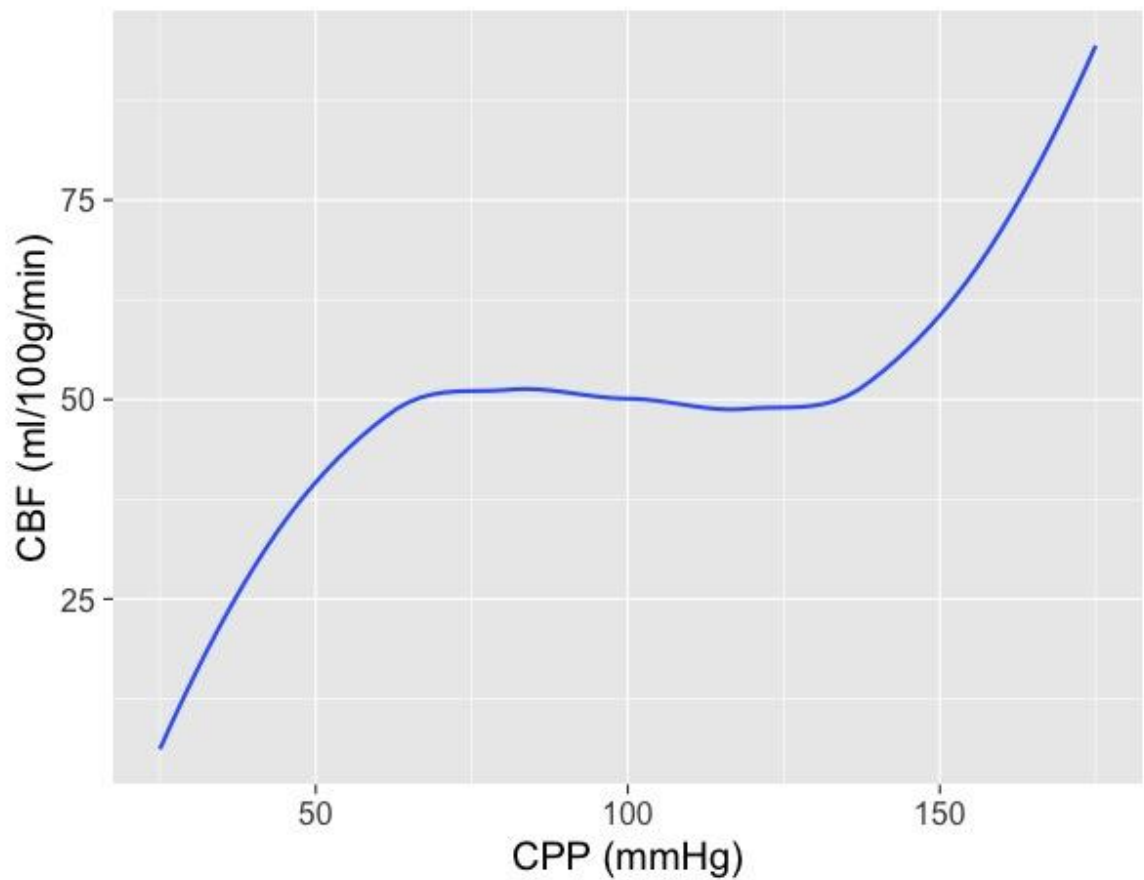
Figure 2.8: Illustration of the maintenance of cerebral blood flow across a range of cerebral perfusion pressures.

2.3.5.2 Mathematical Models of Autoregulation

As discussed above, there is an extensive literature on the mathematical modelling of ICP dynamics. Several of these models incorporate descriptions of cerebral autoregulation. The models can be primarily physiology based, and aim to improve our understanding of the interaction between ICP dynamics and autoregulation, or they can have a more statistical basis and aim to provide an index of the state of autoregulation. Examples of each type of model shall be considered in turn below.

2.3.5.3 Physiological Models of Autoregulation

Ursino and Lodi published a simplified mathematical model of the interaction between ICP and cerebral haemodynamics that is a cut down version of Ursino's earlier work(41-43). The model is a two compartment model which incorcopates the hemodynamics of the arterial-arteriolar cerebrovascular bed, CSF production and reabsorption processes, the pressure-volume relationship of the craniospinal compartment, and a Starling resistor mechanism for the cerebral veins (Figure

2.9). Importantly, it includes a parameter to account for the maximum autoregulatory gain. Using this model in a series of 20 patients with severe TBI, Ursino *et al* were able to classify the state of cerebral autoregulation and predict the response of ICP to PVI testing(42).
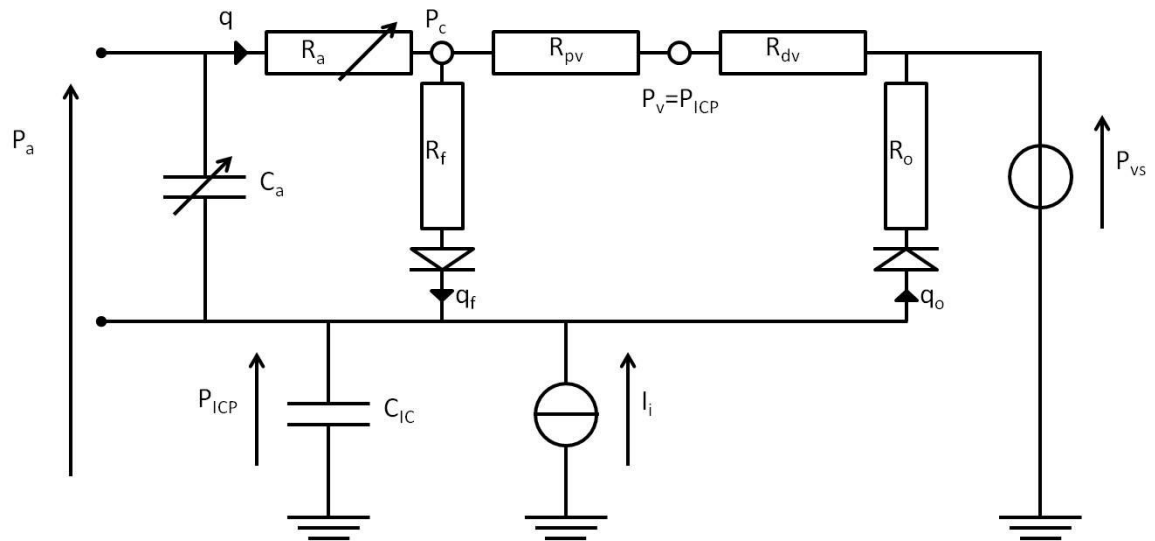
Figure 2.9: Reproduction of the Electrical Equivalence Circuit of the Ursino Model(43). Capacitors are used to represent physiological compartments, resistors restriction to flow of blood or CSF and diodes unidirectional flow. CBF (q) enters the intracranial space at systemic arterial pressure (P_a). It is subject to arterial resistance (R_a) and the cerebrovascular bed has some storage capacity (C_a). CBF is then through proximal (R_{pv}) and distal (R_{dv}) venous resistance. Venous pressure (P_v) is assumed to equal ICP (P_{ICP}). P_{ICP} is dependent upon the volume stored in intracranial compliance (C_{IC}). This is dependent upon blood volume in C_a, CSF inflow (q_f) through inflow resistance (R_f) and CSF outflow (q_o) through outflow resistance (R_o), which is itself dependent upon venous sinus pressure (P_{vs}). The system can be disturbed by mock CSF injection (I_i).

Czosnyka has also proposed compartment model of CBF and CSF circulation(44). It is a three compartment model that consists of two vascular storage compartments (arterial and venous) and one CSF storage compartment (Figure 2.10). Again, this model is able to simulate the state of autoregulation. Using data taken from 82 patients admitted to ICU with moderate and severe TBI, comparison was made between measured clinical responses and simulated model responses to events such carotid artery compression, systemic arterial

hypotension and ICH. The mathematical modelling results were found to be helpful with interpretation of the clinical phenomena. In particular, the model demonstrated that the correlation between arterial blood pressure (ABP) and ICP is dependent on the state of autoregulation. Czosnyka exploited this fact in development of the pressure reactivity index (PRx), which will be discussed in the following section.
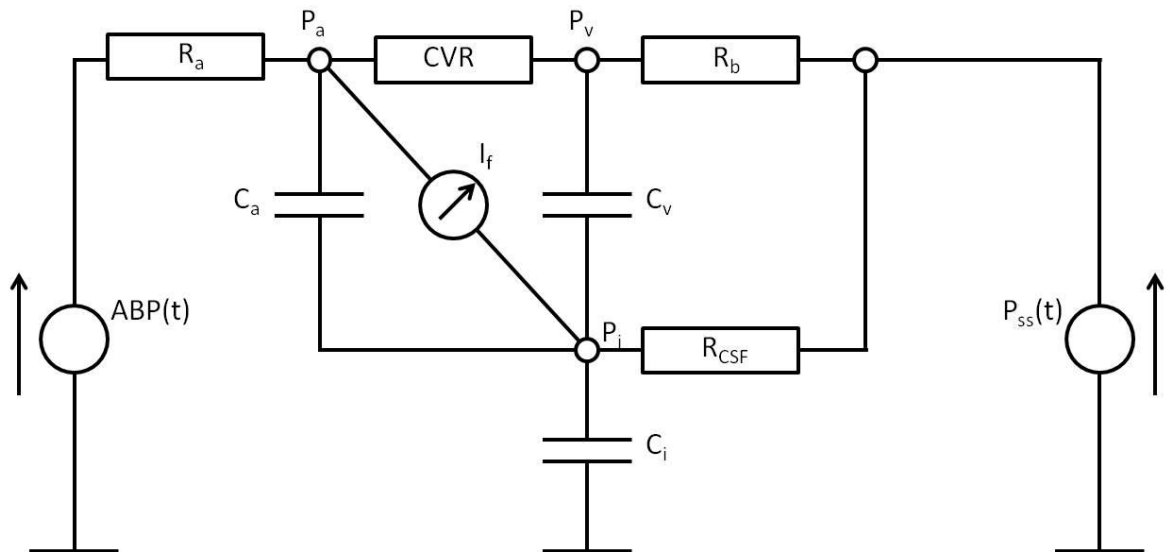
Figure 2.10: Reproduction of the Electrical Equivalent Circuit of the Czosnyka model(44). Capacitors are used to represent physiological compartments and resistors restriction to flow of blood or CSF. The model illustrates the presence of three storage compartments (C_a = compliance of the great cerebral arteries, C_v = compliance of capillaries and small veins, C_i = compliance of the CSF containers). Other parameters are arterial blood pressure (ABP), cerebral arterial pressure in the small arteries (P_a), pressure in the cortical veins (P_v), ICP (P_i), sagital sinus pressure (P_{ss}), resistance of great cerebral arteries (R_a), cerebrovascular resistance (CVR), resistance of cortical and bridging veins (R_b), CSF outflow resistance (R_{CSF}) and CSF secretion (I_f).

An example of a model bridging the gap between physiological and more statistical or data driven models of autoregulation is provided by Daley *et al*(45). The high frequencies of cerebrovascular pressure transmission of ABP to ICP are reduced by vasoconstriction and increased by vasodilation. The highest modal frequency (HMF) at which energy is transferred from ABP to ICP can be calculated from digitised ABP and ICP waveforms. Pairs of ABP and ICP values are processed using an autoregressive moving average (ARMAX) technique to numerically define a difference equation representing the change of ICP relative to ABP at 4 millisecond sampling epochs. The difference equation can be converted to a continuous description of cerebrovascular pressure transmission. The constants of this continuous model can then be used to determine HMF.

In a piglet model of raised ICP it was found that when cerebral autoregulation was intact (as assessed by measurement of pial artery diameter), a rise in CPP led to a decrease in HMF. In contrast, when there was autoregulatory impairment, a rise in CPP was met with an increase in HMF (Figure 2.11). Similar results have been seen in patients admitted to ICU with severe TBI(46).
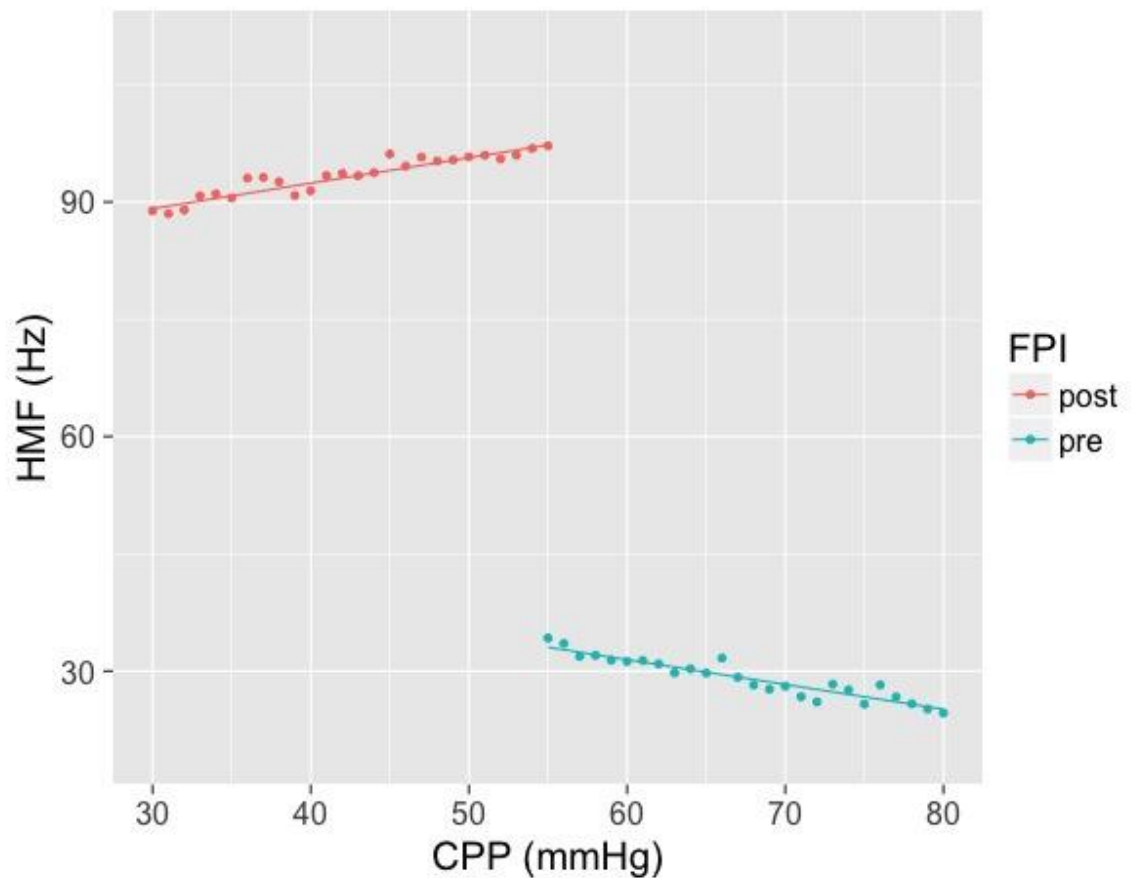
Figure 2.11: Examples of the relationships between HMF and CPP during challenge with norepinephrine before and after fluid percussion injury (FPI). A) Before FPI (in blue): challenge with norepinephrine resulted in a response consistent with active vasoconstriction with a negative correlation value (R = −0.77) and negative slope (m) of the regression line (m = −0.317 Hz/mm Hg) between HMF and CPP were demonstrated. B) After FPI (in red): challenge with norepinephrine resulted in a response consistent with passive vasodilation with a positive correlation value (R = 0.34) and positive slope of regression line (m = 0.325). Adapted from Daley *et al*(45).

2.3.5.4 Data Driven Indices of Cerebral Autoregulation

The most systematically investigated of the statistical approaches to autoregulatory assessment, using ICP as an input parameter, is the Pressure Reactivity Index (PRx) described by Czosnyka *et al*(47). It is based on the hypothesis that naturally occurring slow oscillations of arterial blood pressure can be used to evaluate the cerebrovascular reactivity. In theory, when pressure reactivity is intact, an increase in ABP would result in cerebral vasoconstriction and a reduction in ICP (negative PRx). Conversely, when pressure reactivity is absent, an increase in ABP would result in a passive rise in ICP (positive PRx).

Pressure reactivity has a complex relationship with cerebral autoregulation rather than the expressions being analogous.

The PRx is a moving correlation coefficient between 40 consecutive samples of values for ABP and ICP averaged over a period of five seconds. By employing this averaging interval, most of the frequency changes above 0.2 Hz in the ABP and ICP recordings are filtered out. In addition, Nyquist's sampling theorem dictates that the highest frequency that can be represented by a signal sampled every five seconds is 0.1 Hz or 6 oscillations per minute. As a result, the dynamical system relationship between ABP and ICP cannot be precisely defined by PRx.

Nevertheless, PRx has been found to be a very useful tool in clinical research. In TBI it has been demonstrated to provide a reliable index of cerebral autoregulation as validated by TCD(47) and PET(48) derived measurements. Clinical observations show that the PRx is high both during the occurrence of plateau waves and also during refractory raised ICP(49). In addition, the PRx has been used to guide proposed therapies and calculation of an "optimal CPP" for the management of patients with TBI(50).

2.3.5.5   Comparison of Models of Cerebral Autoregulation

Despite illustrating a number of the approaches that can be taken, this is by no means an exhaustive list of models of CBF autoregulation. It is not clear which approach is most clinically practical or useful. The models take different input parameters and yield different output indices, thus making comparison difficult. In an attempt to address this issue, Shaw *et al* re-worked and normalized three of the models so that a fair evaluation could be made on a standardized dataset of ABP, ICP and MCA flow velocity readings taken from piglets pre and post fluid percussion injury(51, 52). The state of autoregulation predicted by the models could then be compared to changes in pial artery diameter as a direct measure of autoregulation. One of the interesting conclusions from this work was that before application of a number of optimization approaches, none of the models performed particularly well. Overall, Ursino's physiological model performed best and after optimization of the data driven models, Daley's HMF autoregulatory index performed marginally better than Czosnyka's PrX. This work is limited by the use of only one small dataset for comparison. What is

certain, however, is that further studies comparing autoregulatory methods and optimization approaches are warranted before widespread clinical adoption of a standarised autoregulation model is possible.

In recognition of this challenge, an international group of those working in both experimental and clinical autoregulation research have setup a new consortium called the "Cerebral AutoRegulation Network" or CAR-Net(53).

2.4 Current Controversies

2.4.1 Should ICP be Monitored in Severe TBI?

Monitoring of ICP has become a standard of care in severe TBI and its use is supported by internationally applied guidelines. The Brain Trauma Foundation makes a level IIb recomendation that patients with severe TBI should be managed using information from ICP monitoring to reduce in-hospital and 2-week post-injury mortality(54). Further, Treating ICP >22 mm Hg is recommended because values above this level are associated with increased mortality.

The evidence for and against ICP monitoring in TBI has been appraised in several excellent reviews(55-57). Supporting the use of ICP monitoring are retrospective comparisons of historical cohorts at the same centre suggesting that protocols incorporating ICP monitoring improve outcome(58, 59). Similarly, there has been an association between centres monitoring ICP more frequently and better outcome(60). In contrast, a retrospective comparison of 2 trauma centres revealed an increase in therapy levels without an improvement in outcome in the centre that monitored ICP(61).

On the basis of the wealth of conflicting evidence, there was demand for a randomised controlled trial (RCT) to assess the impact of ICP monitoring on clinical outcomes. An RCT of 324 patients with severe TBI was subsequently performed in Latin America(13). Patients were assigned to protocolised therapy directed by either ICP monitoring or clinical examination and imaging. There was no difference between groups in the primary outcome of a composite of survival

time, impaired consciousness, and functional status at 3 months and 6 months and neuro-psychological status at 6 months.

This study has been subject to extensive discussion and editorial review(62-65) including by the lead investigator(66). Irrespective of the applicability of the findings to the routine practice of ICP monitoring in severe TBI, the results certainly strengthen the argument for more clearly defining the use of ICP targeting strategies as part of an individualised and multimodal approach to this patient group.

2.4.2 What Modality Should be Used to Monitor ICP?

2.4.2.1 Introduction

The two techniques most commonly used in clinical practice to monitor ICP are via an intraventricular or intraparenchymal catheter with a microtransducer system. Both of these techniques are invasive and are thus associated with complications such as haemorrhage and infection. For this reason, significant research effort has been directed towards development of a non-invasive method to measure ICP.

2.4.2.2 Intraventricular Catheter

Following Lundberg's description of the use of intraventricular catheters for the continuous measurement of CSF pressure(16), the technique has remained the gold standard for ICP monitoring(67). It is performed by inserting a catheter into either lateral ventricle through a frontal burr hole. In 1960, Lundberg was already using electronic measurement equipment by connecting the ventricular cannula via a strain gauge transducer to a potentiometer recorder. In modern practice, the ventricular catheter can similarly be connected to an external strain gauge or the ICP waveform can be transduced via fibreoptic or micro strain gauges within the catheter itself.

An advantage of measuring ICP using an intraventricular catheter is the opportunity to perform drainage of CSF as an ICP lowering therapy. It is also possible to recalibrate the monitor while in situ and thus retain accuracy for several days of monitoring. However, as suggested above, the technique is not without risk. It can be technically difficult in the case of ventricular effacement

or midline shift. There is a risk of CSF infection but this can be kept to as low as 10% with a "Bundle" based approach to care(68). The incidence of haemorrhage following ventriculostomy is around 1%, although the number requiring surgical evacuation is likely to be lower(67).

2.4.2.3   Intraparenchymal Catheter

In cases where intraventricular ICP monitoring is not possible, or in many centres as the preferred technique, an intraparenchymal device can be placed. The principle difference with the intraparenchymal devices is the inability to recalibrate them following insertion with the consequent problem of zero drift. Bench testing of devices using both fibreoptic tips (Camino OLM ICP monitor; Camino Laboratories, San Diego, CA) and micro strain gauges (Codman Microsensor ICP Transducer; Codman & Shurtlef Inc., Randolph, MA) have shown 24 hour zero drift of <0.8 mmHg(69). Similarly, laboratory testing of an intraparenchymal device incorporating a micro strain gauge with complete Wheatstone bridge circuit incorporated into the tip (Raumedic AG, Helmbrechts, Germany), demonstrated a mean zero drift of 0.6 mmHg at 5 days(70). However, in the more demanding clinical environment, a multicentre evaluation concluded that the zero drift rate remained a concern and catheter performance was similar that of other manufacturers(71).

Intraparenchymal ICP monitoring devices are typically placed via a small burr hole into the white mater of the non-dominant frontal hemisphere. These devices measure a compartmentalised local pressure and significant supratentorial pressure gradients have been demonstrated between monitoring ipsi and and contralateral to the side of focal haematomas(72).

2.4.3 Non-invasive ICP Monitoring

For a non-invasive measure of ICP to replace the commonly used invasive measures above it must provide an accurate absolute measure of ICP that can be performed continuously at the bedside. There is no current technique that satisfies these criteria. An in depth review of all of the available technologies is outwith the scope of this article and has been covered in detail elsewhere(73-75). Techniques considered include imaging based studies using CT and magnetic resonance imaging (MRI), transcranial Doppler sonography (TCD), near-infrared

spectroscopy (NIRS), tympanic membrane displacement (TMD), visual-evoked potentials (VEPs), measurements of optic nerve sheath diameter (ONSD) and other measurements of the optic nerve, retina and pupil. Of these, approaches using TCD and ONSD have perhaps received the most clinical interest.

Using low frequency TCD, it is possible to measure flow velocity in the middle cerebral artery (MCA)(76). Several authors have published equations using the MCA flow velocity metrics of peak systolic velocity (PSV), mean flow velocity (mFV), end diastolic velocity (EDV) and pulsatility index (PI, PSV-EDV/mFV) to estimate ICP and CPP.

Schmidtt *et al* examined 25 patients admitted with severe TBI and calculated non-invasive CPP (nCPP) as MAP x EDV/mFV +14 mmHg(77). For these patients, 81% of 1 minute averages of nCPP (n = 12 275) were different from invasively measured CPP (iCPP) by <10 mm Hg. In 81 brain injured patients, including 21 with TBI, Bellner *et al* calculated non-invasive ICP (nICP) as 10.93 x PI – 1.28(78). Bland and Altman analysis of all measurements (n = 658) revealed that the difference between nICP and invasively measured ICP was less than 4.2 mmHg for 95% of measurements. Edouard *et al* calculated nCPP as [mFV/(mFV-EDV)] x (MAP-DAP) in patients with severe TBI and bilateral injury(79). In 10 patients, repeated measurements were made during their clinical course (n = 89) and a significant correlation was found between nCPP and iCPP. However, in a further 10 patients in whom hypercapnoea was induced, the strength of this correlation was reduced.

The performance of the above three equations in estimating ICP was compared in 45 patients with severe TBI by Brandi *et al*(80). Under standardised conditions, including continuous sedation, normocapnoea and normothermia, daily nICP measurements were compared to ICP measured using an intraparenchymal device. On the basis of Bland and Altman analysis, the authors concluded that the equation by Bellner *et al*(78) was superior in assessing nICP. However, as has been noted elsewhere(55), the Bellner equation failed to predict all cases of ICH in this series and is therefore not likely to be clinically useful as a screening test in TBI.

Like TCD measurements, assessment of ONSD using ultrasound potentially provides a simple bedside screening test for ICH in TBI. The technique exploits the fact that the optic nerve is part of the central nervous system and therefore, a rise in ICP will be transmitted through the CSF surrounding the nerve. Several studies comparing ultrasound derived ONSD assessment to iICP(81-86) have been included in a recent meta-analysis(87). This was limited by the fact that it included only 231 patients, 89 of whom had suffered TBI. However, using the ONSD thresholds reported in the individual studies, the pooled sensitivity and specificity to detect ICH were 0.9 and 0.85 respectively. Dubourg *et al* are now collecting data for an individual patient data meta-analysis with the objective of defining the cutoff value for ultrasound derived ONSD in the detection of ICH(88).

2.4.4 Should ICP or CPP be the Target?

Whatever modality is chosen to monitor ICP in severe TBI, the clinician must then decide whether to primarily target therapy at attempting to optimise CPP or lower ICP. CPP oriented therapy, as proposed by Rosner *et al*(89), requires pressure autoregulation and the ability to manipulate CPP within the autoregulatory range. During intact pressure regulation, increases of CPP cause constriction of the arterial-arteriolar vascular bed and lowering of ICP by a reduction in cerebral blood volume. In addition, the resulting reduction of pre- and post-capillary pressure decreases fluid filtration and increases absorption, thus reducing brain oedema. However, the application of CPP oriented therapy when autoregulation has been lost may result in an imbalance of Starling forces at the capillaries leading to increased net fluid filtration and further brain injury by increased production of vasogenic oedema.

Avoiding vasogenic oedema is one of the underlying tennets of the "Lund" approach to management of severe TBI based on lowering ICP(90, 91). Asgeirsson *et al*, working at the University Hospital of Lund, described a protocol aimed at inducing transcapillary fluid absorption through reduction of hydrostatic capillary pressure and preservation of normal colloid osmotic pressure. This included pharmacological interventions such as the reduction of systemic hypertension with metoprolol and clonidine, and precapillary vasoconstriction with dihydroergotamine.

In an attempt to determine whether an ICP or CPP based approach was preferable, Roberston *et al* conducted an RCT in 189 patients admitted with severe TBI(92). Patients were randomised to an ICP based protocol or a CBF based protocol. The major differences between the protocols were the CPP targets (>50 mmHg in the ICP group and >70 in the CBF group) and the option to treat ICH with hyperventilation in the ICP group. In terms of the primary outcome of this study, cerebral ischaemia as measured by jugular venous desaturations, the CBF based protocol was associated with a lower risk of ischaemia. However, this did not translate into improved neurological outcome and indeed was associated with an increased frequency of systemic complications such as adult respiratory distress syndrome (ARDS).

It is likely that the choice of ICP or CPP based approach to ICU management of severe TBI should be made on an individual patient basis. For this to be possible, the state of autoregulation needs to be assessed.

Support for the clinical utility of a pressure reactivity index has been provided by Howells *et al*(93). The approach of two neurosurgical ICUs to ICP management in TBI was compared using a PRx based index, averaged over many hours per day, and a machine learning Bayesian Neural Network (BANN) model, which predicted the probability of good or bad clinical outcome. In one centre, the predominant management approach was CPP targeted therapy and in the other, the approach was ICP targeted therapy. The model showed that not only was pressure reactivity related to clinical outcome but also that it's relationship to outcome was management approach dependant (Figure 2.12). From these data, a principally CPP targeted approach was more successful when pressure reactivity was intact, while a principally ICP targeted approach was more successful when pressure reactivity was impaired. Of course, there could be other factors influencing clinical outcome that were not considered in the analysis. Nevertheless it is compelling evidence for what appears to be common sense: a management strategy that considers the brains ability to regulate its

blood flow is more successful than one that does not.
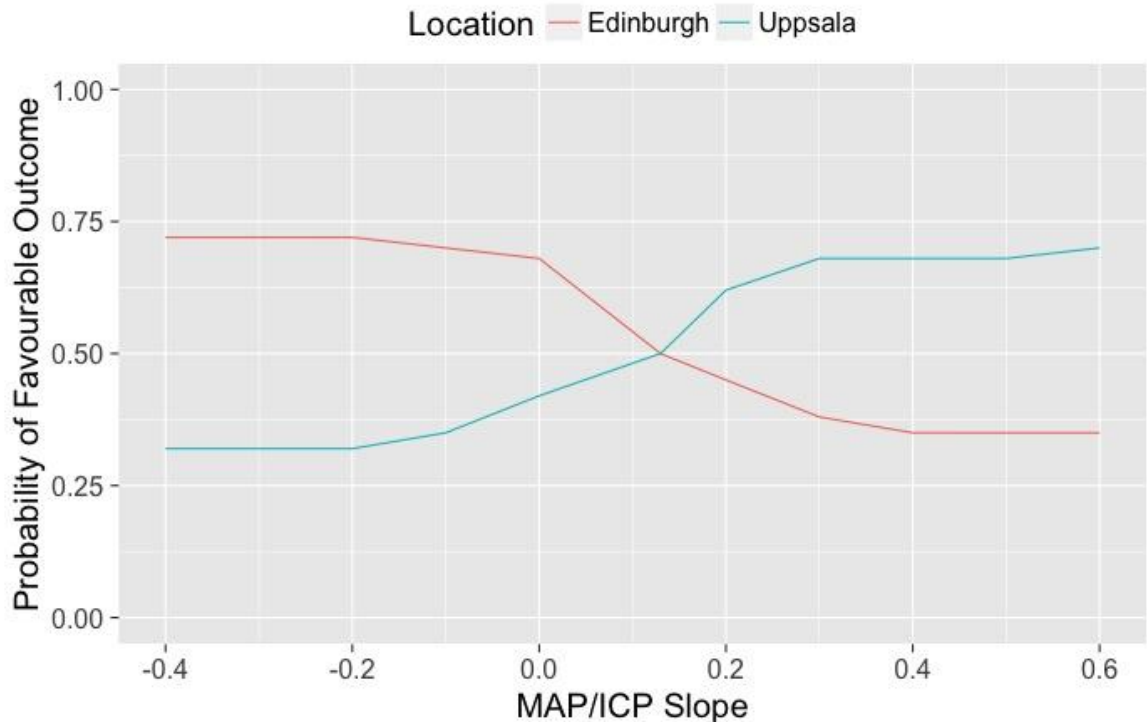
Figure 2.12: Representation of BANN generated probability distribution plots for the mean likelihood of a favourable clinical outcome for patient populations managed in two different centres. In these data, the optimal point at which to switch from one treatment strategy to the other in a given patient is at an MABP/ICP trend with a slope of approximately 0.13. Adapted from Howells *et al*(93).

2.5   Future Directions

2.5.1 Introduction

The field of ICP research is a wide ranging one and, to date, has been the subject of 16 international symposia embracing such diverse disciplines as neurosurgery, intensive care, anaesthesia, radiology, biophysics, electronic and mechanical engineering, mathematics and computer science(94). This multidisciplinary and collaborative approach is highlighted by research groups such as International Mission for Prognosis and Analysis of Clinical Trials in TBI (IMPACT)(95), Brain Monitoring with Information Technology (BrainIT)(96) and the recently funded CENTER-TBI project(97).

At present, there is no level 1 evidence to support the targeting of a specific ICP or CPP using clinical interventions. Indeed the recently reported RESCUEicp study, which evaluated the role of decompressive craniectomy in treatment of

uncontrollable ICH, concluded that the rates of good recovery were not improved by the intervention(98). Similarly Eurotherm3235, which appraised the role of targeted temperature therapy (32 to 35°C) for the management of ICH, suggested that outcomes were worse with hypothermia than with standard care alone(99).

In the face of these negative results, there is considerable effort to extract more information, rather than simply a generic threshold value, from the ICP signal and use this to provide patient specific targets and to forecast secondary ICP insults. In addition, there is ongoing effort to develop novel non-invasive techniques to measure ICP and thus widen its clinical application. Some key areas of current research shall be discussed below.

2.5.2 Individualised ICP and CPP Targets

As an alternative to using a universal CPP threshold for all TBI patients, a more dynamic patient tailored CPP target, based upon the autoregulation capacity of the cerebral vasculature, has been proposed. In retrospective analysis, Steiner *et al*(50) demonstrated that by plotting PRx against CPP for the entire monitoring period, a "U-shaped" curve could be produced in about 60% of patients. The CPP corresponding to the minimum PRx was taken to represent the optimal CPP (CPPopt) for each patient. Patients who were managed with CPPs closer to CPPopt were more likely to have a good outcome.

The feasibility of using PRx to prospectively calculate CPPopt in TBI patients in a clinical environment has subsequently been demonstrated by Aries *et al*(100). Using a four hour moving window, updated every minute, CPPopt could be calculated for 55% of the monitoring period. Again, patients were more likely to have a good outcome if their actual CPP deviated less from CPPopt.

In similar work, Lazaridis *et al*(101) have used PRx to identify patient specific ICP thresholds in TBI. By plotting PRx against ICP for the entire monitoring period, the threshold ICP was taken to be that at which the PRx was consistently >0.2. It was possible to calculate a threshold ICP in 68% of patients. Time spent above an individually calculated ICP threshold was more strongly predictive of

mortality than using a generic threshold of 20 or 25 mmHg. This further supports the concept of patient specific targets of ICP or CPP in the management of TBI.

However, calculation of PRx and most other measures of autoregulation require high frequency data (> 50 Hz) sampling. Capturing and processing this data frequency is not routine in many NICUs. Consequently, Depretiere *et al* have developed a new index of cerebrovascular reactivity that requires only minute by minute data sampling(102). Known as LAx, the index is the moving median of minute-by-minute ICP/MAP correlation coefficients over different time intervals (3-120 min). They demonstated that not only does it correlate with PRx and GOS but also is able to produce a CPPopt recommendation. DATACAR (Dynamic Adaptive Target of Cerebral Autoregulation) combines different LAx values and time windows in a weighted manner to issue a CPPopt recommendation. They observed significant differences between PRx-based and LAx-based CPPopts. DATACAR was able to issue a CPPopt recommendation in 92% of monitoring time, as opposed to 44% for PRx-based CPPopt.

Certainly, a method for continuous and robust determination of a patient's optimal CPP, that can work with normal NICU data capture rates, is an attractive concept. A prospective study comparing a number of these indices is warranted. These developments show clearly the benefits possible through the combination of sharing and analysis of large ICU datasets with the development and application of mathematical models.

2.5.3 Prediction of Secondary ICP Insults

An interesting approach to forecasting ICH is based on preceding changes to waveform morphology. In recognition that most clinical decision making only takes into account the mean ICP, Hu and colleagues have proposed a technique for automatically extracting useful information from the ICP waveform(103). Morphological clustering and analysis of continuous intracranial pressure (MOCAIP) detects the P_1, P_2 and P_3 peaks within the ICP waveform. The technique was developed and validated using an annotated database of ICP waveforms collected from 66 patients admitted to an adult hydrocephalus centre. For every 3 minute section of ICP recording, the MOCAIP algorithm performs beat-by-beat pulse detection followed by pulse clustering to generate

a dominant ICP pulse. Artifactual pulses are removed prior to the detection and optimal designation of pulse peaks. This process has been generalized as MOCAIP++ and validated on a larger dataset collected from 128 patients(104).

The application of MOCAIP to ICP monitoring in TBI has been demonstrated(105). In a dataset from 66 patients, including 23 admitted with TBI, ICP pulse morphological metrics were correlated with low CBF as measured by an intravenous ^{133}Xenon clearance technique. Of particular interest, was the association of an elevated P_3 peak and low CBF. However, in this study, the correlation of pulse morphological metrics to low CBF was less in the TBI patients than in those admitted with other diagnoses such as subarachnoid haemorrhage.

In the first efforts to use MOCAIP analysis to forecast episodes of elevated ICP, an ICP waveform dataset recorded from 34 patients presenting with suspected idiopathic intracranial hypertension, CSF shunts and Chiari malformation was evaluated(106). Using 24 metrics of the ICP waveform it was possible to classify recording segments as either control or pre-IH prior to episodes of elevation of ICP to >20 mmHg over a period of at least 20 minutes. This was done with a sensitivity of 37% and 21% and specificity of 99% and 99% for 5 and 20 minutes respectively. These results are encouraging but may not generalise to TBI because of the difference in underlying pathophysiological mechanisms.

An alternative approach to prediction of ICH, which has been developed using data collected from patients admitted to NICU with TBI, is through the use of Gaussian processes(107). Using 4 hour windows of minute-by-minute recordings of ICP and MAP, Guiza *et al* generated over 1000 potential dynamic predictors from which a subset of 73 was selected. These included median values for non-overlapping time intervals, measures of variability, clustering of values based on their trajectory, frequency domain analysis and correlation of ICP with MAP. Gaussian processes are a machine learning algorithm that generate a probabilistic prediction based on the known outcomes of similar data instances. The model was developed in a cohort of 178 patients to predict 30 minutes in advance of an elevation of ICP to >30 mmHg over a period of at least 10

minutes. It was then evaluated in a further cohort of 61 patients achieving a sensitivity of 82% and specificity of 75%.

Future predictive models may incorporate both ICP waveform features and dynamic predictors to optimise their predictive capacity. The value of these predictions would then need to be assessed by providing them to clinicians and formally assessing the impact on patient management and outcome.

2.5.4 Innovative Non-Invasive ICP Monitoring

As suggested above, no methodology in current clinical use provides an accurate absolute measure of ICP. A novel technique, which provides an absolute value of ICP, has recently been described by Ragauskas *et al*(108). A two-depth TCD device is used to identify the intracranial and extracranial components of the ophthalmic artery (IOA and EOA). Following the assumption that the Doppler waveform of the IOA is dependent on compression by ICP and that of the EOA by externally applied pressure (P_e), a ring cuff is applied to the orbit and automatically inflated from 0 to 28 mmHg in 4 mmHg steps. The P_e at which the waveforms of the IOA and EOA are identical is taken to represent the ICP. A comparison study of this technique to CSF pressure measured by lumbar puncture was performed in 62 patients presenting to a neurology clinic, including 37 with suspected IIH and 20 with multiple sclerosis. For invasively measured CSF pressures in the range of 4 to 24, the non-invasive technique achieved a 98% confidence interval for the absolute error of ± 4 mmHg.

In a study of a similar group of patients, the two-depth TCD technique was compared to the ONSD technique in its ability to predict raised CSF pressure as measured by LP(109). Using a CSF pressure threshold of 14.7 mmHg, and an ONSD cut-off of 5 mm, the two-depth TCD technique outperformed the ONSD technique with sensitivities of 0.68 and 0.37 and specificities of 0.84 and 0.59 respectively.

Further work is required to confirm the safety of the innovative two-depth TCD technique in terms of pressure effects on the globe and exposure of the lens to Doppler US. The applicability of the technique to the TBI population and across a wider range of ICP values has yet to be demonstrated.

2.6   Summary of the Current State of Intracranial Pressure Monitoring in Traumatic Brain Injury

Despite the fact that ICP monitoring in TBI has become a standard of care, there is no level I evidence to support its use in targeting generic ICP thresholds. However, there can be little doubt that investigation of ICP and the intracranial pressure-volume relationship has led to an improved understanding of cerebral physiology. It is now time to exploit this knowledge and integrate ICP monitoring into a multimodality and individualised approach to care. Future RCTs of ICP monitoring should utilise autoregulatory assessment to provide patient specific thresholds for ICP and CPP. The use of non-invasive monitors of ICP is an attractive prospect but not yet supported by the technology.

2.7   Transcranial Bioimpedance Measurement

2.7.1 Introduction

A study investigating the relationship between transcranial bioimpedance and invasive intracranial pressure measurement in patients with traumatic brain injury (BioTBI) is presented in the following three chapters of this thesis. It is therefore necessary to consider the principles of transcranial bioimpedance (TCB) measurement and the rationale for its consideration as a surrogate measure of ICP.

As has already been discussed in detail, elevated ICP is associated with poor outcome following traumatic brain injury(9) and The Brain Trauma Foundation recommends that ICP should be monitored in patients with a severe traumatic brain injury(54). ICP is typically measured using invasive pressure monitors that are associated with specific complications and can generally only be inserted in specialist centres. To provide ICP monitoring to a wider clinical population, multiple attempts have been made to develop a non-invasive technique. Transcranial bioimpedance measurement was considered to be a potential approach to non-invasive ICP monitoring.

2.7.2 Fundamentals of Bioelectrical Impedance Analysis

Bioimpedance is the ability of biological tissue to impede electric current. Techniques are available to measure bioimpedance from whole or part of the body in a process known as bioelectrical impedance analysis (BIA). The principles and methods of BIA have been extensively reviewed by Kyle *et al*(110) and shall be summarised below.

Bioimpedance is the sum of capacitive resistance (or reactance) and resistive resistance (simply called resistance). The capacitive effect arises principally from charge distributed across cell membranes (acting like the plates of a capacitor) and the resistance from the conductance of current through the ionic solutions in extra and intracellular fluid paths. Electric current of low frequency will tend to be conducted through the extracellular space when the cell membrane is acting as an insulator, whereas electric current of high frequency will be conducted through both the extra and intracellular spaces. An electrical circuit model of the two current paths is shown in Figure 2.13.
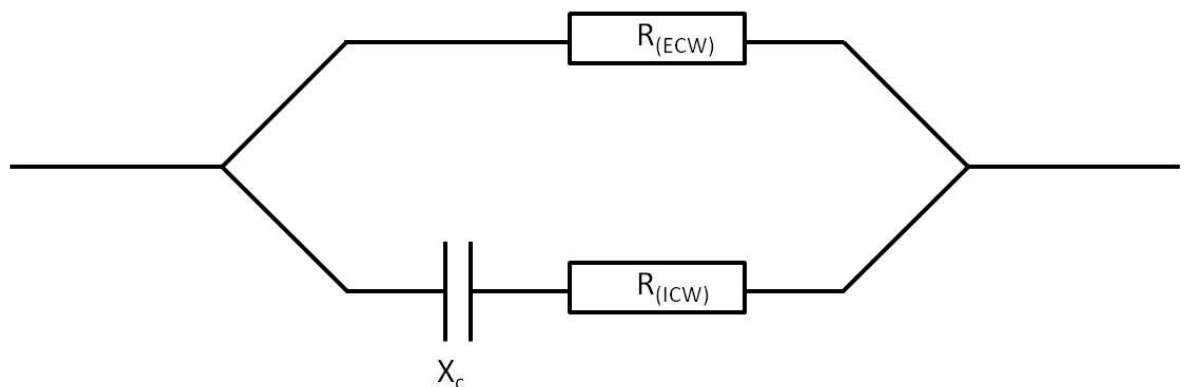
Figure 2.13: A parallel electrical circuit model demonstrating extra and intracellular current paths where R$_{(ECW)}$ is resistance through extracellular water, X$_c$ is impedance from the cell membrane and R$_{(ICW)}$ is resistance through intracellular water.

The equation relating the different factors is:

$$Z = R + iX_c \tag{2.6}$$

where *Z* is overall impedance, *R* is resistance and *iX$_c$* is reactance. The magnitude of bioimpedance can be calculated by:

$$|Z| = \left(R^2 + iX_c{}^2\right)^{\frac{1}{2}} \qquad \text{(2.7)}$$

In whole body measurements, two cutaneous electrodes are placed on the patient's foot and another two on the ipsilateral hand. Resistance is proportional to length and inversely proportional to cross-sectional area of the conducting body (Figure 2.14). This means that whole body impedance measurements are corrected according to height (a surrogate of path length) for use in body composition analysis.
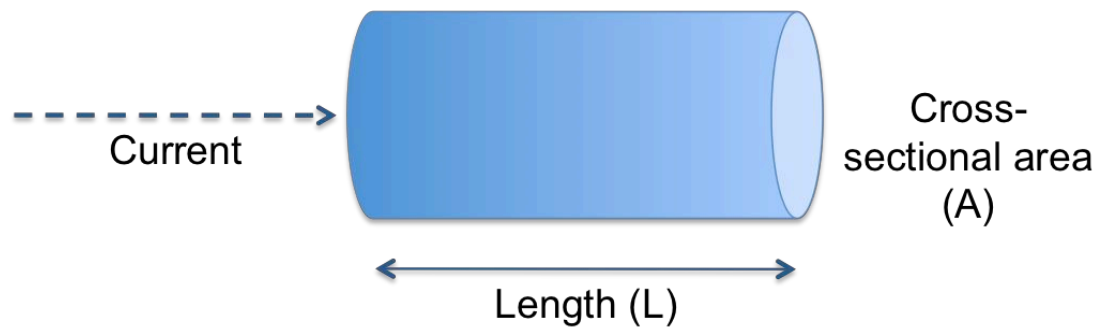
Figure 2.14: Illustration of the cylinder model relating resistance to geometry.

2.7.3 Bioelectrical Spectroscopy

Bioimpedance measurement obtained using devices capable of delivering a broad band of frequencies (typically around 1 to 1000 kHz) is known as bioelectrical spectroscopy. Under these circumstances it is possible to plot the reactance and resistance measurements made at each frequency to construct a Cole-Cole plot (Figure 2.15), (111). Using the impedance values extracted from the Cole-Cole plot, body composition analysis can subsequently be performed. Equations exist to relate resistance, reactance and impedance at a variety of frequencies to fat free mass, body fat, total body water, extracellular water and intracellular water.
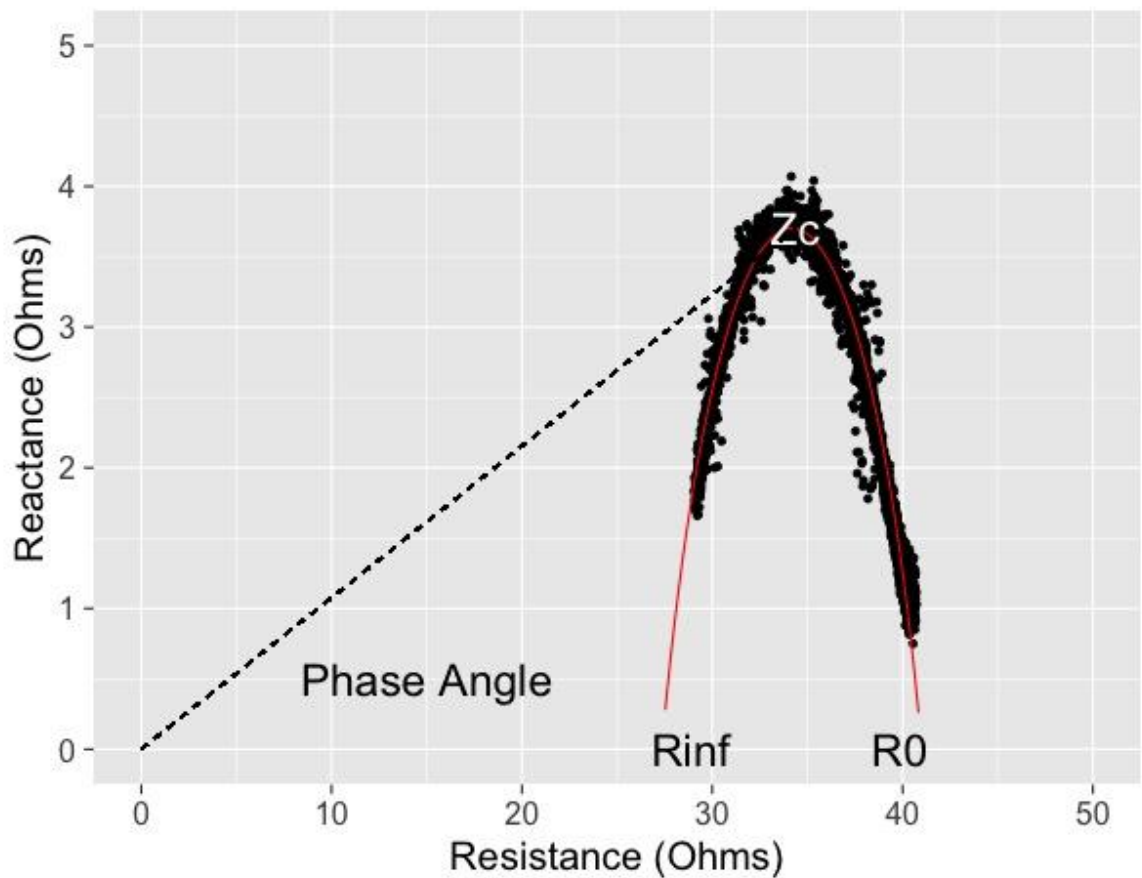
Figure 2.15: A graphical representation of a Cole-Cole plot with reactance plotted against resistance, where R₀ represents resistance measured with a direct current and R$_{inf}$ the resistance measured with an infinitely high frequency alternating current. Z$_c$ is the impedance measured at maximum reactance and θ is the phase angle.

In body composition analysis, the assumptions of homogeneous composition and uniform distribution of current across a fixed cross-sectional area are required. These assumptions are reasonable in healthy subjects, but are unlikely to apply in the context of disease. In this context, the phase angle has been the most extensively studied index of BIA. It is calculated as:

$$\theta = tan^{-1} + \left(\frac{X_c}{R}\right)$$

$$(2.8)$$

where θ is the phase angle (PhA). Calculation of PhA is typically performed at 50 Hz in single frequency BIA and at Z$_c$ in bioelectrical spectroscopy. Higher values of PhA are thought to represent higher cellularity and efficient cell membrane and intracellular functioning(112). Lower phase angles have been correlated

with poor outcome and markers of increased disease severity in a number of pathological processes including renal failure(113, 114), cardiac failure(115, 116) and several malignancies(117, 118).

2.7.4 Bioimpedance Measurements of the Brain

Application of bioimpedance measurements to the human brain is not a new development. Indeed rheoencephalography (REG), or electrical impedance measurement of brain circulation, has been investigated for several decades without transitioning into clinical practice(119). The principle of REG is based on the assumption that blood is a better conductor of electrical current than brain parenchyma. Therefore as arterial blood flows into the cranial cavity, there is a pulsatile reduction in continuously measured bioimpedance.

As well as REG there have been several studies using intermittent measures of TCB in the detection of brain pathology. In a study of 100 healthy controls and 50 patients with a variety of brain pathologies, Grasso *et al* made TCB measurements using a single frequency bioimpedance device(120). The pathologies studied were tumours, intraparenchymal haemorrhage and hydrocephalus. TCB measurements were made using pairs of cutaneous electrodes placed on the closed eyelids and at the base of the occiput. The relationship between resistance (R), brain water content (V) and head circumference (HC) was modelled as:

$$V = \frac{HC^2}{R} \tag{2.9}$$

A significant increase in V was detected between the patients with brain pathology and the healthy controls. This supported their hypothesis that TCB could be used to detect pathological processes associated with brain oedema secondary to both extracellular and intracellular mechanisms.

More recently Liu *et al* have compared TCB measurements made in 200 healthy controls to those made in 78 patients with haemorrhagic stroke and 51 patients with ischaemic stroke(121). Cutaneous electrodes were placed in frontal and occipital positions and a 50 Hz current applied using their "non-invasive

cerebral-edema monitior". TCB was measured and then converted into a "perturbative index". Unfortunately there are no details of how this index is calculated in this paper or related publications using the same device(122-124). The authors reported an increased perturbative index measured from the pathological side in both haemorrhagic and ischaemic stroke.

Of particular relevance to the BioTBI study, Seonne *et al* have reported TCB measurements made using the same Impedimed SFB7 Bio-impedance Spectroscopy Unit (125). In their study of ten patients with ischaemic or haemorrhagic stroke, they compared TCB measurements made from each cerebral hemisphere using silver EEG electrodes. Nine out of the ten patients demonstrated either asymmetry or values outside those measured in control patients. It was not possible to differentiate between ischaemic and haemorrhagic stroke.

Other authors have investigated the use of TCB measurements in TBI. Harting *et al* used a controlled cortical injury rat model of TBI to demonstrate a difference in brain impedance measurement made both post mortem and *in vivo* between sham and injured animals(126). In these experiments the measurements were made using bipolar electrodes in direct contact with the brain. Impedance measurements were found to correlate with brain water content, supporting the theory that bioimpedance could detect cerebral oedema following TBI.

Previous attempts have been made to determine the relationship between TCB and ICP. Using a neonatal piglet model of brain hypoxia, Lingwood *et al* were first able to demonstrate that non-invasive TCB measurements correlated well with invasive measurements(127). They focussed on the bioimpedance parameter of R_0 on the basis that the pathophysiology of brain hypoxia was likely to lead to intracellular oedema with a consequent reduction in the size of the extracellular space. The reduction in the extracellular space would lead to a significant increase in the impedance to a direct current. The presumed cerebral oedema was also associated with an increase in the invasively measured ICP. There was a strong correlation between the change from baseline of the non-invasive measurements of TCB and ICP in the six animals subjected to severe hypoxia (correlation coefficients between 0.72 and 0.97).

In subsequent neonatal piglet experiments, Lingwood *et al* were able to demonstrate that the significant changes from baseline of non-invasive TCB measurements associated with severe hypoxia correlated well with clinical and histological markers of poor neurological outcome(128). They suggested that TCB measurements could therefore be used to help in prognosticating the degree of neurological impairment following severe perinatal asphyxia. Unfortunately it was not possible to confirm the association in a study of 24 human newborns with evidence of severe acute intrapartum hypoxia and encephalopathy(129).

Other attempts have been made to explore the relationship between TCB and ICP using an animal model. Shaw *et al* performed a series of experiments in sheep, again using the Impedimed SFB7 device(130). TCB measurements were made via 21G needles inserted into the scalp on either side of the head. ICP was invasively measured with an intraventricular catheter and manipulated via the injection of a mock CSF injection to cause a stepwise increase in ICP up to 50 mmHg. It was demonstrated that when Z_c was normalised against a baseline value for each animal, there was a clear relationship between the log of ICP and the inverse of Z_c:

$$ICP = exp\left(\frac{a}{Z_{norm}} + b\right) \tag{2.10}$$

where Z_{norm} is the normalised Z_c. In parallel with this animal study, Shaw *et al* performed a study in healthy human volunteers to determine the normal values for TCB recorded using transcutaneous electrodes.

In terms of previous work that has investigated TCB measurements of the brain, it is finally necessary to mention the evolving technique of electrical impedance tomography (EIT)(131). Using an array of surface electrodes, multiple electrical impedance measurements can be made between rotating electrode pairs. Advanced signal processing is then required to construct a cross sectional image of the object being measured. An adaptation of the technique has been applied to a porcine model of traumatic brain injury using a combination of cutaneous electrodes and an EIT electrode incorporated onto an intraparenchymal ICP

monitoring device(132). As a proof of concept study, it was possible to some degree, to detect intracranial injuries in real time.

2.7.5 Postulate

It is clear that multiple studies have demonstrated a potential role for bioimpedance measurements of the brain in clinical practice. Indeed there is some evidence from the animal studies above that TCB measurements are related to invasively measured ICP. As stated above, development of a reliable non-invasive ICP monitoring technique would have wide clinical applicability in TBI. It was therefore postulated that TCB measurements could provide an estimate of ICP in patients admitted following a TBI.

Following TBI intracranial compliance is dependant upon the degree of intracellular swelling and the size of the extra cellular space. Similarly in TCB measurement, brain impedance depends upon intracellular swelling and the size of the extra cellular space. As there is a well-defined exponential relationship between ICP and intracranial compliance, it was proposed that there should also be a definable relationship between ICP and TCB.

3. Materials and Methods for the BioTBI Study

3.1 Overview

This chapter describes in detail the materials and methods for the Relationship Between Transcranial <u>Bio</u>impedance and Invasive Intracranial Pressure Measurement in <u>T</u>raumatic <u>B</u>rain Injury <u>P</u>atients (BioTBI) Study. The study protocol and related documents are available on request.

3.2 Objective

The primary objective of this study was to define the relationship between non-invasive bioelectrical impedance measurements of the brain and skull and intracranial pressure (ICP) in traumatic brain injury (TBI) patients. This would act as a pilot project to assess the feasibility of transcranial bioimpedance (TCB) as a non-invasive estimate of ICP.

3.3 Ethical Approval

Ethical approval was granted for the study by Scotland A Research Ethics Committee following the meeting on 23rd June 2011 and chaired by Dr Ian Zealley (Reference Number: 11/AL/0320). The study was sponsored by NHS Greater Glasgow and Clyde and supported by funding from The Association of Anaesthetists of Great Britain and Ireland/ Anaesthesia via the National Institute of Academic Anaesthesia (WKR0-2011-0039).

3.4 Summary of Study Design

This was a single centre pilot study comparing TCB measurements to invasively monitored ICP in patients with TBI. The aim was to enrol 15 patients with a view to performing 300 individual TCB measurements.

3.5 Patient Recruitment

Study participants were prospectively recruited from patients admitted to the Neurological Intensive Care Unit (NICU) at the Institute of Neurological Sciences.

Included patients were over 16 years of age, admitted with a traumatic brain injury and undergoing invasive ICP monitoring as part of their routine clinical care.

Due to the nature of their injuries and ongoing intensive care, patients were unable to consent to inclusion in the study. For this reason, the nearest relatives were approached on their behalf. The nearest relatives were provided with a Relative's Information Sheet and a verbal description of the study procedure. They were allowed time to ask questions and for consideration prior to consenting to their relative's participation in the study.

Patients were excluded from participation in the study if their relative refused consent or if there was soft tissue injury preventing application of the TCB electrodes.

3.6 Patient Monitoring

As part of their routine clinical care on the NICU, all participants were undergoing measurement of their physiological vital signs through the Philips IntelliVue MX700 bedside patient monitor (Philips Healthcare, Netherlands). Vital signs recorded included, but were not limited to, pulse oximetry (SpO_2), end-tidal carbon dioxide ($ETCO_2$), electrocardiogram (ECG), invasive arterial blood pressure (IABP) and core temperature.

As stated in the inclusion criteria, all patients were undergoing invasive ICP monitoring. This was done through a Neurovent-P catheter-tip pressure sensor (Raumedic, Germany). The sensor was typically placed in the intraparenchymal compartment through a cranial bolt-housing overlying the frontal cortex. Interface to the Philips IntelliVue MX700 was provided by the NPS2 Philips/HP adapter cable.

Minute by minute summaries of all vital signs, including ICP, were recorded and archived to the local patient management database (Microsoft SQL Server, 2008).

3.7   Study Procedure

3.7.1 Transcranial Bioimpedance Measurement

Transcranial bioimpedance measurements were performed using the Impedimed SFB7 Bio-impedance Spectroscopy Unit (ImpediMed, Australia). The device is a single channel BIA unit that acquires 256 separate measurements between 4 and 1000kHz. The SFB7 device was connected through application of 3M Red Dot Paediatric Monitoring Electrodes (3M, USA) to the scalp. In a previous study of healthy volunteers, our group had demonstrated the ease of obtaining TCB measurements using this device and have established a normative data set with varying electrode position, age and gender(130). From this it was concluded that temporal to temporal or frontal to occipital electrode positions were likely to give equally reliable data. The temporal to temporal position was anticipated to be the easiest to perform in TBI patients and was thus chosen as the primary configuration (Figure 3.1).

Following patient recruitment to the study, TCB measurements were made with at least one hour intervals so that they could be considered as discrete measurements. There was a target of 20 measurements per participant, but this was subject to continuation of invasive ICP monitoring and ongoing feasibility of TCB measurement. At each measurement time point the device was programmed to perform 40 separate TCB recordings. This process took approximately one minute and ensured that any variation of instantaneous readings through pulsatile changes in either brain or scalp could be accounted for at the analysis stage.

Figure 3.1: SFB7 device connected with electrodes in the temporal position. An identical pair of electrodes are on the opposite side.

3.7.2 Whole Body Bioimpedance Analysis

Whole body bioimpedance measurements were anticipated to be an important variable when modelling TCB against ICP. To enable this, whole body bioelectrical impedance analysis (BIA) was performed six hourly during the study period using the SFB7 device and the standard technique.

3.7.3 Waveform Data Capture

In addition to routine clinical monitoring of participants, high frequency capture of physiological vital signs was performed throughout the study period. This was achieved by continuously streaming data from the Philips Intellivue MX700 Medical Interface Bus (MIB) to a Dell Inspiron laptop (Dell Inc., USA) using ixTrends software(133). The purpose of this high frequency data capture was to allow better inspection of data for artifact and to allow future comparison of TCB against features of the ICP waveform.

3.7.4 Additional Clinical Data

A number of participant variables were recorded in the clinical record form (CRF) to allow data stratification for the process of modelling TCB against ICP. These variables included age, gender, body weight and height. Additional variables extracted from the participants computed tomography scan (CT) of their brain for consideration in the modelling process included brain diameter

and measurements of soft tissue swelling. To ensure that the population of patients studied was an appropriate representation of patients admitted with TBI, details of aetiology of TBI, primary diagnosis and any surgical procedures were also collected in the clinical record form (CRF).

3.8   Analysis

3.8.1 Introduction

As stated in the introduction, data processing and analysis were performed using the "R" statistical programming environment(7). Specifically R Studio Version 0.98.1102 running R Version 3.1.2 (R Core Team, 2014) was used. Individual R Packages used for each stage of analysis are detailed in the appropriate sections. All data visualisation was done using the package *ggplot*(134).

3.8.2 Data Preparation

3.8.2.1   Bioimpedance Data

TCB and whole body BIA data were downloaded from the SFB7 device using the BioImp Body Composition Analysis Software provided with the device. The capabilities of this software in terms of Cole-Cole plotting and body composition estimates were not used. Instead the downloaded comma separated value (csv) files were imported into R for subsequent analysis. An annotated example of an SFB7 output file is shown in Figure 3.2.

```
SFB7 BioImp v1.55 #SFB7-16E110002 biotbi001-0180.mfu
17-Dec-2011 09:03:12 PM
h 185.0
w 85.0
a 45
s M
ref 235.50
rif 894.20
rem 273.90
rim 937.20
d 1.05
p 4.30
hy 0.732
3.084,36.91,0.86
3.147,37.03,0.66
3.210,37.05,0.74
3.273,37.07,0.69
3.367,37.15,0.84
3.430,37.08,0.88
3.525,37.00,0.91
3.588,37.07,0.76
3.682,37.02,0.74
3.777,37.09,0.83

...

...

...

...

...
815.263,30.05,3.50
833.988,29.88,3.56
853.123,29.88,3.47
872.698,29.86,3.46
892.745,29.85,3.54
913.233,29.78,3.50
934.193,29.63,3.39
955.625,29.66,3.42
977.560,29.70,3.44
999.999,29.61,3.38
```

Header information including file number, date, time and patient demographic details

Bioimpedance data in the format frequency, resistance, reactance

Figure 3.2: Excerpt from a SFB7 data file, which includes header information and resistance and reactance measurements across 256 frequencies.

Manipulation of TCB data into a standardised format for ease of repeatable analysis was performed using the packages *dplyr*(135) and *stringr*(136). Cole-Cole plots were then constructed for each TCB and whole body bioimpedance measurement using a circle fitting function used in previous work(51). Summary values for Z_c, R_0 and R_{inf} were created by performing a composite fit using data from all of the 40 measurements made at each time point. Data were excluded

if the circle fitting function was unable to successfully calculate all of Z_c, R_0 and R_{inf}.

3.8.2.2   ICP Data

The ICP data necessary for modelling against TCB data were extracted from the high frequency data collected by the ixTrends software. These waveform data were stored with a resolution of 128 Hz and were output to a csv file. The processing of waveform data was done using techniques developed by Martin Shaw as part of a parallel project to which the BioTBI study contributed pilot data(137, 138). In brief, the waveform data underwent pulse detection and subsequent summarisation to 1 Hz frequency. ICP data were then extracted and imported into R. As for TCB data, manipulation of ICP data into a standardised format for ease of repeatable analysis was performed using the packages *dplyr*(135) and *stringr*(136).

In preparation for modelling their relationship, a unique ICP value was needed for each TCB measurement. As a pragmatic sample, median ICP was calculated for the five minutes following each TCB measurement.

3.8.3 Modelling ICP Using TCB Data
3.8.3.1   Sample Size

When calculating the appropriate sample size for the study, the range of ICP was assumed to be 0 to 50 mmHg. In the first instance, we expected to detect a minimum correlation between ICP and impedance of 0.2 (or 10 mmHg). Therefore a sample size of 280 was required to achieve a power of 0.9. We anticipated that this number of samples could easily be collected if 15 patients were recruited and TCB measurements made every hour for 24 hours.

3.8.3.2   Modelling Process

Attempts were made to model ICP using both absolute and normalised values of Z_c and R_0. In the animal studies referred to in the introduction, Z_c had an inverse relationship with ICP, while R_0 had a direct relationship(127, 130). An unadjusted linear modelling approach was first taken to confirm some degree of relationship between TCB and ICP.

An adjusted linear modelling approach was subsequently taken to explore which patient specific variables could be used to further define the relationship between ICP and Z_c or R_0. Each of the patient variables of gender, age, weight and height, along with CT derived measurements of soft tissue swelling and brain diameter, as well as whole body bioimpedance measurement and temperature, were included in linear models. Patient variables that did not significantly contribute to the model were sequentially removed. The simplified model was then compared against the original using analysis of deviance testing to confirm that they were not significantly different.

The final modelling approach was to use the Akaike information criterion (AIC) in backward stepwise regression to select the models with the best balance of goodness of fit and low complexity. All modelling was done using the *stats* package in R(7).

4 Results for the BioTBI Study

4.1 Overview

The principle results of the transcranial Bioimpedance in Traumatic Brain Injury study are presented. There is first a description of patient demographics and measurements made, followed by a description of the attempts to model intracranial pressure using transcranial bioimpedance measurements. These results were presented in June 2016 at the 16th International Symposium on Intracranial Pressure and Neuromonitoring, Boston, Massachusetts.

4.2 Data Collection

4.2.1 Data Collection Period

The initial plan for the BioTBI study was to recruit 15 patients to achieve a data set of 300 independent TCB measurements. Data were collected over the period 17/12/2011 to 21/01/2014. TCB data were collected from a total of 11 patients during this period. In one of these patients, a technical problem with the neurological intensive care unit network led to a failure to store sufficient ICP data to model against TCB measurements. Consequently there were 10 patients with data suitable for inclusion in the study.

In an audit of admissions to NICU at the Institute of Neurological Sciences in 2010 there were 17 patients with TBI who underwent ICP monitoring. For this reason, it had been felt that recruiting the sample size of 15 patients in a two year period would be achievable. There were a number of reasons that meant that this was ultimately not the case. These ranged from a higher than expected number of relatives refusing consent, the unavailability of relatives to conduct the consent process, coincident admission of patients when there was only sufficient equipment to recruit one and short ICP monitoring periods meaning adequate data collection would not be possible.

4.2.2 Patient Demographics

All patients met the inclusion criteria of age over 16 years, admitted to NICU with a traumatic brain injury and were undergoing ICP monitoring as a routine part of their clinical care. Table 4.1 summarises the demographic characteristics of each of the 10 final participants. There were nine male patients and one female and the median age was 51 (29 – 61) years.

ID	Gender	Age (Yrs)	Aetiology	Primary Diagnosis	Hospital Survivor
001	m	45	Fall	ASDH	y
003	m	54	Fall	EDH	y
004	f	61	Fall	EDH	y
005	m	51	Fall	ASDH	y
007	m	48	Fall	ASDH	y
009	m	59	Fall	Contusions	y
010	m	61	Fall	Contusions	y
011	m	41	Assault	EDH	y
013	m	53	Fall	Contusions	y
018	m	29	MVC	DAI	n

Table 4.1: Demographic summaries for each of the ten patients included in the BioTBI study, where MVC = motor vehicle crash, ASDH = acute subdural haematoma, EDH = extradural haematoma, DAI = diffuse axonal injury.

The aetiology of TBI was a fall in eight cases, with one assault and one motor vehicle crash. Most patients had several abnormalities identified on their admission CT brain scan, but the primary diagnosis was subdural haematoma, extradural haematoma or contusions in three cases each, with a single case of diffuse axonal injury. Four patients underwent craniotomy for haematoma removal prior to the period of TCB measurement. Subsequent to the study period, one further patient underwent craniotomy, two underwent burr hole drainage of chronic subdural haematoma and a further patient underwent insertion of an external ventricular drain followed by decompressive craniectomy. The extent of mixed pathology within and between patients is likely to have been significant in terms of the ability to model ICP using TCB and will be considered in detail later.

Nine out of the ten patients survived until discharge from hospital. The median length of stay in ICU was 8.6 (4.2 – 18.6) days, while the median length of acute hospital stay was 24.6 (16.2 – 143.5) days.

4.2.3 Transcranial Bioimpedance Measurements

In the ten patients who were ultimately included in the study, 168 valid temporal to temporal TCB measurement episodes were available. Preliminary Cole-Cole plots could be displayed on the SFB7 device and it was therefore possible to reject any clearly invalid measurements and repeat. In some patients it was impossible to achieve a valid measurement and the reasons for this will be explored in the discussion section. In the first five patients, initial attempts were made to measure TCB in alternative electrode positions (for example frontal to mastoid). It became clear however, that these measurements could often not be made due to the presence of a cervical collar or due to the risk of head position changes impacting on ICP. For each of the 168 episodes, there were 40 separate TCB measurement sweeps across the frequency spectrum.

The TCB measurements from each measurement episode underwent Cole-Cole analysis to fit a single composite curve as a summary measure of the data. An example of the Cole-Cole plots for one patient is shown in Figure 4.1 and an example of the curve fitting has already been shown in Figure 2.15.
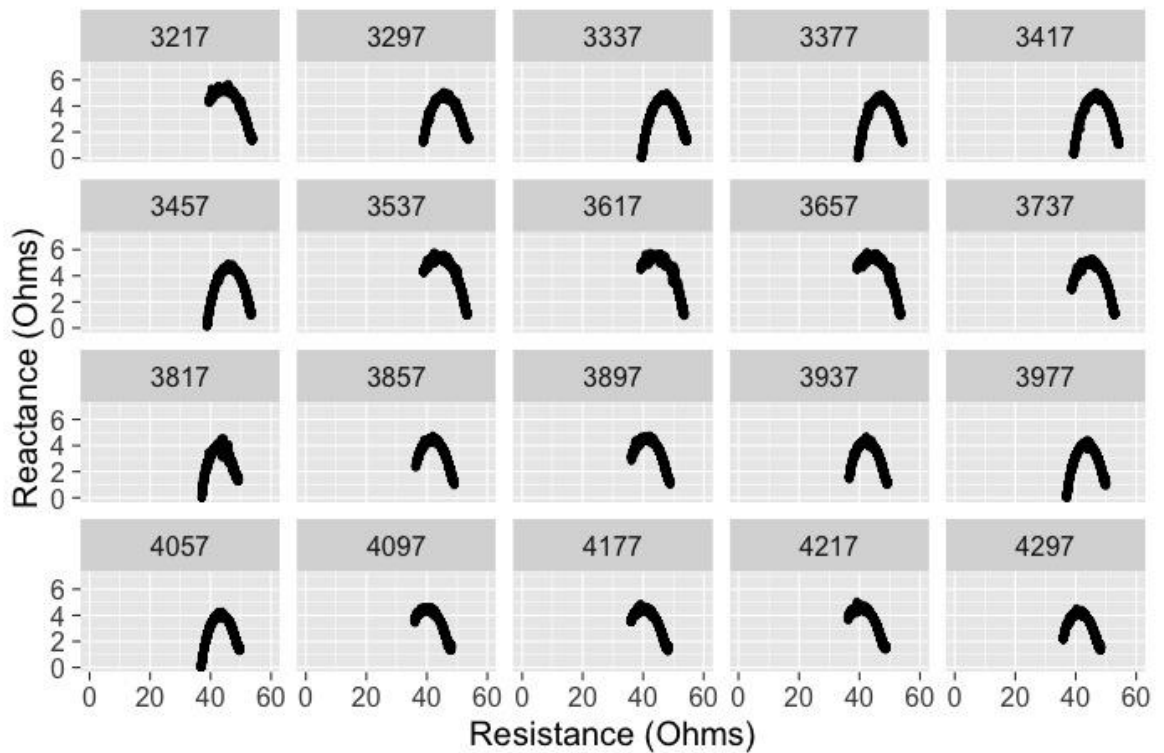
Figure 4.1: An example of composite Cole-Cole plots for one patient (ID = 011).

4.2.4 Whole Body Bioimpedance Measurements

A total of 39 whole body bioimpedance measurements were made. This represented at least one measurement for every six hour period for the patients included in the study. As for the TCB measurements, for each of the 39 episodes, there were 40 separate measurement sweeps across the frequency spectrum.

4.2.5 Intracranial Pressure Measurements

ICP was calculated as a summary measure of two time windows surrounding each TCB measurement. The first time window was the five minutes immediately following the measurement, when the median value across the study period for all patients was 16.3 (9.5 – 28.9) mmHg. Boxplots showing the distribution of ICP for each patient are shown in Figure 4.2. The median ICP value using a second time window from 15 minutes before to 15 minutes after each TCB measurement was 16.2 (9.5 – 29.4) mmHg. The distributions of ICP values for each patient were essentially identical between the first and second time windows. For this reason, the decision was made to use only the ICP values calculated during the first time window during the process of modelling ICP using TCB.
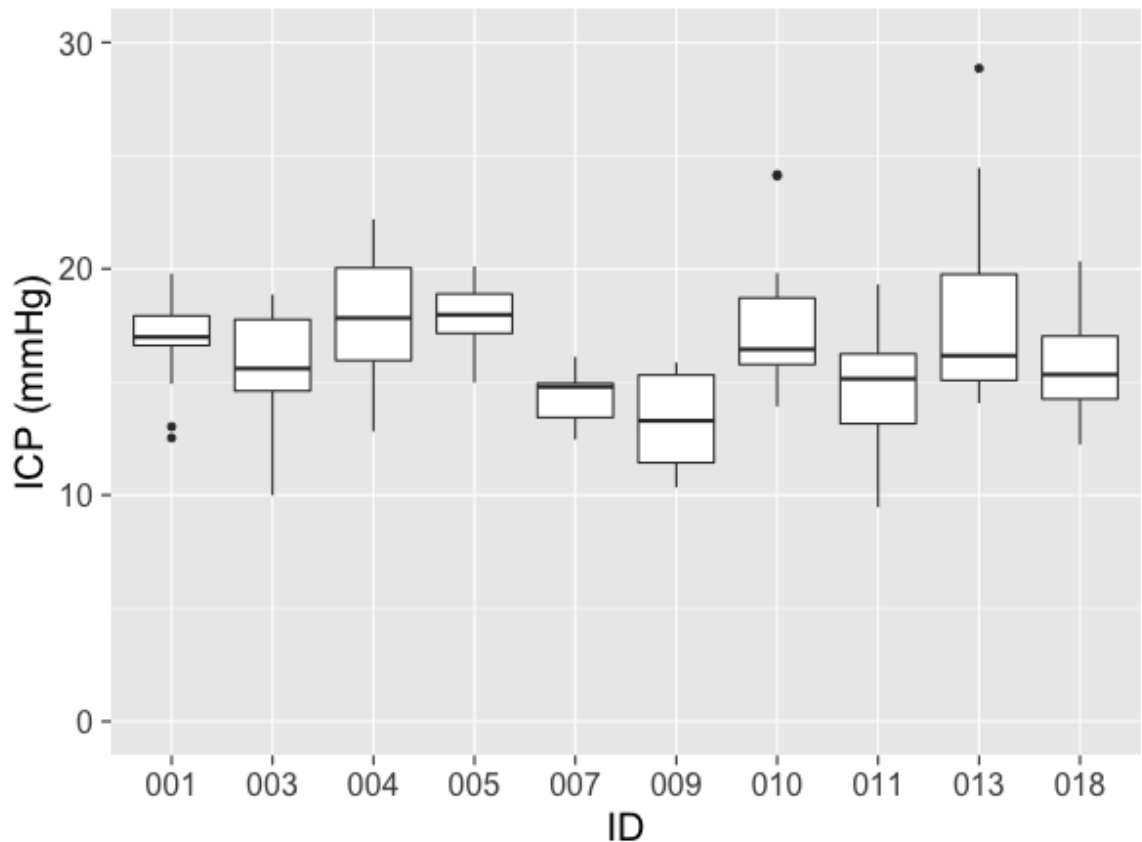
Figure 4.2: Boxplots showing the distribution of ICP values measured across the study period for each patient.

4.3 Modelling of ICP Using TCB Data

4.3.1 Introduction

A number of modelling approaches were taken in an attempt to find the most effective technique to predict ICP using TCB measurements. The results of these analyses shall be discussed in turn below. TCB measurements entered the models either as the raw measured value or as a value normalised against the overall median value for the individual patient.

4.3.2 Unadjusted Linear Models

ICP was first plotted against measured Z_c and normalised Z_c to allow visual inspection for any obvious relationship (Figure 4.3). From these plots there was no clear relationship between TCB and ICP, so the plots were then repeated for each individual patient (Figure 4.4). In the absence of any clear visual relationship the decision was made to use an unadjusted linear modelling approach to explore the relationship between both measured Z_c and normalised

Z_c and ICP. On the basis of the previously discussed sheep study(130), the inverse relationship between normalised Z_c and the log of ICP was also explored.

On the basis of the previously discussed neonatal piglet study(127), the relationship between ICP and R_0 was also explored. Combined and individual patient plots are displayed in Figures 4.5 and 4.6. Again there was no clear relationship between TCB and ICP, so on the basis of the piglet experiment a direct relationship between R_0 and ICP was assumed.
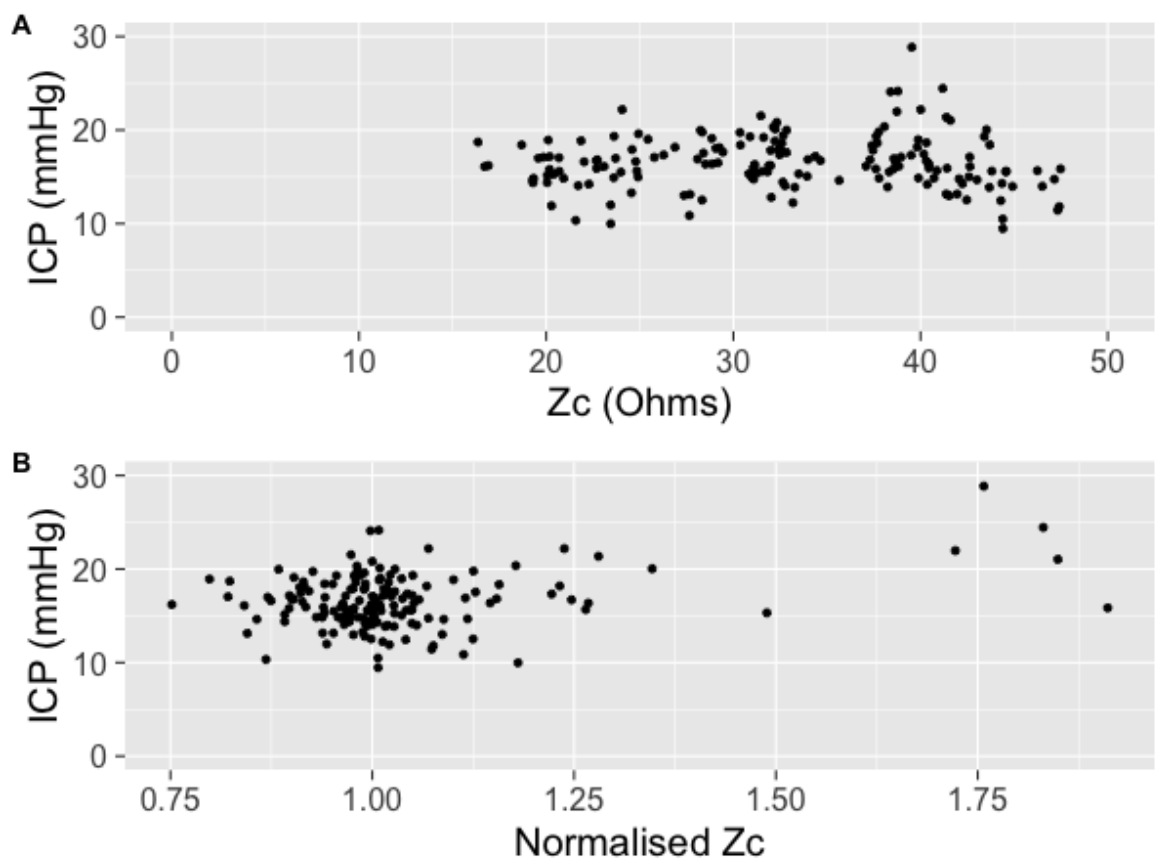
Figure 4.3: Plot of ICP against measured (A) and normalised (B) Z_c for the entire study population.
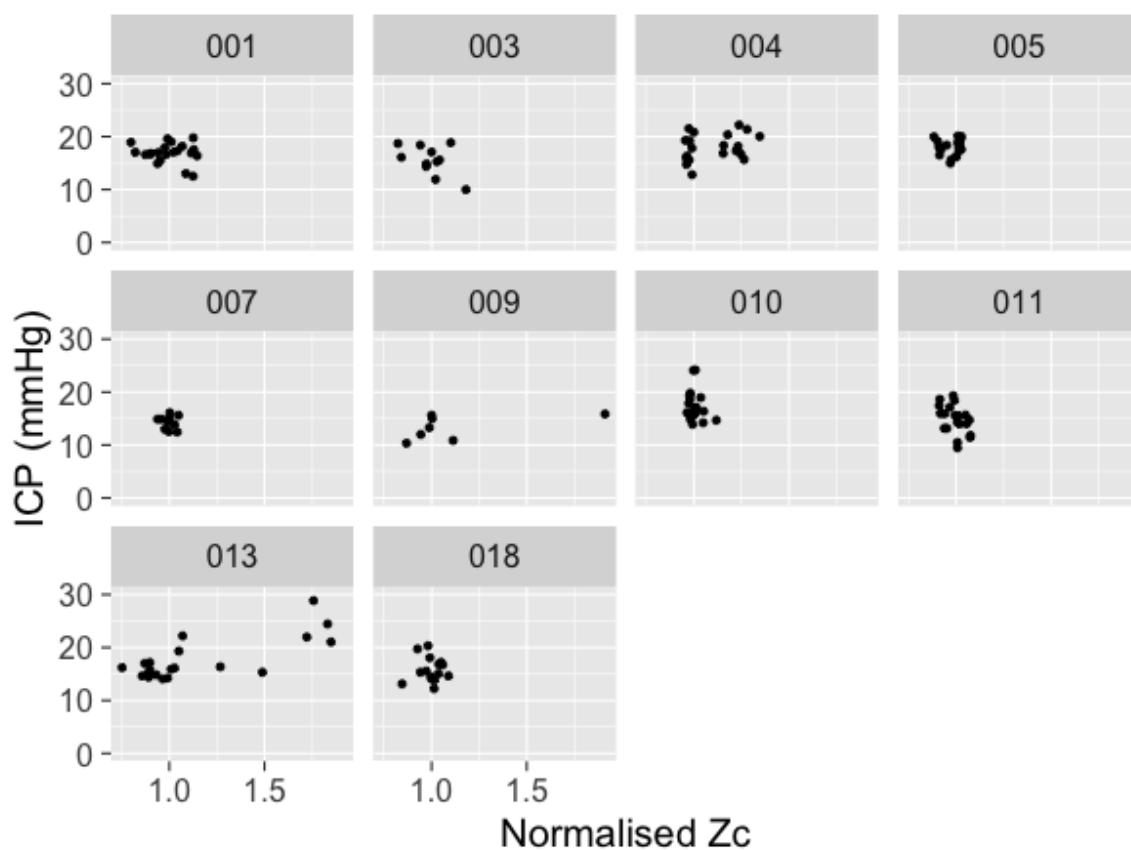
Figure 4.4: Plots of ICP against normalised Z$_c$ for each patient.
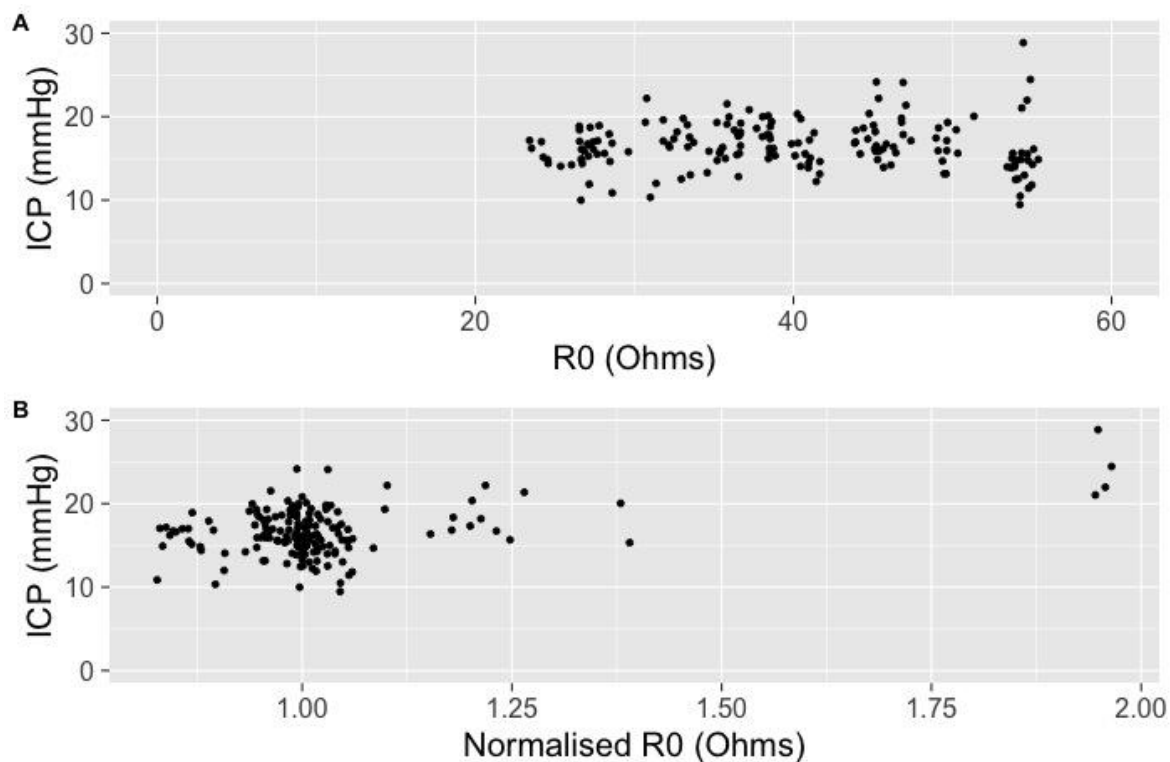
Figure 4.5: Plot of ICP against measured (A) and normalised (B) R$_0$ for the entire study population.
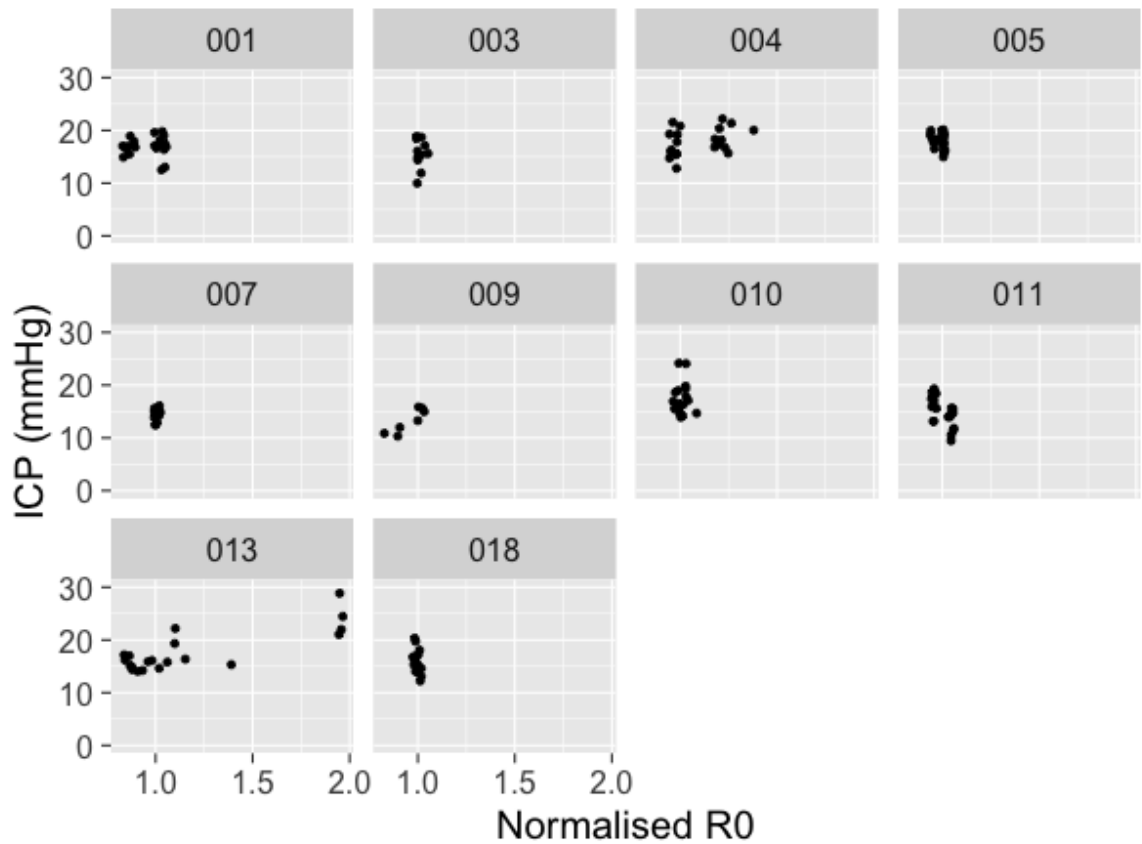
Figure 4.6: Plots of ICP against normalised R_0 for each patient.

There was no significant relationship between ICP and Z_c or R_0. There was a significant relationship between ICP and normalised Z_c ($p < 0.001$), a significant inverse relationship between the log of ICP and normalised Z_c ($p < 0.01$) and a significant relationship between ICP and normalised R_0 ($p < 0.001$). The adjusted r-squared value for each of these relationships was small (0.09, 0.06 and 0.18 respectively). Attempts were therefore made to explore the relationship between ICP and TCB parameters by adjusting the linear models for patient specific variables.

4.3.3 Adjusted Linear Models

To explore which patient specific variables could be used to further define the relationship between ICP and Z_c or R_0, each of the patient variables of gender, age, weight and height, along with CT derived measurements of soft tissue swelling and brain diameter, as well as whole body bioimpedance measurement and temperature, were included in linear models. Patient variables that did not significantly contribute to the model were sequentially removed. The simplified model was then compared against the original using analysis of deviance testing

to confirm that they were not significantly different. The following models were considered:

$$ICP = a_1 Z_c + a_2 V_2 \dots a_n V_n + b \tag{4.1}$$

$$ICP = exp\left(\frac{a_1}{Z_c} + a_2 V_2 \dots a_n V_n + b\right) \tag{4.2}$$

$$ICP = a_1 R_0 + a_2 a_2 \dots a_n V_n + b \tag{4.3}$$

$$ICP = a_1 Z_{norm} + a_2 V_2 \dots a_n V_n + b \tag{4.4}$$

$$ICP = exp\left(\frac{a_1}{Z_{norm}} + a_2 V_2 \dots a_n V_n + b\right) \tag{4.5}$$

$$ICP = a_1 R_{norm} + a_2 V_2 \dots a_n V_n + b \tag{4.6}$$

where Z_{norm} and R_{norm} are normalised Z_c and R_0, $V_1 \dots V_n$ are patient specific variables and $a_1 \dots a_n$ and b are constants. To assess whether or not the inclusion of both Z_c and R_0 strengthened the relationship between TCB parameters and ICP, the following models were considered:

$$ICP = a_1 Z_c + a_2 R_0 \dots a_n V_n + b \tag{4.7}$$

$$ICP = exp\left(\frac{a_1}{Z_c}\right) + a_2 R_0 \dots a_n V_n + b \tag{4.8}$$

$$ICP = a_1 Z_{norm} + a_2 R_{norm} \dots a_n V_n + b \tag{4.9}$$

$$ICP = exp\left(\frac{a_1}{Z_{norm}}\right) + a_2 R_{norm} \dots a_n V_n + b \tag{4.10}$$

Using measured TCB parameters, the simplified model with the greatest r-squared value was:

$$ICP = a_1 R_0 + a_2 G + a_3 W + a_4 H + a_5 BD + a_6 WBZ_c + b \qquad (4.11)$$

where G is gender, W is weight, H is height, BD is brain diameter and WBZ_c is whole body bioimpedance (p < 0.0001, r-squared = 0.19, estimates in Table 4.2).

	Estimate	95% Confidence Intervals	P-value
a_1	0.20	0.12 to 0.29	< 0.0001
a_2	-5.68	-7.51 to -3.85	< 0.0001
a_3	0.08	0.01 to 0.15	< 0.05
a_4	0.28	0.16 to 0.40	< 0.0001
a_5	-0.41	-0.65 to -0.17	< 0.001
a_6	-0.02	-0.03 to -0.01	< 0.0001
b	15.03	-4.92 to 34.98	0.14

Table 4.2: Estimates for model 4.11.

The simplified model with the greatest r-squared value using normalised bioimpedance measurements was:

$$ICP \qquad (4.12)$$
$$= exp\left(\frac{a_1}{Z_{norm}}\right) + a_2 R_{norm} + a_3 G + a_4 ST + a_5 T + a_6 WBZ_{norm} + b$$

where ST is soft tissue thickness and T is temperature (p < 0.0001, r-squared = 0.32, estimates in Table 4.3).

	Estimate	95% Confidence Intervals	P-value
a_1	2.92	1.07 to 4.78	< 0.01
a_2	9.60	6.10 to 13.09	< 0.0001
a_3	-3.81	-5.40 to -2.22	< 0.0001
a_4	0.13	0.08 to 0.19	< 0.0001
a_5	0.90	0.29 to 1.51	< 0.01
a_6	12.12	2.21 to 22.03	< 0.05
b	-48.50	-74.51 to -22.49	< 0.001

Table 4.3: Estimates for model 4.12.

4.3.4 Backward Stepwise Regression

The models selected and their r-squared values calculated using a backward stepwise regression approach were essentially the same as those selected using the adjusted linear modelling approach.

5   Discussion and Conclusions for the BioTBI Study

5.1   Overview

A discussion of the results of the BioTBI Study is presented below. Limitations of the study are addressed and the results are considered in terms of those of similar studies attempting to model intracranial pressure (ICP) using a non-invasive technique. There is then a description of work performed as a direct result of the BioTBI Study with suggestions for future directions of research into the modelling of ICP in patients with traumatic brain injury (TBI).

5.2   Rationale for the Study

Monitoring of ICP is well established in the clinical management of TBI and the practise is supported by international guidelines(54). ICP monitoring is typically performed using an intraventricular or intraparenchymal catheter with a microtransducer system. Both of these techniques are associated with significant complications such as bleeding and infection and their availability in TBI is largely restricted to specialist neurosurgical centres. A safe, simple and accurate non-invasive device would therefore increase the clinical availability of ICP monitoring.

Transcranial bioimpedance (TCB) has been considered for the early detection of multiple brain pathologies in humans(120, 121, 125). In addition, previous animal experiments have shown a relationship between TCB and ICP(127, 130). Based on the known relationship between bioimpedance and the volume of the intracellular and extracellular spaces, the potential use of TCB was investigated as an estimate of ICP in TBI.

5.3   Data Collection

5.3.1 Study Population

All study patients were recruited from the neurological intensive care unit (NICU) and had been admitted with severe TBI. The patients were representative

of the typical population of patients suffering a TBI in terms of age range and the diverse pathologies identified on computed tomography (CT) scanning of the brain. While the range of pathologies was a strength of the study in terms of its clinical applicability it may have limited the prospects of successfully identifying a relationship between TCB and ICP.

In the animal studies that had previously defined a relationship between TCB and ICP, the experimental models resulted in a uniform pathological process that would effect TCB measurements in a predictable manner. In the neonatal piglet model described by Lingwood *et al*(127), brain hypoxia was presumed to lead to intracellular swelling and a consequent decrease in the extra-cellular fluid space that was associated with a rise in ICP. In the sheep model described by Shaw *et al*(130), intracranial hypertension (ICH) was induced by injection of mock cerebrospinal fluid (CSF) into the ventricle. The nature of the brain injuries in the patients recruited to the BioTBI study meant that there were likely to be multiple pathological processes evolving, even within an individual patient. The aetiology of increases in ICP could include intracellular or vasogenic oedema, expansion of intra or extra-axial haematoma or a disruption to CSF flow. All of these pathologies are likely to have had different influences upon TCB measurements that complicated the process of modelling ICP.

A failure to translate promising animal research into successful human studies has been a very well recognised problem in TBI(139) and over the past 30 years more than 20 large phase III trials have failed to show a significant treatment effect of a neuroprotective agent(140). Many of the issues related to therapeutic trials relate equally well to monitoring studies. One of the primary problems in converting positive findings in animal models of TBI into positive findings in the clinical environment is believed to be the heterogeneity of human TBI compared to that in controlled animal models(141). The International Mission on Prognosis and Clinical Trial Design in TBI (IMPACT) study group was initiated in 2003(142). They were given access to individual patient data from several large randomised controlled trials (RCTs) with the aim of optimising the design and analysis of trials in TBI. Proposed techniques for dealing with heterogeneity in TBI have been to maintain broad inclusion criteria but to pre-specify covariate adjustment into analyses(143).

As already detailed in the results section, recruitment to the BioTBI Study was slower than had been anticipated. Although the intended sample size was not achieved, the number of patients and individual TCB measurements should have been sufficient to detect a strong relationship between TCB and ICP if it existed.

5.3.2 TCB Measurements

Measurement of TCB proved to have a number of technical difficulties in the population of TBI patients studied. The presence of rigid collars to immobilise the cervical spine in a number of patients meant that positioning the electrodes in mastoid or occipital positions was not feasible. Similarly the risk of undiagnosed cervical spine injury in this patient population means that the head and neck can only be moved with caution to allow electrode attachment.

In several patients the application of electrodes was complicated by the position of dressings following cranial surgery or because of associated maxillo-facial injuries. Indeed the presence of significant soft-tissue swelling in some cases made the successful measurement of TCB difficult. In these cases there was the concern that a significant portion of the current path would be extra-cranial and therefore impedance would not necessarily reflect intra-cranial pathology. Attempts were made to mitigate this risk by measuring soft tissue thickness and brain diameter on CT scan and including these measurements in the adjusted models.

5.3.3 ICP Measurements

In the BioTBI Study, only patients who were undergoing ICP monitoring as part of their routine clinical care following severe TBI were recruited. In these patients, one of the principle aims of NICU care is to prevent ICH and thus intervene when ICP is rising. As can be seen from Figure 4.2, the vast majority of ICP summary measures from all patients were in the range of 10 to 25 mmHg. Therefore there were a limited number of extreme ICP values to facilitate model building. All studies investigating non-invasive ICP devices in the real clinical environment face a similar problem. For example in the study by Brandi *et al*, comparing multiple transcranial Doppler sonography (TCD) derived models of ICP, across

601 measurements in 45 patients, there were only four values above 25 mmHg(80).

ICP values used for modelling purposes were taken as a median of ICP in the five minutes following a TCD measurement. This time window was chosen as being long enough to provide a stable value but short enough to reflect any changes in pathophysiology. The R code used to provide the summary measure would allow the window length to be easily adjusted in any future studies.

5.4 Modelling of ICP Using TCB Data

5.4.1 Unadjusted Linear Models

The TCB parameters selected for modelling were based upon the animal studies referred to above. Shaw *et al* had demonstrated an inverse relationship between the log of ICP and Z_c(130), while Lingwood *et al* had demonstrated a direct relationship between ICP and R_0(127). Visual inspection of plots of ICP against the Z_c and R_0 (Figures 4.3 and 4.5) did not suggest any strong relationship. Given the low sample size, plots were performed for each individual patient (Figures 4.4 and 4.6) but even on an individual patient basis there was no clear trend between either Z_c or R_0 and ICP.

The lack of a strong relationship was then supported by the results of the linear modelling approach, where there was no demonstrable relationship between the measured values of either Z_c or R_0 and ICP. When TCB variables were normalised per patient (as was done in the previous animal studies) there was a small but significant relationship.

5.4.2 Adjusted Models

In an attempt to account for some of the patient heterogeneity in the study population, a number of patient specific variables were used in adjusted linear models and backward stepwise regression. Using measured values, the TCB parameter R_0 in combination with the variables of gender, age, weight, height, brain diameter and whole body Z_c provided the adjusted linear model of ICP (4.11) with the largest adjusted r-squared value (0.19). Using normalised values, the TCB parameters of $1/Z_c$ and R_0 in combination with the variables of gender,

soft tissue thickness, temperature and whole body Z_c provide the model of ICP (4.12) with the largest adjusted r-squared value (0.32). The models and values calculated using backward stepwise regression were almost identical.

The relatively low r-squared values in the above models mean that a large component of ICP is unexplained by the model incorporating TCB measurements. This is particularly relevant given that there is a significant risk of model over fitting to the small study population. Therefore the likelihood that either of the models could be generalised to provide clinically meaningful estimates of ICP in a population of patients admitted with severe TBI is low.

5.4   Results in the Context of Similar Studies

5.4.1 Non-Invasive ICP Measurement

The two most extensively investigated non-invasive techniques to estimate ICP are TCD and optic nerve sheath diameter (ONSD) derived measures, as already discussed. The complexity of TCB measurements and the training required to perform them would be less than either of these ultrasound-derived measures. On the basis of the BioTBI study however, TCB does not show more potential overall.

It is not possible to perform an exact comparison of the techniques, but the r-squared value of 0.19 achieved by modelling ICP using measured values of TCB suggests the technique would be far inferior to either TCD or ONSD. The TCD technique proposed by Bellner *et al*(78) and recommended by Brandi *et al*(80) was initially demonstrated to detect an ICP of over 20 mmHg with a sensitivity of 0.83 and specificity of 0.99. It is worth mention that in the comparative study by Brandi *et al*, the technique failed to detect all cases of intracranial hypertension. In the meta-analysis of ONSD techniques performed by Dubourg et al, the pooled sensitivity and specificity to detect ICH were 0.9 and 0.85 respectively(87).

The TCB, TCD and ONSD techniques all share the disadvantage of providing a surrogate measure of ICP, rather than an absolute measure. The technique described by Ragauskas *et al*(108), based on detecting ophthalmic artery pulse

waveforms following increments of intra-occular pressure, provides an interesting alternative. The safety and applicability to a wide range of clinical situations are yet to be demonstrated for this technique.

5.4.2 Clinical Application of TCB

The BioTBI study suggests that TCB techniques will require considerable development before application to estimation of ICP in TBI. Other authors have proposed the use of TCB to detect alternative pathologies. Both of Liu *et al*(121) and Seonne *et al*(125) have studied the use of TCB measurement in the early detection of stroke. The use of TCB in this population does not face the same difficulties in terms of movement of the head and neck or electrode application in the context of soft tissue injury that are encountered in TBI.

There is no detailed description of the TCB measurements made by Liu *et al*. In the study by Seonne *et al*, comparison was made between TCB measurements made with central and lateral electrode positions and with left and right electrode positions. The ratios of resistance in these electrode positions was found to be outside the range of healthy controls in nine out of ten stroke patients. This is an interesting result and does support the hypothesis that TCB measurements can help to identify a patient with brain injury. It is difficult however to envisage how TCB would be applied in the acute care of stroke, where the requirement for early diagnostic imaging is already established in national guidelines(144).

5.5   Related and Future Work

5.5.1 Introduction

Despite disappointing results in terms of modelling ICP, the ICP and ABP waveform data collected as part of the BioTBI Study have been a valuable research resource. They have been used as pilot data to test some of the models described in the introductory chapter and bring them closer to implementation in clinical practice. Examples of recent and ongoing projects that are using the data to develop novel ICP analysis, address issues related to artifact in high volume data capture and embed these complex analyses into the clinical environment are provided below.

5.5.2 Multi-resolution Convolution Analysis of the ICP Waveform

From the database of ICP waveforms collected as part of the BioTBI Study, examples of the recognised ICP states of high and low compliance and 'a' and 'b' waves were selected(145). Multi-resolution convolution analysis was used to identify features of the ICP waveform associated with each of the clinical states that could then be used to create an impulse function. It was then possible to identify these waveform features in a separate study dataset. These pilot results require further optimisation on a larger ICP waveform dataset. As with the previously discussed work on morphological clustering and analysis of continuous intracranial pressure (MOCAIP)(103), they do suggest that automated analysis of the ICP waveform may be able to identify clinically important ICP states.

5.5.3 Calculation of Optimal CPP

There has already been detailed discussion of the potential use of indices of cerebral autoregulation (CA) to calculate optimal cerebral perfusion pressure (CPPopt) in TBI. One of the potential limitations of this approach is the fact that the most established techniques to calculate CPPopt fail to successfully find a value in a significant percentage of monitoring episodes(100). Arterial blood pressure (ABP) and ICP waveforms collected during the BioTBI Study have been used to compare indices of CA(146) and explore alternative methods of estimating CPPopt(147). If targeting of CPPopt in the management of TBI is to be tested by RCT, there will need to be consensus agreement on the most appropriate means of its estimation.

5.5.4 Detecting Artifact in Physiological Waveforms

The BioTBI Study tested a new system for high frequency data capture on the NICU (ixTrends(133)). One of the well recognised problems with automatic high frequency data capture is the inadvertent collection of artifactual data(148). The ABP data collected during the BioTBI Study were used as pilot data for a Chief Scientist Office (Scotland) funded project (CHZ/4/801) into the automatic detection of artifactual events in vital signs monitoring data(149, 150). As high frequency data capture becomes the norm in ICU there will be a requirement for systems to ensure the quality of these data.

5.5.5 Embedding Automatic Data Analysis into the NICU

At around the same time that the IMPACT Group were addressing issues surrounding the failure of multiple large RCTs to confirm the efficacy of promising therapies in TBI, the Brain monitoring with Information Technology (BrainIT) Group were suggesting an alternative solution(96). As a collaboration across 22 NICUs in 11 European countries (coordinated from the Institute of Neurological Sciences in Glasgow), the group have worked towards development of more information technology based tools for collection and analysis of standardised high resolution data in TBI. By sharing and analysing these high resolution data it is expected that a better understanding of variations in patient physiology and treatment will lead to more targeted therapies in the future.

In the BrainIT projects, the data collection frequency was 1 Hz. In the BioTBI project, the data collection frequency of the ICP and ABP waveforms was 128 Hz, while the frequency for the electrocardiogram (ECG) signal was 512 Hz. The collection of this resolution of data means that analyses of brain physiology, for example the assessments of cerebral autoregulation mentioned above, can be performed. However, the vast quantities of data generated require specialised infrastructure for transfer, storage and analysis. The Connecting Healthcare and Research Through A Data-Analysis Provisioning Technology (CHART-ADAPT) Project has been funded by Innovate UK (Reference: 102113) to address these issues along with the unique challenge of returning results to the patient bedside in a clinically useful timeframe(151).

5.5.6 Alternative Monitors of Brain Physiology

In the context of managing TBI, the importance of ICP monitoring relates to the information it can provide clinicians in terms of indicating the extent of the pathological process and guiding interventions. The interventions can be targeted at reducing ICP and optimising CPP as a means of ensuring adequate cerebral blood flow (CBF) and consequently maintaining oxygen and nutrient delivery to the injured brain. Direct measures of these endpoints exist but a review of their function and efficacy is outwith the scope of this thesis. The Brain Trauma Foundation (BTF) guidelines acknowledge the current low level of evidence surrounding devices designed to monitor CBF, brain oxygenation and the metabolic state of the brain. Despite this, the future of TBI care will

potentially involve integrating ICP measurement with multiple additional monitors of brain physiology.

5.5.7 Alternative Applications for TCB Measurement

All of the applications of TCB measurement described above have been in the monitoring and investigation of acute pathologies. As an estimate of ICP it may be more appropriate in future studies to consider a role for TCB in monitoring more chronic conditions. For example, idiopathic intracranial hypertension (IIH) is a syndrome of raised intracranial pressure without identifiable aetiology(152) and hydrocephalus is a disorder of excessive accumulation of CSF with multiple aetiologies(153). In both of these clinical conditions there is often an indication for measurement of CSF pressure in individuals over a long period of time, frequently resulting in multiple invasive procedures. Therefore the need for new techniques to assist with the diagnosis of hydrocephalus is recognised as an opportunity for hydrocephalus research(154). In IIH and hydrocephalus, TCB would benefit from the lack of soft tissue injury, the potential to make a calibrating invasive measurement at the time of diagnosis, followed by the ability to trend non-invasive measures over time.

5.6 Conclusions

The pilot results from the BioTBI Study confirm some degree of relationship between TCB parameters and invasively measured ICP. The magnitude of this relationship is small and on the basis of the study, TCB is unlikely to provide a clinically useful estimate of ICP in patients admitted with TBI.

6 Pharmacokinetic Pharmacodynamic Modelling in Anaesthesia

6.1 Overview

Target controlled infusion (TCI) systems deliver intravenous drugs with the aim of achieving and maintaining set levels of drug in either the plasma or an effect site. In anaesthetic practice the effect site of interest is most commonly the brain. TCI systems apply population based pharmacokinetic (PK) models that attempt to account for inter-individual variability by adjusting model parameters according to covariates such as age, sex and weight(155). Most PK models in anaesthesia are compartment models, where drug is infused into a central compartment and can re-distribute to peripheral compartments as described by the rate constants. The delay between measured or predicted plasma concentrations and clinical effect can be accounted for by the incorporation of an effect site compartment, with an associated rate constant for elimination from this compartment (k_{e0}). The resulting model is known as a pharmacokinetic pharmacodynamic, or PKPD model (Figure 6.1).

In anaesthetic practice, the drug most commonly administered by TCI is propofol. A detailed discussion of the pharmacodynamic and pharmacokinetic features of propofol that make it ideally suited for TCI is provided below. There is a description of the PKPD models for propofol that are commonly used in clinical practice, alongside a consideration of their most significant differences. This is followed by an introduction of the Covariates Model, which is the subject of the PKPD study (VaSCoM) that forms the subsequent sections of this thesis. Finally there is a discussion of the modelling techniques available to determine the appropriate k_{e0} to use with a given PK model.
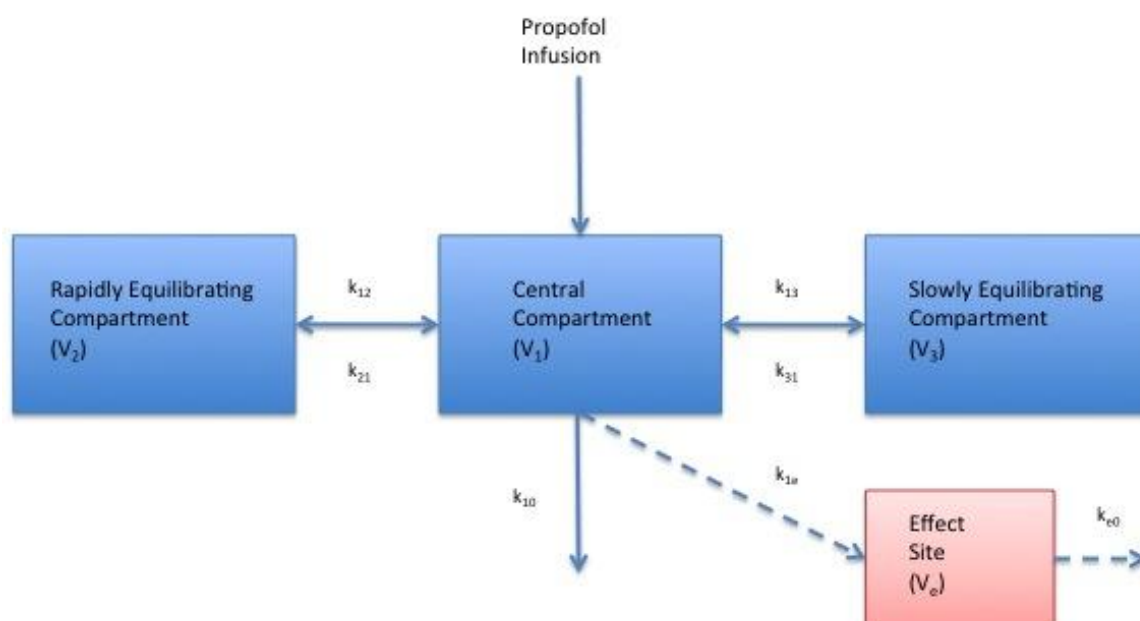
Figure 6.1: Three compartment mammillary model with model parameters V (compartment volumes) and k (microrate constants). The effect site is assumed to be infinitely small and does not effect the disposition of drug from the central compartment. Keo is the model parameter that describes the time course of clinical effect.

6.2   Total Intravenous Anaesthesia

Total intravenous anaesthesia (TIVA) has a number of theoretical advantages over inhalational anaesthesia that relate both to the drug delivery mechanism (Table 6.1) and the pharmacodynamic properties of the drugs used. TIVA is most commonly provided using a combination of a hypnotic agent (typically propofol) and a short acting opioid analgesic (typically remifentanil). In an audit of National Health Service (NHS) activity performed in 2013, 5.8% of anaesthetics in the United Kingdom are delivered by propofol infusion(156). The establishment of TIVA in routine anaesthetic practice has been facilitated by the development of PKPD models for propofol to allow its delivery via TCI systems.

Selected Advantages of Total Intravenous Anaesthesia
No requirement for anaesthetic machine with vapourisers
No risk of atmospheric pollution
Continuous delivery of anaesthesia during airway surgery
Continuous delivery of anaesthesia during patient transfer
Safe for use in patients with malignant hyperthermia

Table 6.1: Advantages of TIVA

6.3   Propofol

6.3.1 Chemistry

Propofol (2,6-diisopropylphenol) is the most commonly used intravenous anaesthetic agent. It is a highly lipophylic compound and was initially introduced during the late 1970s formulated in Cremophor EL(157). Due to an association between Cremophor EL and anapylactoid reactions, this preparation of the drug was withdrawn and propofol has been subsequently formulated as a lipid emulsion. The first preparation chosen for development (Diprivan®) was based on the composition of the parenteral fat formulation Intralipid® (10% soybean oil, 2.25% glycerol, 1.2% egg yolk lecithin) with the pH adjusted by sodium hydroxide. The soybean emulsion in Diprivan® contains long chain triglycerides and these are thought to be responsible for the associated pain on injection. Alternative formulations containing mixed long and medium chain triglycerides (Propofol-Lipuro®) have been associated with similar pharmacokinetic and pharmacodynamic properties but with less injection pain(158).

Selected Effects of Propofol	
Airway	⇓⇓ Haemodynamic response to intubation
Respiratory	⇓⇓ Central inspiratory drive
	⇓⇓ Minute volume
	⇓⇓ Tidal volume
	⇓⇓ Ventilatory response to increased $ETCO_2$
Cardiovascular	⇓⇓ Arterial blood pressure
	⇓⇓ Systemic vascular resistance
	⇓ Cardiac output
	⇓ Stroke volume
Cerebral physiology	⇓⇓ $CMRO_2$
	⇑⇓ Vascular reactivity
	⇑⇓ Autoregulation
	⇓⇓ Blood flow
	⇓⇓ Blood volume
	⇓⇓ ICP
	⇓ CPP

Table 6.2: Selected Effects of Propofol. ⇓⇓ = consistently reduced across multiple studies, ⇓ = tendency towards reduction or a less significant effect, ⇑⇓ = no change or conflicting evidence, $ETCO_2$ = end tidal carbon dioxide, $CMRO_2$ = cerebral metabolic rate for oxygen consumption, ICP = intracranial pressure, CPP = cerebral perfusion pressure.

6.3.2 Pharmacodynamics

Propofol induces unconsciousness through activity on the γ-Aminobutyric acid A receptor (GABA$_A$) on cortical and subcortical inhibitory interneurones[159]. The systemic effects of propofol have been well documented [160-162] and are summarised in Table 6.2. Propofol meets a number of the requirements of the ideal drug for intravenous anaesthesia by providing a rapid, smooth induction without excitation or respiratory distress and quick recovery to clear consciousness without post-operative nausea and vomiting.

6.3.3 General Pharmacokinetics

The decline of plasma propofol concentration following an intravenous bolus dose or infusion has been well described and will be discussed in detail below in the context of disposition kinetics and existing PK models.

Propofol is highly bound to plasma proteins with 97-98% binding (predominantly to albumin) in both control patients and patients with known cirrhosis but maintained plasma albumin levels(163). In contrast, clinical situations resulting in a reduction in the plasma protein concentration, such as cardiopulmonary bypass, have been associated with a rise in the concentration of unbound propofol(164). This rise in the free fraction of the drug is thought to result in increased pharmacodynamic effect despite a stable whole blood concentration(165).

As well as being highly bound to plasma proteins, propofol is bound to erythrocytes. In whole blood samples, propofol has been shown to be 50% bound to erythrocytes, 48% bound to plasma protein and 2% free drug(166).

The metabolism of propofol is thought to be primarily hepatic. There is likely to be at least some contribution from other organs due to the fact that apparent systemic clearance only reduced by around 40% during the anhepatic phase of liver transplant(167). Some authors have argued for a significant role of the kidney in propofol metabolism(168), although this could not be confirmed through measurement of propofol concentration in renal artery and vein in a swine experiment(169). Similarly there is some discussion over the relative contributions of the small intestine, lung and brain in propofol metabolism(167, 170).

Analysis of the urine metabolite profile for propofol has demonstrated an important contribution of both glucoronidation and hydroxylation prior to excretion(171). Only a small amount of propofol is excreted unchanged in the urine.

6.3.4 Disposition Kinetics

The decline of the plasma concentration of propofol following an intravenous bolus dose can be mathematically modelled. The most commonly described pharmacokinetic model is the mammillary model(172). In this type of modelling, drug is delivered into a central compartment and then can either be redistributed to other tissue compartments or can be eliminated. The compartments do not represent real anatomical regions but rather groups of tissues that have similar blood flow and affinity for drug. Assumptions made by this type of modelling are that there is instantaneous mixing of drug delivered to the central compartment and there is uniform drug distribution within each peripheral compartment.

Several early studies investigated the disposition kinetics of propofol following an intravenous bolus dose and all described the kinetics using a three-compartment model(163, 173-175). These are a heterogeneous group of studies in that blood sampling was done from either arterial or venous systems, young and old patients were studied and propofol was either given alone or in combination with other drugs. However, key pharmacokinetic parameters were of a consistent magnitude and are summarised in Table 6.3.

The structure of a three-compartment mammillary model has already been shown in Figure 6.1. A three compartment model was selected because of the triphasic decline of propofol concentration (Figure 6.2). The first phase represents rapid decline due to a combination of elimination, redistribution to the second compartment and slower redistribution to the third compartment. The second phase represent slower decline due to a combination of elimination and redistribution to the third compartment when the central and second compartments are in equilibrium. The third phase represents a terminal elimination phase when the central compartment is in equilibrium with both the second and third compartments.

Reference	Sampling	Group (n)	V_1 (l)	Cl (l min^{-1})	Cl (ml min^{-1} kg^{-1})
Kay(173)	Venous	Males (6)	42.3	1.81	23.6
		Females (6)	36.1	1.8	29.1
Cockshott(174)	Venous	Control (6)	41.3	1.91	32.9
		Fentanyl (6)	21.8	1.29	23.7
		Halothane (6)	34.5	1.79	30.4
Kirkpatrick(175)	Venous	Young (12)	26.3	NA	27.7
		Elderly (12)	19.6	NA	23.2
Servin(163)	Arterial	Control (10)	20.6	2.30	NA
		Cirrhosis (10)	20.2	1.99	NA

Table 6.3: Key pharmacokinetic parameters from studies of the disposition pharmacokinetics of propofol following an intravenous bolus. n = number of patients, V_1 = central compartment volume, Cl = clearance from the central compartment.
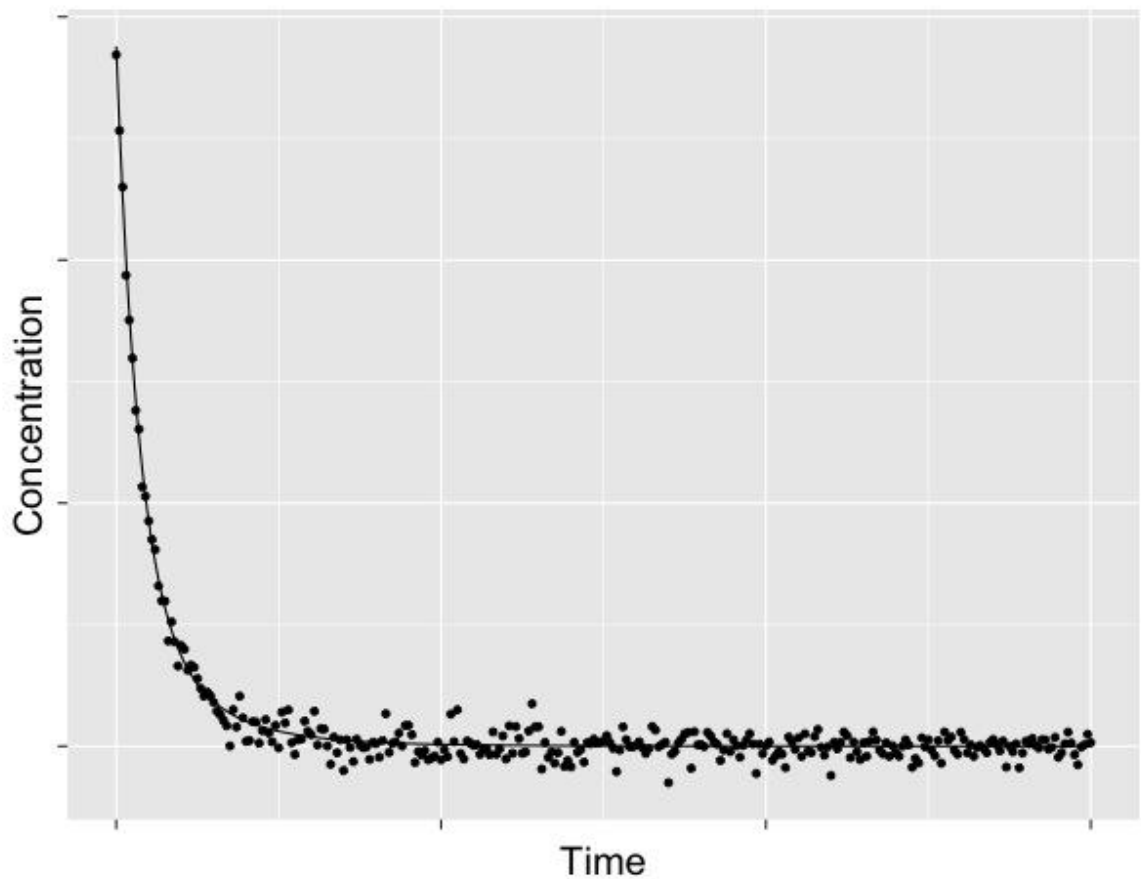
Figure 6.2: Simulated plot of the decline of propofol concentration following an intravenous bolus dose.

The tri-exponential decline of plasma propofol concentration according to the three compartment model can be described by the following equation:

$$C_p = Ae^{-\alpha t} + Be^{-\beta t} + Ce^{-ct} \tag{6.1}$$

where C_p is the plasma concentration and t is time. Following fitting of the curve to identify the constants A, B, C and a, b, c, these can then be used to calculate the compartment volumes and the rate constants that predict the rate of elimination from the central compartment and transfer of drug between the central and peripheral compartments. For example:

$$V_1 = \frac{D_0}{A + B + C} \tag{6.2}$$

$$k_{10} = \frac{a.b.c(A + B + C)}{A.b.c + B.a.c + C.a.b} \tag{6.3}$$

where V_1 is the volume of the central compartment and D_0 is the bolus dose of propofol administered and k_{10} is the rate constant for elimination from the central compartment (C_p or C_1). Clearance from the central compartment (Cl) can subsequently be calculated as:

$$Cl = k_{10}.V_1 \tag{6.4}$$

The two models currently available for TCI of propofol in clinical practice are the Marsh(6) and Schnider(176, 177) models. The development of these models and their significant differences shall be discussed in detail below.

6.4 Pharmacokinetic Models for Propofol

6.4.1 The Marsh Model

The Marsh Model is an adaptation of the pharmacokinetic parameters described by Gepts *et al* in two studies investigating the disposition kinetics of propofol following fixed rate infusions(178, 179). In the first of these studies(178), 18

patients were allocated to receive propofol at 3, 6 or 9 mg/kg/hr (in combination with regional anaesthesia) depending on the perceived clinical need. A radial artery cannula was inserted in the contralateral arm to the intravenous access and arterial blood samples were taken for quantification of whole blood propofol concentrations at regular time intervals. The tri-exponential model (Equation 6.1) was then fitted to the individual blood concentration datasets. Mean values calculated for V_c and Cl were 16.9 l and 1.77 l/min respectively.

In the second Gepts study(179), 11 patients received a constant rate propofol infusion (6 mg/kg/hr) in combination with an exponentially decreasing infusion of alfentanil to achieve general anaesthesia. As before, arterial blood samples were taken for propofol quantification and the tri-exponential model fitted. Mean values calculated for V_c and Cl were 19.7 l and 1.91 l/min respectively. White and Kenny described the process of incorporating a PK model into a computer controlled infusion device and using it to deliver propofol anaesthesia in 33 patients undergoing general surgery(180). In this publication they referred to the second Gepts paper(179) as the source of their PK model but did not print the exact model parameters. The publication by Marsh *et al*, the first paper to state the model parameters, was in fact a follow up study using the adult model to anaesthetise children(6). This "Marsh Model" was identical to the PK model published in the first Gepts paper(178), with the exception of a typographical error where the k_{12} was changed from 0.114 min^{-1} to 0.112 min^{-1} and a weight based value for V_c was incorporated (Table 6.3).

The 'Diprifusor™' was the first commercially available TCI device and used the Marsh Model (with a k_{12} of 0.114 min^{-1}). The technological challenges of developing this system and the rationale for selecting the Marsh Model over other published PK models have been discussed in detail by Glen(181). To allow predictions of effect site concentration, a k_{e0} of 0.26 min^{-1} was implemented with the model, although the reasoning for this decision was never published.

6.4.2 The Schnider Model
The development of the Schnider Model for propofol was entirely different from that of the Marsh Model. It was derived from a combined PKPD study in 24

healthy adult volunteers and published as separate PK(176) and PD(177) papers. Each individual received a 2 mg/kg bolus of propofol (or 1 mg/kg if aged over 65 years) and then one hour later received a randomly allocated fixed rate infusion of 25, 50, 100 or 200 mcg/kg/min for 60 minutes. Blood samples to quantify plasma propofol concentrations were taken from a radial artery cannula at frequent intervals following the bolus dose and during and after the fixed rate infusion. To assess the pharmacodynamic effects of propofol, the timing of loss of consciousness and return of consciousness were recorded along with a novel electroencephalogram (EEG) processing technique, known as semilinear canonical correlation, leading to calculation of a canonical univariate parameter for propofol $CUP_{propofol}$.

One of the end points of this study was to compare the pharmacokinetics of propofol with and without Ethylenediaminetetraacetic acid (EDTA). All individuals were therefore studied on two separate occasions. The PK model was constructed using plasma propofol concentrations collected during the infusions phase of the EDTA containing preparation. Fitting of a three compartment model to the data and the influence of subjects' covariates were calculated using non-linear mixed effect modelling (NONMEM)(182). The final model had a fixed central compartment volume, while compartment two was adjusted according to subjects' age (Table 6.4). k_{10} was adjusted according to subjects' weight, lean body mass (LBM) and height, while k_{12} was adjusted according to subjects' age. Calculation of LBM was done using the James formula:

Females:

$$LBM = 1.07 \times weight - 148 \times \left(\frac{weight}{height}\right)^2 \tag{6.5}$$

Males:

$$LBM = 1.1 \times weight - 128 \times \left(\frac{weight}{height}\right)^2 \tag{6.6}$$

and the implications of this will be discussed below(183). The PK study demonstrated that the pharmacokinetics of propofol differ after a bolus dose compared to an infusion. The presence or absence of EDTA did not effect propofol pharmacokinetics.

One of the primary purposes of the PD study was to develop a rate constant for equilibration between the plasma and effect site (k_{e0}). k_{e0} was calculated using both non-parametric and parametric techniques for each individual and then the median taken to represent the population value. For the non-parametric technique, measured plasma propofol concentrations were compared to the calculated $CUP_{propofol}$. For the parametric technique, plasma propofol concentrations predicted by their PK model were compared to the calculated $CUP_{propofol}$. The non-parametric k_{e0} was estimated to be 0.316 min^{-1}, while the parametric k_{e0} was estimated to be 0.456 min^{-1}. It was this parametric k_{e0} that the authors recommended for use with their PK model.

6.4.3 Significant Differences Between the Marsh and Schnider Models

There is considerable debate in the anaesthesia community over whether the Marsh or the Schnider PK Model is best suited to provide TCI of propofol in clinical practice. As mentioned above, the Diprifusor™ was the first commercially available TCI device and was programmed with the Marsh model to be used in a plasma targeting mode. The device only accepted specially designed syringes pre-filled with the Diprivan® formulation of propofol. Following the expiry of Diprivan® patent protection in Europe, a new generation of "Open TCI" devices were developed that could accept any syringe(184). These devices allowed the user to select different drugs to deliver along with a choice of PKPD model. It thus became possible to select either the Marsh or Schnider Model to be used in a plasma or effect site targeting mode.

The differences between the Marsh and Schnider Models have been discussed previously by Absalom *et al*(185). The structural components of the models are summarised in Table 6.3 and the most significant differences will be discussed in order below:

1. Central compartment volume (V_1)

The central compartment volume of the Marsh Model is proportional to total body weight. This means that the bolus dose of propofol required to achieve a chosen plasma target concentration will increase with weight. In the Schnider Model, the central compartment volume is fixed, meaning that for a chosen plasma target concentration, the bolus dose will be the same irrespective of weight, age or gender.

2. Adjustment for multiple patient covariates

The Marsh Model is a relatively simplistic PK model, where all body compartment volumes are proportional to weight, and all rate constants are fixed. The Schnider Model is a more complex model, which accounts for more patient covariates. The only compartment volume that varies with patient covariates is V_2, which is adjusted according to patient age. Similarly the rate constants k_{12} and k_{21} are influenced by patient age. The elimination rate constant k_{10} is adjusted according to body weight, lean body mass (and thus indirectly by gender, weight and height) and height. By accounting for more patient covariates, the Schnider Model could theoretically enable a more individualised dosing strategy.

3. LBM calculation

As mentioned above, the Schnider Model adjusts the elimination rate constant according to both body weight and LBM. A feature of the James formula for calculating LBM means that as body weight increases into the obese range, there is a paradoxical decrease in the calculated LBM. The consequence of this for the Schnider Model is that for a body mass index (BMI) of greater than 42 kg m^{-2} in males and 37 kg m^{-2} in females, there is an exponential increase in the magnitude of k_{10}. The ways that pump manufacturers have compensated for this irregularity in the model, that could lead to dangerous overdosing in obese patients, is summarised in a letter by Engbers *et al*(186).

4. Rate constant for effect site elimination (k_{e0})

In their original, clinically implemented forms, the Marsh Model has a k_{e0} of 0.26 min^{-1}, while the Schnider Model has a k_{e0} of 0.456 min^{-1}. The consequence of this difference is that the Schnider Model predicts more rapid equilibration between

the plasma and the effect site. This means that when using the Schnider Model in effect site targeting mode, TCI devices make more gentle manipulations of the predicted plasma concentration to achieve a desired effect site concentration.

Model Parameter	Marsh	Schnider
V_1	0.228 litre kg^{-1}	4.27 litre
V_2	0.463 litre kg^{-1}	18.9 - 0.391 x (age - 53) litre
V_3	2.893 litre kg^{-1}	238 litre
k_{10} (min^{-1})	0.119	0.443 + 0.0107 x (weight - 77) – 0.0159 x (LBM-59) + 0.0062 x (height-177)
k_{12} (min^{-1})	0.112	0.302 - 0.0056 x (age - 53)
k_{13} (min^{-1})	0.042	0.196
k_{21} (min^{-1})	0.055	[1.29 – 0.024 x (age - 53)] / [18.9 – 0.391 x (age - 53)]
k_{31} (min^{-1})	0.0033	0.0035
k_{e0} (min^{-1})	0.26	0.456

Table 6.4: Structural parameters of the Marsh and Schnider Models for propofol. V = compartment volume, k = rate constant, LBM = lean body mass as calculated by the James formula. Age is measured in years, weight in kg and height in cm.

A pragmatic approach recommended by most experts is to use the Marsh Model in plasma targeting mode and the Schnider Model in effect site targeting mode. Anaesthetists are encouraged to use the model with which they are most familiar and with caution if using TCI in a population of patients in whom the models have not been successfully validated.

6.4.4 The Covariates Model

The Marsh Model has been criticised for not taking into account patient covariates such as age and gender. Age is well known to have significant effects on body composition and hepatic and renal function, which influence the disposition and elimination of drugs(187). Indeed in one of the early studies of propofol pharmacokinetics following a bolus dose, Kirkpatrick *et al* compared patients aged 18 to 35 years old to those aged 65 to 80(175). The older patients had a significantly smaller central compartment volume and reduced clearance

of propofol. In a study of patients aged 65 to 91 years, who received a bolus followed by a fixed rate infusion of propofol, Vuyk *et al* demonstrated that compartment volumes and clearances were affected by gender(188) in this older age group.

In an attempt to further improve the understanding of the effects of age and gender on the pharmacokinetics of propofol, White *et al* conducted a large population study in patients undergoing anaesthesia using TCI propfol(5). The study will be described in some detail, as a validation of the PK model proposed by the authors is presented later in this thesis.

In 113 patients undergoing elective general surgery, anaesthesia was administered using the Marsh Model as implemented by the Diprifusor™ TCI device. Precise details of the propofol infusion required for anaesthesia were automatically archived. Patients also received an infusion of alfentanil, breathed a mixture of 66% nitrous oxide in oxygen and were given a single bolus of atracurium if endotracheal intubation was required. After induction of anaesthesia, a cannula was inserted into the arm contralateral to the propofol infusion to allow removal of intravenous blood samples at regular intervals. Whole blood propofol concentrations were measured using a gas liquid chromatography-mass spectrometry technique.

Using a NONMEM technique, the parameters of the Marsh model were optimised for each individual patient to provide the best prediction of the measured blood propofol concentrations. Only the volume of the central compartment and the clearance from the central compartment were adjusted as none of the other model parameters improved the goodness of fit by more than 2.5%. The relationship between age and central compartment volume for male and female patients volume is shown in Figure 6.3. The slopes of these regression lines are as follows:

Females:

$$V_1 = 191.78 - 0.669 \times Age \qquad\qquad (6.7)$$

Males:

$$V_1 = 175.5 + 0.046 \times Age \tag{6.8}$$

where V_1 is measured in ml kg^{-1} and age in years. In this population there was a very clear decline in central compartment volume with age in females but not in males.
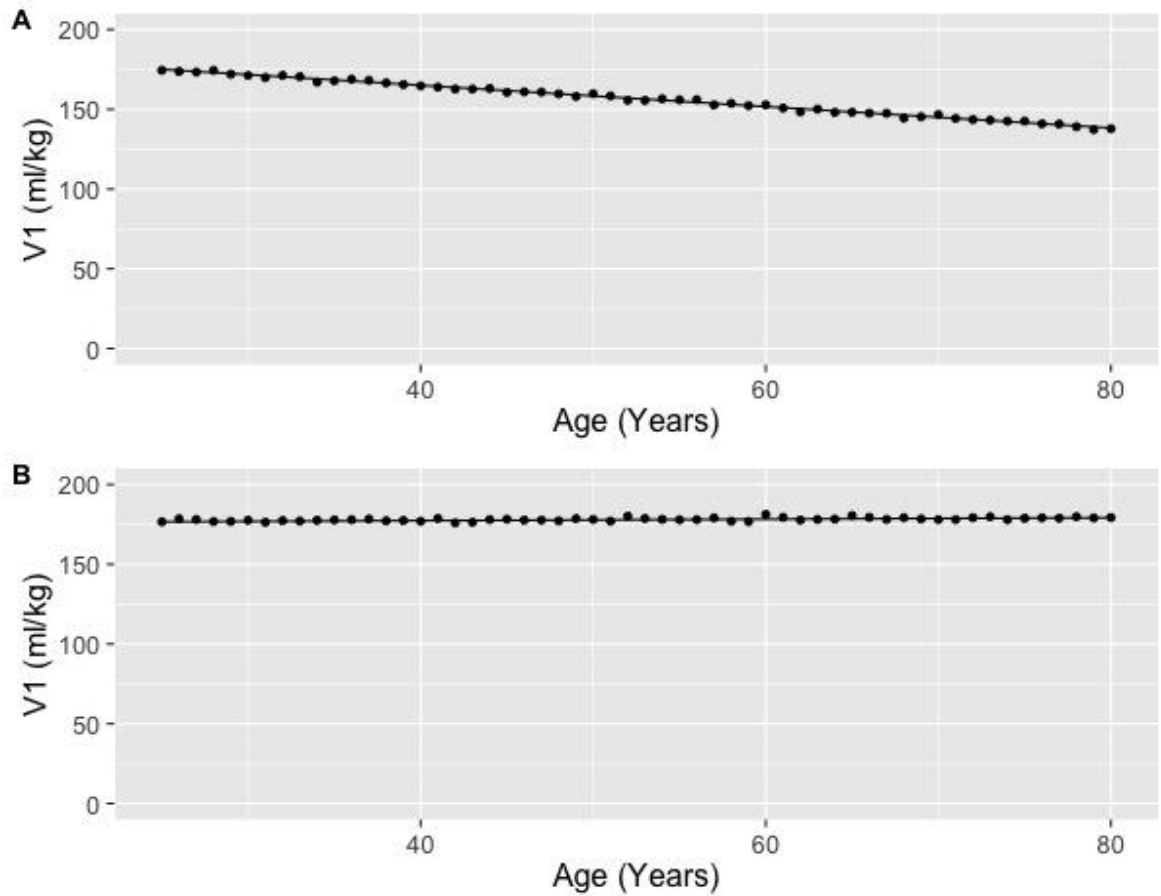
Figure 6.3: Simulated plot of V_1 against age for the Covariates Model in female (A) and male (B) patients.

Similarly, the relationship between age and clearance from the central compartment is shown in Figure 6.4 for females and males. The slopes of these regression lines are as follows:

Females:

$$Clearance = 37.87 - 0.198 \times Age \qquad (6.9)$$

Males:

$$Clearance = 26.88 - 0.029 \times Age \qquad (6.10)$$

where clearance is measured in ml kg^{-1} min^{-1} and age in years. Again there is a very clear decline in clearance from the central compartment with age in females but not in males.
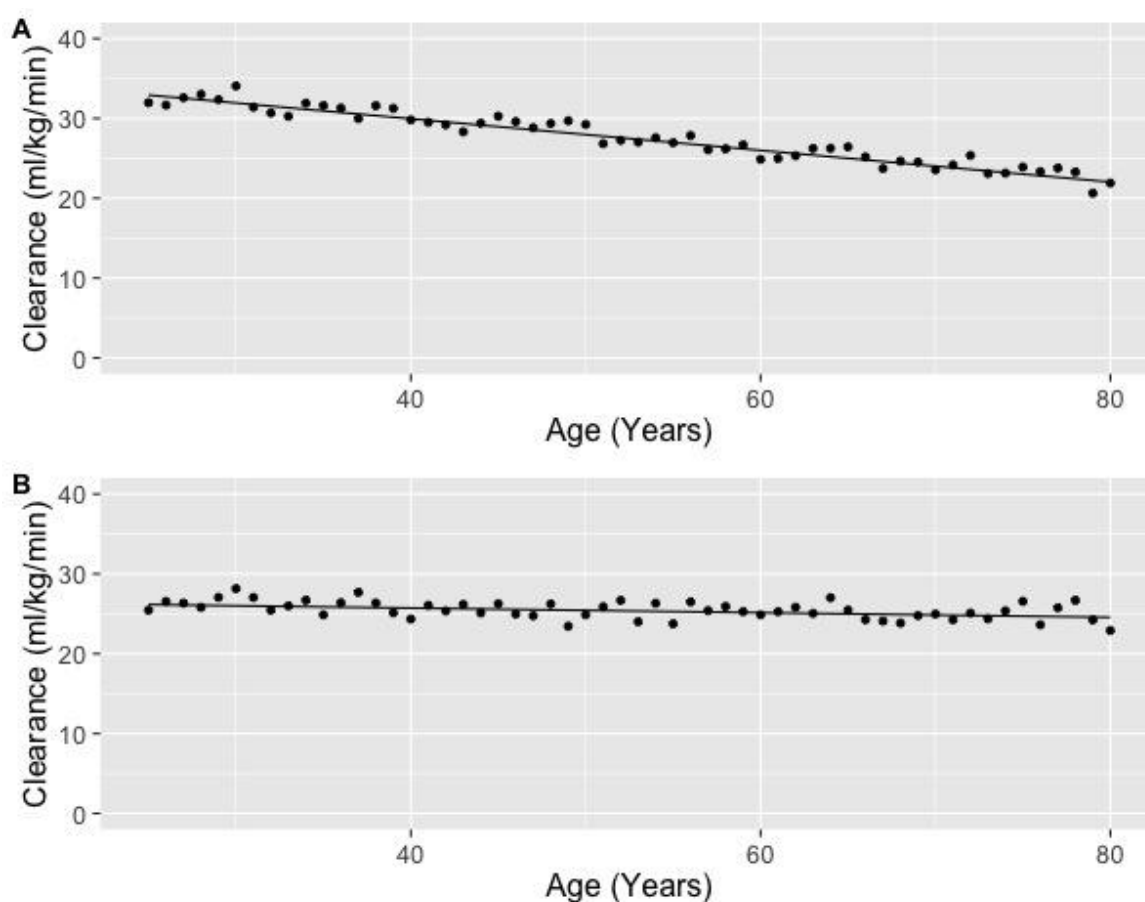
Figure 6.4: Simulated plot of clearance against age for The Covariates Model in female (A) and male (B) patients.

The revised "Covariates Model" thus maintained the original Marsh Model parameters but was optimised by the addition of gender and age covariates to adjust central compartment volume and clearance. The propofol infusion data

for each patient were then used to perform pharmacokinetic simulation of the blood concentrations predicted by the new model. In the study population, the predictions made by the Covariates Model were closer to the measured blood propofol concentrations than those predicted by the Marsh Model. The VASCoM Study had the primary objective of confirming this robust performance of the Covariates Model.

6.4.5 Physiologically Based Pharmacokinetic Models

Despite attempts to optimise compartmental PK models, it is well known that in the early phase after a bolus dose, they do not perform well in predicting plasma concentrations of anaesthetic drugs(189, 190). This is in part due to the erroneous assumption that there is instantaneous mixing of drug within the central compartment. There is also a failure to consider the effects of cardiac output and differing blood flow between organ groups. The development of physiologically based PK (PBPK) models attempts to address these deficiencies and thus improve the understanding of drug disposition.

An example of a PBPK model for propofol has been developed by Upton and Ludbrook(191). Their initial work was done using a chronically instrumented sheep model, where propofol concentrations were measured from the carotid artery and the sagital sinus following bolus injection into the right atrium(192, 193). The effects of propofol on cerebral blood flow and metabolism were measured by Doppler flow of the sagital sinus and oxygen extraction between the carotid artery and sagital sinus. Analysis of the data from these experiments allowed them to build a six compartment model that could explain the kinetics and dynamics of induction of anaesthesia with propofol(194, 195).

They subsequently developed the principles of their animal model using human data to define propofol kinetics and dynamics in a "standard" man. This model was a simplified version of the PBPK model, known as a recirculatory model. The necessary estimates of organ blood volume and blood flow for a 30 year old, 69 kg man were averaged from those derived from the Third National Health and Nutrition Examination Survey(196). The final model consisted of brain and lung sub-models in parallel with liver and fast and slow distribution compartments. The brain sub-model represented cerebral kinetics and dynamics derived from

experiments where arterial and jugular venous propofol concentrations were measured, along with processed EEG following a propofol infusion in man(197). To derive the lung sub-model, data from a study involving simultaneous measurement of pulmonary and radial artery concentrations of propofol following a central venous infusion were used(198). The remainder of the systemic model was built to fit the propofol concentrations predicted by the Schnider Model following rapid and slow infusions in a standard man.

One of the most interesting possibilities for PBPK models in general and for Upton and Ludbrook's model in particular, is the potential to improve our understanding of how changes in cardiac output or regional blood flow can effect the kinetics and dynamics of anaesthetic drugs. The approach used by Upton and Ludbrook also introduces many of the concepts that are explored in this thesis including data sharing between research groups and the continuous evolution and optimisation of physiological models.

6.4.6 Methodology for Pharmacokinetic Model Comparison

If one PK model for propofol was clearly superior in all clinical situations, then it can be assumed that all TCI devices would exclusively implement this model. As this has not been the case, it is necessary to have a framework to allow PK model comparison so that newly defined models can be compared against those already used in clinical practice in terms of their predictive performance. Following such a comparison, if the performance of the new model was significantly better than the existing models, there would be a reasonable case to support its introduction into clinical practice.

Varvel *et al* proposed an approach to allow systematic comparison of PK models used in TCI devices, referred to in the paper as computer controlled infusion pumps (CCIPs), that has become widely adopted in the anaesthetic literature(199). They tested their approach using a dataset collected during a study of CCIPs comparing the performance of two PK models for alfentanil(200). For 51 patients they had between 10 and 24 blood samples with measured alfentanil concentrations to compare to the concentrations predicted by the CCIP.

Central to their methodology was measurement of the performance error (PE). The PE represents the difference between the drug concentration measured in blood and the drug concentration predicted by the TCI device. It is calculated using the equation:

$$PE_{ij} = \frac{Cb_{ij} - Cp_{ij}}{Cp_{ij}} \times 100$$

(6.11)

where PE_{ij} is the percentage performance error i in the jth patient, Cb is the concentration measured in blood and Cp is the concentration predicted by the TCI device.

The PE is expressed as a percentage of the predicted concentration because this is felt to be of more clinical utility. If a summary measure for the size of the PE is known, then for a given predicted concentration the clinician can estimate the range of the associated blood concentration. The same would not apply expressing the PE as a percentage of the measured concentration, which is not known at the time the TCI device is being used in clinical practice.

Following calculation of the PEs for each sample in each individual, the authors advocate the calculation of four summary measures in each individual to describe the clinical utility of CCIPs. Firstly the median performance error (MDPE) represents the bias, or overall direction of the PEs, and thus the tendency of a CCIP to over or under-predict the blood concentration. Secondly the median absolute performance error (MDAPE) represents the inaccuracy, or overall magnitude of the PEs, and is not affected by the direction of the PEs. Thirdly divergence represents the tendency of PEs to either increase or decrease with time and is calculated from the slope of the linear regression of an individual's PEs against time. Finally wobble represents the variability of an individual's PEs and is calculated as the median absolute deviation of PEs from the MDPE.

The overall population performance of a CCIP requires further summarisation of the four summary measures described above. This can be done using either a two stage, pooled data or variance weighted approach. The two stage approach

simply takes a mean (or median) of all of the individuals summary measures. This inappropriately weights results towards individuals with fewer blood samples. The pooled data approach uses the number of samples for an individual to weight the contribution of that individual to the overall summary. Finally the variance weighted approach accounts for the intra-individual variability in PEs by weighting the contribution of an individual to the overall summary by the variance of the estimates for that individual. The authors suggest that in their analysis of several large datasets there is actually little difference in the summary measures calculated using each of the three approaches.

6.4.7 Pharmacokinetic Model Comparison Studies

The above methodology has been utilised in a number of studies to compare published PK models for propofol in their predictive performance. Coetzee *et al* randomly assigned 30 patients to receive propofol TCI by one of either the Tackley(201), Marsh or Dyck models(202). These were the same three models evaluated during the development of the Diprifusor™ in 1993. Arterial and venous blood samples were collected at regular intervals and the summary measures of MDPE, MDAPE, divergence and wobble calculated. Although all models provided adequate clinical anaesthesia, the Tackley and Marsh Models were superior in terms of MDPE and MDAPEs. It was noted that arterial propofol concentrations were significantly greater than venous concentrations but that this difference decreased with time.

Three recent simulation studies have compared the performance of the two PK models in common clinical use (Marsh and Schnider) and two of these included the Covariates Model introduced above(203-205). In the first, Glen *et al* used the standardised propofol infusion profiles from nine control patients (6 male and 3 female) in a previous PK study(163) to simulate the plasma concentrations predicted by each of the Marsh, Schnider, Covariates and Schuttler(206) Models(203). PEs were then calculated for a total 286 arterial propofol concentration measurements. In terms of overall performance there was little to differentiate between the four models. In this group, the Covariates Model had a tendency to over-predict the plasma concentrations compared to the Marsh Model but compared favourably in terms of MDAPE. Although the Schnider Model

showed negligible overall bias, there was a tendency to over-predict during the early phases of infusion and under-predict during the recovery phase.

In the second simulation study, Matsui *et al* used PK data from four previous studies, with distinct propofol infusion regimen(204). A total of 108 patients contributed PK data to the study, who had received propofol by either bolus(207), short infusion(208), long infusion(209) or TCI(202). Simulation studies were performed to calculate the plasma propofol concentrations predicted by each of the Marsh, Schnider and Schuttler PK models and an adaptation of the Upton physiologically based recirculation model(191). When all infusion regimen were taken into account, the Schnider Model more often displayed significantly better performance in terms of MDPE and MDAPE compared to the other models. This was particularly true when compared to the Marsh Model using data from the bolus and short infusion studies. All of the models performed with similar bias and inaccuracy when compared using data from the TCI study.

In the third simulation study, Glen and White(205) used data from 41 patients in a previous study evaluating the predictive performance of the Diprifusor TCI system(210). Predicted plasma propofol concentrations for each of the Marsh, Schnider and Covariates Models were calculated and PEs measured for a total of 530 arterial propofol samples. In this study, the MDPE of the Covariates Model was significantly improved compared to the Marsh and Schnider Models and the MDAPE was significantly improved compared to the Marsh Model. An important observation made by the authors was that for all three models, bias varied depending on whether plasma propofol concentration was increasing, steady or decreasing.

6.5   Pharmacodynamic Models for Propofol

6.5.1 Modelling the Effect Site

As part of their review "Contributions of PK/PD Modelling to Intravenous Anesthesia", Minto and Schnider described the theory of the effect site compartment in detail(155). The principles of the effect site and the techniques available to model its behaviour are central to the PD component of the VaSCoM study and will be considered below.

In response to the observation that the clinical effects of a drug are delayed relative to the plasma concentration (a fact that is well recognised by all practising anaesthetists), Sheiner *et al* proposed the concept of a hypothetical effect site compartment(211). The model parameter k_{eo} was introduced to characterise the delay between C_p and effect and therefore accounts for the processes of perfusion, diffusion, partition, drug-receptor interaction and the relationship between receptor occupancy and effect. In the original publication the nomenclature of k_{eo} was chosen to represent the rate constant for equilibration between the effect site compartment and "outside". It is now more generally referred to using more standardised PKPD terminology as k_{e0} or the rate constant for elimination from the effect site. The structural model proposed has been illustrated in Figure 6.1 and the association between drug infusion rate and predicted plasma and effect site concentrations illustrated in Figure 6.5.
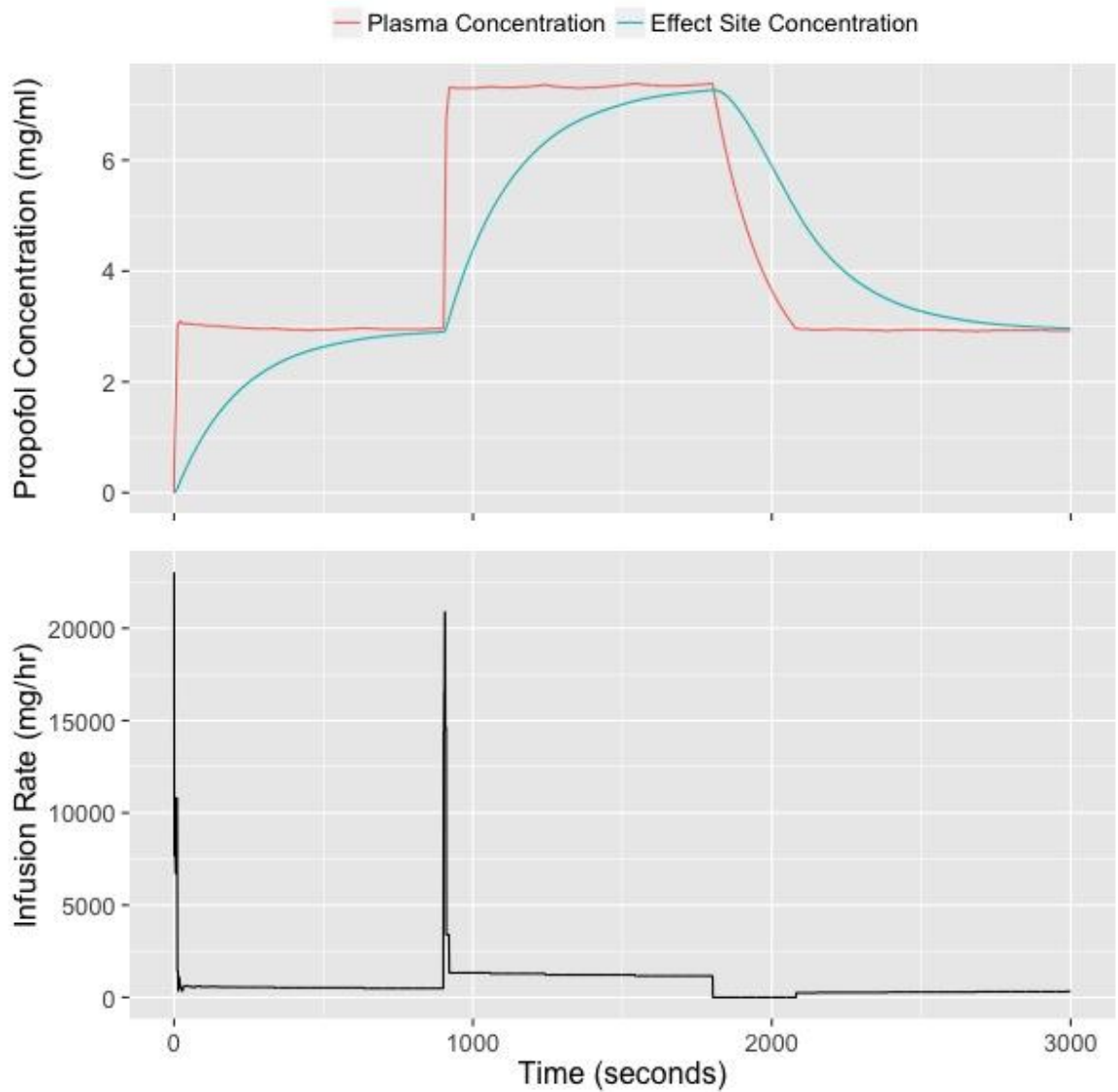
Figure 6.5: Lower panel provides details of propofol infusion regimen. Upper panel demonstrates associated plasma and effect site concentrations predicted by combined PKPD model.

Sheiner *et al* applied their PKPD model to three datasets containing plasma concentrations and associated measures of effect for the drug *d*-tubocurarine. They modelled the relationship between concentration of drug in the effect site compartment and clinical effect using the adaptation of the "Hill Equation" previously proposed by Wagner(212):

$$E = \frac{C_e{}^\gamma}{C_e{}^\gamma + C_e(50)^\gamma} \tag{6.12}$$

where E is the intensity of pharmacological effect expressed as a fraction of maximal effect, C_e is the concentration in the effect site, $C_e(50)$ is a constant giving the value of C_e at 50% effect and γ describes the sigmoidicity of the C_e to E relationship. For hypnotic anaesthetic drugs with an inhibitory effect on brain activity this can be expressed as:

$$E = E_0 - \frac{E_{max}C_e{}^{\gamma}}{C_e{}^{\gamma} + C_e(50)^{\gamma}}$$

(6.13)

where E_0 is the baseline effect with no drug present and E_{max} is the maximum difference from baseline. This sigmoid-E_{max} curve is demonstrated in Figure 6.6.
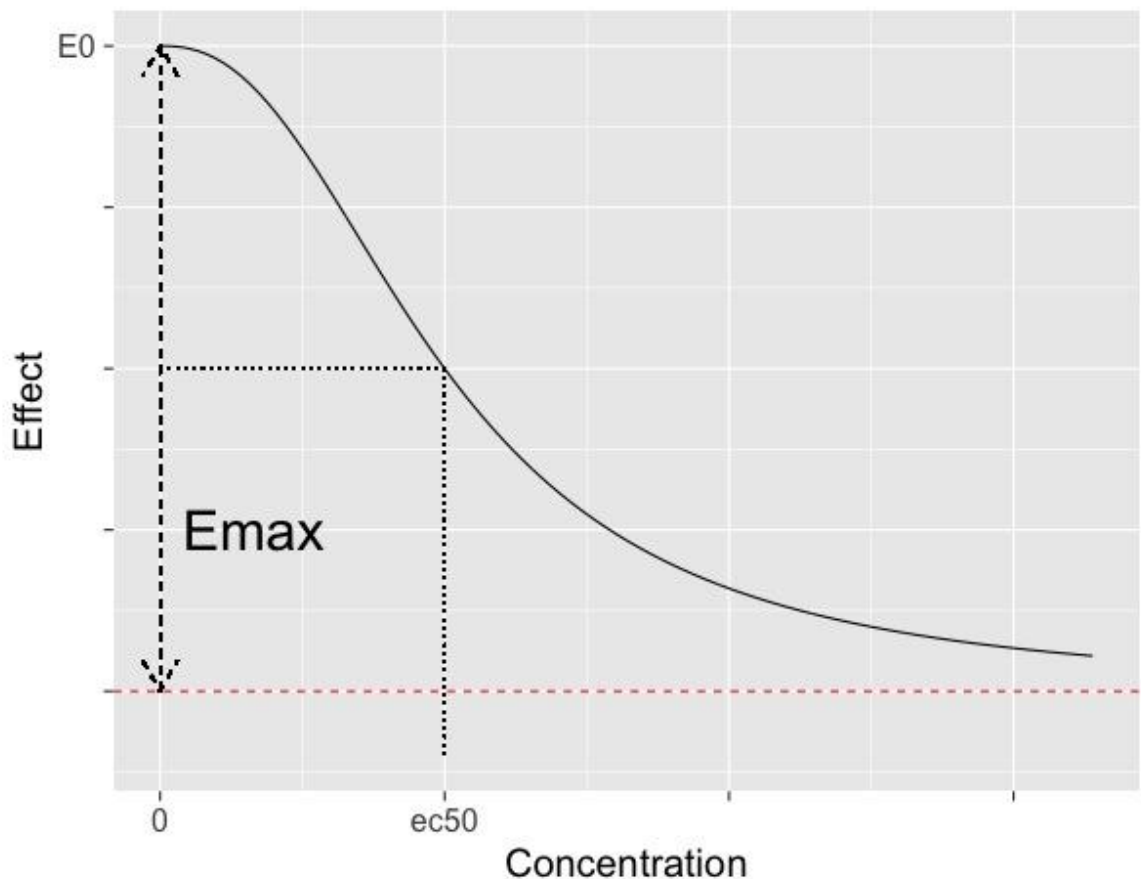
Figure 6.6: Sigmoid-E$_{max}$ Concentration-Effect relationship for a hypnotic anaesthetic drug where E0 = baseline effect with no drug present, Emax = the maximum difference from baseline, ec50 = a constant giving the value of Ce at 50% effect i.e. Ce(50).

The differential equation used to model the temporal relationship between C_p (or C_1) and C_e was:

$$\frac{\delta C_e}{\delta t} = k_{1e} C_1 - k_{e0} C_e \qquad (6.14)$$

where k_{1e} is the rate constant for movement of drug between the plasma and the effect site. The effect site is considered to be of negligible volume and therefore does not influence the behaviour of any associated PK model. For this reason the rate constant k_{1e} is inconsequential and the characterisation of the relationship between C_p and C_e can be described in terms of k_{e0} alone:

$$\frac{\delta C_e}{\delta t} = k_{e0} C_1 - k_{e0} C_e \qquad (6.15)$$

In their study of *d*-tubocurarine, Sheiner *et al* successfully fitted a two-compartment PK model to the data and determined the k_{e0} to describe the time course of the observed PD data. This is an example of parametric determination of the k_{e0}, where the effect site is related to the plasma concentration predicted by a contemporaneous PK model and the magnitude of effect is modelled as a known function of C_e.

It is also possible to determine k_{e0} using a non-parametric approach that makes no assumptions regarding the underlying PK model or the relationship between effect and C_e.(213). In this technique, k_{e0} is adjusted to account for the difference between measured plasma drug concentration and clinical effect. As for the parametric approach described above, this has the requirement to measure both plasma concentrations and pharmacodynamic effect within the same study.

An alternative approach, referred to as the 'time to peak effect site concentration' (t_{peak}), has been proposed by Minto *et al* and allows PD parameters from one study to be combined with PK parameters from another(214). Following a submaximal intravenous bolus dose, t_{peak} is measured as the time taken to reach the maximum observed clinical effect (and thus

maximum C_e). Using an existing PK model, it is then possible to adjust the associated value of k_{e0} to preserve the measured t_{peak}. Minto *et al* performed a number of simulation studies using data from previous PKPD studies of thiopental, remifentanil and propofol and demonstrated that the t_{peak} method provided a better estimate of k_{e0} than simply extending a new PK model by combining a k_{e0} value from a previous PKPD study.

In the Open TCI devices currently commercially available there are a number of very different implementations of k_{e0}. A recent editorial by Cortinez has acknowledged the confusion that this can cause in the clinical use of TCI and discussed the implications of differing k_{e0}s on the effect site concentrations predicted by these devices(215). In most of the studies estimating k_{e0}, an index of the electroencephalogram (EEG) has been used as a surrogate for the clinical hypnotic effect of propofol. The use of differing EEG indices is likely to account for at least some of the difference in the calculated k_{e0}s.

As indicated above, a k_{e0} of 0.26 min^{-1} for the Marsh Model was implemented in the original Diprifusor TCI device. Although the rationale for selection of this k_{e0} was never published, it was very similar to the k_{e0} of 0.2 min^{-1} calculated by Billard *et al* when comparing the Bispectral Index (BIS) to other indices of the EEG using a dataset from 12 patients who received a fixed rate propofol infusion (216). In a study using auditory evoked potentials (AEP) as a measure of the CNS effects of propofol, White *et al* used both parametric and non-parametric techniques to determine k_{e0}. Successful fits of ke0 could be achieved in 14 of the 22 patients using the population parametric approach and 15 of the 22 patients using the individual parametric approach. Mean k_{e0}s for the parametric and non-parametric approaches were 0.2 min^{-1} (median 0.16 min^{-1}) and 0.22 min^{-1} (median 0.24 min^{-1}).

The 'adjusted' k_{e0} often implemented with the Marsh Model is 1.21 min^{-1} and thus predicts much faster equilibration between the plasma and effect site compartments. This comes from using a t_{peak} for propofol of 1.6 minutes as reported by Schnider(177) to adjust the k_{e0}. In a short TCI infusion study of 120 female patients, with no period of decreasing plasma concentration, Struys *et al*

demonstrated that this adjusted k_{e0} more accurately predicts the measured changes in BIS(217).

As has been outlined previously, the parametric k_{e0} of 0.456 min^{-1} is suggested for effect site TCI using the Schnider Model. With the common availability of two PK models and three K_{e0}s clinicians must exercise caution during the use of Open TCI to ensure that they are aware of the pharmacokinetic and pharmacodynamic consequences of their model selection.

The PD component of the VaSCoM Study used the EEG index of BIS to estimate the appropriate k_{e0} to extend the Covariates PK Model. For this reason a brief summary of processed EEG (pEEG) and specifically BIS are provided below.

6.5.2 Processed Electroencephalography

The EEG is the measurement of bioelectric potentials resulting from the postsynaptic potentials produced by the dendrites of pyramidal neurones in the cerebral cortex(218). Needle or gel electrodes are required as transducers to convert the physiological ionic current to an electrical current for further processing by the EEG monitoring equipment. A formal EEG for diagnostic purposes uses a montage of electrodes attached across the whole scalp. For the purposes of monitoring the effect of anaesthetic drugs, gel electrodes connected across the forehead and temple are most commonly used.

Unlike the electrocardiogram (ECG), the EEG has no fixed repeating pattern. If the signal is processed in terms of its time and frequency domain characteristics, there are however some constant statistical properties that can be correlated with differing levels of wakefulness or anaesthesia. A number of depth of anaesthesia monitors (DoA) have been developed in an attempt to quantify the hypnotic component of anaesthetic drugs on the EEG. (219, 220). An effective device would help to prevent awareness under anaesthesia and avoid relative overdosing of anaesthetic drugs. Most DoA monitors attempt to provide an index of anaesthetic depth between 100 (fully awake) to 0 (no brain activity), with values of 40 to 60 often proposed to be adequate for surgical anaesthesia. In the ideal situation, these indices would correlate with clinical measures of anaesthetic effect and be stable across different anaesthetic drugs and clinical

populations. No DoA monitor yet meets these requirements but the BIS has become widely used in anaesthetic practice. Processing of the EEG signal is considered below in terms of BIS.

6.5.3 Calculating the Bispectral Index

The Bispectral Index is a complex parameter that integrates several separate descriptors of the EEG signal to provide a single index as above. It was developed by Aspect Medical Systems (subsequently owned by Covidien and now Medtronic) using data from 1500 anaesthetic administrations and was introduced in 1994. It uses a specialised four electrode sensor placed on the patients forehead to collect the raw EEG from one cerebral hemisphere. The underlying proprietary algorithm has never been published and has undergone continuous update, but the underlying principles of the signal processing have been described in detail by Sigl *et al*(221) and Rampil(218). The stages involved in calculating BIS are summarised in Figure 6.7.
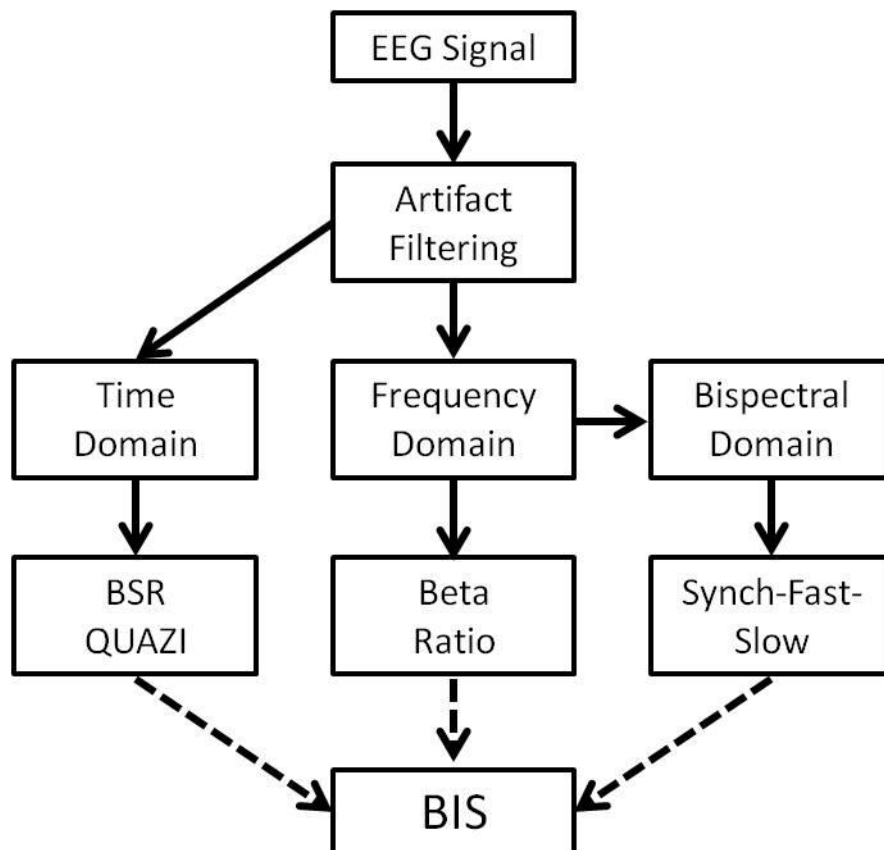
Figure 6.7: Summary of the processing steps involved in calculation of the Bispectral Index (BIS). BSR = burst suppression ratio, QUAZI detects burst suppression in the context of a wandering baseline voltage.

The first stage of EEG processing in BIS calculation involves filtering of high and low frequency artifacts and division of the signal into 2-s epochs. Further artifact filtering is then performed on these epochs to remove signals such as the ECG and electromyogram (EMG). Time domain analysis then uses two measures of burst suppression. During deep anaesthesia the EEG may develop the pattern of periods of normal or high voltage activity followed by periods of low voltage or isoelectricity. The burst suppression ratio (BSR) reports the periods of suppression of greater than 0.5 seconds as a fraction of the epoch length. In circumstances with a wandering baseline voltage, the "QUAZI" suppression index incorporates slow wave information to detect burst suppression that would be missed by the original BSR algorithm.

Fourier's theorem states that any complex repetitive waveform can be decomposed into the sum of simple sine or cosine waves (Figure 6.8). A computationally efficient method of performing this is known as the Fast Fourier transform (FFT). Each frequency component of the complex wave has an associated amplitude and phase component that can then be used for frequency domain analysis of the EEG. The frequency bands in the spectrum are named according to a generally accepted convention (Table 6.5).
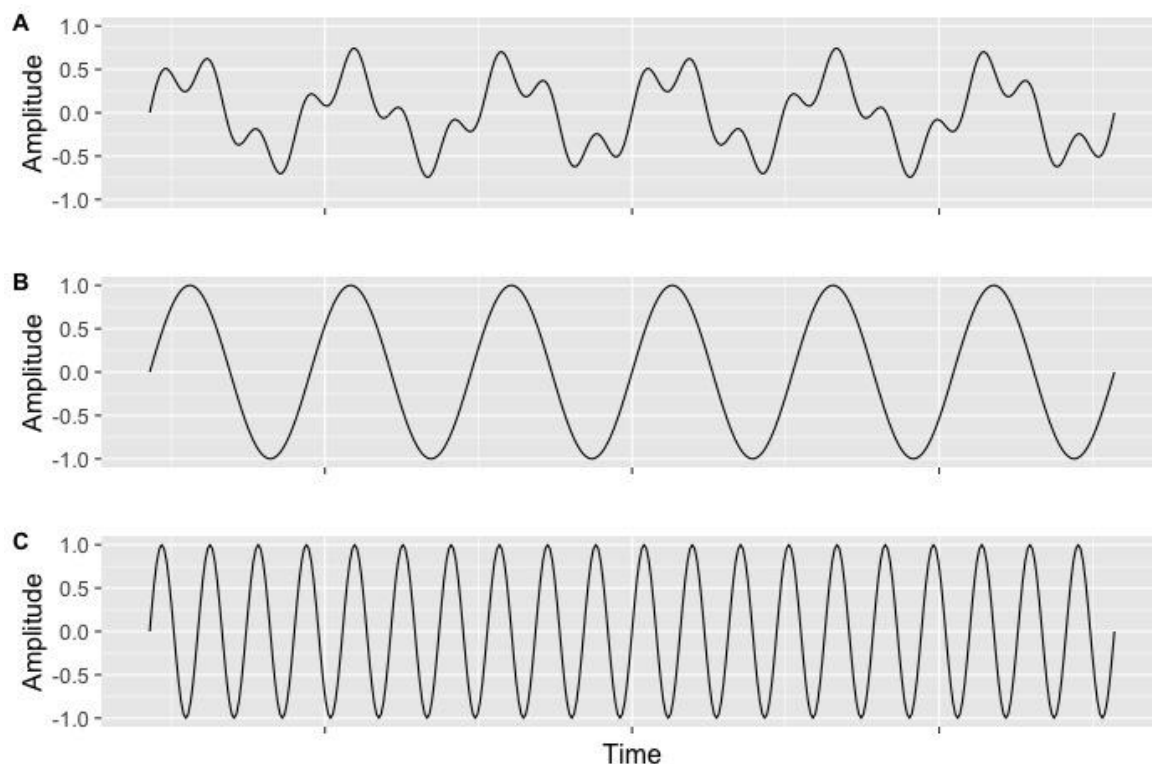
Figure 6.8: An example of Fourrier theorem that a repetitive wave (A) can be deconstructed to a series of simple sine waves (B and C).

Name	Frequency Range (Hertz)
Slow	< 1
Delta	1-4
Theta	5-8
Alpha	9-12
Beta	13-25
Gamma	26-80

Table 6.5: Spectral frequency bands of the EEG

The two measures of frequency domain analysis that contribute to the BIS Index are "BetaRatio" and "SynchFastSlow". BetaRatio is the log ratio of power in the frequency bands 30-47 Hz and 11-20 Hz. SynchFastSlow is the contribution from bispectral analysis. The bispectrum is a complex measurement of the phase relationships between selected frequencies identified following FFT. It has been suggested that strong phase relationships are inversely related to the number of EEG pacemaker elements.

The BIS Index results from a combination of the subparameters of BSR, QUAZI, BetaRatio and SynchFastSlow, each of which was selected to have a specific range of anaesthetic depth where it performs best. SynchFastSlow predominates during the excitation phase and during surgical levels of hypnosis. BetaRatio is weighted more heavily during light sedation and BSR and QUAZI detect deep levels of anaesthesia. Ultimately a single number (BIS) is continuously produced using averaging of preceding epochs, which predicts the depth of anaesthesia.

6.5.4 Clinical Validity of the Bispectral Index

In the United Kingdom, use of BIS in anaesthetic practice is supported by guidance from the National Institute of Health and Care Excellence (NICE)(222). In the diagnostics guidance (DG6, 2012), pEEG depth of anaesthesia monitors, with specific reference to BIS, are recommended as an option during the following clinical situations:

1. In patient groups at higher of risk of unintended awareness during general anaesthesia. These patients would include, but are not limited to, patients with a previous history of unintended awareness, patients with a history of drug or alcohol abuse or patients undergoing certain types of surgery such as airway surgery.

2. In patient groups at higher risk of excessively deep levels of anaesthesia. These patients would include older patients and patients with a history of cardiac, renal or liver disease.

3. In patients receiving total intravenous anaesthesia.

In the NICE guidance, the recommendations regarding BIS were based on a Cochrane review on "Bispectral Index for improving anaesthetic delivery and post-operative recovery"(223). It included 31 randomised controlled trials (RCTs) of BIS monitoring compared with standard clinical practice, but the NICE guidance acknowledged a large amount of heterogeneity between the trials with unintended awareness as an end-point. Two of these trials, on the basis of being the largest and most influential, merit further discussion.

The B-Aware trial was a multicenter RCT of 2463 surgical patients aged 18 yr or older who were at higher risk of awareness(224). Patients were randomized to BIS monitoring with target range of 40 to 60 or routine care. BIS values were manually recorded by the anaesthetist in the intervention group and there was no BIS monitoring in the control group. The primary outcome measure was the incidence of confirmed awareness by use of a structured questionnaire. Until 30 days after enrolment, the number of patients who reported awareness under anaesthesia was significantly less in the BIS group (2, 0.17%) than in the routine care group (11, 0.91%). This represented an odds ratio of 0.18 (95% confidence interval 0.02 to 0.84, p = 0.022) and absolute reduction in the risk of awareness of 0.74%, Therefore the number of high risk patients needed to treat to prevent one episode of awareness was 138. The rates of total intravenous anaesthesia with propofol were similar in the intervention and control groups (43% and 42%).

The BAG-RECALL trial(225) was itself a follow up to the B-Unaware trial which was criticised for being single centre and underpowered to exclude a clinically significant benefit attributable to BIS(226). Therefore BAG-RECALL was a multicentre RCT of 5713 surgical patients aged 18 yr or older who were at higher risk of awareness. Patients were randomized to BIS monitoring with a target range of 40 to 60 or volatile anaesthesia with a targeted minimum alveolar concentration (MAC) of 0.7 to 1.3. BIS and MAC values were recorded at minimum intervals of 1 minute by means of an electronic recording of anaesthesia data. The primary outcome measure was the incidence of intraoperative awareness. Until 30 days after extubation, the number of patients who reported awareness under anaesthesia was not significantly less in the BIS group (7, 0.24%) than in the control group (2, 0.07%). This represented an absolute difference of 0.17% (95% confidence intervals -0.03 to 0.38, p = 0.98) and thus superiority for the the BIS protocol was not demonstrated.

The BAG-RECALL study was performed only in patients undergoing volatile-based anaesthesia and thus does not exclude the possibility that BIS monitoring would lead to lower levels of unintended awareness during total intravenous anaesthesia. Indeed during the recently reported national audit project (NAP5), conducted by the Royal College of Anaesthetists, there was an approximate two-fold over-representation of awareness cases where a propofol infusion was used

for maintenance than would have been expected(227). This led the report authors to suggest that depth of anaesthesia monitors should be considered in patients undergoing TIVA with associated neuromuscular blockade.

One of the major limitations of all pEEG techniques used to monitor the depth of anaesthesia is the underlying assumption that all anaesthetic agents have the same effect on the EEG. Increasing doses of GABAergic anaesthetics (for example propofol) cause a shift in the spontaneous EEG from higher to lower frequency components and an increase in synchronisation. This is not necessarily the case for other agents that are known to increase the clinical depth of anaesthesia (for example ketamine and opioids). The EEG signatures of commonly used anaesthetic drugs and their neurophysiological bases have recently been reviewed in detail(228).

On the basis of the variable effects of anaesthetic drugs on the EEG, some commentators have suggested that it would be more valuable for anaesthetists to be trained to observe the raw EEG waveform than be dependent on the output of a pEEG device(229). Barnard *et al* demonstrated that anaesthetists could be taught to recognise the basic EEG changes associated with GABAergic anaesthetic drugs(230). Following a 15 minute tutorial, anaesthetists were able to categorize EEGs as awake, sedated, or anesthetized with comparable accuracy to the BIS monitor. The authors therefore suggested that the combination of pEEG and a clinician able to interpret the raw waveform would be of more value than a DoA monitor alone.

Despite the recognised limitations of BIS, the continuous nature of its output and its relatively well established place in clinical anaesthesia, mean that it was selected for monitoring of the effect site in the VaSCoM study.

6.5.5 Non-linear Mixed Effect Modelling
The standard technique used for the development of a PKPD model is known as non-linear mixed effect modelling (NONMEM)(231). The NONMEM® software, now distributed by ICON Development Solutions, was initially released by Lewis Sheiner and Stuart Beal at the University of California and has been in use for over 30 years(232). There is an extensive product literature explaining the

ongoing development and instructions on the use of NONMEM®(233). Owen and Fielder-Kelly have provided an excellent non-technical introduction to the principles underlying NONMEM analysis(234).

Non-linear mixed effects models involve both fixed and random effects. The fixed effects are the structural parameters of the PKPD model (such as compartment volumes and rate constants) and can be scaled according to patient covariates. The random effects account for unexplained inter-patient variability and the difference between the individual predicted values and the observations.

Therefore at the population level, the model predicted value (F) can be represented as a function:

$$F = f(\theta, n, x) \qquad (6.16)$$

where the model parameter θ, is scaled according to the covariates *x*, with inter-individual random variation η. At the individual level, the observation (Y) can be represented as a function of F:

$$Y = f(F, \varepsilon) \qquad (6.17)$$

where ε is the intra-individual variability. NONMEM® estimates the fixed and random effects parameters using a maximum likelihood approach(235).

While NONMEM® remains the industry standard for PKPD modelling, open source alternatives are becoming increasingly refined. Using a standard PK dataset, Tornoe *et al* have demonstrated that the R package n*lmeODE*(236) provides accurate parameter estimates, which are consistent with NONMEM®(237). This package was used in the VaSCoM study to provide population and individual estimates of the k_{e0} for the Covariates Model.

6.6 Summary of PKPD Modelling in the Context of the Covariates Model for Propofol

Target controlled infusion of propofol represents a significant component of anaesthetic practice in the United Kingdom. While the physicochemical properties and clinical effects of propofol make it particularly suitable for intravenous infusion, it is the development of pharmacokinetic pharmacodynamic models that has been instrumental in facilitating its clinical use in TCI. There is considerable debate over whether the Marsh or Schnider PKPD model for propofol is better. The Covariates Model represents a potential alternative to these models and has the advantage over the Marsh Model of adjusting for the additional patient factors of age and gender. The VaSCoM Study presented in the coming chapters provides a systematic validation of the Covariates Model and comparison to the Marsh and Schnider Models.

There has so far been no description of the pharmacodynamic component of the Covariates Model. The standard technique for extending a PK model to predict clinical effect is to describe the delay between plasma concentrations and clinical effect using the parameter of k_{e0}, or the rate constant for elimination from a theoretical effect site. Quantifying the magnitude of anaesthetic effect is typically performed using depth of anaesthesia monitors that use specialised algorithms to process the raw electroencephalogram. BIS is the most established of these monitors and has been used is conjunction with a non-linear mixed effects modelling approach to determine the k_{e0} for the Covariates Model.

7 Materials and Methods for the VaSCoM Study

7.1 Overview

This chapter provides a detailed description of the patients and methods used in the Validation Study of the Covariates Model (VaSCoM). The study protocol and related documents are available on request.

7.2 Objectives

The primary objective of this study was to prospectively validate the predictive performance of the Covariates Pharmacokinetic Model for propofol in the study population.

The secondary objectives were:
   a. Effect site modelling to obtain a k_{e0} value for the Covariate Model.
   b. Comparison of propofol concentrations measured in simultaneously sampled arterial and venous blood.

Comparison of the Covariates Model performance to that of the commonly used Marsh and Schnider models was not a stated objective of this study. Throughout the course of the study the question of which model is "best" did naturally arise. For this reason, simulation studies were performed to compare the three models.

7.3 Ethical Approval

Ethical approval was granted for the study by the West of Scotland Research Ethics Service on 9th April 2010 (Reference Number: 10/S0709/8). The study was sponsored by The Golden Jubilee National Hospital and supported by funding from The Department of Anaesthesia and Peri-operative Medicine Endowment Fund.

7.4 Summary of Study Design

The study was a single centre, randomised, non-comparative, validation study of the Covariates Model. The Medicines and Healthcare products Regulatory Agency confirmed that the study was not a Clinical Trial of an Investigational Medicinal Product. The aim was to enrol up to 50 adults with a goal of 30 completed cases. At least ten patients aged over 65 years were required to assess the validity of the model in an older population. The study protocol is summarised in Figure 7.1.

7.5 Patient Recruitment

Study participants were prospectively recruited from patients attending the Golden Jubilee National Hospital, Glasgow for elective surgery between 26th January 2011 and 10th June 2014. Included patients were over 18 years of age and undergoing non-cardiac surgery requiring general anaesthesia and expected to last more than 30 minutes.

Patients were approached during their pre-operative clinic attendance and provided with a Participant Information Sheet and a verbal description of the study procedure. They were either consented at this stage or allowed further time to consider their involvement prior to attendance on the day of surgery.

Patients were excluded from the study if they refused consent or were unable to consent on the basis of lack of capacity. If a patient was due to receive pre-medication or had received sedative or anaesthetic agents the preceding 12 hours they were excluded because of the potential impact on depth of anaesthesia monitoring. For similar reasons, patients with a history of excessive alcohol intake or illicit drug use were excluded. Patients were excluded if they had a body mass index (BMI) of greater than 35, predictors of a difficult airway or a history of allergy to any of the constituents of propofol.

7.6 Patient Monitoring

During conduct of the study protocol, all patients were cared for in either an anaesthetic room or operating theatre by a minimum of two anaesthetists or one anaesthetist and one appropriately trained physician's assistant for anaesthesia.

A skilled anaesthetic assistant was present at all times. Standards of monitoring provided by the Association of Anaesthetists of Great Britain and Northern Ireland (AAGBI) were followed(238). Monitoring was performed using the Draeger Primus anaesthetic machine with integrated monitoring (Draeger Medical UK Ltd.).

7.7   Study Procedure

7.7.1 Intravenous and Intra-arterial Access

Following confirmation of stable vital signs, all patients had an 18G or 20G intravenous cannula inserted into a large forearm vein to allow infusion of propofol. In the contra-lateral arm, a second 18G intravenous cannula was inserted to allow sampling of venous blood. A further cannula was then inserted into the radial artery on this side to allow sampling of arterial blood and beat-to-beat measurement of arterial blood pressure.

7.7.2 Electroencephalographic Monitoring

To allow modelling of the effect site, processed electroencephalography (pEEG) monitoring was performed. The monitor used in the study was the Bispectral Index (BIS XP A2000, Medtronic, Ireland) running software version 3.11 and with a smoothing rate of 15 seconds.

7.7.3 Synchronised Electronic Data Capture

Prior to initiation of the study protocol, the collection of continuous physiological data was confirmed. All routinely collected AAGBI standard monitoring data, invasive arterial blood pressure and details of all medications administered were recorded using the Recall digital anaesthetic record (Informatics, UK). pEEG data were streamed directly to a Dell Latitude Toughbook (Dell, USA) using the Anaesthesia Synchronisation Software (ASYS)(239) (provided by Nadja Bressan).

7.7.4 Propofol Infusion Regime

Propofol (Propofol Lipuro 2%, B. Braun Medical Ltd., UK) was infused using an Injectomat TIVA Agilia syringe pump (Fresinius Kabi, France) programmed with

the Covariates Model. Patency of the intravenous cannula was confirmed by concomitant slow infusion of compound sodium lactate solution. As described in the study protocol (Figure 7.1), patients were alternately randomised to either a 2-5-2 infusion or a 5-2-5 infusion. In the 2-5-2 group, an initial propofol plasma target concentration of 2 μg/ml was maintained for 15 minutes prior to an increase to 5 μg/ml for 15 minutes and finally a reduction to 2 μg/ml for 15 minutes. The reverse was performed in the 5-2-5 group.

The study procedure lasted around 45 minutes in total and was performed prior to the initiation of surgery. During this time, the patient remained spontaneously breathing via a face mask and the concentration of oxygen was titrated to maintain arterial oxygen saturations of at least 95%. Intravenous boluses of metaraminol 0.1 mg and glycopyrrolate 200 mcg were used to treat hypotension and bradycardia as clinically indicated. No medications that could interfere with the pharmacodynamics of propofol, such as volatile anaesthetics agents, benzodiazepines or opioids, were administered during the study procedure.

7.7.5 Blood Sampling Schedule

Throughout the study procedure, arterial and venous blood samples were drawn at pre-specified time points as indicated in Table 7.1. The sampling schedule was designed to allow comparison of arterial and venous propofol concentrations as well as to allow model validation close to plasma target changes and during stable anaesthesia.

Following collection of the final blood sample, the patient was prepared for their surgical procedure. Anaesthetic management from this stage onwards followed local procedures and guidelines and participation in the study did not influence the patient's ongoing clinical care.
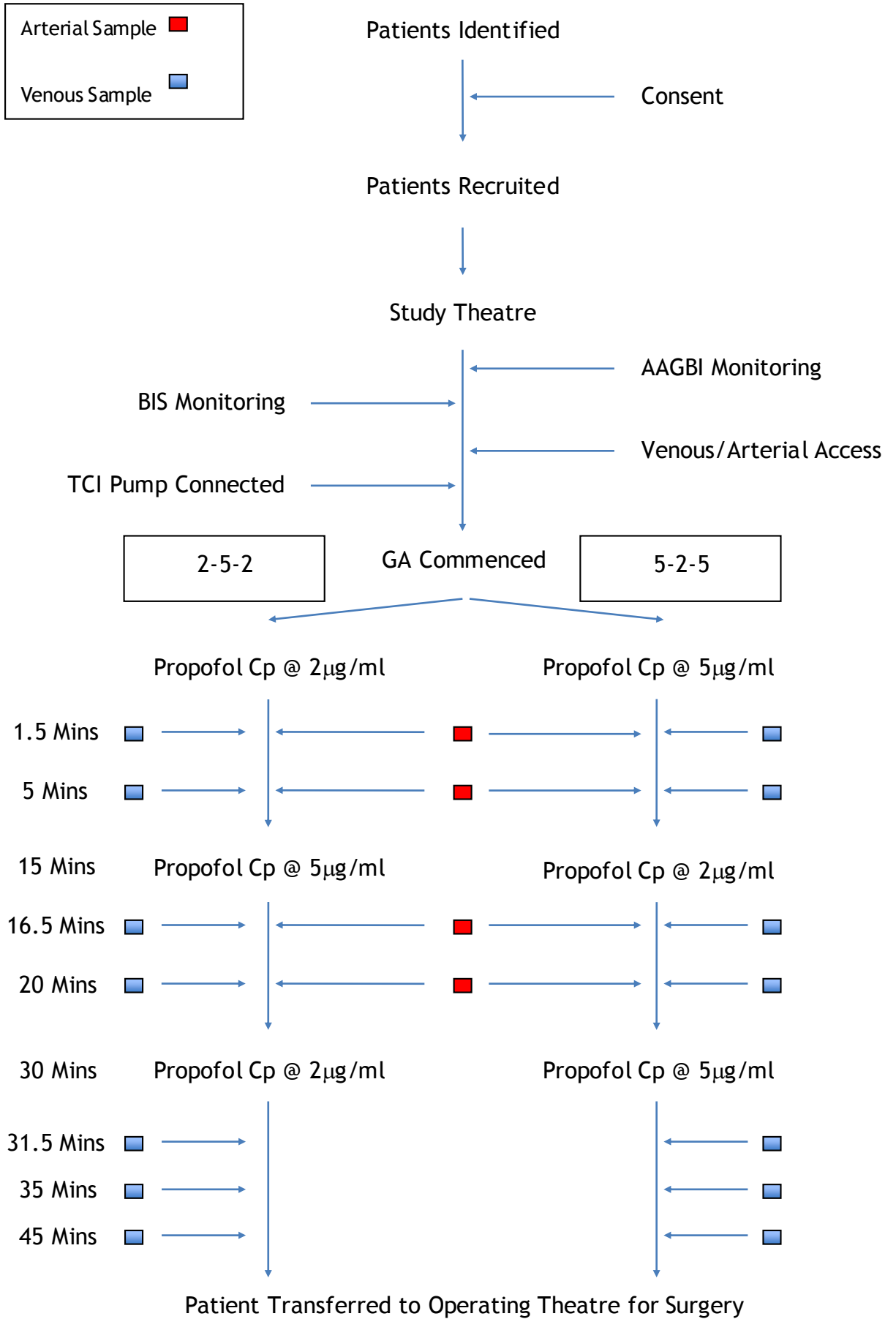
Figure 7.1 (previous page): VaSCoM study algorithm. AAGBI = Association of Anaesthetists of Great Britain and Ireland, BIS = Bispectral Index, TCI = target controlled infusion, GA = general anaesthesia, Cp = target plasma concentration.

Venous Samples		Arterial Samples	
Sample 1	90 seconds	Sample 1	90 seconds
Sample 2	5 minutes	Sample 2	5 minutes
Sample 3	60 – 90 seconds after change of target 1	Sample 3	60 – 90 seconds after change of target 1
Sample 4	20 minutes	Sample 4	20 minutes
Sample 5	60 – 90 seconds after change of target 2		
Sample 6	35 minutes		
Sample 7	45 to 60 minutes		

Table 7.1: Schedule for sampling of venous and arterial blood

7.7.6 Processing of Blood Samples

Arterial and venous blood samples were collected into a blood gas syringe to heparinise. The sample was then transferred into a fluoride oxalate sample bottle to provide stability prior to storage at 4°C. Propofol concentrations in whole blood samples were analysed by C3P Analysis using a validated whole blood high performance liquid chromatography (HPLC) technique(231).

7.8 Analysis

7.8.1 Introduction

The majority of data processing and analysis were performed using RStudio Version 0.98.1102 running R Version 3.1.2 (R Core Team, 2014)(7). Individual R Packages used for each stage of analysis are detailed in the appropriate

sections. The rationale for using R has already been discussed in the introduction to this thesis. All summary measures are reported as *median (range).*

7.8.2 Data Preparation

Infusion profiles from the Injectomat TIVA Agilia syringe pump were downloaded into Microsoft Excel (2007) using the software provided (Partner Agilia, Fresenius Kabi, France). The BIS recordings were exported from the ASYS software into Microsoft Excel. Similarly all arterial and venous blood results and individual patient demographic details were stored in Microsoft Excel. Data were then imported into R using the package *gdata*(240). Manipulation of data into a standardised format for ease of repeatable analysis was performed using the packages *dplyr*(135) and *stringr*(136).

7.8.3 Approach to Pharmacokinetic Model Validation

7.8.3.1   Introduction

The approach to pharmacokinetic model validation published by Varvel *et al* and discussed in the introduction to this thesis was adapted for use in this study(199). The measures of performance felt to be most relevant were "bias" and "precision". The calculations of these metrics as performed in this study are outlined below.

7.8.3.2   Percentage Performance Error

Prior to the calculation of bias and precision, it was first necessary to measure the percentage performance error for each of the arterial and venous blood samples. It was calculated using the equation:

$$PE_{ij} = \frac{Cb_{ij} - Cp_{ij}}{Cp_{ij}} \times 100 \qquad (7.1)$$

where *PE$_{ij}$* is the percentage performance error *i* in the *jth* patient, *Cb* is the concentration measured in blood and *Cp* is the concentration predicted by the TCI device.

7.8.3.3 Bias

The bias of a TCI device is its tendency to over or under predict the actual drug concentration. For each individual this was measured through the median performance error (MDPE), calculated as:

$$MDPE_i = median\{PE_{ij}, j = 1, ..., N_i\}$$ (7.2)

where N_i is the number of performance errors in the *ith* individual.

7.8.3.4 Inaccuracy

In a situation where a TCI device has the tendency to both under and over predict drug concentrations at different stages of the infusion, these PEs may compensate for each other and the bias may be negligible. The overall size of the PEs is thus better represented by the median absolute performance error (MDAPE), calculated as:

$$MDAPE_i = median\{|PE_{ij}|, j = 1, ..., N_i\}$$ (7.3)

7.8.3.5 Population estimates

Following calculation of MDPE and MDAPE for each individual, the TCI device performance was measured for the entire population by finding the overall medians:

$$MDPE = median\{MDPE_i, i = 1, ..., M\}$$ (7.4)

and

$$MDAPE = median\{MDAPE_i, i = 1, ..., M\}$$ (7.5)

where *M* represents the number of study participants. The disadvantage of this two stage approach to finding the population estimates is that MDPE and MDAPE may be known in some participants with more certainty than others. This was accounted for by weighting the calculation by the number of blood samples

performed in each patient, but without adjustment for the intra-patient variability.

7.8.3.6 Sample Size

There is no consensus agreement on the required sample size for this type of PK validation study. Similar published studies have recruited around 30 patients(241) and the same number was determined to be appropriate in this study.

7.8.4 Model Simulation

The TCI device infusion profile for each participant was used to simulate the propofol plasma concentrations predicted by each of the Covariates, Marsh and Schnider Models. For the interim analysis described below, this was first performed using the Tivatrainer software (Version 8.1)(242) to simulate the predictions made by the Covariates Model. Tivatrainer is a specialised pharmacokinetic simulation programme that has been used extensively in anaesthetic pharmacokinetic research. It does not however provide the flexibility of data manipulation and integration of multiple analyses that is provided by R. For this reason, the remainder of the simulation studies were performed using the *deSolve* Package in R, which provides the functions to solve ordinary differential equations as required in compartmental PK modelling(243).

The models were represented in R based on the standard three compartment open model:

$$\frac{\delta C_1}{\delta t} = dose + k_{21}C_2 + k_{31}C_3 - (k_{10} + k_{12} + k_{13})C_1 \tag{7.6}$$

$$\frac{\delta C_2}{\delta t} = k_{12}C_1 - k_{21}C_2 \tag{7.7}$$

$$\frac{\delta C_3}{\delta t} = k_{13}C_1 - k_{31}C_3 \tag{7.8}$$

where *dose* is the quantity of propofol delivered, C_1, C_2 and C_3 are the concentrations of propofol in the first, second and third compartments, k_{12}, k_{13}, k_{21} and k_{31} are the intercompartmental rate constants and k_{10} is the rate constant for elimination.

To ensure that the *deSolve* Package was providing accurate solutions to the modelling studies, the predicted plasma concentrations for the Covariates Model in the interim analysis were compared to the predictions provided by Tivatrainer. This was done using the same methodology as described with calculation of MDPE and MDAPE as measures of bias and inaccuracy.

7.8.5 Interim Analysis

An interim analysis of the study was performed following recruitment of ten male and ten female patients to the study to ensure that MDPE and MDAPE for the Covariates Model were within the expected ranges. This analysis revealed that the PEs were markedly higher in female patients than was anticipated. The decision was therefore made to perform a simulation study at this stage to ensure that the implementation of the Covariates Model by the Fresenius Injectomat TIVA Agilia syringe pump was accurate. Simulation study using both Tivatrainer software and the *desolve* Package revealed that the TCI device programming had been mis-specified and was therefore not appropriately implementing the Covariates Model in female patients (details are provided in the results section). This mis-specification was corrected by the manufacturer and following discussion with the Research Ethics Service, an additional ten female patients were recruited to the study.

7.8.6 Validation Study

Validation of the Covariates Model as implemented by the syringe pump was performed only in the participants who received the correctly specified model. Overall values for bias (MDPE) and inaccuracy (MDAPE) were calculated. Wilcoxon Signed Rank Tests were performed to compare PEs measured using arterial and venous sampling. A p-value of < 0.05 was regarded as significant.

Again using the Wilcoxon Signed Rank Test, specific comparisons were made between male and female patients and younger and older patients to confirm that adjusting the model by the covariates of age and gender resulted in consistent bias.

Finally, the effect of time since a change in target plasma concentration was explored. For arterial and venous samples, linear models were constructed to identify if there was a systematic change in bias with increasing time from a change in target concentration. The absolute difference was then calculated between each pair of PEs from arterial and venous samples (the a-v PE difference) and the magnitude of this difference modelled against time. All modelling was done using the *stats* Package in R(7) and details of the models selected are provided in the results section.

7.8.7 Model Comparison Study
Simulation studies were performed in the *desolve* Package using data from all patients to compare predictions made by the Covariates, Marsh and Schnider Models. Following calculation of the predicted plasma concentrations for each participant according to each of the models, their performances were compared using MDPE and MDAPE. The Friedman Rank Sum Test was used to compare all of the Covariates, Marsh and Schnider Models for a statistically significant difference in inaccuracy. The Nemenyi Multiple Comparison Test could then be used to determine which, if any, models were statistically different. Use of the Nemenyi multiple comparison test removes the need for post-hoc adjustment of p-values and therefore a p-value of <0.05 was regarded as significant.

For each of the models, similar comparisons as for the validation study were performed between female and male and younger and older patients to determine if there were any systematic differences in bias.

For arterial and venous blood sampling, models were compared at early (< 2.5 minutes), intermediate (> 2.5 minutes) and late (> 5.5 minutes) time intervals following a change in target plasma concentration. As above, statistical comparisons of model inaccuracies were performed using the Friedman Rank Sum Test with Nemenyi Multiple Comparison Test. For each of the PK models

there was then construction of linear models to determine systematic changes in bias with time and for a systematic change in the a-v PE difference.

7.8.8 Effect Site Modelling

The central role of the k_{e0} in effect site modelling and its determination using non-linear effect site modelling has been discussed in detail in the introduction. The appropriate k_{e0} for the Covariates Model had not been determined prior to this study. To perform effect site modelling using the standard parametric approach, it is necessary to simultaneously perform monitoring of the anaesthetic effect site while delivering anaesthesia using a validated PK model. In the first instance this meant using only data from patients in whom the correctly specified Covariates Model was delivered and an effect site monitoring profile (i.e. BIS) was available. The analysis was subsequently repeated using simulated PK data in all patients who had an effect site monitoring profile available.

The relationship between anaesthetic effect and the effect site concentration was assumed to be represented by the sigmoid E_{max} model described by Hill(244):

$$E = E_0 - \frac{E_{max}C_e{}^{\gamma}}{C_e{}^{\gamma} + C_e(50)^{\gamma}} \tag{7.9}$$

where E is drug effect, E_0 is the baseline effect with no drug present, E_{max} is the maximum difference from baseline, C_e is the effect site concentration, $C_e(50)$ is the drug concentration producing 50% of the maximum effect and γ describes the slope of the concentration-effect relationship. To describe the relationship between the predicted plasma concentration and the effect site concentration, a further differential equation was added to the existing three-compartment model:

$$\frac{\delta C_e}{\delta t} = k_{e0}(C_1 - C_e) \tag{7.10}$$

where k_{e0} is the rate constant for elimination from the effect site and models the delay between changes in C_1 and clinical effect.

The standard software used for PKPD analysis, and thus estimation of the best k_{e0} to describe drug behaviour in a population is NONMEM® (ICON Plc, Ireland). In this study, the R package nlmeODE(236) was used to perform non-linear mixed effect modelling using differential equations. As discussed earlier, this package has been shown to provide accurate parameter estimates, which are consistent with NONMEM estimates(237).

The analysis was performed in three stages. Firstly by allowing nlmeODE to fit the data by finding the best estimates of k_{e0}, E_0, E_{max}, EC_{50} and γ. Secondly by fixing E_{max} to 100, as this is the maximum anaesthetic effect measurable by the BIS device. Finally by fixing both E_{max} and E_0 to 100, as the theoretical BIS in all patients prior to starting anaesthesia is also 100. In each scenario, an overall population estimate (or fixed effect) as well as an individualised estimate (or random effect) for k_{e0} was provided.

8   Results of the VaSCoM Study

8.1   Overview

The principle results of the Validation Study of the Covariates Model (VaSCoM) for target controlled infusion of propofol are presented. The results are in four sections, relating firstly to an interim analysis, secondly to the pharmacokinetic (PK) validation study, thirdly to a pharmacokinetic PK comparison study and finally to the pharmacodynamic (PD) analysis.

8.2   Data Collection

8.2.1 Data Collection Period

The initial plan for the VaSCoM study was to recruit up to 50 patients to achieve datasets for 30 patients. Data collection took place during the period 26th January 2011 and 10th June 2014. Recruitment was significantly slower than expected for two reasons. The first was the fact that the vast majority of patients undergoing non-cardiac surgery at the Golden Jubilee National Hospital are anaesthetised using regional rather than general anaesthetic techniques. This reduced the pool of eligible patients. The second reason related to the complex logistics of the study requiring three clinicians and a separate clinical area to complete the study procedure without impacting on the efficient running of the theatre list.

As discussed in the methods section, the initial target sample size was increased to 40 to compensate for a calculation error programmed into the TCI device used. One patient was withdrawn from the study prior to any blood samples being collected because airway management became a priority. In addition, there was one female participant who was anaesthetised using the male algorithm. Ultimately there were 40 patients studied, with 29 participants anaesthetised using the correctly specified Covariates Model.

8.2.2 Patient Demographics

25 female patients were studied with median age of 45 (38 – 63) years and median weight of 63 (61 - 71) kg. For the 14 females anaesthetised using the correctly specified Covariates Model, these values were 45.5 (43.25 – 65.25) years and 63 (60.25 – 73.25) kg. There were 15 male patients studied with median age of 51 (43 – 66) years and median weight of 86 (78 – 97) kg. Table 8.1 summarises the demographic characteristics of each of the 40 participants and the infusion protocol that was used.

8.2.3 Blood Samples and BIS Profiles

Whole blood propofol concentrations were measured in 160 arterial blood samples and 274 venous blood samples. For patients who were anaesthetised using the correctly specified Covariates Model, there were 116 arterial samples and 199 venous samples. Bispectral index (BIS) profiles were available for 33 patients, 24 of whom were anaesthetised using the correctly specified Covariates Model.

ID	Model	Gender	Age (Yrs)	Weight (kg)	Height (cm)	Protocol
1	Mis_spec	f	54	66	160	a
11	Covariates	m	32	79	175	a
20	Covariates	m	29	86	180	b
21	Covariates	m	28	93	181	a
23	Mis_spec	f	43	62	161	b
27	Mis_spec	f	35	66	159	a
30	Covariates	m	53	117	185	b
35	Covariates	m	41	99	185	a
39	Covariates	m	51	99	175	b
47	Mis_spec	f	29	59	169	b
49	Mis_spec	f	52	62	166	a
55	Covariates	m	58	79	180	a
56	Covariates	m	46	95	175	b
60	Mis_spec	f	32	73	175	a
61	Mis_spec	f	49	80	171	b
62	Covariates	m	47	80	182	a
63	Covariates	m	45	120	192	b
65	Mis_spec	f	38	67	164	b
71	Mis_spec	f	30	61	171	a
72	Mis_spec	f	73	66	174	a
78	Covariates	f	51	49	156	a
81	Covariates	f	43	60	168	b
83	Covariates	f	46	58	171	a
84	Covariates	f	40	76	161	b
85	Covariates	f	45	63	162	a
87	Covariates	f	45	88	174	b
88	Covariates	f	44	63	159	a
90	Covariates male	f	69	51	164	a
95	Covariates	f	70	69	169	b
101	Covariates	m	65	68	173	b
107	Covariates	f	66	71	151	a
108	Covariates	m	75	75	172	b
110	Covariates	f	63	74	155	b
112	Covariates	f	35	62	167	a
114	Covariates	m	68	77	170	a
117	Covariates	m	67	95	179	a
119	Covariates	f	32	82	176	b
130	Covariates	m	67	73	177	b
132	Covariates	f	70	61	160	b
137	Covariates	f	68	54	158	a

Table 8.1: Demographics, PK model details and study protocol for each of the 40 patients studied in the VaSCoM study.

8.3 Interim Analysis

An interim analysis of data from the first ten male and ten female patients studied was performed and these were presented in June 2012 at the Anaesthetic Research Society Meeting, Aberdeen(245). MDPE and MDAPE were first calculated for the full cohort of patients. MDPE and MDAPE for venous samples were 10 (-49 to 52) and 23 (9 to 54), while MDPE and MDAPE for arterial samples were 27 (-33 to 89) and 34 (13 to 89). The bias and inaccuracy calculated were of a greater magnitude than was anticipated given the optimisation of the Covariates Model through the inclusion of age and gender covariates. To explore this further, separate analyses of male and female patients were performed and the results revealed a much larger performance error in female patients (Table 8.2 and Figure 8.1).

Measure	Female	Male
MDPE Arterial	49 (-33 to 89)	16 (-11 to 72)
MDAPE Arterial	49 (26 to 89)	23 (13 to 72)
MDPE Venous	8 (-49 to 52)	15 (-6 to 29)
MDAPE Venous	40 (12 to 54)	23 (9 to 31)

Table 8.2: Interim results with MDPEs and MDAPEs for venous and arterial sampling in males and females.
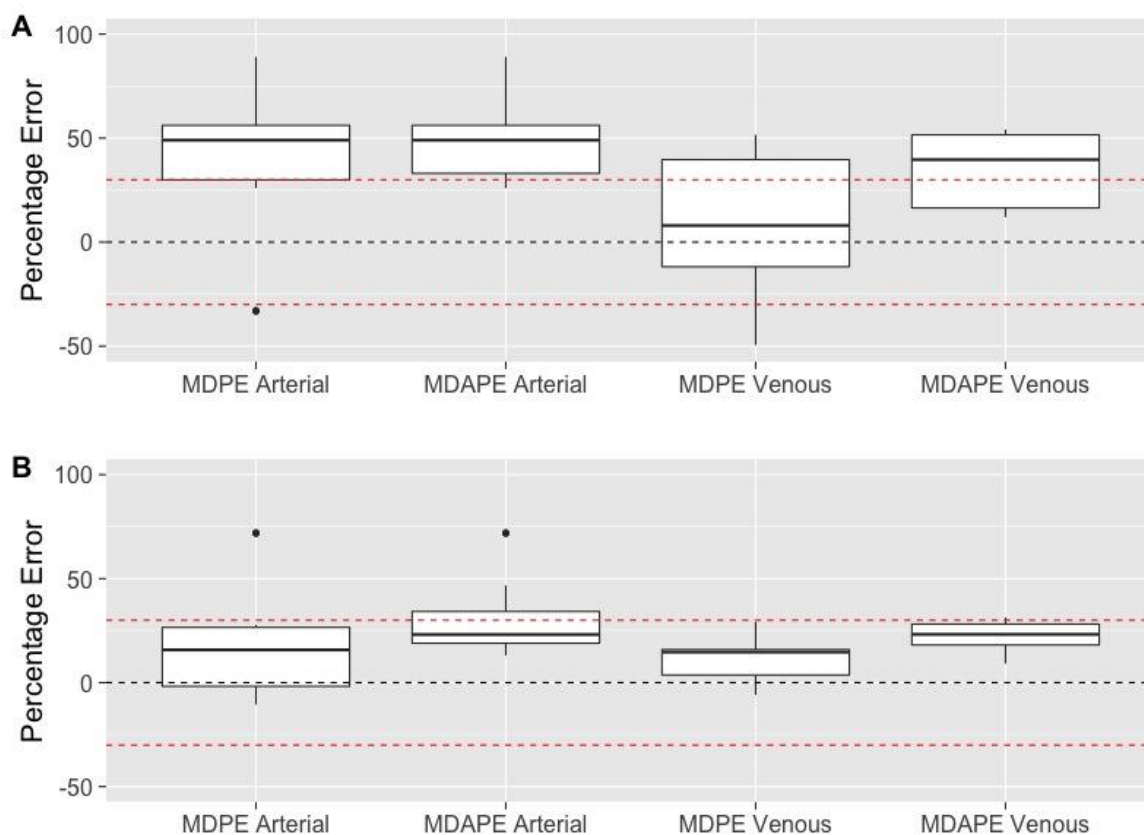
Figure 8.1: Boxplots demonstrating the range of MDPEs and MDAPEs for arterial and venous sampling for females (A) and males (B) in the interim analysis of pump performance.

On the evidence of the MDPE for arterial sampling in females there seemed to be a systematic under prediction of the measured propofol concentrations by the Covariates Model as implemented by the Fresenius Injectomat TIVA Agilia syringe pump. Sample plots of predicted concentrations with measured arterial and venous blood concentrations for female patients anaesthetised using both protocol a (2-5-2) and protocol b (5-2-5) supported this hypothesis (Figure 8.2). This systematic error could be related to either a bias within the Covariates Model itself, or a mis-specification of the Covariates Model within the syringe pump. To elucidate this further, it was necessary to perform simulation studies for each of the patients so far recruited and compare the predicted concentrations from the simulations to those downloaded from the syringe pump (Figure 8.2).
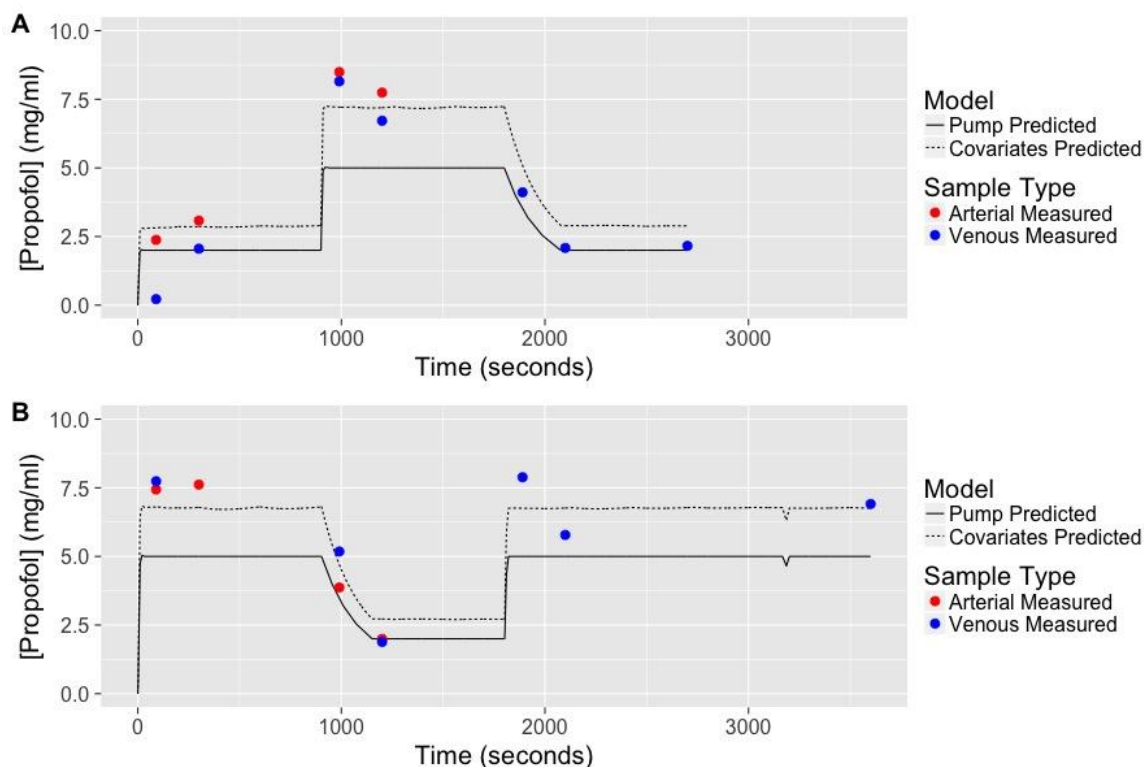
Figure 8.2: Predicted concentration profiles for female patients who had propofol infusions delivered according to protocol a (A) and b (B) for the mis-specified Covariates Model. The measured arterial and venous blood concentrations have been plotted to indicate the significant discrepancy between measured and predicted values. The concentrations predicted by a simulation of the correctly specified Covariates Model are plotted for comparison.

The simulation studies were performed using both the Tivatrainer software and the *deSolve* Package in R with identical input parameters. Performance errors between the concentration predictions made by Tivatrainer and those made by the syringe pump were plotted against time (Figure 8.3). It became immediately clear that in female patients the syringe pump was systematically predicting lower concentrations than those expected by Tivatrainer. This was supported by a MDPE of 35 (23 to 69) and a MDAPE of 35 (23 to 69) in females. There was systematic under prediction of concentrations in males but to a much smaller degree with a MDPE of 5 (3 to 6) and a MDAPE of 5 (3 to 6) (Figure 8.4).
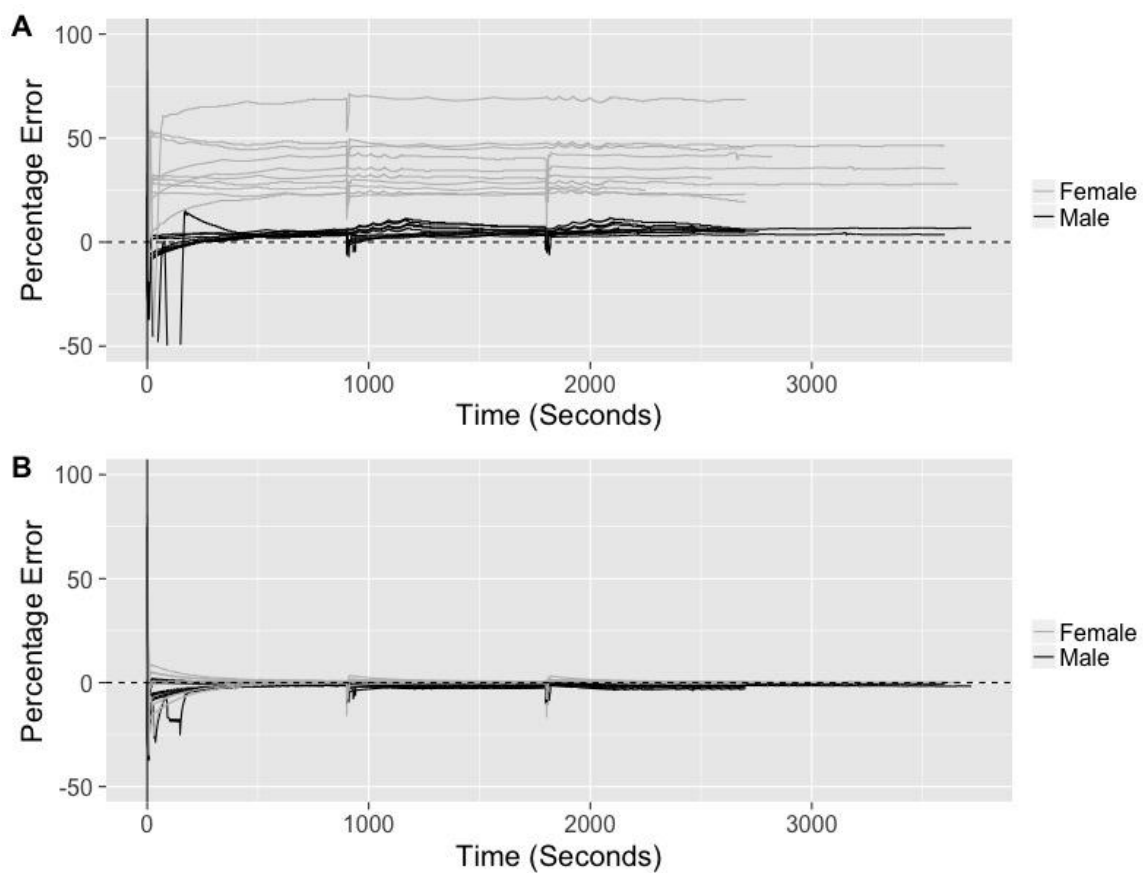
Figure 8.3: Performance error plotted against time for ten male and ten female patients comparing simulated predictions made by Tivatrainer and (A) the predictions made by the syringe pump and (B) the simulated predictions made by the *deSolve* Package.
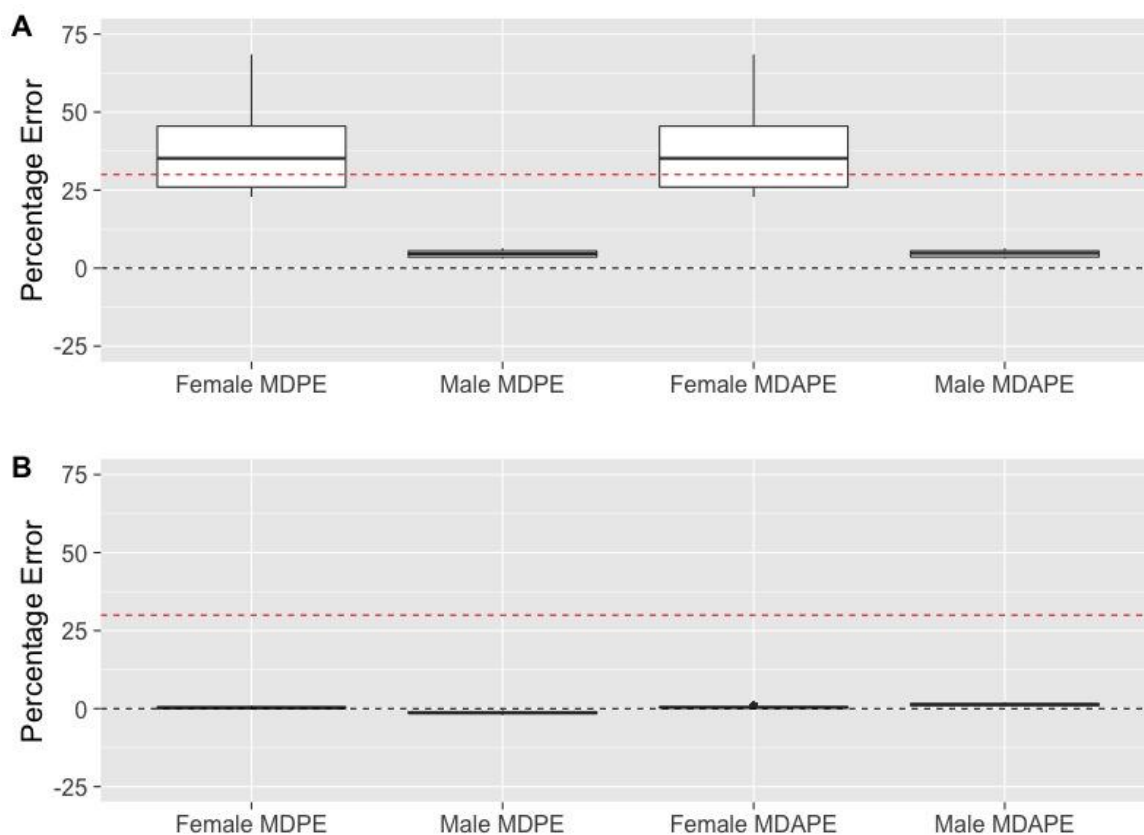
Figure 8.4: Comparison of MDPE and MDAPE for female and male patients between predictions made by Tivatrainer and (A) the predictions made by the syringe pump and (B) the simulated predictions made by the deSolve package.

On the basis of the significant and systematic error between propofol concentration predictions made by the syringe pump and both the measured values and the predictions made by Tivatrainer, the VaSCoM study was put on hold. A review of the input parameters to the Covariates Model as implemented by the syringe pump was performed and revealed a simple arithmetic error. Calculation of the central compartment volume should have been implemented as:

$$V_1 = 191.78 - 0.669 \times Age \tag{8.1}$$

but had instead been implemented as:

$$V_1 = 191.78 + 0.669 \times Age \tag{8.2}$$

with the consequence of increased doses of propofol being delivered to fill the larger compartment volume. All of the syringe pumps used in the study were re-programmed with the correctly implemented model, and following liaison with the Research Ethics Committee a plan was made to recruit an additional 10 female patients to the study.

The results of the simulation studies performed comparing the predictions made by the *deSolve* Package to those made by the syringe pump gave essentially identical results to those using Tivatrainer. Indeed when the performance error between predictions made by Tivatrainer and those made by *deSolve* were plotted against time there was no real systematic difference identified (Figure 8.3). This conclusion was supported by calculation of a MDPE of 0 (-2 to 1) and MDAPE of 1 (0 to 2) (Figure 8.4). On the basis of these results, all subsequent simulation studies were performed using the *deSolve* Package due to the ability to more quickly and efficiently perform multiple simulations.

8.4 Validation Study Results

8.4.1 Overall Validation Results

The results presented below relate to a comparison between the measured arterial and venous propofol concentrations and the concentrations predicted by the syringe pump. Only data from the 29 patients anaesthetised using the correctly specified Covariates Model with the correctly implemented Covariates Model were included in the analysis. These results were presented in part in September 2016 at the World Congress of Anesthesiologists, Hong Kong(246). Overall the implemented model seemed to perform with a reasonable degree of bias and inaccuracy with a MDPE of 9 (-45 to 82) and MDAPE of 24 (9 to 82) for arterial samples and MDPE of -8 (-64 to 70) and MDAPE of 23 (9 to 70) for venous samples (Figure 8.5). There was a statistically significant difference between PEs for each arterial and venous blood sample ($p < 0.0001$) and between the arterial and venous MDPEs for each patient ($p < 0.001$) as tested by the Wilcoxon Signed Rank Test.
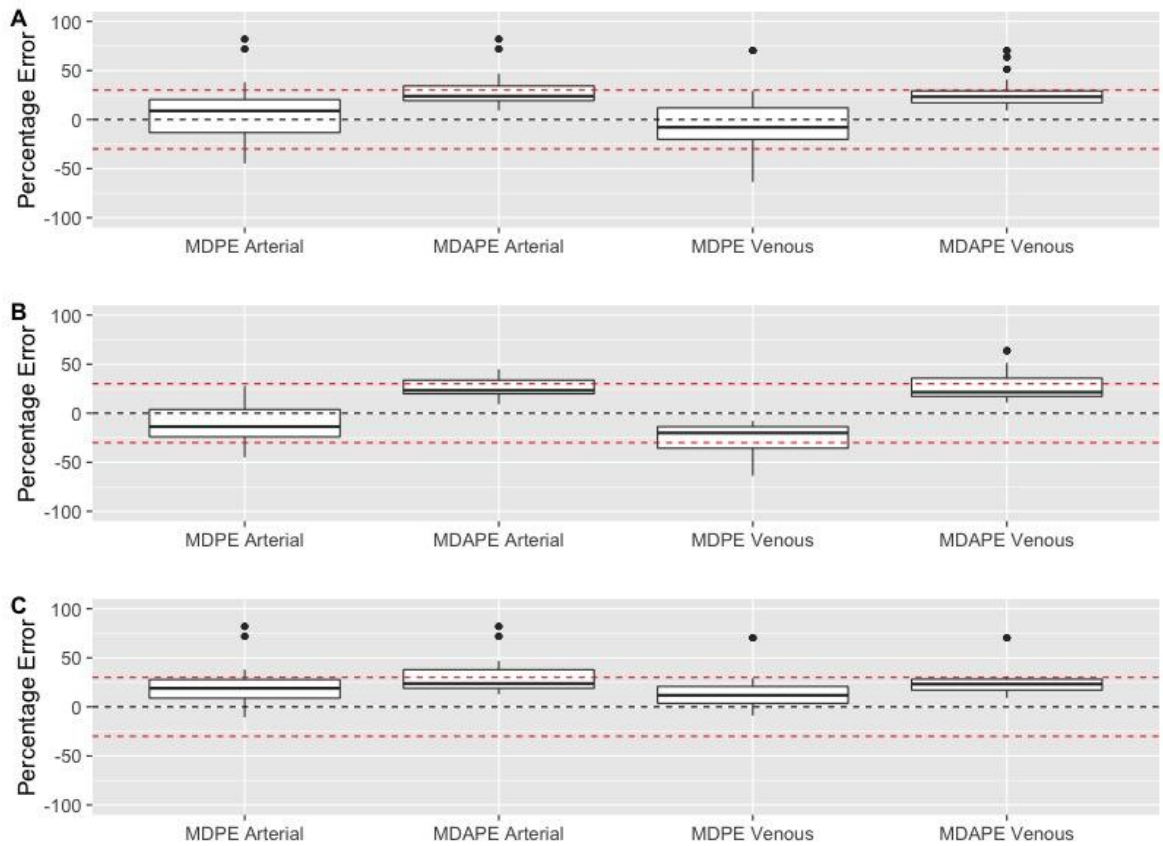
Figure 8.5: Validation study results showing MDPE and MDAPE for arterial and venous samples in (A) the overall population, (B) female patients and (C) male patients.

8.4.2 Female and Male Patient Comparison

On examination of the results for female and male patients, there appeared to be a tendency for the predicted concentrations to be higher than the measured concentrations in female patients but lower than predicted concentrations in male patients (Table 8.3 and Figure 8.5). This was confirmed by significant Wilcoxon Signed Rank Tests comparing MDPEs for female and male patients on arterial (p < 0.001) and venous (p < 0.0001) samples. The result of these opposing biases (over prediction in females and under prediction in males) was that the overall population bias was reduced to nearer to zero.

Measure	Female	Male
MDPE Arterial	-14 (-45 to 28)*	19 (-11 to 82)*
MDAPE Arterial	23 (9 to 45)	24 (13 to 82)
MDPE Venous	-20 (-64 to -8)*	12 (-9 to 70)*
MDAPE Venous	21 (11 to 64)	23 (9 to 70)

Table 8.3: Final validation results with MDPEs and MDAPEs for venous and arterial sampling in females and males. * Denotes statistically significant difference between MDPEs in females and males.

8.4.3 Younger and Older Patient Comparison

There was no clear systematic difference in the bias of model predictions between younger (aged under 65 years) and older patients (Table 8.4). This was confirmed by non-significant Wilcoxon Signed Rank Tests comparing MDPEs for younger and older patients on arterial ($p = 0.36$) and venous ($p = 0.80$) samples. There was a tendency for older age to emphasise existing differences in bias between female and male patients as supported by arterial MDPEs of -12 (-43 to 18) and -23 (-45 to 28) in younger and older females and 16 (-11 to 72) and 27 (13 to 82) in younger and older males (Figure 8.6).

Measure	Younger	Older
MDPE Arterial	1 (-43 to 72)	20 (-45 to 82)
MDAPE Arterial	22 (9 to 72)	27 (13 to 82)
MDPE Venous	-6 (-64 to 29)	-9 (-51 to 70)
MDAPE Venous	22 (9 to 64)	24 (10 to 70)

Table 8.4: Final validation results with MDPEs and MDAPEs for venous and arterial sampling in younger and older patients.
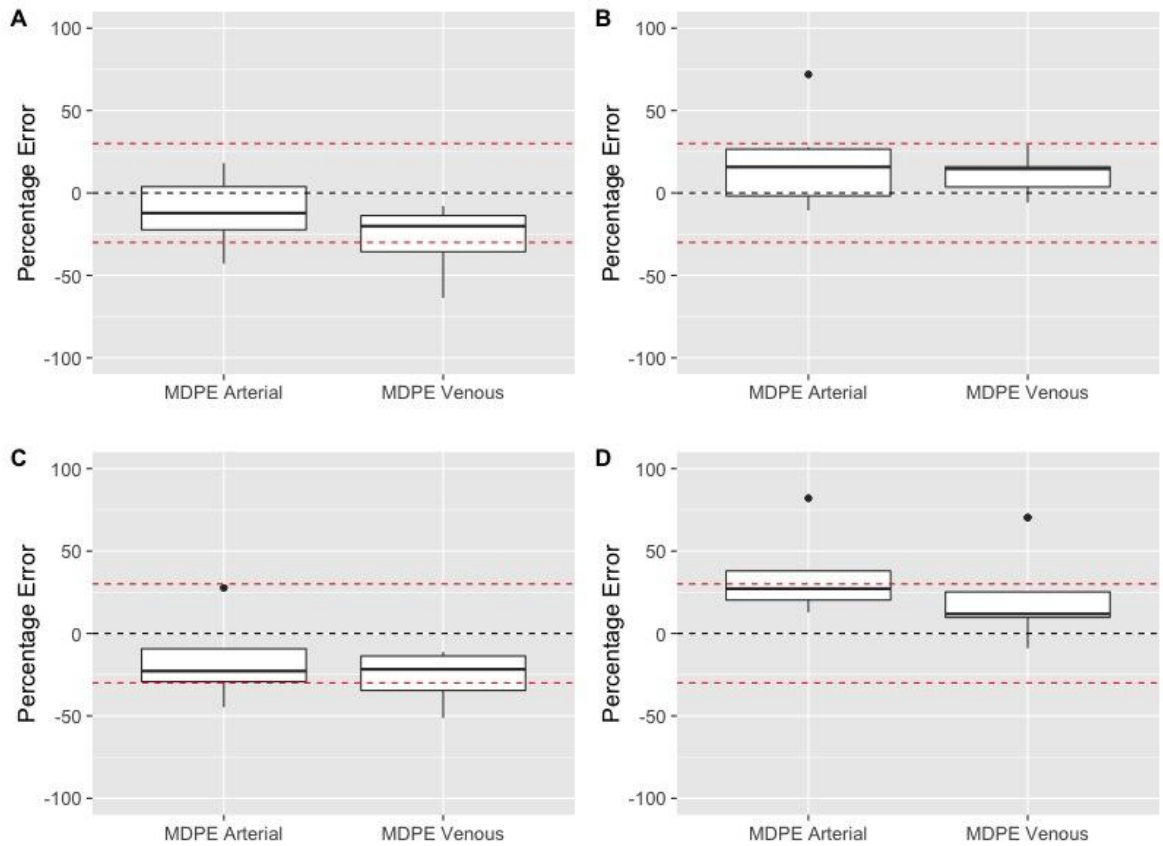
Figure 8.6: Validation study results showing MDPE for arterial and venous samples in (A) younger females, (B) younger males, (C) older females and (D) older males.

8.4.4 Early and Late Sampling Comparison

On visual inspection of the data, there appeared to be a systematic change of PEs with increasing time from an increase in the target plasma concentration. With increasing, time arterial PEs appeared to become more negative and venous PEs appeared to become more positive. This was formally investigated using a linear modelling technique with the model:

$$PE = \alpha_1 \Delta t + \alpha_2 G + \beta \qquad (8.3)$$

where *PE* is the arterial or venous PE, *Δt* is the time since an increase in plasma target concentration and *G* is gender (Table 8.5 and Figure 8.7). There was a significant negative correlation between time from an increase in target plasma concentration and the performance errors measured using arterial samples (p < 0.0001, r-squared = 0.29). In contrast, using performance errors measured using venous samples, the overall model demonstrated statistical significance (p <

0.0001, r-squared = 0.23) but there was no significant relationship between performance errors and time (α_1 p = 0.302).

Sampling	Constant	Estimate	Lower	Upper	p-value
Arterial	β	0.37	-0.26	15.61	0.946
	α_1	-0.03	-0.05	-0.02	0.001
	α_2	38.10	16.92	37.31	0.000
Venous	β	-32.98	-42.41	-23.55	0.000
	α_1	0.01	0.00	0.02	0.302
	α_2	40.00	29.69	50.3	0.000

Table 8.5: Estimates for constants in Equation 8.3 for venous and arterial sampling with upper and lower 95% confidence intervals and associated p-values.
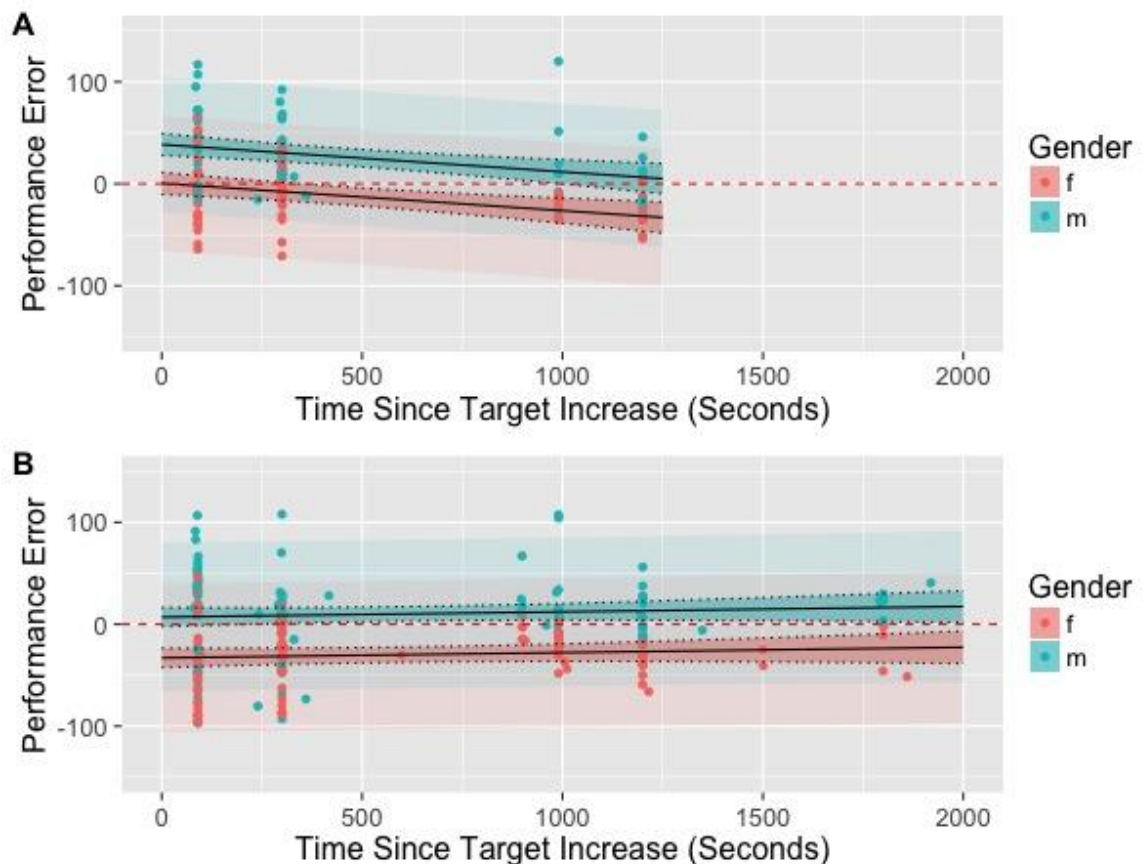
Figure 8.7: Plots of PE against time since an increase in the target plasma concentration for arterial (A) and venous (B) samples. Linear models are displayed as fit +/- 95% confidence interval. The lighter shaded area represents 95% confidence interval of model predictions.

From Figure 8.7, there is a suggestion that the differences between PEs calculated using arterial and venous sampling reduce with time from an increase in plasma target concentration. To explore this further, the difference was calculated between every pair of arterial and venous blood samples (Figure 8.8). After visual inspection of the data, the following linear model was fitted:

$$log(PE_a - PE_v) = \alpha\Delta t + \beta \tag{8.4}$$

where PE_a is performance error calculated from arterial sampling, PE_v is performance error calculated from arterial sampling and Δt is the time since an increase in plasma target concentration (Table 8.6). There was a significant relationship between log(PE_a - PE_v) and time since an increase in target plasma concentration ($p < 0.0001$, r-squared = 0.32).
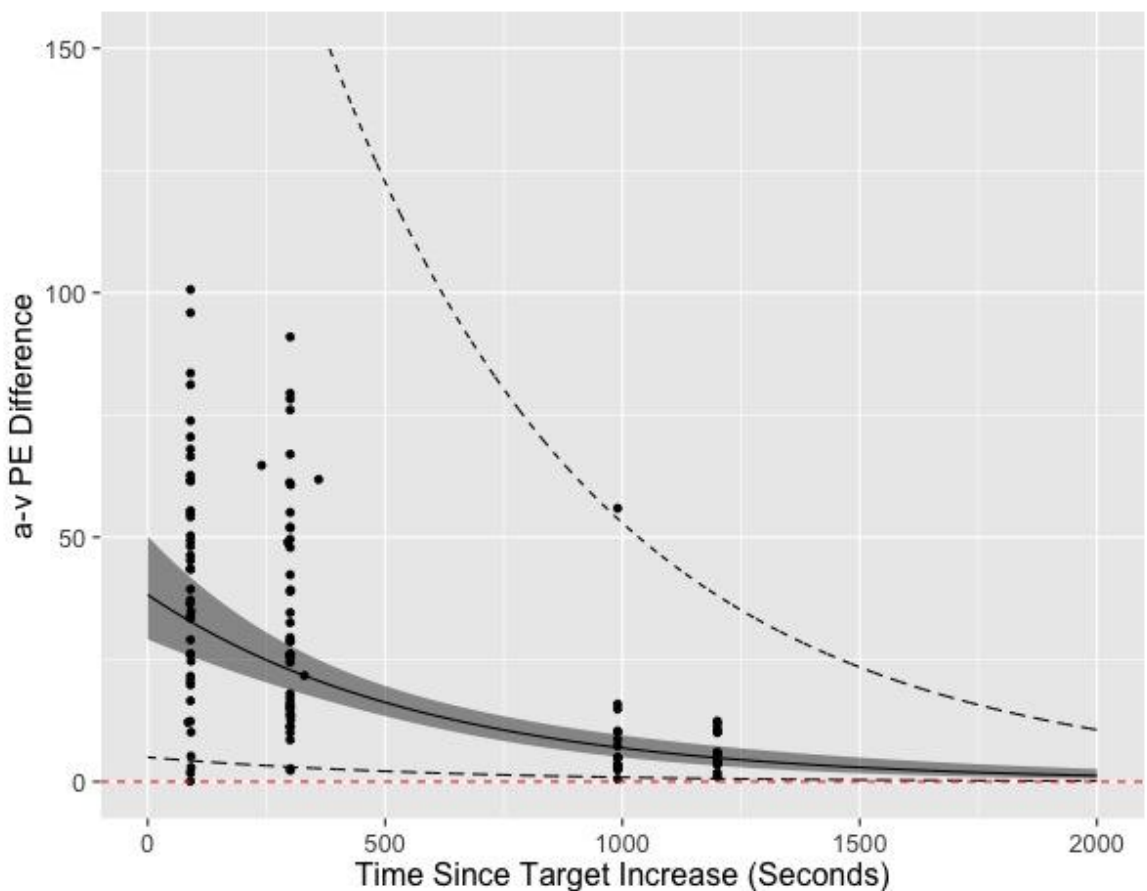
Figure 8.8: Plot of the difference between arterial and venous PEs against time since an increase in target plasma concentration. Linear models are displayed as fit +/- 95% confidence interval. The dashed line represents 95% confidence interval of model predictions.

Constant	Estimate	Lower	Upper	p.value
α	3.643	3.385	3.847	0.000
β	-0.002	-0.002	-0.001	0.000

Table 8.6: Estimates for constants in Equation 8.4 with upper and lower 95% confidence intervals and associated p-values.

8.5 Model Comparison Results

8.5.1 Introduction

All of the validation study results presented above have used the Fresenius implementation of the Covariates Model. For consistency in comparison, the Covariates Model, Marsh Model and Schnider Model were all re-simulated using the *deSolve* Package in R from the Fresenius Agilia Pump infusion profile for all 40 patients. In the simulations performed for the interim analysis results above, predictions made using *deSolve* were very close to those made by the well-established Tivatrainer software.

8.5.2 Model Comparison Based on Overall Performance Error

Comparison was first made between the arterial and venous blood propofol concentrations and the concentrations predicted by each of the Covariates, Marsh and Schnider Model Simulations in all study patients and at all study time points. The summary results for these simulations are displayed in Table 8.7 and Figures 8.9 and 8.10. On the basis of arterial sampling, the overall bias of the Covariates Model was closest to zero, with accuracy similar to that of the Schnider Model. The Marsh Model tended to over-predict with lower accuracy than the other two models. This was confirmed statistically using a Friedman Rank Sum Test to confirm a difference between the MDAPEs for each of the models ($p < 0.0001$). Pairwise comparisons using Nemenyi Multiple Comparison Test confirmed the similarity of the Covariates and Schnider Models, but a significant difference between the Marsh Model and the Covariates and Schnider Models respectively ($p < 0.01$ and $p < 0.0001$). On the basis of venous sampling, the Covariates Model had a greater tendency to under-predict but there was no significant difference in the accuracies of the models ($p = 0.20$).

Model	MDPE Art	MDAPE Art	MDPE Ven	MDAPE Ven
Covariates	3 (-45 to 73)	25 (3 to 73)*	-11 (-64 to 56)	20 (9 to 64)
Marsh	18 (-44 to 112)	34 (9 to 112)*	-5 (-56 to 84)	25 (9 to 84)
Schnider	9 (-40 to 68)	22 (7 to 68)*	-6 (-59 to 40)	26 (9 to 59)

Table 8.7: Summary of results for prediction errors in simulation studies for each of the Covariates, Marsh and Schnider Models. * Denotes statistically significant difference between MDAPEs calculated for each model.
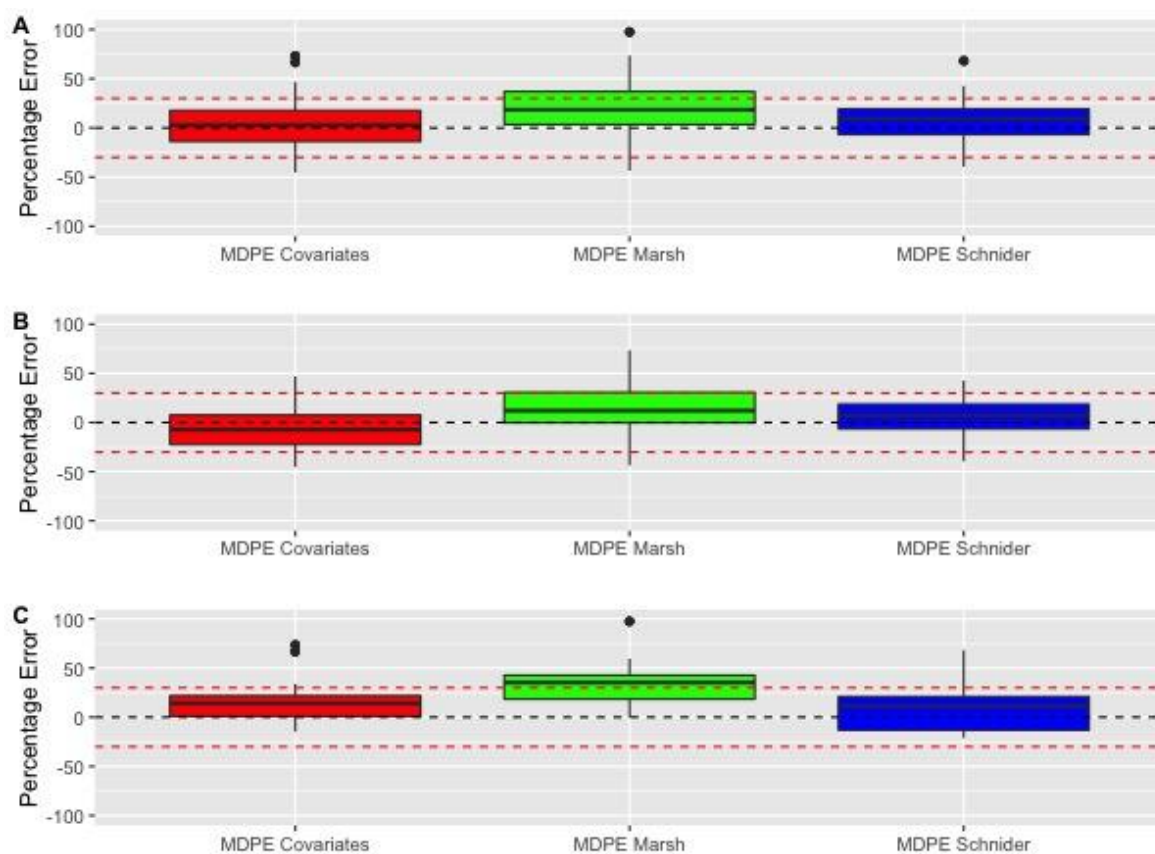
Figure 8.9: Summary of results for prediction errors based on arterial blood sampling in simulation studies for each of the Covariates, Marsh and Schnider Models in all patients (A), females (B) and males (C).
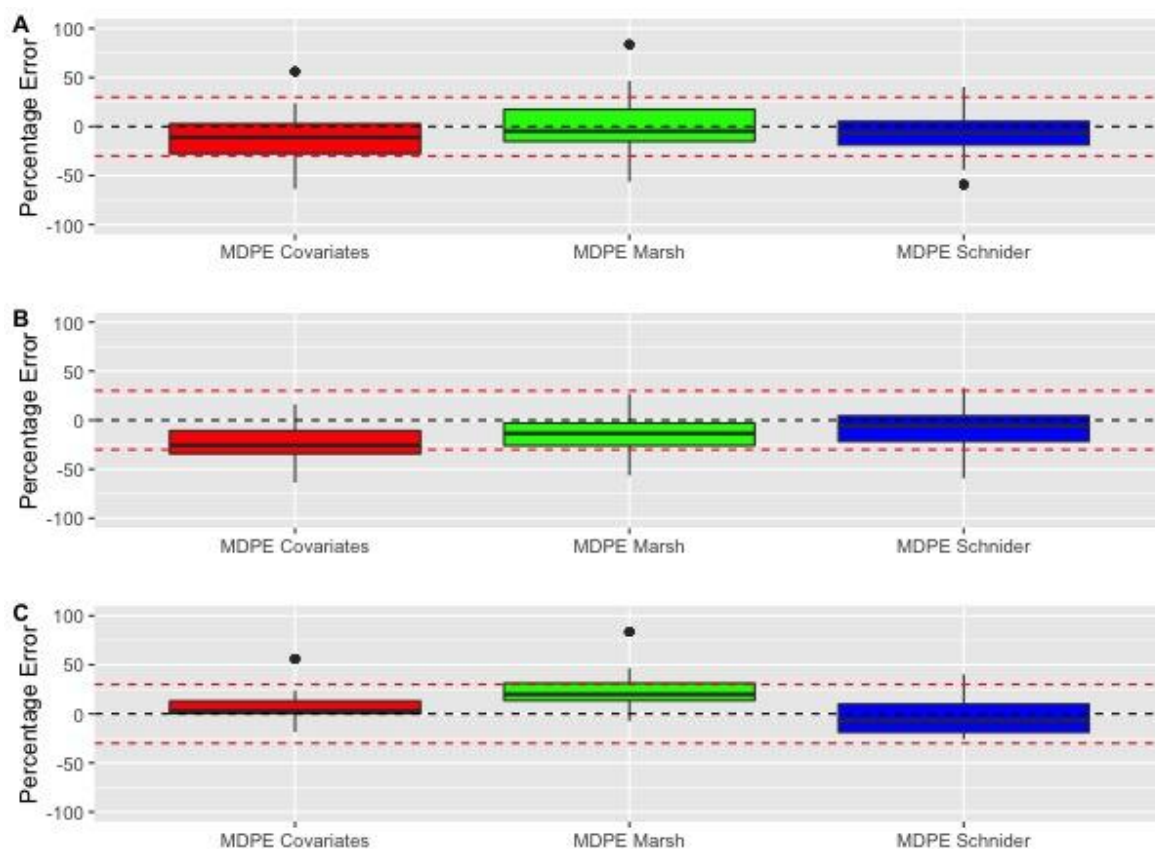
Figure 8.10: Summary of results for prediction errors based on venous blood sampling in simulation studies for each of the Covariates, Marsh and Schnider Models in all patients (A), females (B) and males (C).

8.5.3 Model Comparison By Gender

The predictive performance of the Covariates, Marsh and Schnider Models in female and male patients was compared. The results are summarised in Table 8.8 and Figures 8.9 and 8.10. In line with the Validation Study results, the simulation studies using the Covariates Model confirmed the tendency to over-predict in females and under-predict in males. Again this was confirmed by significant Wilcoxon Signed Rank Tests comparing MDPEs for female and male patients on arterial ($p < 0.0001$) and venous ($p < 0.0001$) samples. The tendency for the Marsh Model to under-predict was consistent across both female and male patients on arterial but not venous samples. There was a statistically significant difference in bias between female and male patients in both arterial ($p < 0.0001$) and venous samples ($p < 0.0001$). In contrast, there was no significant difference in bias between female and male patients in the predictions made by the Schnider Model in either arterial ($p = 0.55$) or venous samples ($p = 0.12$).

Model	Gender	MDPE Art	MDAPE Art	MDPE Ven	MDAPE Ven
Covariates	Female	-7 (-45 to 47)*	24 (3 to 47)	-26 (-64 to 16)*	26 (12 to 64)
	Male	14 (-15 to 73)*	25 (8 to 73)	3 (-18 to 56)*	18 (9 to 56)
Marsh	Female	12 (-44 to 74)*	32 (10 to 74)	-13 (-56 to 27)*	25 (9 to 56)
	Male	36 (0 to 112)*	36 (9 to 112)	20 (-7 to 84)*	24 (17 to 84)
Schnider	Female	7 (-40 to 43)	24 (7 to 48)	-6 (-59 to 33)	27 (9 to 59)
	Male	11 (-21 to 68)	20 (9 to 68)	-7 (-26 to 40)	24 (10 to 59)

Table 8.8: Results for prediction errors in simulation studies for each of the Covariates, Marsh and Schnider Models for female and male patients. * Denotes statistically significant difference between MDPEs in females and males.

8.5.4 Model Comparison By Age

The predictive performance of the Covariates, Marsh and Schnider Models was compared between older and younger patients. The results are summarised in Table 8.9 and Figures 8.11 and 8.12. With the exception of the Schnider Model as assessed on venous blood sampling ($p < 0.05$), there was no statistical difference between the model biases in younger and older patients. There was a non-significant trend for increased under-prediction in older patients for the Marsh Model.

Model	Age Group	MDPE Art	MDAPE Art	MDPE Ven	MDAPE Ven
Covariates	Younger	4 (-45 to 67)	25 (3 to 67)	-8 (-64 to 24)	20 (11 to 64)
	Older	1 (-45 to 73)	24 (8 to 73)	-15 (-51 to 56)	21 (9 to 56)
Marsh	Younger	15 (-44 to 97)	34 (9 to 97)	-6 (-56 to 47)	25 (9 to 56)
	Older	31 (-23 to 112)	36 (10 to 112)	5 (-43 to 84)	22 (10 to 84)
Schnider	Younger	11 (-34 to 43)	19 (8 to 46)	-7 (-59 to 27)*	24 (9 to 59)
	Older	-4 (-40 to 68)	29 (7 to 68)	3 (-31 to 40)*	33 (13 to 58)

Table 8.9: Results for prediction errors in simulation studies for each of the Covariates, Marsh and Schnider Models for younger and older patients. * Denotes statistically significant difference between MDPEs in younger and older patients.
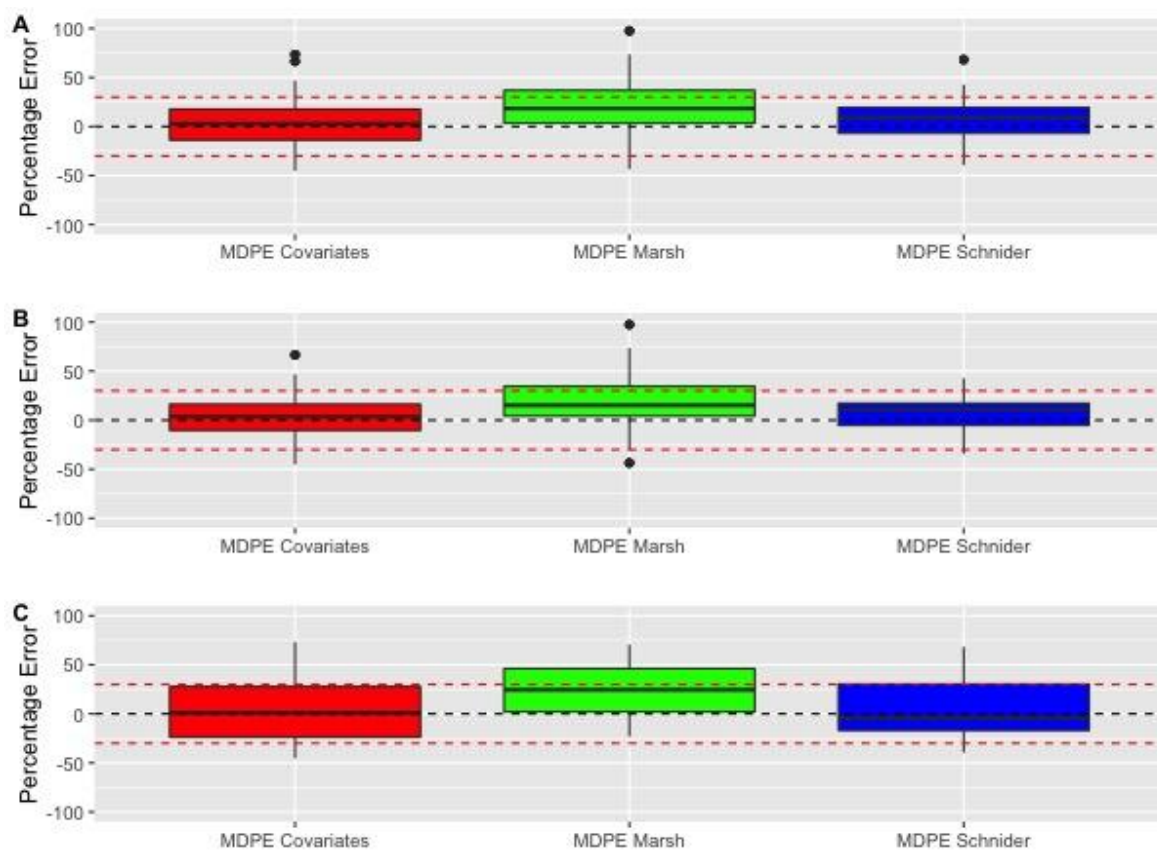
Figure 8.11: Summary of results for prediction errors based on arterial blood sampling in simulation studies for each of the Covariates, Marsh and Schnider Models in all patients (A), younger patients (B) and older patients (C).
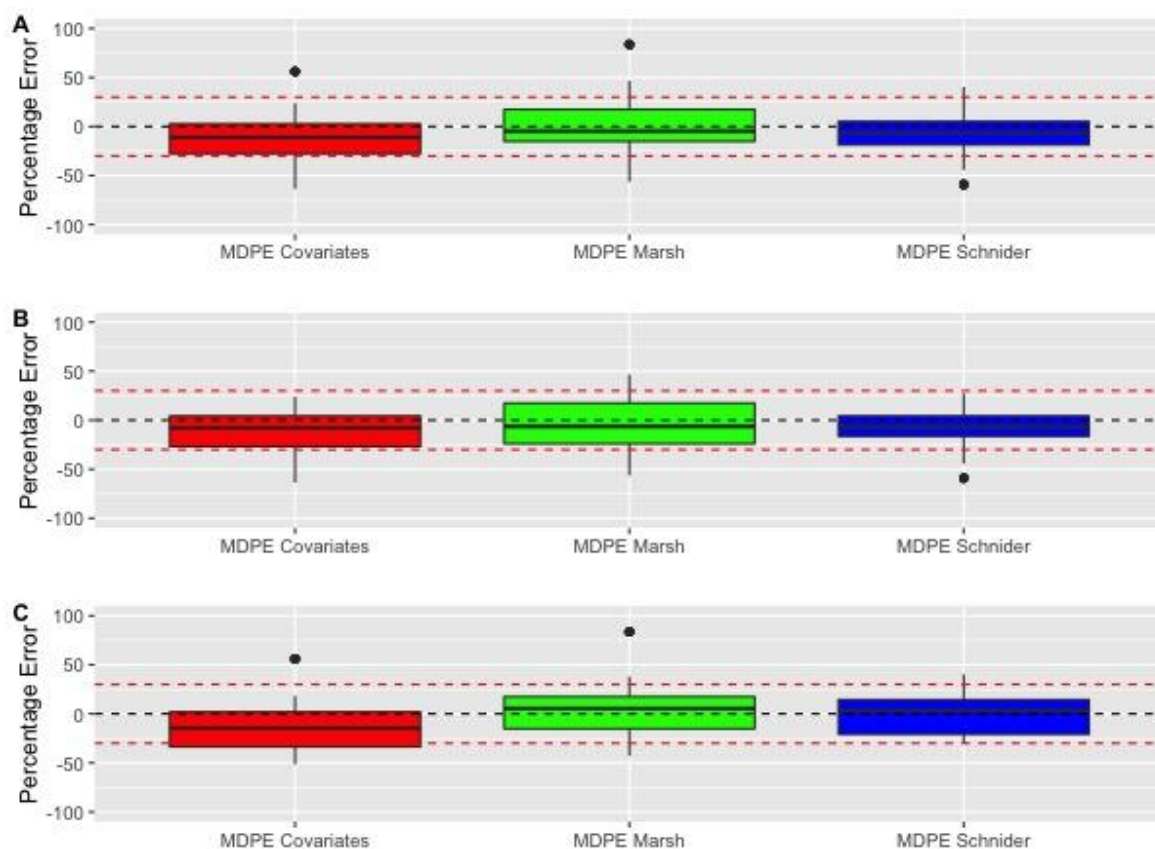
Figure 8.12: Summary of results for prediction errors based on venous blood sampling in simulation studies for each of the Covariates, Marsh and Schnider Models in all patients (A), younger patients (B) and older patients (C).

8.5.5 Model Comparison By Timing Of Blood Sampling

At set times following an increase in plasma target concentration, the predictive performances of the Covariates, Marsh and Schnider Models were compared. The time periods selected were less than 2.5 minutes, greater than 2.5 minutes and greater than 5.5 minutes. The results are summarised in Table 8.10 and Figure 8.13.

For both the Covariates and the Marsh Models there was a trend from the early to the late time window from model under-prediction to over-prediction on the basis of arterial sampling. The reverse was true for the Schnider Model and these trends were explored in detail through linear modelling.

Time	Measure	Covariates	Marsh	Schnider
< 2.5 Mins	MDPE Art	9 (-46 to 113)	43 (-22 to 166)	-15 (-50 to 44)
	MDAPE Art	31 (0 to 113)*	47 (2 to 166)*	27 (1 to 50)*
	MDPE Ven	-20 (-79 to 61)	1 (-73 to 95)	-34 (-77 to 18)
	MDAPE Ven	53 (7 to 79)*	56 (9 to 95)*	47 (7 to 77)*
> 2.5 Mins	MDPE Art	0 (-52 to 80)	2 (-55 to 118)	11 (-34 to 93)
	MDAPE Art	25 (8 to 80)*	30 (5 to 118)*	25 (4 to 93)*
	MDPE Ven	-12 (-58 to 56)	-4.5 (-56 to 84)	3.5 (-52 to 54)
	MDAPE Ven	18 (2 to 58)	21 (6 to 84)	22 (6 to 59)
> 5.5 Mins	MDPE Art	-22 (-53 to 59)	-17 (-58 to 80)	26 (-29 to 135)
	MDAPE Art	26 (6 to 59)	22 (3 to 80)	29 (6 to 135)
	MDPE Ven	-14 (-53 to 50)	-8.5 (-56 to 74)	13 (-27 to 107)
	MDAPE Ven	18 (2 to 53)	21 (6 to 74)	25 (3 to 107)

Table 8.10: Results for prediction errors at specified time intervals in simulation studies for each of the Covariates, Marsh and Schnider Models. * Denotes statistically significant difference between MDAPEs calculated for each model at given time interval.

At the early time window, on the basis of arterial sampling there was a significant difference between the accuracy of the three models as assessed by Friedman Rank Sum Test of the MDAPEs ($p < 0.0001$). Pairwise comparisons using Nemenyi Multiple Comparison Tests confirmed the similarity of the Covariates and Schnider Models, but a significant difference between the Marsh Model and the Covariates and Schnider Models respectively ($p < 0.001$ and $p < 0.01$). A significant difference was also seen between the accuracy of the three models on the basis of venous sampling ($p < 0.01$). Again the similarity of the Covariates and Schnider Models was confirmed, with a significant difference between the Marsh Model and each of the Covariates and Schnider Models ($p < 0.01$ and $p < 0.05$).
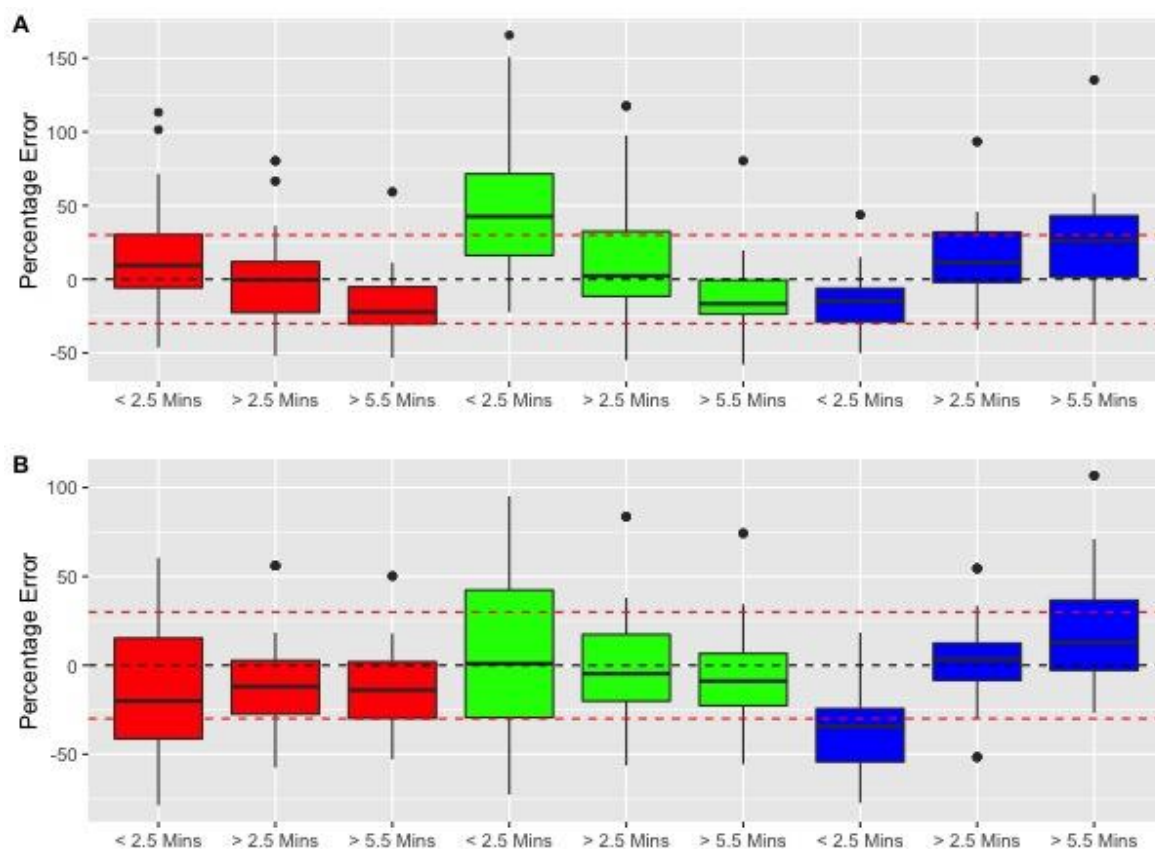
Figure 8.13: Summary of results for prediction errors based on arterial (A) and venous (B) blood sampling in simulation studies for each of the Covariates (red), Marsh (green) and Schnider (blue) Models at set time points following an increase in target plasma concentration.

At the intermediate time window, there was a persisting statistically significant difference in the accuracies of the three models on the basis of arterial (p < 0.05) but not venous sampling (p = 0.50). On pairwise comparison, the statistical difference on the basis of arterial sampling was only present between the Marsh and Schnider Models (p < 0/05).

At the later time window there was no statistically significant difference between accuracies of the three models on arterial (p = 0.25) or venous sampling (p = 0.71).

As for the Fresenius implementation of the Covariates Model, there was further exploration of the relationship between increasing time from a plasma target increase and bias for each of the three simulated models. The same linear model described in Equation 8.3 was used with estimated constants in Table 8.11 and fits in Figures 8.14 and 8.15.

Sampling	Model	Constant	Estimate	Lower	Upper	p-value
Arterial	Covariates	β	7.67	-0.26	15.61	0.058
		α_1	-0.03	-0.05	-0.02	0.000
		α_2	27.12	16.92	37.31	0.000
	Marsh	β	37.73	28.3	47.15	0.000
		α_1	-0.06	-0.07	-0.04	0.000
		α_2	30.97	18.86	43.08	0.000
	Schnider	β	-11.09	-19.41	-2.78	0.009
		α_1	0.04	0.02	0.05	0.000
		α_2	0.49	-10.2	11.17	0.928
Venous	Covariates	β	-29.19	-36.51	-21.86	0.000
		α_1	0.00	0.00	0.01	0.398
		α_2	30.31	21.45	39.17	0.000
	Marsh	β	-12.71	-21.37	-4.06	0.004
		α_1	-0.01	-0.02	0.00	0.135
		α_2	36.79	26.31	47.26	0.000
	Schnider	β	-35.16	-43.51	-26.81	0.000
		α_1	0.04	0.03	0.05	0.000
		α_2	12.76	2.66	22.86	0.014

Table 8.11: Estimates for constants in Equation 8.3 for venous and arterial sampling with upper and lower 95% confidence intervals and associated p-values.

Using arterial sampling, there was a significant negative correlation between the time since an increase in the target concentration and the performance error for the Covariates and Marsh Models, ($p < 0.0001$, r-squared = 0.24 and $p < 0.0001$, r-squared = 0.33). The opposite was true for the Schnider Model, where there was a significant positive correlation ($p < 0.0001$, r-squared = 0.14).

Using venous sampling the overall model demonstrated statistical significance for the Covariates and Marsh Models ($p < 0.0001$, r-squared = 0.14 and $p < 0.0001$ and r-squared 0.15) but there was no significant relationship between performance errors and time (α_1 p = 0.398 and 0.135). There remained a significant positive correlation for the Schnider Model ($p < 0.0001$, r-squared = 0.21 and α_1 p = 0.000).
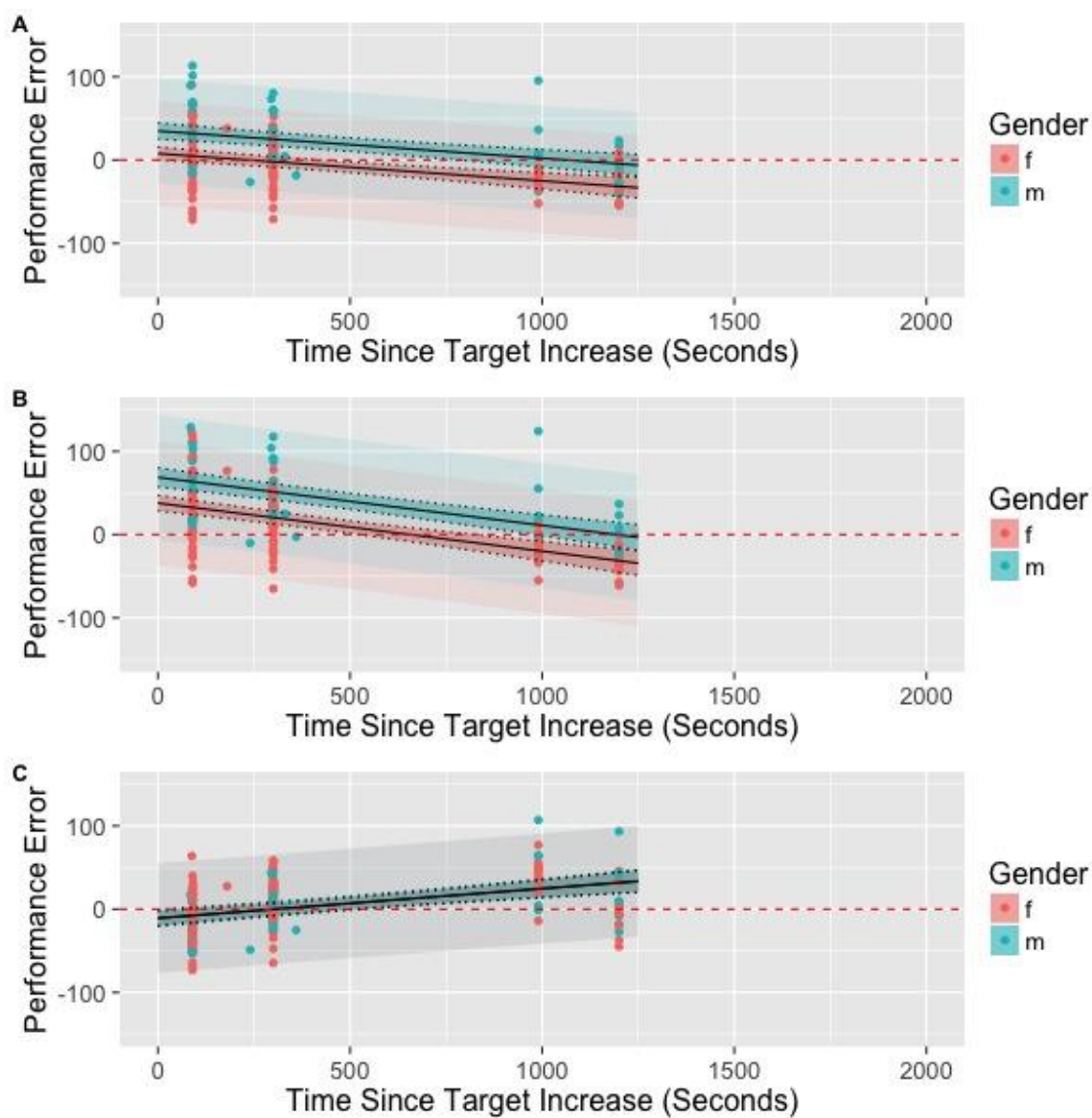
Figure 8.14: Plots of PE for arterial samples against time since an increase in the target plasma concentration for the Covariates (A), Marsh (B) and Schnider (C) Models. Linear models are displayed as fit +/- 95% confidence interval. The lighter shaded area represents 95% confidence interval of model predictions.
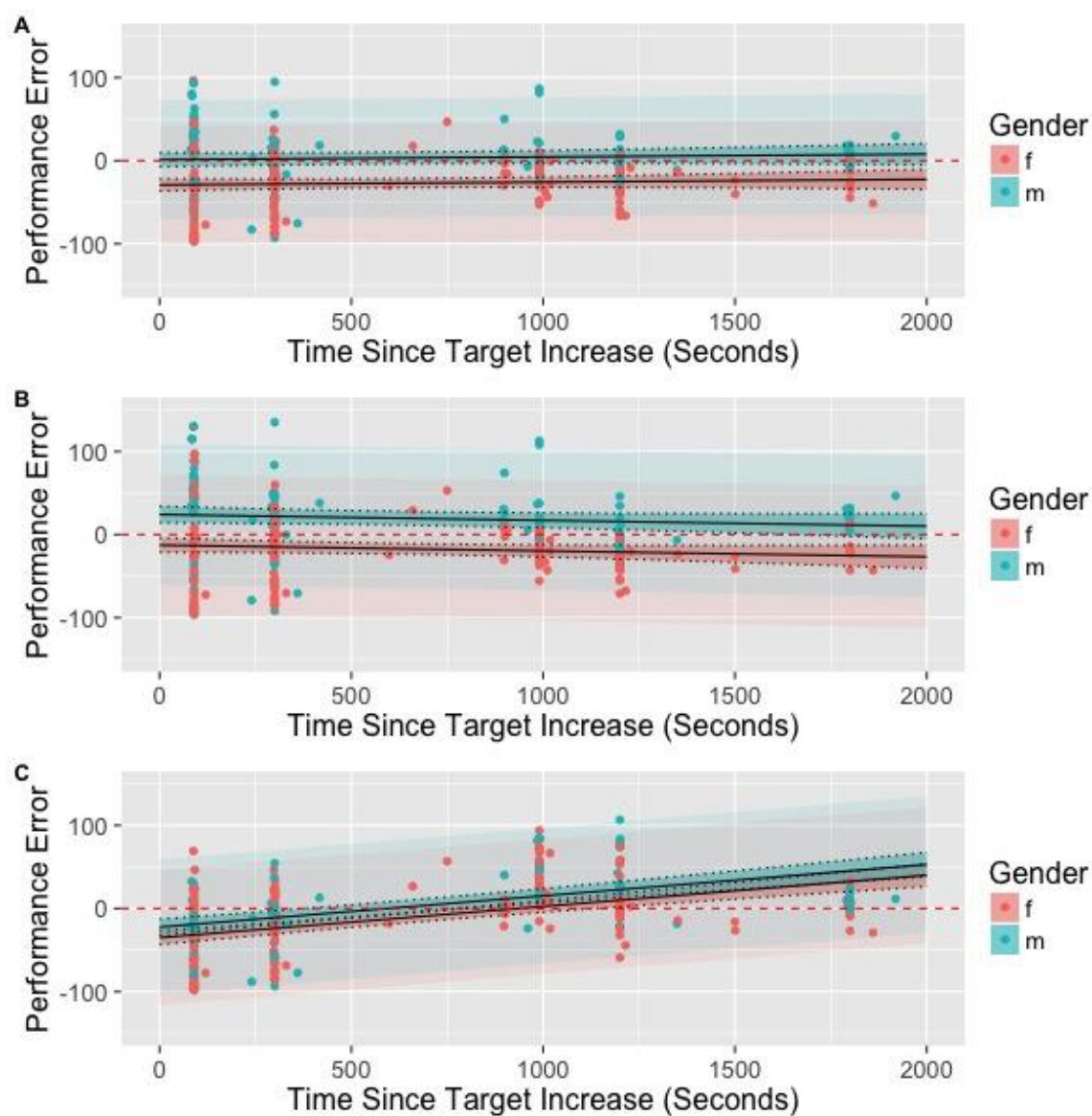
Figure 8.15: Plots of PE for venous samples against time since an increase in the target plasma concentration for the Covariates (A), Marsh (B) and Schnider (C) Models. Linear models are displayed as fit +/- 95% confidence interval. The lighter shaded area represents 95% confidence interval of model predictions.

The difference was calculated between every pair of arterial and venous PEs for each of the three simulated models. The linear model from Equation 8.4 was fitted and demonstrated a significant relationship in each of the Covariates ($p < 0.0001$ and r-squared 0.32), Marsh ($p < 0.0001$ and r-squared 0.37) and Schnider Models ($p < 0.0001$ and r-squared 0.15), (Table 8.12 and Figure 8.16).

Model	Constant	Estimate	Lower	Upper	p-value
Covariates	β	3.616	3.385	3.847	0.000
	α	-0.002	-0.002	-0.001	0.000
Marsh	β	3.875	3.385	3.847	0.000
	α	-0.002	-0.002	-0.001	0.000
Schnider	β	3.34	3.385	3.847	0.000
	α	-0.001	-0.002	-0.001	0.000

Table 8.12: Estimates for constants in Equation 8.4 for each of the simulated models with upper and lower 95% confidence intervals and associated p-values.
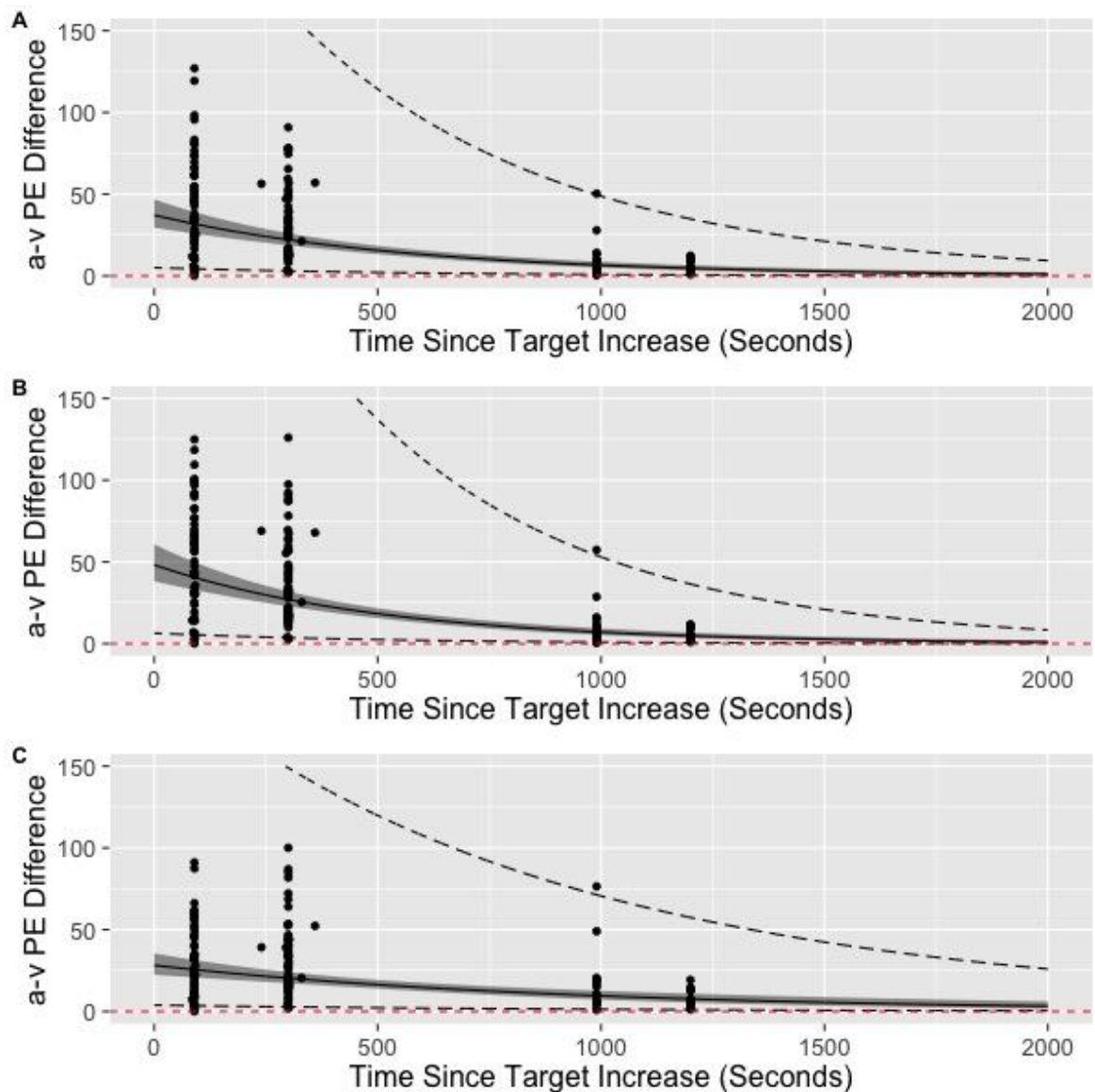
Figure 8.16: Plot of the difference between arterial and venous PEs against time since an increase in target plasma concentration for the Covariates (A), Marsh (B) and Schnider (C) Models. Linear models are displayed as fit +/- 95% confidence interval. The dashed line represents 95% confidence interval of model predictions.

8.6   Pharmacodynamic Model Development

8.6.1 Introduction

The Covariates Pharmacokinetic Model was extended to a pharmacokinetic pharmacodynamic (PKPD) model by calculation of an overall population estimate for k_{e0}. As described in the methods section, this was performed firstly for the patients who received the correctly specified Fresenius implementation of the Covariates Model and secondly for all patients using predicted plasma propofol concentrations simulated by the Covariates Model. The results were presented in part in September 2016 at the World Congress of Anesthesiologists, Hong Kong[247].

8.6.2 Fresenius Implementation

Of the 29 patients who were anaesthetised according to the correctly specified Covariates Model, there were 24 with BIS data available for PKPD model development. Using the *nlmeODE* Package it was possible to successfully provide a population based estimate for k_{e0} with or without fixed values for E_0 and E_{max}. Table 8.13 provides a summary of the population variable estimates in each of the three scenarios. Estimates for k_{e0} were all similar and ranged from 0.21 to 0.25 min^{-1}.

Model	Variable	Estimate	Lower	Upper	p-value
Fresenius	k_{e0} (min^{-1})	0.25	0.20	0.31	0.00
	E_0 (BIS)	106	102	110	0.00
	E_{max} (BIS)	144	0	2.01e+63	0.94
	EC_{50} (μg/ml)	4.39	0.00	9.65e+85	0.99
	γ	2.36	0.00	1.19e+07	0.91
Fresenius with fixed E_0 and E_{max}	k_{e0} (min^{-1})	0.22	0.18	0.27	0.00
	E_0 (BIS)	105	101	108	0.00
	EC_{50} (μg/ml)	2.48	2.14	2.86	0.00
	γ	2.80	2.37	3.31	0.00
Fresenius with fixed E_{max}	k_{e0} (min^{-1})	0.21	0.18	0.25	0.00
	EC_{50} (μg/ml)	2.83	2.53	3.17	0.00
	γ	2.33	1.78	3.07	0.00

Table 8.13: Estimates for variables in Equation n for each of the described scenarios with upper and lower 95% confidence intervals and associated p-values.

8.6.3 Covariates Simulation

There were 33 patients with BIS data available for PKPD model development using simulated plasma propofol predictions for the Covariates Model. It was again possible to successfully provide a population based estimate for k_{e0} with or without fixed values for E_0 and E_{max}. Table 8.14 provides a summary of the population variable estimates in each of the three scenarios. Estimates for k_{e0} were similar to those calculated using the Fresenius implementation of the Covariates Model and ranged from 0.22 to 0.27 min^{-1}. Figure 8.17 displays the fits achieved for population (fixed) and individual (random) estimates for k_{e0} without fixed values for E_0 and E_{max}. Figure 8.18 provides a more detailed display of the fits for a single patient (ID = 137).

Model	Variable	Estimate	Lower	Upper	p-value
Covariates	k_{e0} (min^{-1})	0.27	0.23	0.32	0.00
	E_0 (BIS)	104	102	106	0.00
	E_{max} (BIS)	124	96	160	0.00
	EC_{50} (μg/ml)	4.13	2.50	6.82	0.00
	γ	2.56	1.77	3.70	0.00
Covariates with fixed E_{max}	k_{e0} (min^{-1})	0.24	0.22	0.27	0.00
	E_0 (BIS)	104	101	107	0.00
	EC_{50} (μg/ml)	2.77	2.53	3.04	0.00
	γ	2.21	1.94	2.53	0.00
Covariates with fixed E_0 and E_{max}	k_{e0} (min^{-1})	0.22	0.20	0.25	0.00
	EC_{50} (μg/ml)	3.05	2.81	3.30	0.00
	γ	2.40	1.89	3.05	0.00

Table 8.14: Estimates for variables in Equation n for each of the described scenarios with upper and lower 95% confidence intervals and associated p-values.
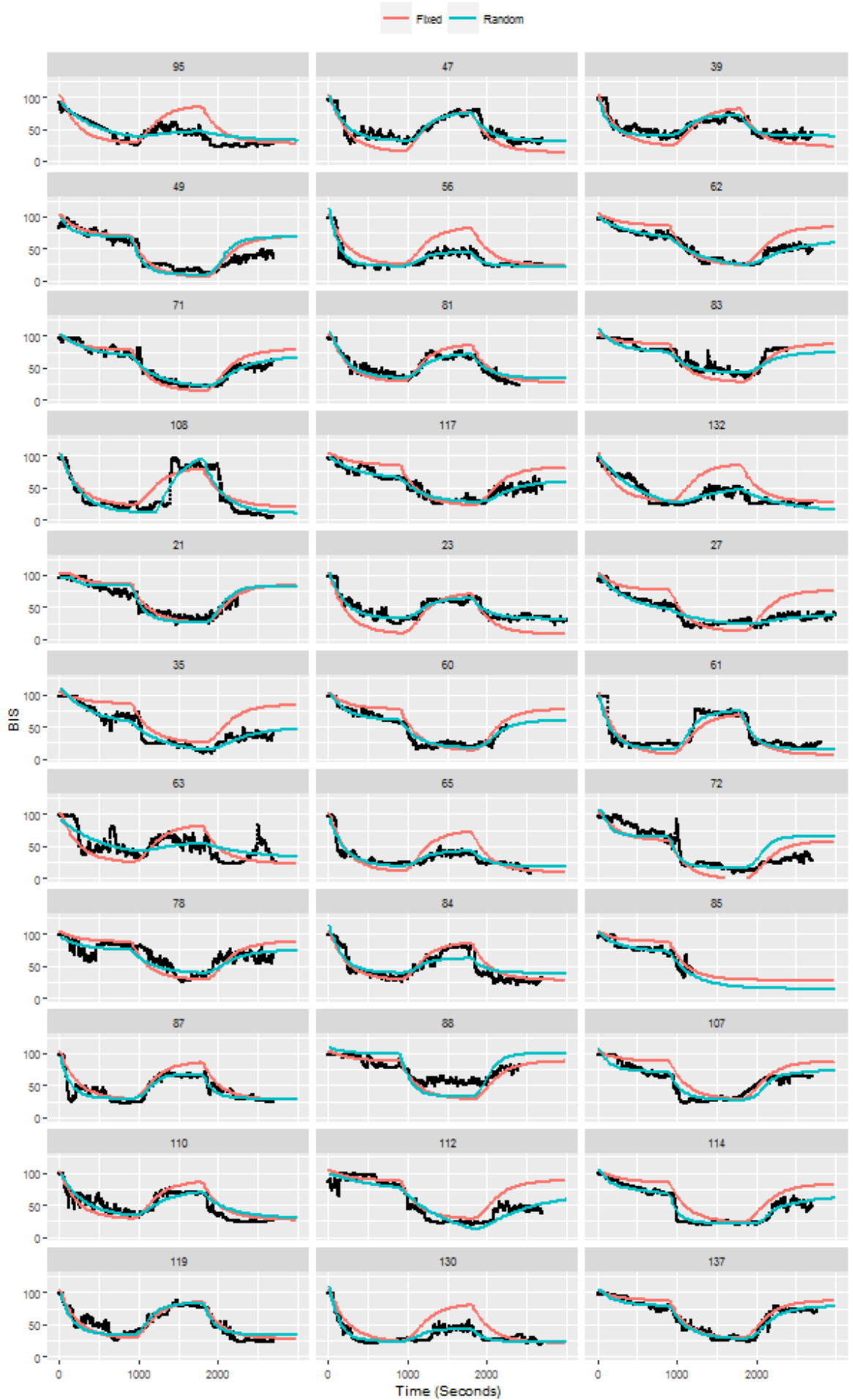
Figure 8.17 (preceding page): Fixed (red) and random (blue) *nlmeODE* fits for all patients with suitable BIS data. Model fits are plotted over the measured BIS values for each patient.
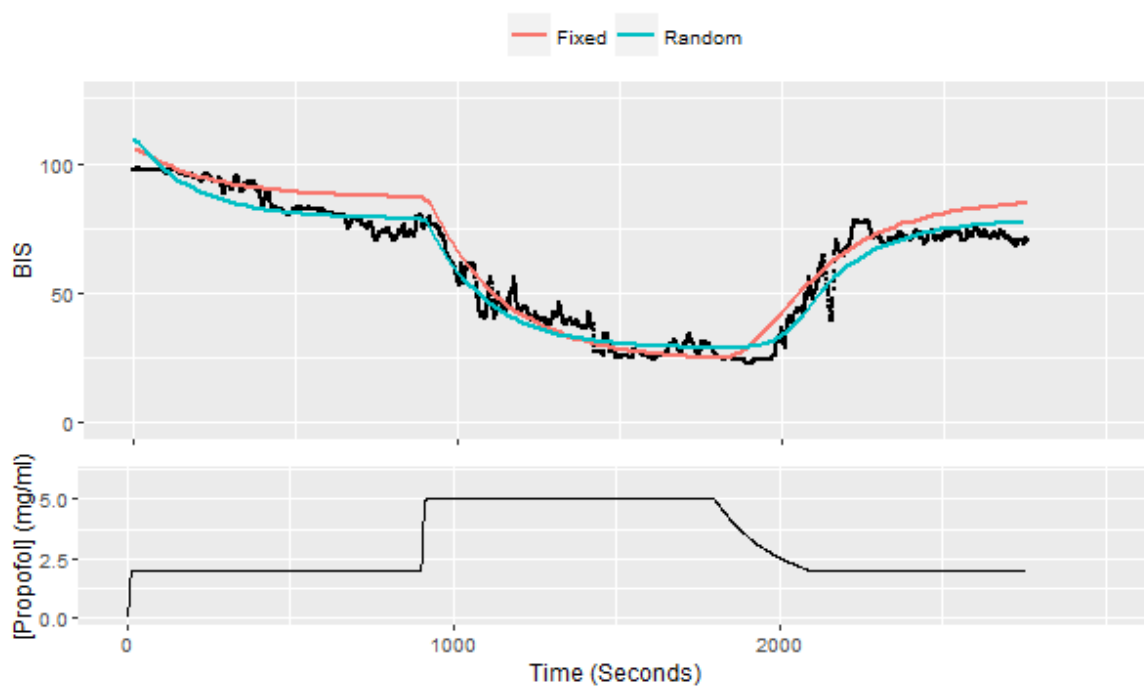
Figure 8.18: Upper panel shows fixed (red) and random (blue) *nlmeODE* fits for an example patient (137). Model fits are plotted over the measured BIS values for each patient. Lower panel shows the associated Covariates Model predictions for plasma propofol concentration.

9 Discussion and Conclusions for the VaSCoM Study

9.1 Overview

A discussion of the results from the VaSCoM Study is presented below. Limitations of the study are addressed and the results are considered in terms of those of similar pharmacokinetic (PK) and pharmacodynamic (PD) studies of propofol. There is then a description of work performed as a direct result of the VaSCoM Study with suggestions for future directions of pharmacokinetic pharmacodynamic (PKPD) modelling in anaesthesia.

9.2 Rationale for the Study

The relative advantages and disadvantages of the Marsh and Schnider Models for target controlled infusion (TCI) of propofol have been discussed in the introductory section. There is currently no overall consensus on which is the more generally applicable model to a wide range of clinical situations. The Covariates Model described by White *et al* represents an update to the Marsh Model that adjusts for the patient covariates of age and gender(5). The VaSCoM Study aimed to prospectively validate the PK component of the Covariates Model, while extending the model to include a PD component by estimating the rate constant for elimination from the effect site (k_{e0}).

9.3 Data Collection

9.3.1 Study Population

All study patients were undergoing anaesthesia to facilitate elective non-cardiac surgery. In this respect they were representative of the population of patients in whom TCI of propofol is used in clinical practice. While patients with significant co-morbidities were excluded, the study was designed to recruit a reasonable number of patients who were aged over 65 years. This was particularly important as firstly this age group represents a significant proportion of anaesthetic caseload(156) and secondly it allowed comparison of model performance in younger and older age groups.

9.3.2 Infusion Regime and Blood Sampling

The infusion regime used in the VaSCoM Study was chosen to be representative of the use of TCI in clinical practice. There were multiple step changes in target plasma concentration of propofol with patients randomised to either a 2-5-2 μg/ml protocol or 5-2-5 μg/ml protocol. Therefore model performance was tested at several target plasma concentrations and also while plasma concentration was both increasing and decreasing. Following a change in target plasma concentration, there were no further target changes for at least 15 minutes to allow time for PD effects to reach a steady state and thus assist with modelling of the effect site compartment.

During the study period there was no administration of any other hypnotic drugs or analgesic drugs. Therefore the risk of other drugs influencing the distribution and metabolism of propofol or modulating the pharmacodynamic effects of propofol were minimised.

In previous studies comparing PK models for propofol, both arterial and venous blood-sampling methods have been used. Some commentators believe that arterial sampling is of more value in PK modelling on the basis of the 'front-end kinetics' delivering the drug to its sites of action. Front-end kinetics refers to early drug distribution following intravenous administration and determines the relationship between the plasma concentration of drug delivered to various tissue groups and time(190). Three compartment PK models, such as the Covariates, Marsh and Schnider Models, ignore the complexity of this early phase and assume instantaneous mixing of drug within the whole of the central (i.e. plasma) compartment. To effectively model this dynamic phase of drug disposition, physiology based pharmacokinetic (PBPK) or recirculatory models, for example the model described by Upton and Ludbrook(191), are required. PBPK models are far more complex and are yet to be implemented in clinical practice.

The development of the Covariates Model was based on venous blood samples taken during anaesthesia delivered using the Marsh Model(5). In the VaSCoM Study, the decision was made to collect a combination of arterial and venous samples. This allowed the comparison of the performance errors (PEs) between

sampling methods and also, as is discussed below, an examination of how arterial and venous PEs change with time. The study schedule involved sampling arterial blood at four specified time points during the first 20 minutes of anaesthesia and sampling venous blood at seven specified time points during the 45 to 60 minutes of the study. In retrospect, a schedule involving paired arterial and venous sampling for the entire duration of the study would have allowed better comparison of the two methods.

9.3.3 BIS Monitoring

The most commonly used approach to modelling the effect site concentration (C_e) of a hypnotic anaesthetic drug in PKPD studies is through processed electroencephalography (pEEG). On the basis of endorsement by national guidelines(222) and use in routine clinical practice at the Golden Jubilee National Hospital, the Bispectral Index (BIS) was selected for the VaSCoM Study. The disadvantages of using BIS to model C_e include the fact that it is a surrogate marker of clinical effects and, as is the case with all pEEG monitors, there is a time delay associated with processing the EEG signal(248). There was no attempt to account for this time delay in the PD modelling study.

Alternative approaches using clinical end-points to estimate the magnitude of the effect site concentration in PKPD studies have been suggested. For example, Lim used the loss of eyelash reflex during different propofol administration regimes to derive a k_{e0} of 0.8 min^{-1}(249). Use of a fixed end-point means that the PKPD model will be dependent upon a single clinical observation in each individual.

More recently Thomson *et al* have described a novel technique for estimating k_{e0} while assessing clinical effect using visual reaction time (VRT)(250). This is an attractive technique as it provides a continuous measure of a true clinical end-point. Unfortunately it is only practical at sedating doses of propofol and cannot be applied to the recovery phase from deeper anaesthesia.

Using the above approach, Thomson *et al* tested several k_{e0}s with the Marsh Model in effect site controlled TCI to see which provided the highest probability of achieving stable clinical effect(250). A k_{e0} of 0.61 min^{-1} was most likely to

maintain a stable VRT when a fixed C_e was programmed. In a subsequent randomised study, they demonstrated that compared to TCI with the Marsh Model in plasma controlled mode or effect site controlled mode with a k_{e0} of 1.2 min^{-1} and the Schnider Model in effect site controlled mode, the Marsh Model with a k_{e0} of 0.6 min^{-1} achieved faster induction but with no associated increase in haemodynamic instability(251).

9.4   Interim Analysis

In the interim analysis performed of data collected in the VaSCoM Study, a marked deviation from expected PEs was identified in female patients. Further investigation revealed a significant Covariates Model mis-specification in the Injectomat TIVA Agilia syringe pump based on a typographical error. Following discussion with the device manufacturer, the model was adjusted and subsequent female patients were anaesthetised using the correct specification of the model. Events like this underline the need for formal testing of PK models in a clinical context before implementation in Open TCI devices and introduction to clinical practice.

Interestingly the plasma concentrations predicted for male patients by the TCI device were not identical to those estimated by the Tivatrainer software (Figure 8.3). However, the deviations were within an acceptable margin of error following import of infusion rates into an external program along with the necessary interpolations of missing values.

Outputs for Covariates Model predictions provided by Tivatrainer were compared to those provided the *desolve* Package in R. The results suggested that this open source alternative provides a suitable means of accurately simulating predictions for multiple PK models from infusion profiles. *desolve* is more suited to batch processing than Tivatrainer and should therefore be considered for future comparative PK studies.

9.5   Validation Study

9.5.1 Overall Validation

Schuttler *et al* suggested that a mean variation in measured drug plasma concentrations of 20 to 30%, with a total bias of 10 to 20% from TCI device predictions, represented acceptable performance(252). At the time of this publication, the use of PEs and the summary measures of median performance error (MDPE) and median absolute performance error (MDAPE) had not yet become established but similar ranges have been suggested by subsequent authors(202). Therefore the VaSCoM Study has demonstrated that the Injectomat TIVA Agilia syringe pump implementation of the Covariates Model achieved an acceptable level of predictive performance, as assessed by both arterial and venous sampling, for use in clinical practice. Whether or not there is a sufficient improvement in performance compared to the Marsh and Schnider Models to justify a shift towards usage of the Covariates Model shall be discussed with consideration of the comparison study results below.

9.5.2 Specific Patient Populations

The overall minimal bias of the Covariates Model (MDPE of 9 for arterial samples and -8 for venous samples) was not consistent across patient subgroups. On both sampling methods there was a consistent and statistically significant tendency to under-predict plasma concentrations in females and over-predict in males. This is a disappointing finding, given that in the development of the Covariates Model the Marsh Model was updated with a specific aim to account for gender differences. The Covariates Model was more successful in adjusting for the covariate of age and there was no significant difference in bias between younger and older patients.

9.5.3 Relationship Between PE and Time

The importance of the choice of blood sampling site (arterial or venous) and the influence of timing since dose on measured drug concentrations has undergone detailed general discussion elsewhere(253, 254). In their comparative study of PK models for propofol, Coetzee *et al* noted marked differences in calculated model performance based on arterial or venous sampling and changes in the

differences between arterial and venous propofol concentrations over time(202). Similar results were noted in the VaSCoM Study.

When explored with a linear modelling technique, performance errors based on arterial samples showed a statistically significant tendency to change from more positive to more negative with time. There was no significant relationship observed for venous samples, although PEs tended to change in the opposite direction. In line with these observations, the difference between arterial and venous PEs (a-v PE difference) could be fitted with an exponentially decreasing model over time. From Figure 8.8 it can be suggested that by between 15 and 20 minutes after an increase in target plasma concentration, arterial and venous PEs will have reached some sort of equilibrium. This has significant implications for planning blood sampling site and sampling schedule for future PK studies of TCI of propofol.

9.6   Model Comparison

9.6.1 Overall Comparison

Simulations of the plasma concentrations predicted by the Covariates, Marsh and Schnider Models were performed using the propofol infusion profile from each patient. This allowed a comparison of each of the model's predictions to the measured blood propofol concentrations. As suggested from the above results, the model biases were different depending on whether venous or arterial sampling was used. On arterial sampling, the Covariates Model had the bias closest to zero, suggesting the least tendency to over or under-predict plasma concentrations. The opposite was true for venous sampling. Statistical comparison between models was performed on the basis of inaccuracy (MDAPEs). This meant that the direction of any bias was irrelevant and models were compared only on the overall magnitude of PEs. The Marsh Model was significantly more likely to provide PEs of greater magnitude than either the Covariates or Schnider Models based on arterial sampling.

9.6.2 Comparison by Specific Patient Population

Statistical comparisons between female and male patients and between younger and older patients were performed for each model based on bias. The reason for

this was that when using a PK model clinically it is important to know if it has a difference in tendency towards over or under-prediction depending on the covariates of the individual patient. Both of the Covariates and Marsh Models, on the basis of both arterial and venous sampling, showed a significant tendency towards more positive bias in male patients. The Schnider Model did not demonstrate any significant difference in bias between female and male patients and therefore can be considered to more effectively account for the covariate of gender than the other models.

In contrast, only the Schnider Model, on the basis of venous sampling, showed a significant tendency towards increased positive bias in older patients. The Marsh Model had a non-significant tendency towards more positive bias in older patients on the basis of arterial sampling. This difference in bias is negligible in the Covariates Model and supports the rationale for adjustment of the central compartment volume (V_1) and clearance (Cl) for age.

9.6.3 Comparison of Relationships Between PE and Time

In the simulation studies, both of the Covariates and Marsh Models showed a similar pattern of arterial and venous PE changes over time as described above for the validation study. The Schnider Model showed distinctly different results. As assessed by linear modelling, on the basis of both arterial and venous sampling, PEs showed a significant tendency to become more positive over time. This is likely related to the fact that the relatively small fixed central compartment volume specified by the Schnider Model resulted in over-prediction of plasma concentrations in the early phase after an increase in target concentration.

Comparisons between model performances were made at early, intermediate and late sampling periods. During the early sampling period, on the basis of both arterial and venous samples, the Marsh Model was associated with significantly increased inaccuracy compared to the other two models. By the late sampling period this difference is no longer significant and indeed the Schnider Model is trending towards increased inaccuracy.

For all three PK models, the relationship between a-v PE difference and time can be fitted with an exponentially decreasing model. The a-v PE difference is relatively smaller for the Schnider Model in the early phases because the model tends to over-predict both arterial and venous blood concentrations.

All of the above results need consideration when using any of the above models in clinical practice. The anaesthetist must be aware of how the bias of the selected model will change with time and be prepared to adjust target plasma or effect site concentrations based on this knowledge.

9.7   Pharmacodynamic Model

The VaSCoM Study has provided a range of estimates for the appropriate k_{e0} to use with the Covariates Model using an adaptation of the parametric approach. In the classic study by Sheiner et al, they described fitting a PK model for d-tubocurarine while explaining the time course of the PD effects with the k_{e0}(211). In the current study there was no new PK model fitted to the available data but there was simultaneous validation of the predictions made by the Covariates Model.

Depending on whether the analysis was restricted to patients who had received the correctly specified Covariates Model or performed in all patients with simulated plasma propofol concentrations predicted by the Covariates Model, the range of k_{e0} estimations were 0.21 to 0.25 min^{-1} and 0.22 to 0.27 min^{-1} respectively. There was minimal effect in restricting the allowed BIS values for E_0 (baseline value with no drug present) and E_{max} (maximum change from baseline). Indeed all estimates were around the value of 0.26 min^{-1} that was originally implemented with the Marsh Model in the Diprifusor™. This is reassuring given that the non-linear mixed effect modelling (NONMEM) was not performed using the standard NONMEM® software but instead the *nlmeODE* Package in R. Further reassurance comes from Figures 8.17 and 8.18 that show the fixed and random effects models provide good fits to the available BIS data. The *nlmeODE* Package therefore provides a realistic alternative to NONMEM® for PKPD modelling that avoids the need to purchase proprietary software.

9.8   Results in the Context of Similar Studies

9.8.1 PK Model Comparison

There are only two prior studies that have compared performance of the Covariates Model to that of Marsh and Schnider Models(203, 205). The first of these studies used data from nine patients who had received a propofol infusion and the second used data from 42 patients undergoing surgery with TCI of propofol via the Diprifusor™.

In terms of assessing the performance of the Covariates Model, the VaSCoM Study has several theoretical advantages over the previous studies. To begin with, the VaSCoM Study is the first to provide a new PK dataset and validated the Covariates Model by directly testing it with a demanding schedule of increasing and decreasing target plasma concentrations. Patients recruited to the VaSCoM Study received no pre-medication and during the study period, anaesthesia was provided only by TCI of propofol. In the two prior studies, patients were routinely pre-medicated and received multiple other drugs that could potentially affect the PK profile of propofol.

Despite the technical differences between the studies, there are important similarities in the results. In common with both the infusion and TCI studies above, the VaSCoM Study highlighted the favourable overall performance of the Covariates Model as assessed by MDAPE compared to the Marsh Model. As was demonstrated in the previous TCI study, the tendency of the Marsh Model to under-predict in males relative to females remained present (albeit to a lesser degree) in the Covariates Model despite the adjustments made to the model on the basis of gender.

The VaSCoM Study confirmed the observation of both earlier studies that the Schnider Model tends to over-predict in the induction phases and under-predict in the later phases of anaesthesia. Indeed the VaSCoM Study also agreed with the finding of the previous TCI study that the bias of all three models did not remain constant across increasing, stable or decreasing target plasma concentrations.

In recognition that all of the published PK models for propofol have been derived from quite distinct patient or volunteer populations, Eleveld *et al* attempted to derive a general purpose PK model with robust performance across multiple patient populations(255). They used PK data from 21 previous studies, obtained either from the Open TCI Initiative or through personal communication with authors. The Open TCI Initiative provides a forum for the discussion of issues related to PKPD modelling and a platform for the sharing of open source code and data for model development(256). A comment on the importance of this type of initiative is included in the concluding remarks of this thesis.

The final PK model constructed by Eleveld et al could theoretically be used to deliver propofol TCI in patient groups ranging from neonates to the elderly and from normal to high to body mass index (BMI). To remain applicable across such a diverse population, the model was necessarily complex and accounted for the patient covariates of gender, age and weight in a scaled manner. The model also distinguished between individuals depending on whether they were patients or healthy volunteers. Despite the complexity, and assessing predictive performance in the same population it was derived from, the Eleveld model actually showed only modest improvement in inaccuracy in an adult population compared to the Covariates Model.

9.8.2 PD Model Development

As stated above, the range of k_{e0} estimates calculated in the VaSCoM Study are very similar to the k_{e0} implemented with the Marsh Model in the Diprifusor™. Furthermore, the range is also similar to the k_{e0} of 0.2 min^{-1} calculated by Billard *et al* using BIS to monitor drug effect during increasing and decreasing plasma concentrations of propofol(216).

Studies using different methodology to calculate k_{e0} have provided markedly different estimates. For example in the study by Thomson et al outlined above the k_{e0} was faster than calculated in the VaSCoM Study. The Thomson study has the strength of having used a clinical measure of drug effect. However, in terms of general applicability, the VaSCoM Study monitored drug effect at a wider range of predicted effect site concentrations and also studied the decline in drug effect with decreasing concentrations. Only patients between the ages of

21 and 65 years were recruited to the Thomson study and therefore the applicability of the k_{e0} to an older population cannot be assumed(250).

Minto *et al* advocated a 'time to peak effect site concentration' (t_{peak}) approach to estimating k_{e0}(155) and Struys *et al* used the technique to estimate an 'adjusted ke0' for the Marsh Model of 1.2 min^{-1}(217). By definition the t_{peak} approach only accounts for the pharmacodynamics relating to onset of drug effect and therefore is unlikely to provide as full a description of PD behaviour as the more detailed approach adopted in the VaSCoM Study.

Inter-individual variation of pharmacokinetics and pharmacodynamics means that a single k_{e0} value will not accurately predict effect site compartment concentrations in all patients. It remains the responsibility of the anaesthetist to monitor the clinical effects of target C_p or C_e and adjust infusions appropriately.

9.9 Related and Future Work

9.9.1 Introduction
In similar with the BioTBI Study, the high-resolution data collected as part of the VaSCoM Study have become a valuable research resource. Examples of recent and ongoing projects that are using the data in PKPD analysis are provided below.

9.9.2 Non-Parametric Estimation of Ke0
To confirm the parametric k_{e0} estimated in the VaSCoM Study, the arterial blood propofol concentrations and BIS profiles were used to estimate a non-parametric k_{e0}(257). The overall population estimate was 0.27 and thus within the range estimated in the VaSCoM Study.

9.9.3 Unique Modelling Approaches to PKPD
Physiology based pharmacokinetic models provide an alternative to compartmental PK models by attempting to incorporate existing knowledge of physiological behaviour. The opposite of this approach is a purely data driven or 'machine learning' system (Figure 1.1). Data from the VaSCoM Study have been

used in an input-output non-linear dynamical system to model pharmacodynamic behaviour of multiple physiological effects in individual patients(258). The need to consider multiple effect site compartments was acknowledged in early work by Fuseau and Sheiner(213) and the delay between hypnotic and haemodynamic effects of propofol has previously been explored(217, 259). Attempts to apply input-output non-linear dynamical systems beyond the individual patient level are currently underway.

9.9.4 The Future of PKPD Modelling in Anaesthesia

The Food and Drug Administration (FDA) has never approved the use of TCI devices to deliver anaesthesia in the United States of America. A recent series of editorials in *Anesthesia and Analgesia* detailed the history, technology and safety of TCI and concluded with a review of the potential pathways to FDA approval(184, 260-262). Licensing of TCI in the United States would undoubtedly lead to a substantial rise in usage and further increase the demand for more refined and generally applicable PKPD models.

One approach to this challenge, as demonstrated in the Eleveld study above, is to use bigger datasets with more patients, to develop increasingly complex compartmental models. Alternative modelling approaches may include the adaptation of PBPK models or machine learning models for clinical practice. A final methodology that is likely to influence the future of PKPD modelling in anaesthesia is the concept of 'feedback control'(263). Closed-loop TCI for hypnotic drugs in anaesthesia would involve using the PK models as the starting point for drug delivery and adapting the infusion rate based on some observation of the system. The observations may be pharmacodynamic, for example a pEEG measure of hypnosis, or pharmacokinetic, for example bed-side measurement of blood propofol concentration(264). A suitable measurement device has been evaluated in comparison to reference techniques(265, 266) but it is as yet unclear if it will become adopted into clinical practice. Similarly, for any closed-loop control systems to be introduced into routine use in anaesthesia there will need to be extensive assessment of their safety and value.

9.10 Conclusions

The VaSCoM Study has validated the Covariates Model for target controlled infusion of propofol and confirmed that it improves inaccuracy compared to the Marsh Model. There remains a difference in bias between female and male patients such that anaesthetists would need to respect this if using the model in clinical practice. A k_{e0} in the range of 0.21 to 0.27 min^{-1} has been estimated for implementation with the Covariates Model.

10   Overall Conclusions to the Thesis

The management of patients with traumatic brain injury (TBI) on the neurological intensive care unit (NICU) and the use of target controlled infusions (TCI) in the operating theatre provide two excellent examples of how mathematical modelling can enhance knowledge and influence the practice of anaesthesia and critical care. As has been demonstrated with the BioTBI and VaSCoM Studies the modelling approaches and techniques can be adapted to suit the particular clinical questions. There is however one underlying theme that can unite all modelling studies of critically ill patients. An increasing quantity of high-frequency physiological data are collected from these patients with a correspondingly high financial and resource cost. It is therefore imperative that these data are appropriately used.

To facilitate the most effective exploitation of physiological data, networks of clinicians and scientists must share the data and the associated analytic techniques. Examples of such networks have already been discussed in terms of TBI (BrainIT(96), CENTER-TBI(97), IMPACT(142)) and TCI (Open TCI Initiative(256)). The most well established repository for sharing data and code in the critical care domain is the Medical Information Mart for Intensive Care (MIMIC) Database(267, 268). Now onto its third iteration it is an openly available dataset comprising de-identified health data associated with around 40,000 patients. Collaboration such as this represents one of the keys to leveraging technology to improve the care of critically ill patients.

In support of the above theme, all of the analyses in this thesis have been performed using the open source statistical programming environment 'R' (7). Ultimately the code will be made available via BrainIT for the BioTBI Study and via the Open TCI Initiative for the VaSCoM Study.

11   References

1.   Celi LA, Mark RG, Stone DJ, Montgomery RA. "Big data" in the intensive care unit. Closing the data loop. Am J Respir Crit Care Med. 2013;187(11):1157-60.

2.   Cobelli C, Carson E. Introduction to Modeling in Physiology and Medicine. Oxford: Academic Press; 2008.

3.   Barnes DJ, Chu D. Introduction to Modeling for Biosciences. London: Springer; 2010.

4.   Carson E, Cobelli C. Modeling Methodology for Physiology and Medicine. Bronzino J, editor. New York: Academic Press; 2001.

5.   White M, Kenny GN, Schraag S. Use of target controlled infusion to derive age and gender covariates for propofol clearance. Clin Pharmacokinet. 2008;47(2):119-27.

6.   Marsh B, White M, Morton N, Kenny GN. Pharmacokinetic model driven infusion of propofol in children. Br J Anaesth. 1991;67(1):41-8.

7.   R Core Team. R: A Language and Environment for Statistical Computing. Vienna, Austria: R Foundation for Statistical Computing; 2014.

8.   Hawthorne C, Piper I. Monitoring and Modelling of Intracranial Pressure in Patients with Traumatic Brain Injury. Frontiers in Neurology. 2014;5.

9.   Marmarou A, Anderson RL, Ward JD, Choi SC, Young HF, Eisenberg HM, et al. Impact of ICP instability and hypotension on outcome in patients with severe head trauma. J Neurosurg. 1991;75(1s):S59-S66.

10.   Maas AI, Stocchetti N, Bullock R. Moderate and severe traumatic brain injury in adults. Lancet Neurol. 2008;7(8):728-41.

11.   Dunn LT. Raised intracranial pressure. Journal of neurology, neurosurgery, and psychiatry. 2002;73 Suppl 1:i23-7.

12.   Bratton SL, Chestnut RM, Ghajar J, McConnell Hammond FF, Harris OA, Hartl R, et al. Guidelines for the management of severe traumatic brain injury. VIII. Intracranial Pressure Thresholds. J Neurotrauma. 2007;24 Suppl 1:S55-8.

13.   Chesnut RM, Temkin N, Carney N, Dikmen S, Rondina C, Videtta W, et al. A trial of intracranial-pressure monitoring in traumatic brain injury. N Engl J Med. 2012;367(26):2471-81.

14.   Czosnyka M, Smielewski P, Timofeev I, Lavinio A, Guazzo E, Hutchinson P, et al. Intracranial pressure: more than a number. Neurosurg Focus. 2007;22(5):E10.

15.   Mokri B. The Monro–Kellie hypothesis: Applications in CSF volume depletion. Neurology. 2001;56(12):1746-8.

16.   Lundberg N. Continuous recording and control of ventricular fluid pressure in neurosurgical practice. Acta Psychiatr Scand Suppl. 1960;36(149):1-193.

17.   Lundberg N, Troupp H, Lorin H. Continuous recording of the ventricular-fluid pressure in patients with severe acute traumatic brain injury. A preliminary report. J Neurosurg. 1965;22(6):581-90.

18.   Langfitt TW, Weinstein JD, Kassell NF, Simeone FA. Transmission of increased intracranial pressure. II. Within the craniospinal axis. J Neurosurg. 1964;21:989-97.

19.   Langfitt TW, Weinstein JD, Kassell NF, Gagliardi LJ. Transmission of increased intracranial pressure. II. Within the supratentorial space. J Neurosurg. 1964;21:998-1005.

20.   Lanier WL, Warner DO. Intracranial Elastance versus Intracranial Compliance: Terminology Should Agree with That of Other Disciplines. Anesthesiology. 1992;77(2):403.

21.   Drummond JC. Elastance Versus Compliance. Anesthesiology. 1995;82(5):1309-10.

22.   Marmarou A. A theoretical and experimental evaluation of the cerebrospinal fluid system.: Drexel University; 1973.

23.   Wakeland W, Goldstein B. A review of physiological simulation models of intracranial pressure dynamics. Computers in Biology and Medicine. 2008;38(9):1024-41.

24.   Marmarou A, Shulman K, LaMorgese J. Compartmental analysis of compliance and outflow resistance of the cerebrospinal fluid system. J Neurosurg. 1975;43(5):523-34.

25.   Davson H. Physiology of the cerebrospinal fluid. Churchill: London; 1967.

26.   Gray WJ, Rosner MJ. Pressure-volume index as a function of cerebral perfusion pressure. Part 1: The effects of cerebral perfusion pressure changes and anesthesia. J Neurosurg. 1987;67(3):369-76.

27.	Gray WJ, Rosner MJ. Pressure-volume index as a function of cerebral perfusion pressure. Part 2: The effects of low cerebral perfusion pressure and autoregulation. J Neurosurg. 1987;67(3):377-80.

28.	Lavinio A, Rasulo FA, Peri E, Czosnyka M, Latronico N. The relationship between the intracranial pressure–volume index and cerebral autoregulation. In: Pinsky MR, Brochard L, Hedenstierna G, Antonelli M, editors. Applied Physiology in Intensive Care Medicine 1: Springer Berlin Heidelberg; 2012. p. 153-6.

29.	Lozier AP, Sciacca RR, Romagnoli MF, Connolly ES, Jr. Ventriculostomy-related infections: a critical review of the literature. Neurosurgery. 2002;51(1):170-81; discussion 81-2.

30.	Beer R, Lackner P, Pfausler B, Schmutzhard E. Nosocomial ventriculitis and meningitis in neurocritical care patients. Journal of neurology. 2008;255(11):1617-24.

31.	van de Beek D, Drake JM, Tunkel AR. Nosocomial Bacterial Meningitis. New England Journal of Medicine. 2010;362(2):146-54.

32.	Avezaat CJJ, van Eijndhoven JHM. Cerebrospinal Fluid Pulse Pressure and Craniospinal Dynamics: A Theoretical, Clinical and Experimental Study: A. Jongbloed en Zoon; 1984.

33.	Cardoso ER, Rowan JO, Galbraith S. Analysis of the cerebrospinal fluid pulse wave in intracranial pressure. J Neurosurg. 1983;59(5):817-21.

34.	Avezaat CJ, van Eijndhoven JH, Wyper DJ. Cerebrospinal fluid pulse pressure and intracranial volume-pressure relationships. Journal of Neurology, Neurosurgery & Psychiatry. 1979;42(8):687-700.

35.	Leyden E. Beiträge und Untersuchungen zur Physiologie und Pathologie des Gehirns. Archiv f pathol Anat. 1866;37(4):519-59.

36.	Löfgren J, Essen Cv, Zwetnow NN. The pressure-volume curve of the cerebrospinal fluid space in dogs. Acta Neurol Scand. 1973;49(4):557-74.

37.	Panerai RB. Assessment of cerebral pressure autoregulation in humans--a review of measurement methods. Physiol Meas. 1998;19(3):305-38.

38.	Hamner JW, Tan CO. Relative Contributions of Sympathetic, Cholinergic, and Myogenic Mechanisms to Cerebral Autoregulation. Stroke. 2014;45(6):1771-7.

39.	Overgaard J, Tweed WA. Cerebral circulation after head injury. Journal of Neurosurgery. 1974;41(5):531-41.

40.	Czosnyka M, Smielewski P, Piechnik S, Steiner LA, Pickard JD. Cerebral autoregulation following head injury. Journal of Neurosurgery. 2001;95(5):756-63.

41.	Ursino M. A mathematical study of human intracranial hydrodynamics part 1—The cerebrospinal fluid pulse pressure. Annals of Biomedical Engineering. 1988;16(4):379-401.

42.	Ursino M. A mathematical study of human intracranial hydrodynamics part 2—Simulation of clinical tests. Annals of Biomedical Engineering. 1988;16(4):403-16.

43.	Ursino M, Lodi CA. A simple mathematical model of the interaction between intracranial pressure and cerebral hemodynamics. Journal of Applied Physiology. 1997;82(4):1256-69.

44.	Czosnyka M, Piechnik S, Richards HK, Kirkpatrick P, Smielewski P, Pickard JD. Contribution of mathematical modelling to the interpretation of bedside tests of cerebrovascular autoregulation. Journal of Neurology, Neurosurgery & Psychiatry. 1997;63(6):721-31.

45.	Daley ML, Pourcyrous M, Timmons SD, Leffler CW. Assessment of Cerebrovascular Autoregulation: Changes of Highest Modal Frequency of Cerebrovascular Pressure Transmission With Cerebral Perfusion Pressure. Stroke. 2004;35(8):1952-6.

46.	Daley ML, Leffler CW, Czosnyka M, Pickard JD. Intracranial pressure monitoring: modeling cerebrovascular pressure transmission. In: Hoff J, Keep R, Xi G, Hua Y, editors. Brain Edema XIII. Acta Neurochirurgica Supplementum. 96: Springer Vienna; 2006. p. 103-7.

47.	Czosnyka M, Smielewski P, Kirkpatrick P, Laing RJ, Menon D, Pickard JD. Continuous assessment of the cerebral vasomotor reactivity in head injury. Neurosurgery. 1997;41(1):11-7; discussion 7-9.

48.	Steiner LA, Coles JP, Johnston AJ, Chatfield DA, Smielewski P, Fryer TD, et al. Assessment of cerebrovascular autoregulation in head-injured patients: a validation study. Stroke. 2003;34(10):2404-9.

49.	Czosnyka M, Smielewski P, Piechnik S, Schmidt EA, Al-Rawi PG, Kirkpatrick PJ, et al. Hemodynamic characterization of intracranial pressure plateau waves in head-injury patients. J Neurosurg. 1999;91(1):11-9.

50.	Steiner LA, Czosnyka M, Piechnik SK, Smielewski P, Chatfield D, Menon DK, et al. Continuous monitoring of cerebrovascular pressure reactivity allows

determination of optimal cerebral perfusion pressure in patients with traumatic brain injury. Crit Care Med. 2002;30(4):733-8.

51.   Shaw M. Modelling the time-series of cerebrovascular pressure transmission variation in head injured patients.: University of Glasgow; 2012.

52.   Shaw M, Piper I, Daley M. Autoregulatory model comparison and optimisation methodology. Acta Neurochir Suppl. 2012;114:135-9.

53.   Cerebral Autoregulation Research Network [cited 2017 18th March]. Available from: www.car-net.org.

54.   Carney N, Totten AM, O'Reilly C, Ullman JS, Hawryluk GWJ, Bell MJ, et al. Guidelines for the Management of Severe Traumatic Brain Injury, Fourth Edition. Neurosurgery. 2017;80(1):6-15.

55.   Lavinio A, Menon DK. Intracranial pressure: why we monitor it, how to monitor it, what to do with the number and what's the future? Curr Opin Anaesthesiol. 2011;24(2):117-23.

56.   Smith M. Monitoring intracranial pressure in traumatic brain injury. Anesth Analg. 2008;106(1):240-8.

57.   Steiner LA, Andrews PJD. Monitoring the injured brain: ICP and CBF. British Journal of Anaesthesia. 2006;97(1):26-38.

58.   Patel HC, Menon DK, Tebbs S, Hawker R, Hutchinson PJ, Kirkpatrick PJ. Specialist neurocritical care and outcome from head injury. Intensive Care Med. 2002;28(5):547-53.

59.   Fakhry SM, Trask AL, Waller MA, Watts DD. Management of brain-injured patients by an evidence-based medicine protocol improves outcomes and decreases hospital charges. J Trauma. 2004;56(3):492-9; discussion 9-500.

60.   Alali AS, Fowler RA, Mainprize TG, Scales DC, Kiss A, de Mestral C, et al. Intracranial pressure monitoring in severe traumatic brain injury: results from the American College of Surgeons Trauma Quality Improvement Program. J Neurotrauma. 2013;30(20):1737-46.

61.   Cremer OL, van Dijk GW, van Wensen E, Brekelmans GJ, Moons KG, Leenen LP, et al. Effect of intracranial pressure monitoring and targeted intensive care on functional outcome after severe head injury. Crit Care Med. 2005;33(10):2207-13.

62.   Hutchinson PJ, Kolias AG, Czosnyka M, Kirkpatrick PJ, Pickard JD, Menon DK. Intracranial pressure monitoring in severe traumatic brain injury. Bmj. 2013;346:f1000.

63.   Melhem S, Shutter L, Kaynar AM. A trial of intracranial pressure monitoring in traumatic brain injury. Crit Care. 2014;18(1):302.

64.   Romner B, Grande PO. Traumatic brain injury: Intracranial pressure monitoring in traumatic brain injury. Nature reviews Neurology. 2013;9(4):185-6.

65.   Kirkman MA, Smith M. Intracranial pressure monitoring, cerebral perfusion pressure estimation, and ICP/CPP-guided therapy: a standard of care or optional extra after brain injury? British Journal of Anaesthesia. 2014;112(1):35-46.

66.   Chesnut RM. Intracranial pressure monitoring: headstone or a new head start. The BEST TRIP trial in perspective. Intensive Care Med. 2013;39(4):771-4.

67.   Bratton SL, Chestnut RM, Ghajar J, McConnell Hammond FF, Harris OA, Hartl R, et al. Guidelines for the management of severe traumatic brain injury. VII Intracranial pressure monitoring technology. J Neurotrauma. 2007;24 Suppl 1:S37-44.

68.   Leverstein-van Hall MA, Hopmans TE, van der Sprenkel JW, Blok HE, van der Mark WA, Hanlo PW, et al. A bundle approach to reduce the incidence of external ventricular and lumbar drain-related infections. J Neurosurg. 2010;112(2):345-53.

69.   Czosnyka M, Czosnyka Z, Pickard JD. Laboratory testing of three intracranial pressure microtransducers: technical report. Neurosurgery. 1996;38(1):219-24.

70.   Citerio G, Piper I, Cormio M, Galli D, Cazzaniga S, Enblad P, et al. Bench test assessment of the new Raumedic Neurovent-P ICP sensor: a technical report by the BrainIT group. Acta Neurochir (Wien). 2004;146(11):1221-6.

71.   Citerio G, Piper I, Chambers IR, Galli D, Enblad P, Kiening K, et al. Multicenter Clinical Assessment of the Raumedic Neurovent-P Intracranial Pressure Sensor: A Report By the Brainit Group. Neurosurgery. 2008;63(6):1152-8.

72.   Sahuquillo J, Poca MA, Arribas M, Garnacho A, Rubio E. Interhemispheric supratentorial intracranial pressure gradients in head-injured patients: are they clinically important? J Neurosurg. 1999;90(1):16-26.

73.   Rosenberg JB, Shiloh AL, Savel RH, Eisen LA. Non-invasive methods of estimating intracranial pressure. Neurocrit Care. 2011;15(3):599-608.

74.   Raboel PH, Bartek J, Andresen M, Bellander BM, Romner B. Intracranial Pressure Monitoring: Invasive versus Non-Invasive Methods - A Review. Critical Care Research and Practice. 2012;2012:14.

75.   Kristiansson H, Nissborg E, Bartek J, Jr., Andresen M, Reinstrup P, Romner B. Measuring elevated intracranial pressure through noninvasive methods: a review of the literature. J Neurosurg Anesthesiol. 2013;25(4):372-85.

76.   Aaslid R, Markwalder T-M, Nornes H. Noninvasive transcranial Doppler ultrasound recording of flow velocity in basal cerebral arteries. Journal of Neurosurgery. 1982;57(6):769-74.

77.   Schmidt EA, Czosnyka M, Gooskens I, Piechnik SK, Matta BF, Whitfield PC, et al. Preliminary experience of the estimation of cerebral perfusion pressure using transcranial Doppler ultrasonography. Journal of neurology, neurosurgery, and psychiatry. 2001;70(2):198-204.

78.   Bellner J, Romner B, Reinstrup P, Kristiansson KA, Ryding E, Brandt L. Transcranial Doppler sonography pulsatility index (PI) reflects intracranial pressure (ICP). Surg Neurol. 2004;62(1):45-51; discussion

79.   Edouard AR, Vanhille E, Le Moigno S, Benhamou D, Mazoit JX. Non-invasive assessment of cerebral perfusion pressure in brain injured patients with moderate intracranial hypertension. Br J Anaesth. 2005;94(2):216-21.

80.   Brandi G, Bechir M, Sailer S, Haberthur C, Stocker R, Stover JF. Transcranial color-coded duplex sonography allows to assess cerebral perfusion pressure noninvasively following severe traumatic brain injury. Acta Neurochir (Wien). 2010;152(6):965-72.

81.   Geeraerts T, Launey Y, Martin L, Pottecher J, Vigue B, Duranteau J, et al. Ultrasonography of the optic nerve sheath may be useful for detecting raised intracranial pressure after severe brain injury. Intensive Care Med. 2007;33(10):1704-11.

82.   Geeraerts T, Merceron S, Benhamou D, Vigue B, Duranteau J. Non-invasive assessment of intracranial pressure using ocular sonography in neurocritical care patients. Intensive Care Med. 2008;34(11):2062-7.

83.   Kimberly HH, Shah S, Marill K, Noble V. Correlation of optic nerve sheath diameter with direct measurement of intracranial pressure. Academic emergency medicine : official journal of the Society for Academic Emergency Medicine. 2008;15(2):201-4.

84.   Moretti R, Pizzi B. Optic nerve ultrasound for detection of intracranial hypertension in intracranial hemorrhage patients: confirmation of previous findings in a different patient population. J Neurosurg Anesthesiol. 2009;21(1):16-20.

85.   Moretti R, Pizzi B, Cassini F, Vivaldi N. Reliability of optic nerve ultrasound for the evaluation of patients with spontaneous intracranial hemorrhage. Neurocrit Care. 2009;11(3):406-10.

86.   Soldatos T, Karakitsos D, Chatzimichail K, Papathanasiou M, Gouliamos A, Karabinis A. Optic nerve sonography in the diagnostic evaluation of adult brain injury. Crit Care. 2008;12(3):1-7.

87.   Dubourg J, Javouhey E, Geeraerts T, Messerer M, Kassai B. Ultrasonography of optic nerve sheath diameter for detection of raised intracranial pressure: a systematic review and meta-analysis. Intensive Care Med. 2011;37(7):1059-68.

88.   Dubourg J, Messerer M, Karakitsos D, Rajajee V, Antonsen E, Javouhey E, et al. Individual patient data systematic review and meta-analysis of optic nerve sheath diameter ultrasonography for detecting raised intracranial pressure: protocol of the ONSD research group. Syst Rev. 2013;2(1):1-6.

89.   Rosner MJ, Rosner SD, Johnson AH. Cerebral perfusion pressure: management protocol and clinical results. J Neurosurg. 1995;83(6):949-62.

90.   Asgeirsson B, Grände PO, Nordström CH. A new therapy of post-trauma brain oedema based on haemodynamic principles for brain volume regulation. Intensive Care Medicine. 1994;20(4):260-7.

91.   Naredi S, Eden E, Zall S, Stephensen H, Rydenhag B. A standardized neurosurgical neurointensive therapy directed toward vasogenic edema after severe traumatic brain injury: clinical results. Intensive Care Med. 1998;24(5):446-51.

92.   Robertson CS, Valadka AB, Hannay HJ, Contant CF, Gopinath SP, Cormio M, et al. Prevention of secondary ischemic insults after severe head injury. Critical Care Medicine. 1999;27(10):2086-95.

93.   Howells T, Elf K, Jones PA, Ronne-Engstrom E, Piper I, Nilsson P, et al. Pressure reactivity as a guide in the treatment of cerebral perfusion pressure in patients with brain trauma. J Neurosurg. 2005;102(2):311-7.

94.   16th International Conference on Intracranial Pressure and Brain Monitoring [cited 2017 18th March]. Available from: http://www.rle.mit.edu/icp2016/.

95.   Maas AI, Murray GD, Roozenbeek B, Lingsma HF, Butcher I, McHugh GS, et al. Advancing care for traumatic brain injury: findings from the IMPACT studies and perspectives on future research. Lancet Neurol. 2013;12(12):1200-10.

96.   Piper I, Citerio G, Chambers I, Contant C, Enblad P, Fiddes H, et al. The BrainIT group: concept and core dataset definition. Acta Neurochir (Wien). 2003;145(8):615-28; discussion 28-9.

97.   CENTER-TBI [cited 2017 18th March]. Available from: www.center-tbi.eu.

98.   Hutchinson PJ, Kolias AG, Timofeev IS, Corteen EA, Czosnyka M, Timothy J, et al. Trial of Decompressive Craniectomy for Traumatic Intracranial Hypertension. New England Journal of Medicine. 2016;375(12):1119-30.

99.   Andrews PJD, Sinclair HL, Rodriguez A, Harris BA, Battison CG, Rhodes JKJ, et al. Hypothermia for Intracranial Hypertension after Traumatic Brain Injury. New England Journal of Medicine. 2015;373(25):2403-12.

100.   Aries MJ, Czosnyka M, Budohoski KP, Steiner LA, Lavinio A, Kolias AG, et al. Continuous determination of optimal cerebral perfusion pressure in traumatic brain injury. Crit Care Med. 2012;40(8):2456-63.

101.   Lazaridis C, Desantis SM, Smielewski P, Menon DK, Hutchinson P, Pickard JD, et al. Patient-specific thresholds of intracranial pressure in severe traumatic brain injury. J Neurosurg. 2014.

102.   Depreitere B, Güiza F, Van den Berghe G, Schuhmann MU, Maier G, Piper I, et al. Pressure autoregulation monitoring and cerebral perfusion pressure target recommendation in patients with severe traumatic brain injury based on minute-by-minute monitoring data. Journal of Neurosurgery. 2014;120(6):1451-7.

103.   Hu X, Xu P, Scalzo F, Vespa P, Bergsneider M. Morphological clustering and analysis of continuous intracranial pressure. IEEE Trans Biomed Eng. 2009;56(3):696-705.

104.   Scalzo F, Asgari S, Kim S, Bergsneider M, Hu X. Robust peak recognition in intracranial pressure signals. Biomedical engineering online. 2010;9:61.

105.   Hu X, Glenn T, Scalzo F, Bergsneider M, Sarkiss C, Martin N, et al. Intracranial pressure pulse morphological features improved detection of decreased cerebral blood flow. Physiol Meas. 2010;31(5):679-95.

106.   Hu X, Xu P, Asgari S, Vespa P, Bergsneider M. Forecasting ICP elevation based on prescient changes of intracranial pressure waveform morphology. IEEE Trans Biomed Eng. 2010;57(5):1070-8.

107.   Guiza F, Depreitere B, Piper I, Van den Berghe G, Meyfroidt G. Novel methods to predict increased intracranial pressure during intensive care and

long-term neurologic outcome after traumatic brain injury: development and validation in a multicenter dataset. Crit Care Med. 2013;41(2):554-64.

108.   Ragauskas A, Matijosaitis V, Zakelis R, Petrikonis K, Rastenyte D, Piper I, et al. Clinical assessment of noninvasive intracranial pressure absolute value measurement method. Neurology. 2012;78(21):1684-91.

109.   Ragauskas A, Bartusis L, Piper I, Zakelis R, Matijosaitis V, Petrikonis K, et al. Improved diagnostic value of a TCD-based non-invasive ICP measurement method compared with the sonographic ONSD method for detecting elevated intracranial pressure. Neurol Res. 2014;36(7).

110.   Kyle UG, Bosaeus I, De Lorenzo AD, Deurenberg P, Elia M, Gomez JM, et al. Bioelectrical impedance analysis--part I: review of principles and methods. Clin Nutr. 2004;23(5):1226-43.

111.   Cole KS, Cole RH. Dispersion and Absorption in Dielectrics I. Alternating Current Characteristics. The Journal of Chemical Physics. 1941;9(4):341-51.

112.   Norman K, Stobaus N, Pirlich M, Bosy-Westphal A. Bioelectrical phase angle and impedance vector analysis--clinical relevance and applicability of impedance parameters. Clin Nutr. 2012;31(6):854-61.

113.   Maggiore Q, Nigrelli S, Ciccarelli C, Grimaldi C, Rossi GA, Michelassi C. Nutritional and prognostic correlates of bioimpedance indexes in hemodialysis patients. Kidney Int. 1996;50(6):2103-8.

114.   Segall L, Mardare NG, Ungureanu S, Busuioc M, Nistor I, Enache R, et al. Nutritional status evaluation and survival in haemodialysis patients in one centre from Romania. Nephrology, dialysis, transplantation : official publication of the European Dialysis and Transplant Association - European Renal Association. 2009;24(8):2536-40.

115.   Colin-Ramirez E, Castillo-Martinez L, Orea-Tejeda A, Asensio Lafuente E, Torres Villanueva F, Rebollar Gonzalez V, et al. Body composition and echocardiographic abnormalities associated to anemia and volume overload in heart failure patients. Clin Nutr. 2006;25(5):746-57.

116.   Doesch C, Suselbeck T, Leweling H, Fluechter S, Haghi D, Schoenberg SO, et al. Bioimpedance analysis parameters and epicardial adipose tissue assessed by cardiac magnetic resonance imaging in patients with heart failure. Obesity (Silver Spring, Md). 2010;18(12):2326-32.

117.   Gupta D, Lammersfeld CA, Burrows JL, Dahlk SL, Vashi PG, Grutsch JF, et al. Bioelectrical impedance phase angle in clinical practice: implications for prognosis in advanced colorectal cancer. Am J Clin Nutr. 2004;80(6):1634-8.

118.   Gupta D, Lammersfeld CA, Vashi PG, King J, Dahlk SL, Grutsch JF, et al. Bioelectrical impedance phase angle in clinical practice: implications for prognosis in stage IIIB and IV non-small cell lung cancer. BMC cancer. 2009;9:37.

119.   Bodo M. Studies in Rheoencephalography (REG). Journal of Electrical Bioimpedance. 2010;1:18-40.

120.   Grasso G, Alafaci C, Passalacqua M, Morabito A, Buemi M, Salpietro FM, et al. Assessment of human brain water content by cerebral bioelectrical impedance analysis: a new technique and its application to cerebral pathological conditions. Neurosurgery. 2002;50(5):1064-72; discussion 72-4.

121.   Liu L, Dong W, Ji X, Chen L, He W, Jia J. A new method of noninvasive brain-edema monitoring in stroke: cerebral electrical impedance measurement. Neurol Res. 2006;28(1):31-7.

122.   Liu LX, Dong WW, Wang J, Wu Q, He W, Jia YJ. The role of noninvasive monitoring of cerebral electrical impedance in stroke. Acta Neurochir Suppl. 2005;95:137-40.

123.   He LY, Wang J, Luo Y, Dong WW, Liu LX. Application of non-invasive cerebral electrical impedance measurement on brain edema in patients with cerebral infarction. Neurol Res. 2010;32(7):770-4.

124.   Lou JH, Wang J, Liu LX, He LY, Yang H, Dong WW. Measurement of Brain Edema by Noninvasive Cerebral Electrical Impedance in Patients with Massive Hemispheric Cerebral Infarction. European Neurology. 2012;68(6):350-7.

125.   Seoane F, Reza Atefi S, Tomner J, Kostulas K, Lindecrantz K. Electrical Bioimpedance Spectroscopy on Acute Unilateral Stroke Patients: Initial Observations regarding Differences between Sides. BioMed research international. 2015;2015:12.

126.   Harting MT, Smith CT, Radhakrishnan RS, Aroom KR, Dash PK, Gill B, et al. Regional differences in cerebral edema after traumatic brain injury identified by impedance analysis. J Surg Res. 2010;159(1):557-64.

127.   Lingwood BE, Dunster KR, Colditz PB, Ward LC. Noninvasive measurement of cerebral bioimpedance for detection of cerebral edema in the neonatal piglet. Brain Res. 2002;945(1):97-105.

128.   Lingwood BE, Dunster KR, Healy GN, Ward LC, Colditz PB. Cerebral impedance and neurological outcome following a mild or severe hypoxic/ischemic episode in neonatal piglets. Brain Res. 2003;969(1-2):160-7.

129.   Lingwood BE, Healy GN, Kecskes Z, Dunster KR, Gray PH, Ward LC, et al. Prediction of outcome following hypoxia/ischaemia in the human infant using cerebral impedance. Clinical neurophysiology : official journal of the International Federation of Clinical Neurophysiology. 2009;120(2):225-30.

130.   Shaw M, Piper I, Campbell P, McKeown C, Britton J, Oommen K, et al. Investigation of the relationship between transcranial impedance and intracranial pressure. Acta Neurochir Suppl. 2012;114:61-5.

131.   Metherall P, Barber D, Smallwood R, Brown B. Three dimensional electrical impedance tomography. Nature. 1996;380(6574):509-12.

132.   Manwaring PK, Moodie KL, Hartov A, Manwaring KH, Halter RJ. Intracranial electrical impedance tomography: a method of continuous monitoring in an animal model of head trauma. Anesth Analg. 2013;117(4):866-75.

133.   ixellence GmbH. ixTrends. Germany;2011.

134.   Wickham H. ggplot2: Elegant Graphics for Data Analysis. New York: Springer-Verlag; 2009.

135.   Wickham H, Francois R. dplyr: A Grammar of Data Manipulation. R package version 0.4.1. 2015.

136.   Wickham H. stringr: Make it easier to work with strings. R package version 0.6.2. 2012.

137.   Georgatzis K, Lal P, C. H, Shaw M, Piper I, Tarbert C, et al. Artifact in physiological data collected from brain injured patients: quantifying the problem and providing a solution through a factorial switching linear dynamical systems approach. Proceedings of the 15th International Symposium on Brain Monitoring and Intracranial Pressure, Singapore, November 2013.

138.   Lal P, Williams CKI, Georgatzis K, Hawthorne C, McMonagle P, Piper I, et al. Detecting Artifactual Events in Vital Signs Monitoring Data2015. Available from:
http://homepages.inf.ed.ac.uk/ckiw/projects/adult_icu/CSOreport230915.pdf.

139.   Maas AI, Steyerberg EW, Murray GD, Bullock R, Baethmann A, Marshall LF, et al. Why have recent trials of neuroprotective agents in head injury failed to

show convincing efficacy? A pragmatic analysis and theoretical considerations. Neurosurgery. 1999;44(6):1286-98.

140.   Maas AI, Roozenbeek B, Manley GT. Clinical trials in traumatic brain injury: past experience and current developments. Neurotherapeutics : the journal of the American Society for Experimental NeuroTherapeutics. 2010;7(1):115-26.

141.   Roozenbeek B, Lingsma HF, Maas AI. New considerations in the design of clinical trials for traumatic brain injury. Clinical investigation. 2012;2(2):153-62.

142.   Maas AI, Marmarou A, Murray GD, Teasdale SG, Steyerberg EW. Prognosis and clinical trial design in traumatic brain injury: the IMPACT study. J Neurotrauma. 2007;24(2):232-8.

143.   Maas AI, Steyerberg EW, Marmarou A, McHugh GS, Lingsma HF, Butcher I, et al. IMPACT recommendations for improving the design and analysis of clinical trials in moderate to severe traumatic brain injury. Neurotherapeutics : the journal of the American Society for Experimental NeuroTherapeutics. 2010;7(1):127-34.

144.   National Institute for Health and Care Excellence. Acute stroke. 2017.

145.   Shaw M, Piper I, Hawthorne C. Multi-resolution Convolution Methodology for ICP Waveform Morphology Analysis. Acta Neurochir Suppl. 2016;122:41-4.

146.   Ward A, Hawthorne C, Shaw M, editors. Cerebral autoregulation model extension using high frequency ICU data. British Journal of Anaesthesia Research Forum (Submitted to conference proceedings); 2016; Glasgow, UK.

147.   Hawthorne C, Shaw M, Moss L, Piper I, Elliott R, Lee C, et al. 761: Improvements to the optimal cerebral perfusion pressure calculation. Critical Care Medicine. 2016;44(12):266.

148.   Takla G, Petre JH, Doyle DJ, Horibe M, Gopakumaran B. The problem of artifacts in patient monitor data during surgery: a clinical and methodological review. Anesth Analg. 2006;103(5):1196-204.

149.   Georgatzis K, Lal P, Hawthorne C, Shaw M, Piper I, Tarbert C, et al. Artefact in Physiological Data Collected from Patients with Brain Injury: Quantifying the Problem and Providing a Solution Using a Factorial Switching Linear Dynamical Systems Approach. Acta Neurochir Suppl. 2016;122:301-5.

150.   Lal P, Williams CK, Georgatzis K, Hawthorne C, McMonagle P, Piper I, et al. Detecting artifactual events in vital signs monitoring data. 2016. In: Machine

Learning for Healthcare Technologies [Internet]. Institution of Engineering and TechnologyHealthcare Technologies; [7-32].

151.   [cited 2017 31st March]. Available from: www.chartadapt.org.

152.   Biousse V, Bruce BB, Newman NJ. Update on the pathophysiology and management of idiopathic intracranial hypertension. Journal of neurology, neurosurgery, and psychiatry. 2012;83(5):488-94.

153.   Pople IK. Hydrocephalus and shunts: what the neurologist should know. Journal of neurology, neurosurgery, and psychiatry. 2002;73 Suppl 1:i17-22.

154.   McAllister JP, 2nd, Williams MA, Walker ML, Kestle JR, Relkin NR, Anderson AM, et al. An update on research priorities in hydrocephalus: overview of the third National Institutes of Health-sponsored symposium "Opportunities for Hydrocephalus Research: Pathways to Better Outcomes". J Neurosurg. 2015;123(6):1427-38.

155.   Minto CF, Schnider TW. Contributions of PK/PD modeling to intravenous anesthesia. Clin Pharmacol Ther. 2008;84(1):27-38.

156.   Sury MR, Palmer JH, Cook TM, Pandit JJ. The state of UK anaesthesia: a survey of National Health Service activity in 2013. Br J Anaesth. 2014;113(4):575-84.

157.   Baker MT, Naguib M. Propofol: the challenges of formulation. Anesthesiology. 2005;103(4):860-76.

158.   Doenicke AW, Roizen MF, Rau J, O'Connor M, Kugler J, Klotz U, et al. Pharmacokinetics and pharmacodynamics of propofol in a new solvent. Anesth Analg. 1997;85(6):1399-403.

159.   Brown EN, Lydic R, Schiff ND. General anesthesia, sleep, and coma. N Engl J Med. 2010;363(27):2638-50.

160.   Sebel PS, Lowdon JD. Propofol: a new intravenous anesthetic. Anesthesiology. 1989;71(2):260-77.

161.   Smith I, White PF, Nathanson M, Gouldson R. Propofol. An update on its clinical use. Anesthesiology. 1994;81(4):1005-43.

162.   Aun CS. New i.v. agents. Br J Anaesth. 1999;83(1):29-41.

163.   Servln MDF, Desmonts MDJM, Haberer MDJP, Cockshott PDID, Plummer HNCGF, Farinotti PDR. Pharmacokinetics and Protein Binding of Propofol in Patients with Cirrhosis. Anesthesiology. 1988;69(6):887-91.

164.   Hiraoka H, Yamamoto K, Okano N, Morita T, Goto F, Horiuchi R. Changes in drug plasma concentrations of an extensively bound and highly extracted

drug, propofol, in response to altered plasma binding. Clin Pharmacol Ther. 2004;75(4):324-30.

165.   Takizawa E, Hiraoka H, Takizawa D, Goto F. Changes in the effect of propofol in response to altered plasma protein binding during normothermic cardiopulmonary bypass. British Journal of Anaesthesia. 2006;96(2):179-85.

166.   Mazoit JX, Samii K. Binding of propofol to blood components: implications for pharmacokinetics and for pharmacodynamics. British journal of clinical pharmacology. 1999;47(1):35-42.

167.   Takizawa D, Sato E, Hiraoka H, Tomioka A, Yamamoto K, Horiuchi R, et al. Changes in apparent systemic clearance of propofol during transplantation of living related donor liver. Br J Anaesth. 2005;95(5):643-7.

168.   Takizawa MDD, Hiraoka MDPDH, Goto MDPDF, Yamamoto PDK, Horiuchi PDR. Human Kidneys Play an Important Role in the Elimination of Propofol. Anesthesiology. 2005;102(2):327-30.

169.   Takata K, Kurita T, Morishima Y, Morita K, Uraoka M, Sato S. Do the kidneys contribute to propofol elimination? Br J Anaesth. 2008;101(5):648-52.

170.   Hiraoka H, Yamamoto K, Miyoshi S, Morita T, Nakamura K, Kadoi Y, et al. Kidneys contribute to the extrahepatic clearance of propofol in humans, but not lungs and brain. British journal of clinical pharmacology. 2005;60(2):176-82.

171.   Favetta P, Degoute CS, Perdrix JP, Dufresne C, Boulieu R, Guitton J. Propofol metabolites in man following propofol induction and maintenance. Br J Anaesth. 2002;88(5):653-8.

172.   Loftsson T. Chapter 2 - Basic Concepts of Pharmacokinetics. Essential Pharmacokinetics. Boston: Academic Press; 2015. p. 9-84.

173.   Kay NH, Sear JW, Uppington J, Cockshott ID, Douglas EJ. Disposition of propofol in patients undergoing surgery. A comparison in men and women. Br J Anaesth. 1986;58(10):1075-9.

174.   Cockshott ID, Briggs LP, Douglas EJ, White M. Pharmacokinetics of propofol in female patients. Studies using single bolus injections. Br J Anaesth. 1987;59(9):1103-10.

175.   Kirkpatrick T, Cockshott ID, Douglas EJ, Nimmo WS. Pharmacokinetics of propofol (diprivan) in elderly patients. Br J Anaesth. 1988;60(2):146-50.

176.   Schnider TW, Minto CF, Gambus PL, Andresen C, Goodale DB, Shafer SL, et al. The influence of method of administration and covariates on the

pharmacokinetics of propofol in adult volunteers. Anesthesiology. 1998;88(5):1170-82.

177.   Schnider TW, Minto CF, Shafer SL, Gambus PL, Andresen C, Goodale DB, et al. The influence of age on propofol pharmacodynamics. Anesthesiology. 1999;90(6):1502-16.

178.   Gepts E, Camu F, Cockshott ID, Douglas EJ. Disposition of propofol administered as constant rate intravenous infusions in humans. Anesth Analg. 1987;66(12):1256-63.

179.   Gepts E, Jonckheer K, Maes V, Sonck W, Camu F. Disposition kinetics of propofol during alfentanil anaesthesia. Anaesthesia. 1988;43 Suppl:8-13.

180.   White M, Kenny GN. Intravenous propofol anaesthesia using a computerised infusion system. Anaesthesia. 1990;45(3):204-9.

181.   Glen JB. The development of 'Diprifusor': a TCI system for propofol. Anaesthesia. 1998;53 Suppl 1:13-21.

182.   Beal S, Sheiner LB, Boeckmann A, Bauer RJ. NONMEM User's Guides. (1989-2009). Icon Development Solutions, Ellicott City, MD, USA2009.

183.   James WPT, Waterlow JC. Research on obesity: a report of the DHSS/MRC group: HM Stationery Office; 1976.

184.   Absalom AR, Glen JI, Zwart GJ, Schnider TW, Struys MM. Target-Controlled Infusion: A Mature Technology. Anesth Analg. 2016;122(1):70-8.

185.   Absalom AR, Mani V, De Smet T, Struys MM. Pharmacokinetic models for propofol--defining and illuminating the devil in the detail. Br J Anaesth. 2009;103(1):26-37.

186.   Engbers FH, Sutcliffe N, Kenny G, Schraag S. Pharmacokinetic models for propofol: defining and illuminating the devil in the detail. British Journal of Anaesthesia. 2010;104(2):261-4.

187.   Klotz U. Pharmacokinetics and drug metabolism in the elderly. Drug metabolism reviews. 2009;41(2):67-76.

188.   Vuyk J, Oostwouder CJ, Vletter AA, Burm AGL, Bovill JG. Gender differences in the pharmacokinetics of propofol in elderly patients during and after continuous infusion. British Journal of Anaesthesia. 2001;86(2):183-8.

189.   Fisher DM. (Almost) everything you learned about pharmacokinetics was (somewhat) wrong! Anesth Analg. 1996;83(5):901-3.

190.   Krejcie TC, Avram MJ. What determines anesthetic induction dose? It's the front-end kinetics, doctor! Anesth Analg. 1999;89(3):541-4.

191.   Upton RN, Ludbrook G. A physiologically based, recirculatory model of the kinetics and dynamics of propofol in man. Anesthesiology. 2005;103(2):344-52.

192.   Ludbrook GL, Upton RN, Grant C, Gray EC. Cerebral effects of propofol following bolus administration in sheep. Anaesth Intensive Care. 1996;24(1):26-31.

193.   Ludbrook GL, Upton RN, Grant C, Gray EC. Brain and blood concentrations of propofol after rapid intravenous injection in sheep, and their relationships to cerebral effects. Anaesth Intensive Care. 1996;24(4):445-52.

194.   Upton RN, Ludbrook GL. A physiological model of induction of anaesthesia with propofol in sheep. 1. Structure and estimation of variables. Br J Anaesth. 1997;79(4):497-504.

195.   Ludbrook GL, Upton RN. A physiological model of induction of anaesthesia with propofol in sheep. 2. Model analysis and implications for dose requirements. Br J Anaesth. 1997;79(4):505-13.

196.   Price PS, Conolly RB, Chaisson CF, Gross EA, Young JS, Mathis ET, et al. Modeling interindividual variation in physiological factors used in PBPK models of humans. Critical reviews in toxicology. 2003;33(5):469-503.

197.   Ludbrook GL, Visco E, Lam AM. Propofol: relation between brain concentrations, electroencephalogram, middle cerebral artery blood flow velocity, and cerebral oxygen extraction during induction of anesthesia. Anesthesiology. 2002;97(6):1363-70.

198.   He YL, Ueyama H, Tashiro C, Mashimo T, Yoshiya I. Pulmonary disposition of propofol in surgical patients. Anesthesiology. 2000;93(4):986-91.

199.   Varvel JR, Donoho DL, Shafer SL. Measuring the predictive performance of computer-controlled infusion pumps. J Pharmacokinet Biopharm. 1992;20(1):63-94.

200.   Raemer DB, Buschman A, Varvel JR, Philip BK, Johnson MD, Stein DA, et al. The prospective use of population pharmacokinetics in a computer-driven infusion system for alfentanil. Anesthesiology. 1990;73(1):66-72.

201.   Tackley RM, Lewis GT, Prys-Roberts C, Boaden RW, Dixon J, Harvey JT. Computer controlled infusion of propofol. Br J Anaesth. 1989;62(1):46-53.

202.   Coetzee JF, Glen JB, Wium CA, Boshoff L. Pharmacokinetic model selection for target controlled infusions of propofol. Assessment of three parameter sets. Anesthesiology. 1995;82(6):1328-45.

203.   Glen JB, Servin F. Evaluation of the predictive performance of four pharmacokinetic models for propofol. Br J Anaesth. 2009;102(5):626-32.

204.   Masui K, Upton RN, Doufas AG, Coetzee JF, Kazama T, Mortier EP, et al. The performance of compartmental and physiologically based recirculatory pharmacokinetic models for propofol: a comparison using bolus, continuous, and target-controlled infusion data. Anesth Analg. 2010;111(2):368-79.

205.   Glen JB, White M. A comparison of the predictive performance of three pharmacokinetic models for propofol using measured values obtained during target-controlled infusion. Anaesthesia. 2014;69(6):550-7.

206.   Schuttler J, Ihmsen H. Population pharmacokinetics of propofol: a multicenter study. Anesthesiology. 2000;92(3):727-38.

207.   Struys MM, Coppens MJ, De Neve N, Mortier EP, Doufas AG, Van Bocxlaer JF, et al. Influence of administration rate on propofol plasma-effect site equilibration. Anesthesiology. 2007;107(3):386-96.

208.   Masui K, Kira M, Kazama T, Hagihira S, Mortier EP, Struys MM. Early phase pharmacokinetics but not pharmacodynamics are influenced by propofol infusion rate. Anesthesiology. 2009;111(4):805-17.

209.   Doufas AG, Bakhshandeh M, Bjorksten AR, Shafer SL, Sessler DI. Induction speed is not a determinant of propofol pharmacodynamics. Anesthesiology. 2004;101(5):1112-21.

210.   Swinhoe CF, Peacock JE, Glen JB, Reilly CS. Evaluation of the predictive performance of a 'Diprifusor' TCI system. Anaesthesia. 1998;53 Suppl 1:61-7.

211.   Sheiner LB, Stanski DR, Vozeh S, Miller RD, Ham J. Simultaneous modeling of pharmacokinetics and pharmacodynamics: application to d-tubocurarine. Clin Pharmacol Ther. 1979;25(3):358-71.

212.   Wagner JG. Kinetics of pharmacologic response I. Proposed relationships between response and drug concentration in the intact animal and man. Journal of Theoretical Biology. 1968;20(2):173-201.

213.   Fuseau E, Sheiner LB. Simultaneous modeling of pharmacokinetics and pharmacodynamics with a nonparametric pharmacodynamic model. Clin Pharmacol Ther. 1984;35(6):733-41.

214.   Minto CF, Schnider TW, Gregg KM, Henthorn TK, Shafer SL. Using the time of maximum effect site concentration to combine pharmacokinetics and pharmacodynamics. Anesthesiology. 2003;99(2):324-33.

215.   Cortínez LI. What is the ke0 and what does it tell me about propofol? Anaesthesia. 2014;69(5):399-402.

216.   Billard V, Gambus PL, Chamoun N, Stanski DR, Shafer SL. A comparison of spectral edge, delta power, and bispectral index as EEG measures of alfentanil, propofol, and midazolam drug effect. Clin Pharmacol Ther. 1997;61(1):45-58.

217.   Struys MM, De Smet T, Depoorter B, Versichelen LF, Mortier EP, Dumortier FJ, et al. Comparison of plasma compartment versus two methods for effect compartment--controlled target-controlled infusion for propofol. Anesthesiology. 2000;92(2):399-406.

218.   Rampil IJ. A primer for EEG signal processing in anesthesia. Anesthesiology. 1998;89(4):980-1002.

219.   Bruhn J, Myles PS, Sneyd R, Struys MM. Depth of anaesthesia monitoring: what's available, what's validated and what's next? Br J Anaesth. 2006;97(1):85-94.

220.   Palanca BJ, Mashour GA, Avidan MS. Processed electroencephalogram in depth of anesthesia monitoring. Curr Opin Anaesthesiol. 2009;22(5):553-9.

221.   Sigl JC, Chamoun NG. An introduction to bispectral analysis for the electroencephalogram. Journal of clinical monitoring. 1994;10(6):392-404.

222.   National Institute for Health and Care Excellence. Depth of anaesthesia monitors – Bispectral Index (BIS), E-Entropy and Narcotrend-Compact M (DG6). 2012.

223.   Punjasawadwong Y, Phongchiewboon A, Bunchungmongkol N. Bispectral index for improving anaesthetic delivery and postoperative recovery. Cochrane Database of Systematic Reviews. 2014(6).

224.   Myles PS, Leslie K, McNeil J, Forbes A, Chan MT. Bispectral index monitoring to prevent awareness during anaesthesia: the B-Aware randomised controlled trial. Lancet. 2004;363(9423):1757-63.

225.   Avidan MS, Jacobsohn E, Glick D, Burnside BA, Zhang L, Villafranca A, et al. Prevention of intraoperative awareness in a high-risk surgical population. N Engl J Med. 2011;365(7):591-600.

226.   Avidan MS, Zhang L, Burnside BA, Finkel KJ, Searleman AC, Selvidge JA, et al. Anesthesia Awareness and the Bispectral Index. New England Journal of Medicine. 2008;358(11):1097-108.

227.   Pandit JJ, Andrade J, Bogod DG, Hitchman JM, Jonker WR, Lucas N, et al. 5th National Audit Project (NAP5) on accidental awareness during general

anaesthesia: summary of main findings and risk factors. Br J Anaesth. 2014;113(4):549-59.

228. Purdon PL, Sampson A, Pavone KJ, Brown EN. Clinical Electroencephalography for Anesthesiologists Part I: Background and Basic Signatures. Anesthesiology. 2015;123(4):937-60.

229. Bennett C, Voss LJ, Barnard JP, Sleigh JW. Practical use of the raw electroencephalogram waveform during general anesthesia: the art and science. Anesth Analg. 2009;109(2):539-50.

230. Barnard JP, Bennett C, Voss LJ, Sleigh JW. Can anaesthetists be taught to interpret the effects of general anaesthesia on the electroencephalogram? Comparison of performance with the BIS and spectral entropy. Br J Anaesth. 2007;99(4):532-7.

231. Rigby-Jones AE, Priston MJ, Wolf AR, Sneyd JR. Concentration-dependent instability of propofol in whole human blood: A-464. European Journal of Anaesthesiology. 2005;22:122.

232. NONMEM History [cited 2017 31st March]. Available from: http://www.iconplc.com/innovation/nonmem/history/.

233. NONMEM Documentation [cited 2017 31st March]. Available from: https://nonmem.iconplc.com.

234. Owen JS, Fiedler-Kelly J. Introduction to Population Pharmacokinetic / Pharmacodynamic Analysis with Nonlinear Mixed Effects Models. First ed: John Wiley & Sons, Inc.; 2014.

235. Kim M-G, Yim D-S, Bae K-S. R-based reproduction of the estimation process hidden behind NONMEM® Part 1: first-order approximation method. Transl Clin Pharmacol. 2015;23(1):1-7.

236. Tornoe CW. nlmeODE: Non-linear mixed-effects modelling in nlme using differential equations. R package version 1.1. 2012.

237. Tornoe CW, Agerso H, Jonsson EN, Madsen H, Nielsen HA. Non-linear mixed-effects pharmacokinetic/pharmacodynamic modelling in NLME using differential equations. Computer methods and programs in biomedicine. 2004;76(1):31-40.

238. The Association of Anaesthetists of Great Britain and Ireland. Recommendations for standards of monitoring during anaesthesia and recovery. 2007.

239.   Bressan N, Paulo Moreira A, Amorim P, Nunes CS. Anaesthesia synchronization software: target controlled infusion system evaluation. Conf Proc IEEE Eng Med Biol Soc. 2010;2010:6777-80.

240.   Warnes GR, Bolker B, Gorjanc G, Grothendieck G, Korosec A, Lumley T, et al. gdata: Various R programming tools for data manipulation. R package version 2.13.3. 2014.

241.   Absalom A, Amutike D, Lal A, White M, Kenny GN. Accuracy of the 'Paedfusor' in children undergoing cardiac surgery or catheterization. Br J Anaesth. 2003;91(4):507-13.

242.   Eurosiva. Tivatrainer 2015 [cited 2015 November 26]. Available from: http://www.eurosiva.org/TivaTrainer/tivatrainer_main.htm.

243.   Soetaert K, Petzoldt T, Setzer RW. Solving Differential Equations in R: Package deSolve. Journal of Statistical Software. 2010;33(9):25.

244.   Hill AV. The possible effects of the aggregation of the molecules of haemoglobin on its dissociation curves. The Journal of Physiology. 1910;40:iv-vii.

245.   Al Hashimi M, Calo G, Guerrini R, Thompson JP, Lambert DG, Arblaster L, et al. Proceedings of the Anaesthetic Research Society MeetingAberdeen Exhibition Centre, Aberdeen, 21–22 June 2012. British Journal of Anaesthesia. 2012;109(4):655P-68P.

246.   Hawthorne C, Schraag S, Suttcliffe N, McKelvie S, Shaw M, Chandran M. Abstract PR438: Validation Study of the Covariates Model for Target Controlled Infusion of Propofol. Anesthesia & Analgesia. 2016;123(3S_Suppl):554-5.

247.   Hawthorne C, Schraag S, Suttcliffe N, McKelvie S, Shaw M, Chandran M. Abstract PR437: Calculating the Keo for the Covariates Model for Target Controlled Infusion of Propofol. Anesthesia & Analgesia. 2016;123(3S_Suppl):552-3.

248.   Zanner R, Pilge S, Kochs EF, Kreuzer M, Schneider G. Time delay of electroencephalogram index calculation: analysis of cerebral state, bispectral, and Narcotrend indices using perioperatively recorded electroencephalographic signals. Br J Anaesth. 2009;103(3):394-9.

249.   Lim TA. A novel method of deriving the effect compartment equilibrium rate constant for propofol. Br J Anaesth. 2003;91(5):730-2.

250.   Thomson AJ, Nimmo AF, Engbers FH, Glen JB. A novel technique to determine an 'apparent ke0 ' value for use with the Marsh pharmacokinetic model for propofol. Anaesthesia. 2014;69(5):420-8.

251.   Thomson AJ, Morrison G, Thomson E, Beattie C, Nimmo AF, Glen JB. Induction of general anaesthesia by effect-site target-controlled infusion of propofol: influence of pharmacokinetic model and ke0 value. Anaesthesia. 2014;69(5):429-35.

252.   Schuttler J, Kloos S, Schwilden H, Stoeckel H. Total intravenous anaesthesia with propofol and alfentanil by computer-assisted infusion. Anaesthesia. 1988;43 Suppl:2-7.

253.   Chiou WL. The phenomenon and rationale of marked dependence of drug concentration on blood sampling site. Implications in pharmacokinetics, pharmacodynamics, toxicology and therapeutics (Part I). Clin Pharmacokinet. 1989;17(3):175-99.

254.   Chiou WL. The phenomenon and rationale of marked dependence of drug concentration on blood sampling site. Implications in pharmacokinetics, pharmacodynamics, toxicology and therapeutics (Part II). Clin Pharmacokinet. 1989;17(4):275-90.

255.   Eleveld DJ, Proost JH, Cortinez LI, Absalom AR, Struys MM. A general purpose pharmacokinetic model for propofol. Anesth Analg. 2014;118(6):1221-37.

256.   Open TCI [cited 2017 31st March]. Available from: http://opentci.org.

257.   Croall A, Hawthorne C, Shaw M, editors. Modelling the effect site compartment in a target controlled infusion of Propofol. British Journal of Anaesthesia Research Forum (Submitted to conference proceedings); 2016; Glasgow, UK.

258.   Georgatzis K, Williams CKI, Hawthorne C. Input-Output Non-Linear Dynamical Systems applied to Physiological Condition Monitoring. In: Finale D-V, Jim F, David K, Byron W, Jenna W, editors. Proceedings of the 1st Machine Learning for Healthcare Conference; Proceedings of Machine Learning Research: PMLR; 2016. p. 1-16.

259.   Kazama T, Ikeda K, Morita K, Kikura M, Doi M, Ikeda T, et al. Comparison of the effect-site k(eO)s of propofol for blood pressure and EEG bispectral index in elderly and younger patients. Anesthesiology. 1999;90(6):1517-27.

260.   Dryden PE. Target-Controlled Infusions: Paths to Approval. Anesth Analg. 2016;122(1):86-9.

261.   Schnider TW, Minto CF, Struys MM, Absalom AR. The Safety of Target-Controlled Infusions. Anesth Analg. 2016;122(1):79-85.

262. Struys MM, De Smet T, Glen JI, Vereecke HE, Absalom AR, Schnider TW. The History of Target-Controlled Infusion. Anesth Analg. 2016;122(1):56-69.

263. Dumont GA, Ansermino JM. Closed-loop control of anesthesia: a primer for anesthesiologists. Anesth Analg. 2013;117(5):1130-8.

264. Pelorus [cited 2017 31st March]. Available from: http://www.spheremedical.com/products/pelorus.

265. Cowley NJ, Laitenberger P, Liu B, Jarvis J, Clutton-Brock TH. Evaluation of a new analyser for rapid measurement of blood propofol concentration during cardiac surgery. Anaesthesia. 2012;67(8):870-4.

266. Liu B, Pettigrew DM, Bates S, Laitenberger PG, Troughton G. Performance evaluation of a whole blood propofol analyser. J Clin Monit Comput. 2012;26(1):29-36.

267. MIMIC [cited 2017 31st March]. Available from: https://mimic.physionet.org.

268. Johnson AE, Pollard TJ, Shen L, Lehman LW, Feng M, Ghassemi M, et al. MIMIC-III, a freely accessible critical care database. Scientific data. 2016;3:160035.